Norwegian University
of Life Sciences

Master's Thesis 2018 60 ECTS
Faculty of Environmental Sciences and Natural Resource Management

Soil Carbon and Glacifluvial Deposits in the Deglaciation Landscape of Gausdal Vestfjell

Lina Bøe
Environment and Natural Resources

Preface

This project marks the end of a two-year master's degree in Environment and Natural Resources studied at the Faculty of Environmental Sciences and Natural Resource Management (MINA) at the Norwegian University of Life Sciences (NMBU). The project is based on one month of fieldwork carried out in Gausdal Vestfjell in July-August 2017, followed by two months of laboratory work in the autumn of 2017 at NMBU, Ås.

I would like to extend my sincerest thanks to the people who have facilitated the work. Supervisors Mona Henriksen and Line Tau Strand, for the opportunity to write a dissertation that combines geology and soil science, and for all help, valuable feedback, constructive criticism and interesting discussion. Leif Vidar Jakobsen, for patience and expertise during GPR data collection and processing. Artūrs Putniņš, for excellent guidance with ArcGIS, especially at a time when his own doctoral thesis was due. Irene Elisabeth Eriksen Dahl, Magdalena Izabela Rygalska, and Valentina Zivanovic, for help and guidance with soil chemical analysis in the laboratory, without whose expertise and pleasant company would be significantly more difficult. Michael Heim, for sharing specialist knowledge of the bedrock of the Lillehammer Map Sheet. Finn-Audun Grøndahl and Kittilbu Utmarksmuseum, for generously providing the facilities that made a month of solitary fieldwork *på vidda* possible. Finally, all the MINA master's students who made the work on both the dissertation and the degree into such an enjoyable experience.

I would also like to thank the people without whom this would not have been possible. My family, for a lifetime of support of me and my education. My father, Reidulv, for help with logistics, some of the physical work that the field of study requires, proof-reading and other suggestions for improvement. My mother, Frida, for helpfully checking all references. My sisters, Mari and Åsne, for being my sisters and otherwise beautiful people to the world. Jodi, for building my confidence and believing in me. Eva, for having pushed towards the path of the right resistance for 10+ years, been my friend even when the scholastic focus has gone *over stokk og stein,* literally and metaphorically, and always been there upon my return from academic endeavours. Maria, for inspiration and for the valuable knowledge that we study nature for the sake of humanity and that the natural sciences can only fulfil their purpose through social application. Gita, for a grateful approach to education and the knowledge that one belongs in the academic environment just by wanting to do good on the world. James, for motivation, stability and guidance, in academic achievement and in life.

Norwegian University of Life Sciences (NMBU)
Ås, 12.05.2018

Lina Bøe

Abstract

Glacifluvial deposits and their soil carbon stock and stability have been studied in the deglaciation landscape of Gausdal Vestfjell, Norway. Soil profiles are described and sampled for parent material clast analysis, density calculation and soil chemical analysis across a variety of glacifluvial landforms deposited in both flowing and stagnant ice, subaerially as well as subaqueously. The landforms include eskers, kame, kame terraces, delta and fan deposits. The morphology and sedimentology of 17 landforms are described and interpreted from remote sensing and field investigation. Methods have included visualization of LiDAR data in ArcMap, stratigraphic logging, sediment property analysis and Ground Penetrating Radar measurements. Calculation of carbon stock is based on soil density, stone and boulder content, horizon thickness and laboratory measurements of total carbon content.

Gausdal Vestfjell was deglaciated by down-wasting of stagnant ice, where kame terraces at the highest elevations (820-890 masl) record a progressive lowering of the ice surface. Fan, delta and sandur deposits record ice-damming and gradual drainage of meltwater from the lowest elevations (778-810 masl). The glacifluvial deposits are subangular, sorted and mainly composed of sand and gravel although both finer and coarser sediments occur. The deposits are dominated by tabular and through cross bedding, current ripples and horizontal lamination, erosive surfaces and variable discharge mainly in the upper flow regime.

The carbon stocks can be linked to depositional environments and processes during deglaciation. Early and late stage deposition at high (~890 masl) and low elevation (~790 masl), respectively, resulted in low carbon stocks, while deposition in stagnating ice at intermediate elevations is linked to high carbon stocks (~850 masl). The coarse texture of the deposits limits carbon input, decomposition, translocation and stabilisation due to low total particle surface area and water and nutrient retention capacity. Soil texture further exerts a major influence on carbon stocks through organic material occlusion and complexation with minerals, and a doubling of the silt and clay content from 20 % to 40 % nearly triples carbon stock. The texture varies greatly due to large variations between and within depositional environments and processes, and the glacifluvial carbon stocks are thus linked to the formation of the landforms they are found on.

The carbon stock of the soils is estimated down through the Bs horizon, and ranges from ~ 3 to 18 kg/m^2, with a mean estimated to 7.99 kg/m^2. The fraction stored in the mineral soil is highly variable and ranges from ~10 % to ~ 100 %, averaging at 63 %. Soil organic carbon varies with the nutrition status of the nearby bedrock and parent material, the degree of soil formation and the nature of sediment transport and deposition. The degree of soil formation is higher in soils formed from innutritious parent material. The soil carbon stock is higher in soil formed on landforms composed of immature sediment, deposited in the lower flow regime and with a low relief with the surrounding landscape. Stabilisation of organic carbon in the mineral soil depends on the presence of clay minerals in the parent material and soil

weathering products including iron and aluminium oxides and phyllosilicates. Mineral-stabilised carbon in soil of nutritious parent material may show higher chemical recalcitrance, while carbon stabilised in more acidic soils formed from less nutritious parent material may be more labile and to a larger degree stabilised by oxides.

Upscaling of carbon stock estimates from the detailed study of selected landforms was done by georeferencing a bedrock map and a topographic map based on LiDAR data to all landforms mapped by remote sensing in the study area (c. 500). Parent material nutrition status can be inferred from the local bedrock, and the nature of deposition from the shape of landforms and their relationship with the surrounding landscape. The small number of deposits studied provides no statistical significance for extrapolation, however, the trends and variation in the carbon stocks of glacifluvial soils appear to be predictable. By upscaling, the organic horizon carbon stocks of the glacifluvial soils were estimated to be equivalent to ~121 Mg CO_2/ha, and the carbon stocks of the mineral soil horizons to ~ 241 Mg CO_2/ha. The former is unstable and may be lost from the deglaciation landscape to the atmosphere in a warmer climate while the latter may be lost if there is a change in land use. Overall, the landforms show large carbon stock variations for both organic and mineral soil horizons. Calculated values are comparable to values obtained in previous studies for carbon stocks of forest soils in mountainous ecosystems.

Sammendrag

Glasifluviale avsetninger og deres karbonlager er studert i isavsmeltingslandskapet i Gausdal Vestfjell, Oppland. Jordprofiler fra fire glasifluviale landformer er beskrevet, og det er tatt prøver for analyse av opphavsmateriale, jordtetthet og jordkjemiske egenskaper fra tolv landformer. Morfologien og sedimentologien til i alt 17 landformer, inkludert eskere, kame, kameterrasse, delta og vifteavsetninger er beskrevet og tolket basert på fjernanalyse og feltundersøkelse, blant annet ved fremstilling av LiDAR-data i Arc MAP, stratigrafisk logging, analyse av sedimentegenskaper og geroradarmålinger. Beregning av karbonlager er basert på jordtetthet, innhold av stein og blokk, sjikttykkelse, og laboratorieanalyse av jordas innhold av total karbon.

På slutten av siste istid gikk Gausdal Vestfjell gjennom en fase med vertikal nedsmelting av stagnert is, hvor kameterrasser markerer en gradvis lavere isoverflate i de høytliggende områdene (820-890 m.o.h.). Vifter, delta og sanduravsetninger i de lavere områdene (778-815 m.o.h.) viser gradvis drenering av isdemt smeltevann. De glasifluviale avsetningene består hovedsakelig av sortert sand og grus med kantrundede klaster, men det finnes også mer finkornete og grovere sedimenter. Sedimentære strukturer inkluderer kryssjikt, strømrifler, horisontal laminasjon og erosjonsgrenser, og avsetningene gjenspeiler øvre strømregime, men også variabel vannføring.

Avsetningenes karbonlager kan kobles til avsetningsprosessene under isavsmeltingen. Tidlig avsetning i høyereliggende områder (~ 890 moh) og sen avsetning i lavereliggende områder (~790 moh) har resultert i små karbonlager, og avsetninger i stagnerende is i moderat høye områder (~850 moh) kan kobles mot større karbonlager. Avsetningens grove tekstur begrenser tilførsel, nedbryting, translokasjon og stabilisering av karbon i jordsmonnet grunnet partiklenes lave totale overflateareal og potensial for å holde på vann og næring. Jordas tekstur har i tillegg sterk innvirkning på karbonlager gjennom finstoffets evne til å binde organisk materiale, hvor en dobling av silt- og leirinnhold fra 20 % til 40 % nesten tredobler lageret av karbon. Teksturen avhenger av avsetningsmiljø, og jordas karboninnhold kan slik kobles til dannelsen av landformen den er lagret i. Jordtypen som har utviklet seg i avsetningene klassifiseres som ulike podzol.

Karbonlageret i jorda er beregnet til og med Bs-sjiktet, og varierer fra ~ 3-18 kg/m^2, med en gjennomsnittsverdi på 7.99 kg/m^2. Andelen lagret i mineraljord varierer fra ~10 % til ~ 100 %, med ett snitt på 63 %. Karbonlageret varierer med næringsstatusen til opphavsmaterialet og omkringliggende berggrunn, graden av jordsmonnutvikling og sedimentets transport- og avsetningsmåte. Jordsmonnutviklingen er sterkere i jord dannet fra næringsfattig opphavsmateriale. Karbonlageret er høyere i jord dannet i landformer bestående av næringsrikt opphavsmateriale, avsatt i nedre strømregime og med lavt relieff i forhold til landskapet omkring. Stabilisering av organisk karbon i mineraljorda avhenger av opphavsmaterialets innhold av leirmineraler, og forvitringsprodukter som oksider av jern og

aluminium og fyllosilikater. Mineralstabilisert karbon i jord dannet fra næringsrikt opphavsmateriale kan være sterkere nedbrutt, mens karbon stabilisert i surere jord dannet fra mindre næringsrikt opphavsmateriale kan være mindre nedbrutt og i større grad stabilisert av jern- og aluminiumsoksider.

Oppskalering av karbonlagerberegningene fra detaljstudiet av utvalgte landformer til å gjelde alle de ca. 500 glasifluviale landformene kartlagt ved fjernanalyse i studieområdet, ble gjort ved å georeferere området til berggrunnskart og topografiske satelittdata. Næringsstatusen til opphavsmaterialet kan vurderes ut fra lokal berggrunn, og avsetningsmåten til landformene fra form og plassering i landskapet. Det lave antallet studerte avsetninger gir ikke statsistisk grunnlag for oppskalering, men studien tyder på at variasjonen i karbonlager i glasifluviale jordsmonn kan være forutsigbar. Karbonlageret i organiske sjikt i glasifluviale landformer i studieområdet er gjennom oppskaleringen beregnet til å tilsvare ~121 Mg CO_2/ha, og karbonlageret i mineraljorda til ~ 241 Mg CO_2/ha. Førstnevnte er ustabilt og kan gå tapt dersom klimaet blir varmere, mens sistnevnte kan gå tapt ved endring i arealbruken. Totalt sett viser landformene stor variasjon i karbonlager både i organiske sjikt og mineraljordsjikt. De beregnede verdiene og variasjonen i karbonlager er likevel sammenlignbare med tidligere beregnede verdier for skogsjord i høyereliggende utmark.

Table of Contents

1 Introduction

This study is focused around the nature of soils and soil organic carbon preserved on a variety of glacifluvial landforms across the deglaciation landscape in Gausdal Vestfjell (figure 1.1). The formation mechanisms and properties of the soils are described and interpreted with respect to their parent material and landform association.

The processes that distribute, sort and arrange parent material produces characteristic landforms (Bockheim et al., 2005), and their interaction with soils can aid the prediction of soil formation through the landscape (Daniels and Hammer, 1992). The deglaciation landscape records the evolution of a changing environment, as does evolving soils throughout the landscape. Bockheim et al. (2005) stated that "Soils are linked to their resident landforms and their landscapes, by geomorphic processes with which they co-evolve".

The approach of studying soils from a geomorphic perspective is not new (Daniels and Hammer, 1992). Davy (1813) was the first to introduce the geological approach to soil science. Later it was recognized that parent material is one of many factors of significant influence on the nature of soils (Dokuchaey, 1897; Davy, 1813; Joffe, 1936; Joffe, 1949; Chesworth, 1973). Chesworth (1973) stated that it is only a question of time before the effect of a soils parent material is nullified.

Soils are ever-evolving, and young soils are particularly subject to change. A significant number of the soils in the world began to form after the last deglaciation (Torn et al., 1997), many of them in a deglaciation landscape. These soils will continue to develop, and soil carbon continue its interaction with the surrounding environment. Understanding the formation processes, stabilising factors and thresholds for irreversible change of soil carbon in these soils is essential in a world undergoing rapid environmental change.

The soils studied here are young, and the deglaciation processes, through the transportation and deposition of glacifluvial material, are still highly influential for the soil processes and carbon stock and stability. The relationship of the deglaciation landscape and the soil carbon it contains is the focus of the study.

1.1 Aims

The main aim of the project is to evaluate whether soil processes and soil carbon can be linked to the deglaciation processes and the landscape they shaped. The nature and mineral content of glacifluvial sediments and landforms are described and interpreted, and the deep and shallow stock of carbon in the soils that have developed from the deposits evaluated. All soil formation parameters but parent material are kept constant. Hence the soil carbon

variation is likely to be the result of the meltwater processes that created the landforms the soils developed from. The problem statements are as follow:

- How was Gausdal Vestfjell deglaciated and glacifluvial sediment deposited?
- What foundation does glacifluvial deposition give for soil organic carbon storage, and how does carbon stock vary among the deposits?
- Can the carbon stock of a glacifluvial soil be linked to the deglaciation processes, including the time of deglaciation, parent material, local bedrock, and nature and distance of sediment transport and deposition?
- What is the relationship between carbon stock, nutrient status of parent material and degree of soil formation? Can the mineral soil carbon stock be predicted from soil texture, the mineralogy of the parent material and the content of soil weathering products? How does parent material influence the mechanisms of carbon stabilisation?
- How does glacifluvial soil carbon stocks compare to that of other forest soils in mountainous ecosystems, what proportion is unstable, how much is mineral-stabilised and how much carbon might be lost from glacifluvial soils into the atmosphere?
- Can results from remote sensing, field- and laboratory studies of representative landforms be extrapolated to an extended area to estimate of deep soil carbon stock and stability of a deglaciation landscape?

Answers to the questions would provide a functional relationship between deglaciation, soil formation and soil carbon stabilisation. The term “functional relationship” was proposed by Jenny (1941) for analysis of soils in relation to soil forming factors for quantitative description of soil differentiation and distribution. The term was introduced as a general idea for soil formation under present conditions but may useful in the attempt of conceptually linking past geological processes to future soil-environment dynamics.

1.2 Study Area

The study area is in Gausdal Vestfjell between Gudbrandsdalen and Valdres, Oppland County (figure 1.1). The area is around 30 km^2 and resides between 61° 14’- 61° 10’ N and 9° 40’- 10° E. It consists of three valley systems at an elevation around 800 masl in a mountainous outfield (Norwegian: *Utmark*). NMBU has long traditions for soil and vegetation field studies in Gausdal Vestfjell, and a recent study in Quaternary geology was carried out by Putniņš and Henriksen (2017). They mapped c. 17 000 landforms, which provided a starting point for landform selection, verification, characterisation, and study of soil development and soil carbon in this project.

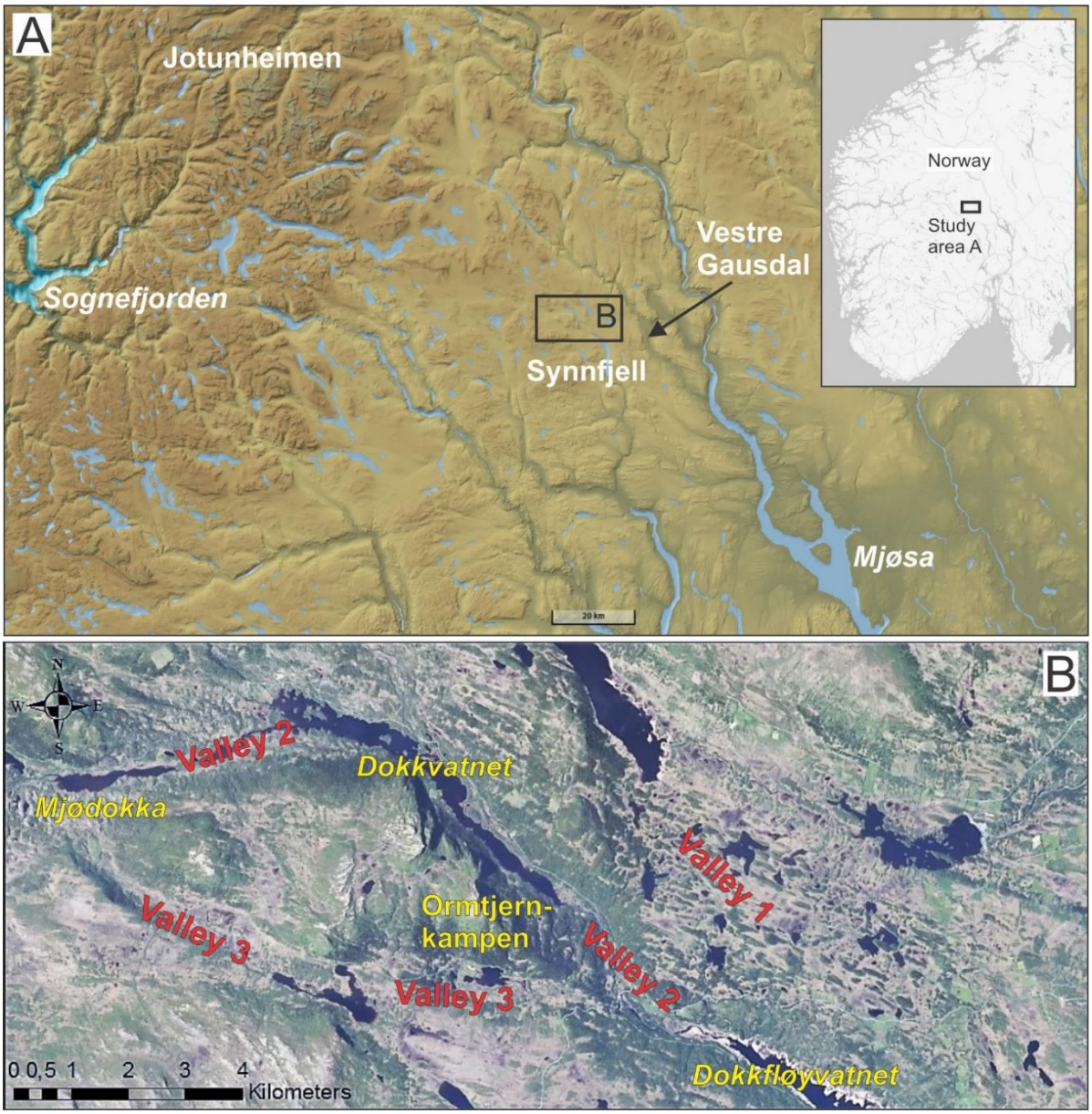

Figure 1.1. Overview of study area.

1.3 Landscape, Vegetation and Climate

The study area resides at high elevation, in a mountainous highland recognized as a palaeo-surface (Norwegian: *Vidde*) (Bergersen and Hofseth, 1987). The surface is a smooth, undulating plateau with an overall dip to the SE (Garnes and Bergersen, 1980). The valley systems in the surrounding area strike NW-SE, including the three valleys incorporated in this study. Valley 1 is wide, at intermediate elevation and located in the NE. Valley 2 is deep, strikes E-W in the N around lake Mjøsdokka and NW-SE in the S from lakes Dokkvatnet to Dokkfløyvatnet. Its Southern end is found at the lowest elevation in the study area. Valley 3 is narrow, shallow, at the highest elevation and located in the SW. Valleys 2 and 3 intersect in the W and SE, and valleys 1 and 2 intersect in the SE.

Gausdal Vestfjell occurs at the border of the Northern and Middle Boreal vegetation zone (Moen, 1987). The tree line resides between 1000 and 1100 masl (Moen, 1998). Average annual precipitation is 1000-1500 mm, and average annual temperature c. 0^{o} C (NVE et al., 2018).

1.4 Geology

The bedrock in Gausdal Vestfjell can be divided into three groups (Englund, 1973). They include (1) the thrusted lithologies known as Jotun Nappe, including gabbro and trondhjemite, (2) Late Precambrian or Eocambrian sedimentary rocks and gneiss-like metamorphosed eruptive rocks known as Valdres Nappe, including coarse sparagmite, fine-grained arkoses and conglomerates, and (3) Cambro-Ordovician sedimentary rocks, including phyllite, shale and quarzitic sandstone (Englund, 1973; Siedlecka et al., 1987; Hossack and Lutro, 2013) (figure 1.2). The thrusting of the Jotun and Valdres Groups and following folding laid the foundation for the structural trends in the area (Englund, 1973).

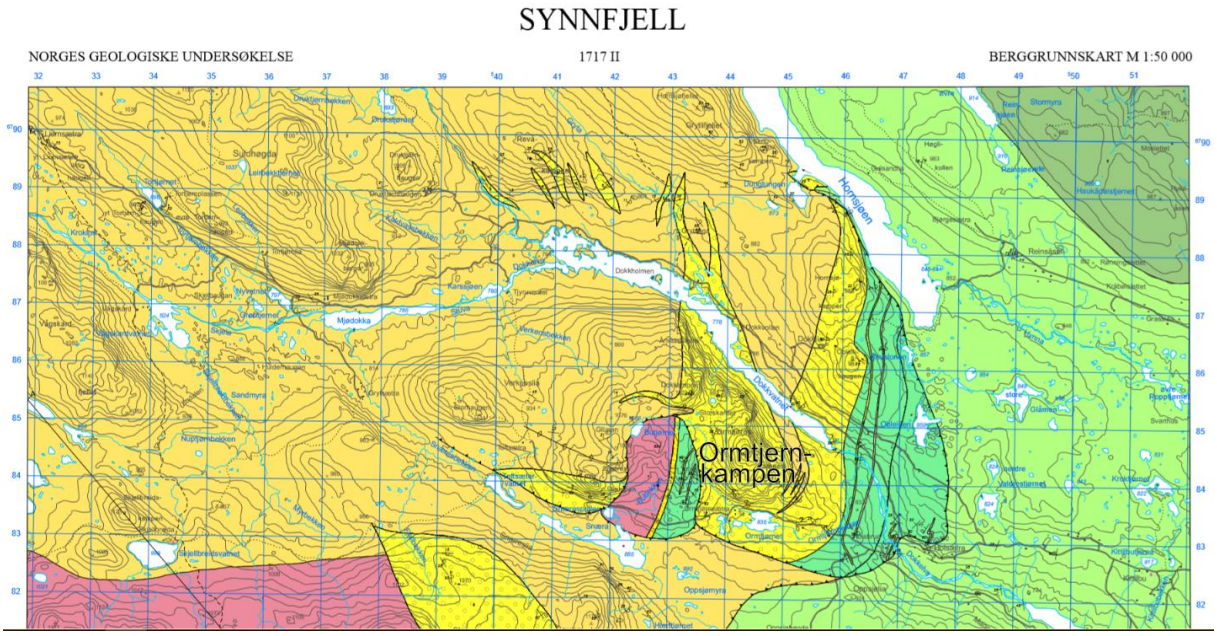

Figure 1.2. Bedrock in the study area. Northern part of map sheet Synnfjell in scale 1:50 000 (Hossack and Lutro, 2013). Pink: Metadiorite; Pale yellow: Coarse-grained arkose and greywacke rich in pink feldspar clasts and white quartz clasts, in places with conglomerate layers; Bright yellow: Conglomerate, consisting mainly of gabbro pebbles; Olive green: Sandstone, dark grey slate, conglomerate, phyllite; Lime green: Slate; Mint green: Dark grey or greyish-black slate. For complete legend, see Hossack and Lutro (2013).

The Fennoscandian Ice Sheet deglaciated between 22 and 9.7 cal. kya BP (Stroeven et al., 2016). At the end of the last deglaciation, the ice divide was NW of the study area, with the main ice movement towards the SE (Vorren, 1977). Stroeven et al. (2016) divided Fennoscandia into sectors depending on the nature of ice retreat, and Gausdal Vestfjell was

wet-based (figure 1.3), with ice-retreat towards the mountain areas in the W and ice-dammed lakes in main and tributary valleys. The isochron in figure 1.3 shows that Gausdal Vestfjell was deglaciated around 10.3 cal. kya BP.

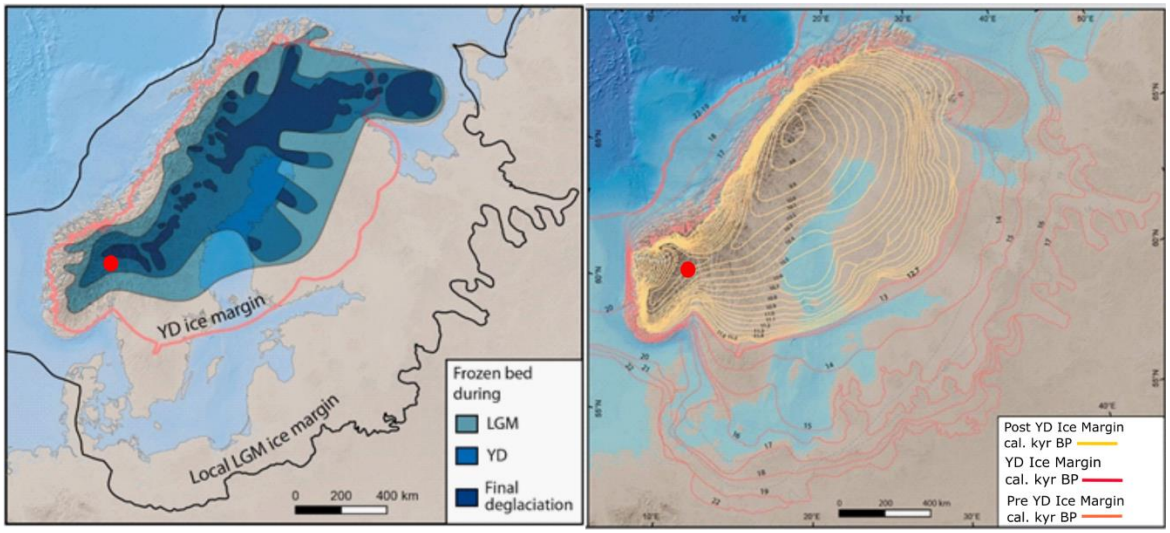

Figure 1.3. The deglaciation of Fennoscandia, red dot marks the location of Gausdal Vestfjell. Left: The extent of the Fennoscandian ice sheet at the Last Glacial Maximum (LGM, c. 20 000 ka) and Younger Dryas (YD, 12.7 cal. kya BP. Right: Deglaciation illustrated by isochrons interpreted from geomorphology and geochronology, where the yellow, hundred-year isochrons show the post-YD margins (up until final decay after 9.7 cal. kya BP). Modified from Stroeven et al. (2016).

The shrinkage of the ice sheet in Gausdal Vestfjell occurred as vertical down-wasting of stagnant ice (Garnes and Bergersen, 1980). Putnins and Henriksen (2017) suggested that thinning of the ice sheet around Gausdal Vestfjell initiated at the same time as at Blåhø 70 km further N at around 25.1 ± 1.0 ^{10}Be cal. Kya BP (Goehring et al., 2008). As the transition from flowing to dynamically dead ice took place, meltwater drainage changed from supraglacial, to englacial and lateral, and eventually, subglacial (Garnes and Bergersen, 1972). Deglaciation probably occurred at the same time as in nearby valleys, at c. 9000 ^{14}C years ago (Garnes and Bergersen, 1980; Putnins and Henriksen, 2017).

The drainage through the area is divdied into five phases: Nunatak-, Krusgrav-, Espedal-, Store Dølasjø- and Gudbrandsdalen-phases (Bergersen and Hofseth, 1987). The ice age was nearly over during the last two phases. The drainage of Gausdal Vestfjell occurred mainly during what (Bergersen and Hofseth, 1987) defined as the Espedal Phase. The drainage intensity and direction varied throughout the deglaciation, and was to a large extent controlled by the thickness of the ice sheet (Bergersen and Hofseth, 1987). It shifted as the meltwater found lower passes with down wasting, and as meltwater dammed by ice surface and moraine ridges burst through. The ice divide moved S during deglaciation, away from the water divide (Bergersen and Hofseth, 1987). During the Espedal Phase, meltwater flowed sub- and ice-laterally and uphill when the ice surface covered the pass points because of the tilt of the surface in relation to the ice surface.

The distribution of sediments surrounding the study area shows a strong topographic coupling (figure 1.4). The deposits generally strike NW-SE in the NW and N-S in the NE. The elevated, undulating palaeo-surface is covered in thin, discontinuous layers of till. Thicker till deposits dominate the valleys. Glacifluvial deposits are found as fan and deltas along the valley sides. The valleys are often filled with fluvial deposits. Peat covers large areas at higher elevation, and exposed bedrock is common in the highest areas. Generally, lower-laying landforms are younger than landforms found at higher elevation (Garnes and Bergersen, 1980).

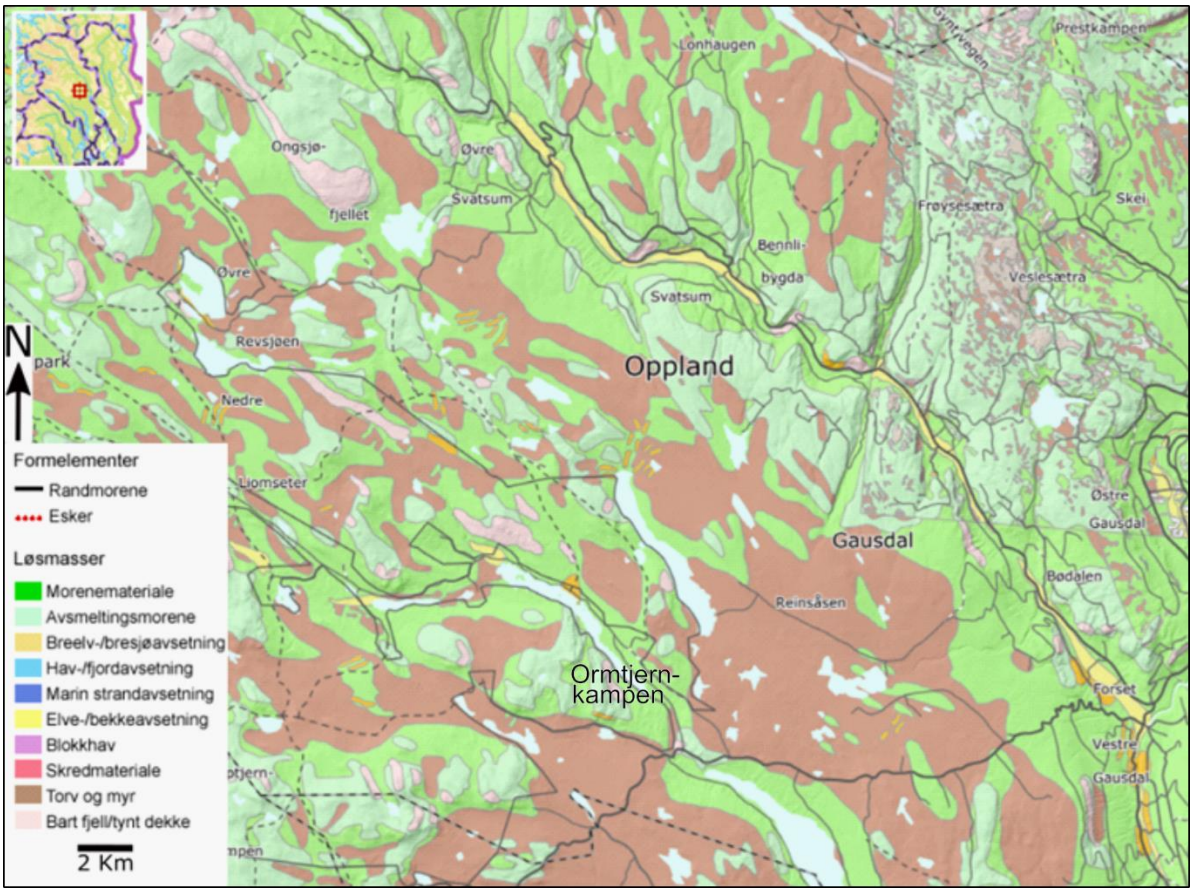

Figure 1.4. Quaternary sediment distribution in Gausdal Vestfjell and nearby areas. Modified from NGU (2018).

In Gausdal Vestfjell, meltwater landforms are spatially and temporally distributed across the landscape. Eskers dominate in the NE (valley 1) and SW (valley 3), while other meltwater landforms (e.g. fans, deltas, outwash plains) dominate the lower-laying areas in the NW (valley 2). The meltwater landforms mapped by Putnins and Henriksen (2017) are shown in figure 1.5. The constitute 512 in total, among them 475 eskers, and cover around six percent of the study area.

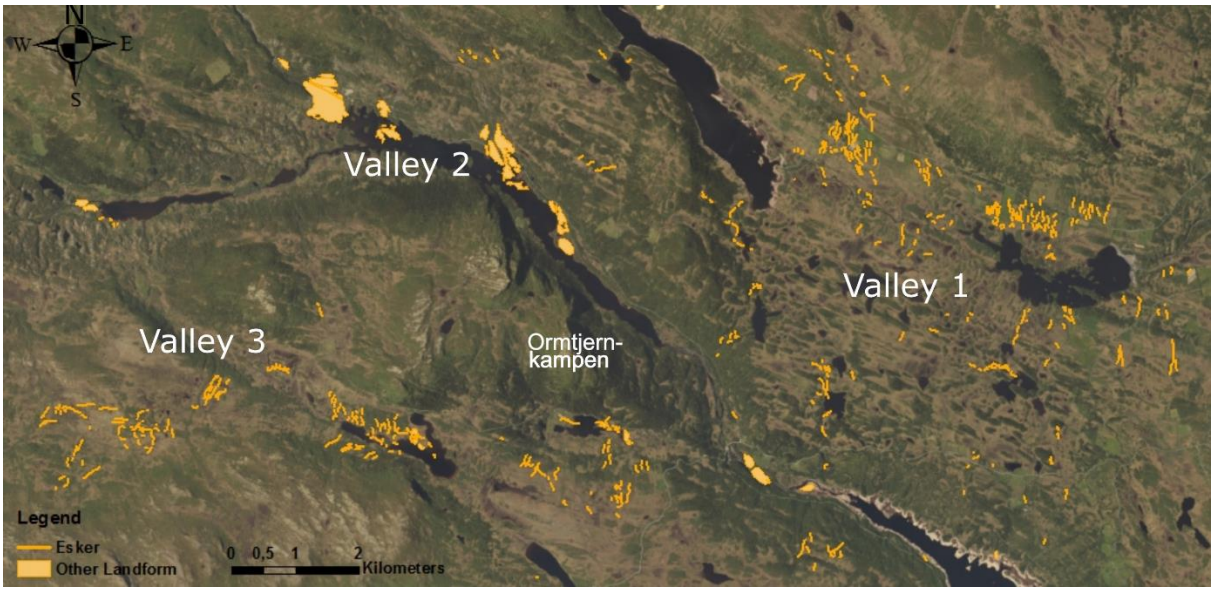

Figure 1.5. Map of meltwater landforms in the study area based on landforms mapped by Artūrs Putniņš. The map shows 512 landforms, among them 475 eskers and 37 other meltwater landforms, including deltas, fans, outwash plains, kames and kame terraces.

1.5 Glacifluvial Deposition

Deglaciation, or the "the uncovering of any area as a result of glacier shrinkage" (Flint, 1957), is a process recorded in glacifluvial sediment deposits and associated landforms. Benn and Evans (2010) stated that meltwater is an essential component of glacier systems, and that as it finds its way from glacier to sea, it shapes the land and leaves vast volumes of gravel, sand and silt behind. Putnins and Henriksen (2017) assumed that the landforms in the area are from the last deglaciation, based on their "fresh appearance and extensive preservation".

Glacifluvial material is recognised by texture, sediment structures, sorting, rounding and nature of layering, and is characterised by large depositional variability, recording environmental or mechanical changes in runoff (Benn and Evans, 2010). Glacifluvial deposits are "secondary" in the glacial sedimentary environment, and viewed as resedimented till not transported and deposited directly by ice (Benn and Evans, 2010), (Lawson, 1981b). Deposition occurs as gravity flows, sheet floods, by bedload transport and suspension settling (Benn and Evans, 2010). The sediment is recognised by a grain size composition consisting mainly of sand, gravel and cobbles and ripple- and cross lamination, scour and channel fill, gravel sheets and silt drapes. The degree of sorting and rounding varies from moderately low to very high. Repetitive appearance of bedding, particle grain size and sorting occurs (Benn and Evans, 2010).

Glacifluvial deposition occurs sub-aerially, sub-aqueously, ice-laterally, sub-, en- and supra-glacially (Jørgensen et al., 1997), in both flowing and stagnant ice, lateral to the ice-margin, near the ice-front, and in ice-dammed meltwater accumulations (Jørgensen et al., 1997).

Glacifluvial landforms include eskers, kames, kame terraces, deltas, fans and sandur plains (Jørgensen et al., 1997). Eskers are often formed near the ice front, either on slopes under high hydrostatic pressure (chute eskers), in tunnels underneath, inside or on the ice surface, or in ice crevasses and between remnant ice blocks (Benn and Evans, 2010). Kames form as meltwater drains into open areas in dead ice, sub-, en- and supra-glacially, and kame terraces between the ice wall and valley side. Deltas, fans and sandur plains often form pro-glacially, but in a landscape dominated by vertical down- wasting, deltas form in ice-dammed meltwater and sandur plains as narrow valleys expand into open areas (Benn and Evans, 2010).

1.6 Soil and Soil Formation

Diagnostic soil horizons and properties can be linked to soil-forming processes (Bockheim et al., 2005), which leads to the recognition of the studied glacifluvial soils as podzols. Podzols contain a spodic horizon, and are found in "cool, wet, sandy, acid, coniferous forests" (Brady and Weil, 2013). The carbon stocks of both the organic and mineral soil on glacifluvial landforms is highly variable.

Soil is, according to Joffe (1936), "a natural body, differentiated into horizons of mineral and of organic constituents, usually unconsolidated, of variable depth, which differs from the parent material below in morphology, physical properties and constitution, chemical properties and composition, and biological characteristics". Defining and understanding soil as a medium has been disagreed upon and evolved through scientific study, but Bockheim et al. (2005) summarises the essential concepts as: "1) The soil is a medium for plant growth. 2) The soil is a mantle of loose and weathered rock. 3) The soil is an independent, natural, evolutionary body. 4) The soil is the ''excited skin'' of the subaerial part of the Earth's crust and a key component of the biosphere. 5) The soil is a natural body composed of solids (minerals and organic matter), liquids, and gases that occurs on the land surface, occupies space, and is characterized by horizons or layers that are distinguishable from the initial materials". The fact that soil is a key component of the biosphere points to the social importance of it as a focus of study. The fact that it is "a mantle of loose and weathered rock" enhances the necessity of studying it from this perspective, and the fact that it is "independent" shows the importance of detailed, site-specific investigation. Finally, realising that soil is "evolutionary", understanding its formation, development and potential destabilisation in rapidly changing ecosystems becomes top priority for human research.

Jenny (1941) stated that the evolution of a soil can be described by its changing properties. The equation $f(S1, S2, S3, S4, S3, \ldots) = 0$ illustrates this process, where soil properties are = S (Jenny, 1941). As a defining property changes sufficiently, a new soil is formed. Jenny (1941) described this as the state of the soil, while the soil classification systems recognize these "states" as specific soil types. The soil forming processes recognised in the meltwater

landforms is podzolization, and the variation among them a result of the parent material of the soils.

Soil formation, and therefore any soil property, is a function of *f(cl,o,r,p,t* where *cl*= climate, *o*= potential organisms (vegetation and fauna), *r*= relief (aspect and topography) *p*= parent material, and *t*= time (Brady and Weil, 2013). All parameters but the parent material is kept constant in this study. Hence the changes in the soil and formation processes are likely to be a result of the meltwater processes that created the landforms the soils are developed from.

Bockheim et al. (2005) stated that parent material is a key soil forming factor, and certainly from a regional perspective. The equation for the soil forming factors simplifies the complex relationship between variables in the environment where the soil evolves. Some authors, e.g. Jenny (1941), state that they are independent, while other, e.g. Dokuchaev (1879b), claim that the factors are interdependent. According to Bockheim et al. (2005), the equation of soil formation has yet to be solved. They summarised the debate as "The soil is a function of the interplay of climate, organisms, relief, and parent material, all operating over time" and "soil-forming factors set the conditions for soil forming processes" (Bockheim et al., 2005). Understanding the influence of minerals the parent material is composed of and the mineral production is promotes on soil carbon is significant for carbon cycling dynamics (Torn et al., 1997).

Soil formation leads to horizon differentiation, which Bockheim et al. (2005) summarises as the result of balances of energy and material through addition, loss, transfer and transformation. Decomposition of organic material produces organic soil, an O horizon (denoted *i, e* or *a* depending on the degree of decomposition) (Brady and Weil, 2013). Sufficient mixing of the underlying mineral soil with organic material trough biological activity (e.g. burrowing and root penetration) produces an A horizon, a mineral horizon with a higher content of organic material (WRB, 2014). Intensive loss and leaching, in the form of downward translocation with precipitation, of clay minerals, iron- and aluminium oxides and organic complexes from the surface soil, eventually produces an eluvial, bleached horizon, an E horizon (Lundstrom et al., 2000). Precipitation and accumulation occurs below, as charged complexes are neutralised, pH increases, and microbial release occurs during degradation, which leads to the development of an illuvial, spodic horizon, or Bs horizon (where the *s* indicates accumulation of sesquioxides) (Lundstrom et al., 2000). Underlying is the C horizon, which resides at the depth where material is still only slightly affected by soil forming processes (Brady and Weil, 2013). Horizon may show attributes from both e.g. a B and C horizon and are then denoted BC. The specific soil formation described here forms Podzols (Lundstrom et al., 2000).

The nature and properties of the soils is used to define and distinguish the podzolization process that formed the soil, with respect to the parent material they formed from. The soil can be considered the representation of the balance between the relative intensity of

weathering and leaching processes, or what is supplied and what is lost (Bockheim et al., 2005). Jenny (1941) defines the horizons as "zones of abundances and deficiencies". Podzols are in these terms recognized by properties of their zone of abundancies, the spodic (Bs) horizon. Podzols are divided into subclasses based on the E horizon thickness, ratio of free Fe/C in the Bs horizon and presence of dispersed organic matter, as well as gleying and permafrost indicators (Lundstrom et al., 2000). The two latter are redundant in this study. The Bs horizon must have a pH (in water) equal to or lower than 5.9, Fe and Al content of oxalate extract and organic carbon content equal to or higher than 0.6% (Lundstrom et al., 2000). It is also required to have a red or dark colour, and/or be cemented and/or contain coated grains (Lundstrom et al., 2000). The glacifluvial soils fulfill these criteria (Appendix 4).

Soil forms as vegetation is established and cause physical and chemical changes to the sediment (Brady and Weil, 2013). Examples include the excretion of acid (as H^+, in exchange for nutrient uptake, to retain charge balance, and from diffusion and dissolution of CO_2 through the roots, and direct organic acid excretion to release nutrients from minerals), oxidation from diffusion of oxygen into the ground through the roots and the transition of chemicals such a nitrogen and phosphorus between organic and inorganic forms through i.e. decomposition of organic material (Pierzynski et al., 2005). The classification of the resulting soil implies certain critical properties and different stabilising factors, which in several ways can lead to significant environmental change, e.g. acid soils of low buffer capacities are sensitive to acid input and can experience acidification beyond repair (Pierzynski et al., 2005).

The degree of podzolization changes linearly with the logarithm of time (Lundstrom et al., 2000). Aluminium, iron and silicon hydr(oxides), base saturation of the E horizon and texture among other properties are used to describe podzolization (Lundstrom et al., 2000). Oxidative-hydrolytic mineral weathering products of silicates and iron (II) minerals are extractable by oxalate (Krogstad and Børresen, 2015) and in this study termed "active oxides". In glacifluvial soils, the content of silt and clay can largely be attributed to soil weathering processes, hence grain size distribution can also indicate the strength of podzolization. The ratio of properties between the illuvial (B) and elluvial (E) horizon is particularly interesting for assessment, as it reflects the degree of downward translocation of energy and material. The podzolization mechanisms are important for translocation and stabilisation of soil organic carbon (Schlesinger and Bernhardt, 2013).

1.7 Soil Carbon

Soil carbon can constitute only a few percent of a soil, but is exerts an important influence on all soil functions and is an essential component of the global carbon cycle (Blume et al., 2016). Soil carbon amounts to 80% of the terrestrial organic carbon that interacts with the modern carbon cycle (Blume et al., 2016). The annual sequestration and cycling of carbon in mountain ecosystems is low because of shallow soils, low rates of net primary productivity,

steep terrain and large seasonal changes in moisture and temperature (Baron, 1992; Körner, 1999; Jandl et al., 2011). Soil organic carbon represent the difference in input (mainly root litter and dissolved organic carbon) and decomposition (Kleja et al., 2008). Carbon stocks of mountain soils vary greatly and average around 100 Mg/ha (megagrams/hectare), where slow decomposition at high altitudes is significant for increased carbon storage (Jandl et al., 2011). As carbon is contributed to the soil through decomposed organic material, it is returned to the atmosphere through microbial respiration (Schlesinger and Bernhardt, 2013). The non-mineralized fraction remains as soil organic material (SOM), and is protected from microbial decomposition and stabilised for hundreds and thousands of years (Blume et al., 2016).

The carbon stock of a soil can be estimated from the total carbon and the bulk density, both measured in the laboratory following soil sampling, and horizon thickness and stone and boulder content, measured in the field. The carbon stock is generally estimated as kg/m^2 for the whole soil profile, for specific horizon or to a specific depth. In this study the carbon stock is estimated down to the lower boundary of the Bs horizon. The carbon stock of the soil can be divided into two components, the stock of the organic soil horizons, and the stock of the mineral soil horizons. The carbon content of the organic horizons is subject to oxidation and microbial decomposition and is not of interest for long-term storage. The fraction is unstable and sensitive to climatic change. The mineral soil stores carbon in a long term perspective, and quantity and variation of this pool is interesting with regards to the global carbon cycle (Schlesinger and Bernhardt, 2013).

The accumulation of SOM requires the inout and decomposition of organic material, as well as soil processes that translocate and stabilise the SOM at depth. The pH, cation exchange capacity (CEC) and total carbon to total nitrogen ratio (C/N) of a soil indicate soil nutrition status and how the biomass experiences the potential for decomposition. Buffering of soil pH occurs through cation exchange reactions, reactions with organic material when pH is moderate, and the release of H^+ from pH dependent charge sites in clay (Brady and Weil, 2013). The buffering of soil is important to prevent drastic changes in acidity. In an organic soil, a pH below 5 allows acidic cations to be exchangeable, resulting in the replacement of essential nutrients with H^+ (Brady and Weil, 2013). Consequently, a pH below 5 can cause the loss of cations through replacement and leaching. In organic soils, the majority of the exchange sites are pH-dependent, and effective CEC therefore increases proportionally with pH (Brady and Weil, 2013). The CEC measures the ability of a soil to retain good structure and availability of nutrients, and the proportion of cations that are bound to exchangeable sites (Pierzynski et al., 2005). The C/N ratio of the organic soil is an indicator for soil chemical recalcitrance. Optimal conditions for decompostion reside between 18-28 :1 (Brady and Weil, 2013). Decomposers utilise carbon for energy as well as growth and consequently need three times the amount of carbon as nitrogen, whereas growth requires a ratio around 8:1, depending on the decomposer (fungi or bacteria) (Brady and Weil, 2013).

2 Methods

2.1 Landform Selection and Verification

Mapping of meltwater landforms in the study area was done by Artūrs Putniņš (Putnins and Henriksen, 2017). In the present project, detailed investigation of 17 of the landforms has been done for an integrated study of meltwater drainage processes and soil carbon content. The selection of landforms was based on 12 criteria: (1) Its identification as a meltwater landform, (2) characterisation as an esker (mapped as polyline) or other meltwater landform, (3) among eskers, directional nature relative to the ice flow direction established by (Putnins and Henriksen, 2017) (4) its potential of natural exposure through cutting by roads or rivers, (5) representativeness, through visual comparison with other landforms in the nearby area, (6) variability, through visual comparison with other landforms in the overall area, in order to study a wide range of deposits based on the size, shape and position of the landform, (7) distance from the NW corner of the area, as material is considered to be transported towards the SE, (8) the underlying bedrock, (9) the dominant phase of ice flow as identified by (Putnins and Henriksen, 2017), (10) general availability of the locality, (11) its potential for ground penetrating radar (GPR) analysis with respect to proximity to roads, density of vegetation and surface boulder content, (12) the potential for soil profile description, with respect to stone- and boulder content.

To verify the mapping of landforms and Quaternary geology done by (Putnins and Henriksen, 2017) using remote sensing, an additional 39 landforms (56 including those studied in detail) were visited. The criteria for selection of these landforms were the following: (1) The four categories mapped by Putnins and Henriksen (2017) should be represented, including meltwater landforms, ribbed moraine ridge type A, ribbed moraine ridge type B and streamlined landform, (2) the representativeness of the landform in terms of its size, shape, directional nature and geographical position and (3) its availability. Landforms were verified as either consisting of glacifluvial material or glacial till. A soil auger and a spade were used to give a brief description of the sediment. The criteria for characterisation as glacifluvial material was the consistent absence of silt and clay. However, the properties (size and shape) of the landform itself was also considered, as moraine ridges and streamlined landforms are frequently covered in glacifluvial material. The mapping by Putnins and Henriksen (2017) is of surface features, yet the surface of many landforms made of till can consist of meltwater material.

Some landforms sampled for soil studies were not described with respect to the sedimentology and geomorphology due to logistical problems, e.g. lack of natural sections. However, the formation and nature of the landforms are interpreted. Along with LiDAR interpretation and field observations, the understanding of depositional processes sufficed to discuss the soil data in relation to landform origin.

2.2 Remote Sensing and Landscape Analysis

Landscape analysis is simplified with high-resolution laser data. LiDAR, or «Light Detecting and Ranging» is a remote sensing method used for terrain mapping (Mulder et al., 2011). The principle is based on emission of light pulses that measure the distance to the surface of the Earth (NORA, 2017). The instrument consists of a laser, scanner and GPS receiver, and data is collected densely across an area in airplanes or helicopter (NORA, 2017). The distance to the surface is determined from the two way travel tie of the light pulse (Grinderud et al., 2008). The LiDAR data used in this study were collected and provided by the Norwegian Mapping Authority (Kartverket).

A Digital Elevation Model (DEM) was constructed from the LiDAR data and aided the description and interpretation of the landforms. Laser scan data can be used to produce DEMs for use in geographic information systems (NORA, 2017). The ESRI (Environmental Systems Research Institute) software Arc Map version 10.3 was used to visualise, interpret and export Lidar-data. The data were received as LAZ files, and first converted to .lasd files in Arc Catalog. The dataset with .lasd files were imported into Arc Map. The data were visualised through the 3D View window. The function "ground truthing" was used to filtrate out reflections not representative of the true terrain, such as trees. A digital elevation model of 20 m horizontal resolution was produced, as well as a hill shade image (azimuth 315°) from the DEM for improved visualisation. The 3D View of the data provided both a bird's-eye view and overview of the landscape that were to be (and later had been) investigated in the field. The elevation profiles of the described transects were extracted from the DEM using the "Interpolate Line"- and "Profile Graph"-functions from the 3D Analyst toolbar.

2.3 Field Sediment Description

Sedimentary deposits record the development of deglaciation. Field description of sedimentary stratigraphy was done through sedimentary logging at nine landforms. Vertical cross-sections, generally in the upper 1-2 meters of the landform, were prepared using a spade and trowel. Description to a deeper level was done at two localities, with a few meters of lateral distance between. Sediment properties, structures, boundaries and flow directions were described. Grain size and degree of sorting was determined after Evans and Benn (2004).

For determining the competence of the meltwater flow, the ten largest clasts observed were measured, and the mean calculated. The degree of rounding was determined through division into four classes (angular, subangular, rounded or well rounded) as described by Olsen (1983). Equally sized clasts around 6 cm dimeter were chosen to avoid variation in degree of

rounding because of proportionality with size. Figure 2.1 shows the procedure for rounding analysis.

2.4 Field Soil Profile Description and Sampling

Soil Profile Description

Figure 2.1. Example is of rounding analysis of clasts from a fan lobe deposit in valley 2. Meter-stick for scale 20 cm.

Soil as a medium is anisotropic, but description and interpretation are enabled by defining a profile. Four soil profiles were described following FAO (2006). The placement of profiles was chosen in similar positions and orientations on the landforms. The intention was to reduce variability in relief and topography and enable comparison of variability between the soils due other factors. A spade was used to dig a hole of about 1x1x1 m and to include potential variation within the profile. A tarpaulin was laid down on one side to collect the removed mineral soil to limit it spreading around and to allow for easier refilling of the hole. The organic soil was kept on a separate side, so that it could be placed back on top afterwards.

Field description of a soil requires physical boundaries, which must be defined in what is a continuous and extensive medium. The description of the profile started with the identification of the boundary between parent material and material affected by soil forming processes. The boundary between mineral soil and organic soil was then determined. Finally, separate horizons were divided based on soil structure, texture and colour (FAO, 2006). The colour determination is based on Munsell (2010). Soil horizons were later divided into subhorizons when significant properties showed large variations. Grain size distribution analysis from the laboratory are included in the soil profile descriptions (Appendix 1).

In addition to the four full soil profiles, eight profiles were sampled down through the Bs horizon. A spade was used to dig three (c. 40 cm) deep holes on topographic highs, at the ends and in the middle of landforms (figures 2.2 and 3.3). The soil horizons were defined as

described above, horizon thicknesses measured and the mean for the landform calculated. Each horizon was sampled in all twelve soils as described in the following paragraph.

Soil Sampling for Chemical Analysis and Density Estimation

Figure 2.2. Procedure for sampling of soil profiles without full descriptions.

Chemical analysis of soil supplements the field investigations. Soil samples were collected from all the soil horizons investigated in the field. Sampling was done using a 100 cm^3 steel cylinder to obtain an accurate volume for bulk density analysis. A spade, hammer, hammer union and knife were used to extract the soil. The spade was used to dig down to the desired soil depth, the cylinder placed in the hammer union, and the hammer to force the cylinder down. The cylinder was thereafter dug out of the soil using the spade, and the knife to cut through roots and ensure a flat soil surface in the cylinder. The soil was transferred to a sample bag. Figure 2.3 illustrates the process.

Figure 2.3. Procedure for soil sampling in 100 cm^3 cylinders for bulk density estimation.

Three cylinder samples were taken from all organic horizons to reduce uncertainty in property analysis and ensure the collection of enough material for further investigation in the laboratory. The mineral soil horizons at localities described as full profiles were sampled twice, and once at the midpoint of the landforms in non-described profiles (figure 3.3). Carbon stock was calculated from volume, dry weight and density of the samples (chapter 2.5).

Soil samples were taken from landforms in an attempt of covering all valleys, bedrock types and ice-flow phases as well as a variety of depositional processes, while at the same time keeping in mind both representativeness and possibility for comparison between landforms. Consequently, not all logged- and GPR-measured landforms were sampled, which, in hindsight, would have been sensible. Describing and interpreting an even larger amount of data, however, would possibly have decreased the quality of the overall discussion and conclusion considering the limited field season and overall time limit of the project.

Most samples contained a large rock fragment/gravel fraction (>2 mm), which gave a smaller fine earth fraction (<2 mm) available for analysis, possibly decreasing the representativeness of the results.

Topography and Transects

Two transects through the landscape were created to visualise the importance of topography and characterise the nature of deposition and corresponding nature of soil formation. According to Bockheim et al. (2005), topography is a key soil-forming factor on the landscape scale. Measurements were done with an observed change in terrain slope, surface boulder content and/or vegetation. Vegetation was described after Larsson (2000) (table 2.1), sedimentary composition after Evans and Benn (2004) and Olsen (1983) and soil horizons after FAO (2006). The soil and sediments were investigated using as spade or augen. The GPS coordinates were recorded at each measurement point.

Classification of Vegetation

A simple characterisation of vegetation was done at all localities where soil was sampled. The interaction of soil and vegetation is significant, and while not the focus of this study, important to note for reference and a holistic soil process understanding. The classification system used is based on dominant species in bottom vegetation (Larsson, 2000). It gives a good indication of the nutritional status and humidity regime of the soil, and can provide valuable information of soil development processes (Larsson, 2000). The five types observed in the area study were “Lavskog (1)”, “Blokkebærskog (2)”, “Bærlyngskog (3)”, “Blåbærskog (4)” and “Småbregneskog (5)”. The classification is based on the respective dominance by lichen, moss, heather, fern or herbs, and the presences of the species important for each category (Larsson, 2000) (table 2.1). As several species occur in a variety of environments, it is the minimum requirement that matters for classification (Larsson, 2000). This implies that the species that can survive the conditions expected for a nutrient-poor vegetation type (lower number after Larsson) can also be found in nutrient-richer types.

The classification in the field was translated into categories according to Fremstad (1997). They are found under “Woodland vegetation”, category A: “Lichen, bryophyte and dwarf-shrub woodland”. The established vegetation types are based on ecological factors such as soil type, soil moisture, nutrient availability and climate (Fremstad, 1997), and can therefore be understood in relation to soil development. The observed vegetation types from Larsson are interpreted to correspond to the following types as established by Fremstad (1997): 1) A1, Lichen woodland (*Cladonia* Woodland), 2) A3b, Heather bog-bilberry – Scots pine mountain woodland (*Calluna vulgaris, Vaccinium uliginosum, Pinus sylvestris* mountain woodland), 3) A2, Cowberry-billberry woodland (*Vaccinium* woodland), 4) A4, Bilberry woodland and 5) A5c, Small-fern mountain woodland. Table 2.1 gives an overview over the vegetation types

after Larsson (2000), the dominant and key species it includes, the corresponding category after Fremstad (1997).

Table 2.1. Vegetation of the glacifluvial landforms from Larsson (2000) and Fremstad (1997).

Larsson (2000)	**Dominant species**	**Key species [1]**	**Fremstad (1997)**
Lavskog (1)	Lichen	Lichen	A1, Lichen woodland
Blokkebærskog (2)	Moss and heather	*Vaccinium uliginosum*, other heather, Sphagnum	A3b, Heather bog-bilberry – Scots pine mountain woodland
Bærlyngskog (3)	Moss and heather	*Vaccinium myrtillus* (blueberry), *Vaccinium vitis-idaea* (lingonberry/cowberry)	A2, Cowberry-billberry woodland
Blåbærskog (4)	Moss and heather	*Maianthemum bifolium, Lysimachia europae, Luzula pilosa*	A4, Bilberry woodland
Småbregneskog (5)	Heather and fern	*Oxalis acetosella, Phegopteris connectilis*	A5c, Small-fern mountain woodland

[1] Minimum requirement

Bedrock Clast Analysis

Analysis of bedrock clasts within the described profiles was done to understand the nature and origin of the parent material the soil developed from, the mineral content of the soil as well as the formation of the landform it is part of. Fifty clasts about 2 cm in diameter were sampled. Maps used for lithological identification are the 1:250 000 map sheet Lillehammer (Siedlecka et al., 1987) and the unpublished mat sheet 1: 50 000 Synnfjell (1717 III) (Hossack and Lutro, 2013). The clasts were described and characterised based on lithology, but not dated. Consequently, categorisation is not based on bedrock unit. The underlying assumption for analysis is that the clasts composition is representative also of the composition of smaller grain sizes.

Visualisation of bedrock clast origins was done by georeferencing a scanned version of the Lillehammer map sheet to a topographic map accessed through the WMS connection provided by Kartverket (2018) as a reference layer. A polygon shapefile was created in Arc Catalog and imported into Arc Map, where the relevant lithologies were sketched out.

2.5 Carbon Stock Estimation

Four soil properties are required in carbon stock calculation; total carbon content, horizon thickness, bulk density and stone and boulder content. Determination of horizon thickness and sampling of soil for density analysis was done in the field (chapter 2.4), and the total carbon and dry weight (which gives bulk density) measured in the laboratory (chapter 2.7). Bulk density is estimated from air-dried weight (chapter 2.7) of the soil sampled in a defined volume cylinder (100 cm^3). Stone and boulder content was estimated by a rod penetration

method described in Eriksson and Holmgren (1996) (see below). The equation used to calculate the carbon stock of a soil horizon reads *C Stock Horizon (kg/m^2)= (100-SB)/100 x (-UHB+LHB) x 0.01 x BD x 1000 x TC*, where SB= Stone and Boulder Content %; UHB= Upper Horizon Boundary in cm; LHB= Lower Horizon Boundary in cm; D= Bulk Density, or Weight (g)/Volume (g/m^3); C= Total Carbon in g/kg. The carbon stock for the full soil profile is calculated from *C Stock Profile= ∑ (C Stock Horizon (1), C Stock Horizon (2), …, C Stock Horizon (n))* (Baritz et al., 2010, Strand et al., 2016).

The content of stones and boulders of the soil was measured to be subtracted from the otherwise exaggerated carbon stock estimation. A steel rod with a diameter of 1 cm was used to penetrate the soil 50 times across an area of about 500 m^2. The shape of the area and number of measurements was adjusted to the landform, which sometimes was smaller than 500 m^2. The depths at which the rod reached a stone or boulder were recorded. When the rod reached a depth of 40 cm, 40 cm was recorded, independently of how much deeper it could reach. A regression equation was used to correlate the average depth of penetration of the rod with the estimated content of stones and boulders. The equation reads *Y= -1.74 X + 73.9*, where Y= estimated content of stones and boulders and X= depth index of the area. The stone and boulder content estimation excludes gravel (2-56 mm). The method is further described in Eriksson and Holmgren (1996).

2.6 Ground Penetrating Radar (GPR)

Ground penetrating radar (GPR) measurements were taken at several of the studies landforms. The radar improved the insight of the structure and composition of the deposits. It reaches a deeper level than can be accessed in the field and provides radargrams that supplement the field observations.

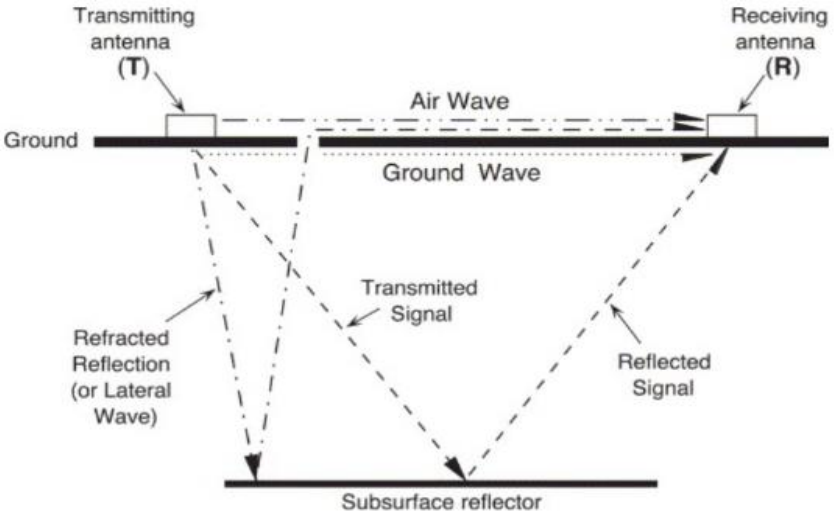

Figure 2.4. Principles of the GPR method, from (Neal, 2004) .

The GPR uses electromagnetic radiation to penetrate dielectric material and provides an image of properties of and structures in the material (Annan, 2003) (figure 2.4). Pulses of radio wave frequencies are transmitted into the ground, and some of the propagating waves

are reflected back and registered by a receiver (Mauring et al., 1995). This process is a result of the interaction of the transmitted energy with the dielectric properties of the ground, such as the ability to transmit electricity (Annan, 2003). Figure 2.4 illustrates the concept. The two-way travel time of the waves is recorded, and its variation is a function of variation in material properties. Dry, coarse material is optimal for good results (Mauring et al., 1995), suggesting that the glacifluvial landforms investigated are suitable for the method.

Three different carts and mobility designs were utilised. At localities with low availability, a terrain cart was used, and a hand-held version of the instrument was used at localities with dense vegetation. For the other localities, a SmartCart was most efficient. All three measurement designs consist of a pulseEKKO 100 GPR system from Sensors & Software Inc. It includes a transmitter, receiver and control unit, as well as an odometer and GNNS (Global Navigation Satellite System) receiver. The transmitter and receiver were connected to the control unit trhough fibre optic cables, and directly connected to two antennas. Two frequencies were used, 100 MHz and 200 MHz, which require different sets of antennas. The antennas were fastened to a frame at 100 cm and 50 cm apart, respectively. When the instrument was used without the cart, the antennas were manually moved an equivalent distance at the time.

An odometer allows the system to record data at continuous intervals, at points known as traces (Mauring et al., 1995). It notifies the control system after movement of a predefined distance, 25 cm and 10 cm for each respective frequency. During use of the standard cart, the control unit was fastened at the front of the frame, and the odomenter at the left back wheel. During use of the terrain cart, the control unit and odometer were manually carried by an operator. Figure 2.5 gives an overview of the setup and different equipment. The time window was set to 500 Ns for all operations.

The standard cart was used in valley 1 and V3-2, the terrain cart in valley 3 and V1-5, and the hand-held GPR in valley 1 (figures 2.5 and 3.3).

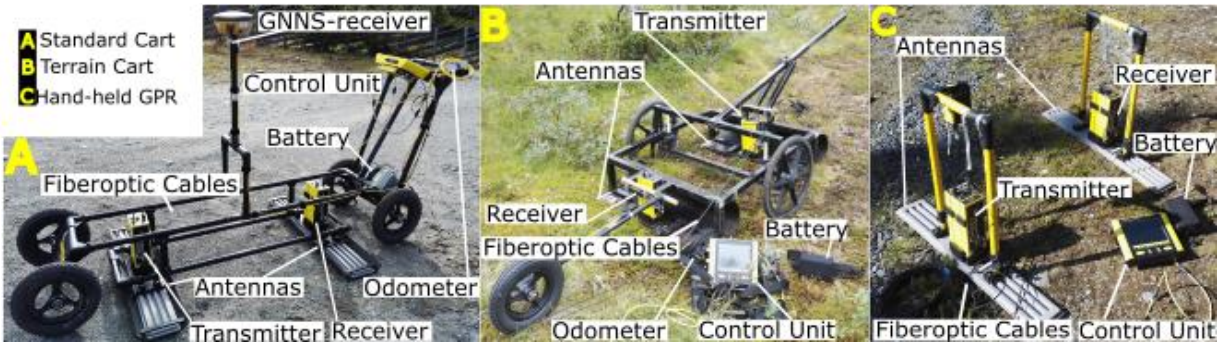

Figure 2.5. GPR set up for the tree measurements methods used.

A Topcon HiPer II GNSS receiver was used to obtain continuous and accurate position data. The lack of network coverage disabled the GNNS at all localities but one. Position- and

elevation data for these radargrams were added in the lab using laser scan data collected by the Norwegian Mapping Authority through remote sensing. Elevation data was not obtained in the field but added to the GPR data using Lidar processed in Arc Map. The tool Stack Profile was used to extract the elevation data along the line of interest. The input was a polyline shapefile where the transect was drawn, the LiDAR data (as a .lasd file) was used as the profile target, and an output table was obtained which was then exported as a text file. The table was converted to a topography file and attached to the GPR file in Ekko_Project

Ekko_Project 4 by Sensors and Software Inc, including the program LineView, was used to visualise, edit and process the data on a computer. Lines taken at the same landforms were merged. The direction was reversed on lines taken in a Southern to Northern directional sense (these lines are recognised from a decreasing horizontal distance on the radargrams) so the view is kept consistent and visualisation improved. Various colour palettes were applied in LineView to identify the main reflectors.

The radargrams were exported from Ekko_Project to the drawing programme InkScape for data interpretation. The main reflectors were sketched out, and the radargram divided into facies based on the nature of the reflections. The clearest reflectors are displayed as thick, black lines, and the weaker as thinner black lines. The radar facies description was based on Neal (2004). The following reflection configurations are identified:

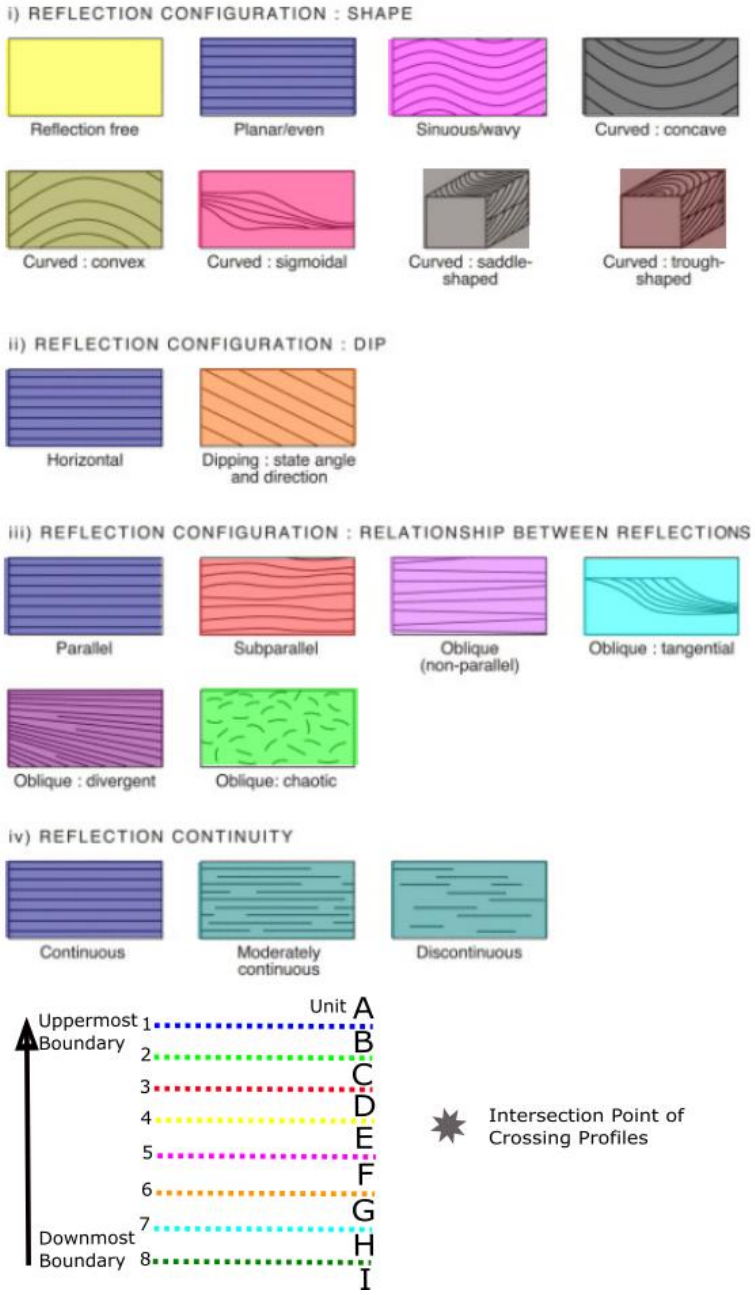

Figure 2.6. Colour scheme applied to reflection patterns for facies identification. Below are the boundary colour scheme and unit identification applied in identification of the GPR facies, and the star identification for intersection points of crossing profiles. Facies in grey were not found in radargrams. Modified from Neal (2004).

Parallel, subparallel, oblique, tangential, divergent, and chaotic. Neal (2004) recommends the separation of descriptive and interpretative terms of reflections, and suggested description based on shape, dip, interrelationship and continuity. For simplicity, the facies are here interpreted based on the relationship between reflectors, while their shape, dip and continuity can be read and analysed from the reflection sketch. Reflection free shapes is the exception and is mapped as a separate facies. Sinusoidal, concave, convex and sigmoidal reflectors are indicated where surrounding areas are reflection free. Continuity of reflectors is considered only when they appear discontinuous.

Prior to facies identification, erosive boundaries were identified from the main continuous reflectors. The boundaries were determined from a top-down approach, based on the principle of cross-cutting relationships, where younger boundaries cut across older (Catuneanu, 2006). The facies found between two erosional boundaries where defined as one unit. This allowed the recognition of facies association, where the presence of different units could be found in different landforms. The erosive boundaries were numbered chronologically, with the youngest as number 1. The units were numbered alphabetically, with the youngest as A. The boundaries are sketched out as dotted lines of a consistent colour scheme illustrated in figure 2.6.

Emphasis on the relationship between the facies rather than separate description is key to interpretation of deposition (Neal, 2004), so the facies identification is done accordingly. The radargrams are therefore interpreted to be dominated by areas of planar, parallel, continuous horizontal, dipping, subparallel, and oblique (non-parallel, tangential, divergent and chaotic) reflectors. Reflection free areas and areas of discontinuous reflectors are also mapped as facies. According to Neal (2004), the emphasis on recognizing facies may lead to an underestimation of the information obtained from the actual radar surfaces. The sole emphasis in geological interpretation is not on identified facies, but also based on individual reflection surfaces. The colour scheme applied in facies description and identification is shown in figure 2.6.

2.7 Soil Chemical Analysis

Soil chemical analysis and grain size distribution was performed on the soil samples from the field. These include twelve profiles and 42 horizons, among which are 30 mineral soil horizons and 12 organic horizons.

Soil Sample Preparation

Drying. The samples were dried to maintain the chemical nature of the soil in preparation for treatment in the laboratory. Dry soil is easier to handle during operation, and microbial processes are reduced (Smith and Mullins, 2001) The samples were air-dried in sample bags

at room temperature (20° C) for 38 to 45 days. Air-drying below 35° C is preferable, because higher temperatures can lead to a changes in soil chemistry (Smith and Mullins, 2001).Weighing, sieving and grinding were done at air-dry conditions.

Dry Sieving. The component of interest when determining the chemical properties of the soil in the laboratory is the percentage < 2mm, the fraction known as "fine earth" that contributes to soil formation. The samples were sieved using a steel sieve (2 mm, with a squared mesh) and a porcelain mortar. The sieving was done under a dust extractor, and between each sample the equipment was cleaned with compressed air. The sieved component was transferred to a sample box, and the residue put back in the sample bag for other analysis.

Weight and Density. Soil density was calculated for carbon stock estimations. The samples were weighed on a scale accurate to +/- 0.01 g both prior to and after sieving. Density of the samples was calculated from dividing the weight by the standard sample volume (100 cm^3). The sieved amount was weighed in a sample box, and the residue was weighed in the original sample bag. Five different sample bags and ten different sample boxes were weighed separately, and their respective average weight was calculated and subtracted from the soil sample weight. The loss during sieving was calculated from subtracting the combined weight of the residue and sieved soil from the initial sample weight. The organic horizon volume sampled is three times higher than the other horizons, compensating for the increased uncertainty during weighing considering its lower density compared to mineral soil.

Grinding. A small spoon (5-6 g) of soil from each sampled horizon was grinded in preparation for analysis of total carbon and nitrogen content. A Retch RM200 mortar grinder was used for four minutes on each sample and was cleaned with a vacuum cleaner between each operation. The machine uses pestle pressure and friction to triturate and grind the soil (Retch, 2017). The grinded amount was transferred to a Kraft soil sample bag.

Total Carbon and Total Nitrogen Content

Soil carbon and nitrogen content are essential for determining the soil environmental condition (Brady and Weil, 2013). The total carbon and total nitrogen content of the samples was measured on 0.2 g of grinded soil in an Leco TruSpec CHN instrument. The samples were dried at 55°C for two weeks. In preparation for analysis they were weighed, wrapped in tin foil and placed in the instrument. The soil undergoes complete dry combustion at 1050° C in the furnace, which produces CO_2, NOx and H2O. The gases are collected in a ballast chamber, and released in portions to the measurement cells (Nelson and Somers, 1982). The weight percentage of carbon and nitrogen in the soil is measured by an IR (infrared light) cell on CO_2 (Nelson and Somers, 1982) and TC (thermal conductivity) on N_2 (Bremmer and Mulvaney, 1982). NOx is reduced to N_2 in a cobber catalyst heater. Ten samples were measured at the time, with two control samples between each measurement for reference and occasional calibration.

pH

The acidity of a soil is an essential variable for chemical properties and its evolution (Brady and Weil, 2013). Soil pH of all the samples was measured using a glass electrode in an aqueous matrix. Krogstad and Børresen (2015) described the measurement of soil pH in water as the closest to the pH of soil solution in the natural environment. A measuring spoon of 10 ml and a graded cylinder of 25 ml was used to transfer soil and ionized water, respectively, to a 50 ml plastic beaker. The solution was thoroughly shaken by hand and left for 20 hours. The solution was then again shaken twice and left for 15 minutes for particles to settle. The pH of the soil solution was then measured using a PHM210 pH-meter from MeterLab. The instrument was calibrated using pH 4.0 and pH 7.0 buffer solutions, respectively, and tested with a theoretical solution at 6.87 prior to use. The pH is measured as a glass electrode is inserted into the suspension so the glass globe and salt bridge stand over the soil/sediment (Krogstad and Børresen, 2015). A ross electrode containing 3 M KCl was used. The pH was read as the instrument stabilised. Calibration was repeated after 15 measurements, to ensure the instrument had not drifted. The electrode was never left in solution for more than two minutes awaiting stabilisation, because then the amount of KCl leaked into the solution would have affected the pH reading.

Loss on Ignition

In a dry soil, the loss on ignition can give an indication of humus content (Brady and Weil, 2013). To determine the loss on ignition in a soil, soil dry matter is measured (Krogstad and Børresen, 2015). The value is corrected for mineral soils of a high clay content, as clay minerals bind water in its crystal structure that is only lost at temperatures above 150°C (Krogstad and Børresen, 2015).

Half a spoon (about 5-10 g) of each soil sample was transferred to a 20 ml, pre-weighed, porcelain crucible. The crucibles were set to dry in a drying cabinet at 105°C for 20 hours. The crucibles with soil dry matter were weighed on a scale accurate to +/- 0.001 g. The crucibles were then transferred to a calcinating oven and left for 5 hours at 550°C. The crucibles were weighed again, and loss on ignition calculated. See figure 2.7 for before-and-after photos of the crucibles.

Acid Oxalate Extractable Fe, Al and Si

Organically complexed and amorphous inorganic forms of iron and aluminium are considered soil weathering products and considered in studies of soil genesis (Brady and Weil, 2013).

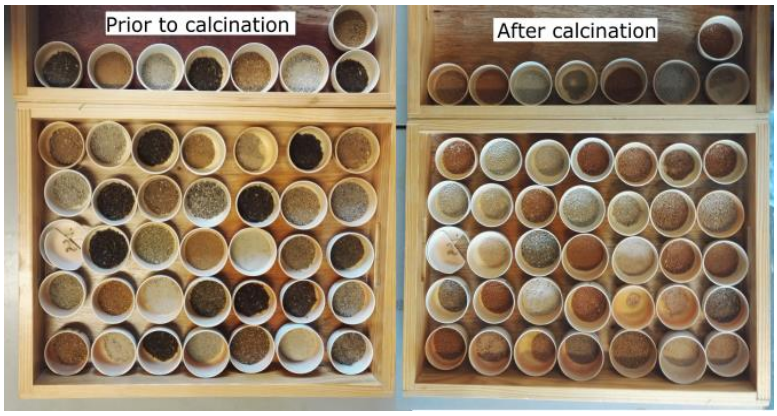

Figure 2.7. Photo that illustrates the effect of humus content removal from soil. The crucibles are displayed in the same order in both photos. Samples that have nearly disappeared after calcination are organic horizons, the white elluvial horizons, the red illuvial horizons, and the grey C horizons.

Acid oxalate is used to extract iron and aluminium oxides in soil, and the content analysed by ICP (see below) (Van Reeuwijk, 1993). The compounds are dissolved as the soil is shaken with an acid ammonium oxalate solution at pH 3 (Krogstad and Børresen, 2015). The reagent is produced from dissolving 81 g $(COONH_4)2 \times H_2O$ and 54 g $(COOH)2 \times H_2O$ in 4.5 liter deionised water (Krogstad and Børresen, 2015). The expected pH is 3, but the acidity of the solution can be adjusted by adding pre-prepared 0.2 M solution of either NH_4-oxalate or oxalic acid. The sample was prepared by transferring 1.00 g of soil and 50 ml acid oxalate to a 100 ml glass shaking bottle. The bottles were transferred to a cardboard box covered in black plastic and placed in an *Edmund Bühler SM-30* horizontal shaker at speed of 112.5 Mot/min for four hours. The sampled are shaken in the dark to avoid the photoinduced degradation of oxalate (Krogstad and Børresen, 2015). The samples were immediately filtered through filters rinsed with ammonium oxalate solution, the clear supernatant was thereafter collected in a 45 ml tube and analysed by ICP. Control samples were also measured, two with a control soil and four with ammonium oxalate only, to rule out the effects of potential contamination.

Cation Exchange Capacity and Base Saturation

The cations that are exchangeable between soil particles and the soil solution are plant-available (Krogstad and Børresen, 2015). It is affected by the clay and humus content of the soil, and a measure of its nutrient status (Krogstad and Børresen, 2015). Clay minerals are permanently negatively charged from isomorphous substitution of cations in the crystal structure and organic material is negatively charged at low pH by disassociation of H^+ from carboxyl- and phenolic groups. These negative charges in the soil limit the loss of nutrients such as calcium, magnesium, potassium and sodium through runoff, while the equilibrium balance of the soil solution allows their release when the soil water concentrations are low (Brady and Weil, 2013). The cation exchange capacity, CEC, is measured as the sum of all cations in cmol/kg. The base saturation is calculated as the cation percentage of the CEC that

does not have an acidifying effect on the soil. Considered here are H^+ and aluminium, which cause hydrolysis at low pH (Brady and Weil, 2013).

The cations were measured by ICP in an extract of soil obtained by 0.05 M ammonium acetate. The reagent is traditionally made from 2 M acetic acid neutralised by ammonia solution and diluted with deionised water (Krogstad and Børresen, 2015). The expected pH is 7, and is adjusted by dilute acetic acid (Krogstad and Børresen, 2015). Here, however, the reagent was made from 770.8 g ammonium acetate diluted to 10 liter, with pH adjustment done by adding either acetic acid or ammonia solution. For measurement of organic soil horizons, 1.5 g of soil was used, and for the mineral horizon 3.0 g soil. Two samples of control soil (standard type A) were included for reference.

The soil and 50 ml of reagent was transferred to a 100 ml Erlenmeyer flask and left for 24 hours. The solution was then washed through ribbon filter paper into a 250 ml flask using a wash bottle with reagent. The filtration was stopped at 250 ml. The procedure is shown in figure 2.8. Titration of 20 ml of the sample extracts was done to estimate the concentration of H^+ in the soil using a pipette, with 0.05 M NaOH, up to pH 7. The pH of the solution was then adjusted to pH 7 using the reagent. Only acidic samples were titrated. The amount of NaOH (measured in ml) required to bring the pH back up to 7 after adding the soil sample is a proportional to the concentration of H^+ in the solution. See paragraph above for description of pH measurements and calibration. The electrode was washed with ammonium acetate between each measurement. Eight clear solutions were measured and averaged to adjust for the amount of NaOH required to bring the solution to pH 7. The samples (42 + eight clear + two control soils) were divided between three rounds of measurement.

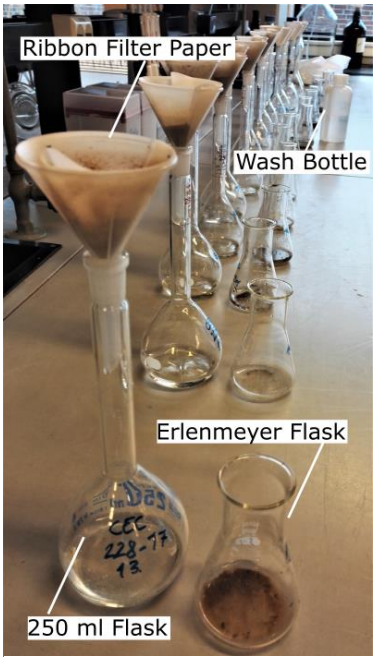

Figure 2.8. Photo of the procedure for cation extraction.

The cation exchange capacity and base saturation are calculated by the following equations:

CEC= (cmol(Na^+)/kg) + (cmol(1/2CMg^+)/kg) + (cmol(K^+)/kg) + (cmol(1/2Ca^+)/kg) + cmol(H^+)/kg

Base Saturation= (CEC - (cmol(H^+)/kg))/CEC

Inductively Coupled Argon Plasma Optical Emission Spectrometer (ICP)

ICP is a method used to analyses elemental concentrations of material in aqueous solution (University of Minnesota, 2017). In this study, it is used for analysis of the total carbon and total nitrogen content of grinded soil samples, as well as the acid oxalate extractable iron and aluminium content of the soils. The content of the elements is determined by spectral

emission from excitation as a mist of the sample is injected into a plasma created from a flowing gas within a high energy field (University of Minnesota, 2017). The compounds in the sample mist dissociate in the hot plasma, their component atoms absorb and emit energy, recognised by a spectrometer as characteristic for each element (University of Minnesota, 2017).

2.8 Grain Size Distribution

Soil texture is a basic soil property, key variable for soil development and provides the surface area for chemical reactions (Brady and Weil, 2013). The grain size distribution of the mineral soil horizons was measured for all samples. An overview of the grain size classes used is given in table 2.2.

The grain size distribution of the samples was measured by both the pipette and the laser method. The soil samples are collected from glacifluvial landforms, and presence of silt and clay is assumed to primarily be the result of soil weathering processes. Additional grain size measurement by laser of clay content is done on samples of Bs horizon to estimate the quantity. Analysis of the grain size distribution of a soil sample gives a grain size percentage definition based on the textural triangle from (WRB, 2014).

Table 2.2. Fractions estimated in grain size distribution from wet sieving (sand), sedimentation by the pipette method (clay and silt) and laser analysis (clay and silt). From Krogstad and Børresen (2015).

Clay		<0.002 mm
Silt	Fine	0.002-0.006 mm
	Medium	0.006-0.020 mm
	Coarse	0.020-0.060 mm
Sand	Fine	0.060-0.200 mm
	Medium	0.200-0.600 mm
	Coarse	0.600-2.000 mm

Pipette Method

The measurement of grain size distribution by the pipette methods is based on Stokes Law and the parameters during measurement are adjusted. The settling time of particles in water is a function on their size, and this assumption is used to measure the grain size distribution of the samples (Gee and Bauder, 1986). Stokes Law reads: $d_e^{\,2} = 18 \times \eta \times h/(\mu_s - \mu_w) \times t \times g$, where d_e = effective particle diameter, h/t= v = settling velocity, η= viscosity of water, $\mu_{s=}$ particle density μ_w= water density and g= gravitational acceleration (Gee and Bauder, 1986). The relationship gives a theoretical estimation, as the solution consists of other liquids than water, the water temperature and viscosity can be inaccurate, the particle density is estimated from quarts whilst the mineralogical composition is complex, and the particles themselves are not

perfect spheres, but irregularly shaped or even flat in the clay fraction (Gee and Bauder, 1986). Iron binds finer particles, and high content of iron can lead to an overestimation of coarse particles (Gee and Bauder, 1986). Preparation of samples before measurement includes removal of organic material, dissolution of inorganic compounds, chemical enhancement of sedimentation and dispersion of material (Krogstad and Børresen, 2015). Seven particle classes were estimated: clay, fine, medium and coarse silt, by the pipette method, and fine, medium and coarse sand by wet sieving.

To measure the grain size distribution of mineral soil, 10 g was transferred to a 1 liter glass beaker. Organic material was oxidized by hydrogen peroxide (H_2O_2) by addition and mixing of 20 ml of deionized water and 10 ml of 35% H_2O_2 with the soil. The reaction left to occur for a few days, and another 10 or 20 ml H_2O_2 was added to the samples with higher content of organic carbon (seen from the loss on ignition) as the initial reaction slowed.

The solution was later heated on a hot plate to 60°C to enhance the speed of reaction to remove the remaining H_2O_2. Deionised water (200 ml) was added to the solution. To allow for evaporation, the solution was left for five hours. To dissolve inorganic material (amorphous compounds), 10 ml 2M HCl was added, and the solution stirred with a glass rod for 1 minute. Deionized water was then added to the solution (up to 900 ml) and left overnight for sedimentation to occur. After sedimentation, the liquid solution was sucked out using a rubber tube connected to a water aspirator, and the measurement glass refilled with deionised water up water to 900 ml. A sieve was used to remove floating organic material remaining in solution. A few drops (2-3 for clearer solutions, 4-5 for opaque solutions) of 1 M $MgCl_2$ was added to increase the sedimentation velocity (figure 2.29). The solutions were left for particles to settle overnight, and the liquid component sucked out again. To ensure that the sediment consists of primary particles only, 50 ml 0.05 M sodium pyrophosphate ($Na_4P_2O_7$) was added for dispersion of the material. The solutions were then stirred for 60 seconds by an electronic overhead stirrer (VWR VOS 16).

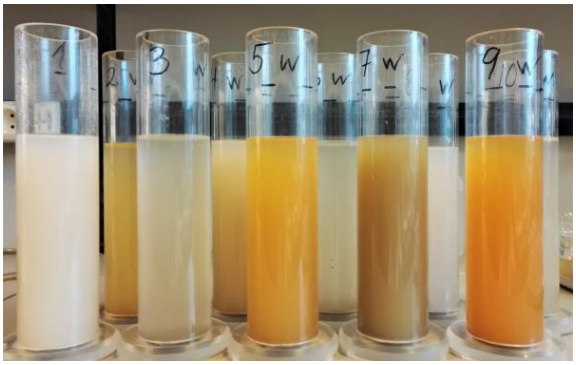

Figure 2.9. Soil samples solution with settling particles. E horizons form white solutions, Bs horizons yellow, orange and brown, and C horizons grey.

The solution was washed into a plastic cylinder with deionised water and filled to 400 ml. The temperature of the solution was measured to 22°C, and the timing of particle settling for each fraction estimated accordingly. Four weighed glasses (one for each fraction) for each sample solution was prepared. Pipetting was initiated by turning on the water jet pump, ensuring that all cocks are closed by blocking the air opening of the pipette (it should bubble in the pressure compensator (Krogstad and Børresen, 2015)), and both tubes in the pressure compensator

adjusted to a four second filling time for both the four cm and 15 cm depth (Krogstad and Børresen, 2015).

Each solution was stirred for 1 minute with a stirring rod. The pipette was raised and lowered into the cylinder to the 15 cm mark. The pipette fills as the cock opens. The first fraction was taken after 44 seconds at 15 cm (<63 microns) and the next after 1 minute and 46 second at 4 cm (20 microns) (Gee and Bauder, 1986). The solution is then stirred again, and the third fraction taken after 19 minutes and 40 seconds (six microns) and the forth fraction after two hours and 57 minutes (2 microns) (Gee and Bauder, 1986). The pipette was washed out between each solution by turning the upper cock releasing deionised water from a container on top (Krogstad and Børresen, 2015). After pipetting, the remaining fractions were sieved (63, 212 and 600 microns). The content was transferred to a stack of three corresponding sieves, the finest fraction at the bottom. Each fraction was transferred to a porcelain dish, excess water decanted, and washed into a beaker. The samples were dried at 105°C, weighed to 1.0 mg accuracy, and the weight percentage of each fraction was calculated.

The grain size distribution after sedimentation is calculated as follows:
The extraction of interest (g) = The extracted fraction - the finer co-extracted fractions) x (400 ml solution/20 ml extracted solution) (Gee and Bauder, 1986). For the clay fraction, the salt from dispersion is subtracted, for fine silt, salt and clay are extracted, etc. (Gee and Bauder, 1986). The result gives a cumulative grain size distribution.

Laser Method

The concentration of various particles sizes in a liquid can be measured from the differential scattering of a ray of light through the solution (Beuselinck et al., 1998). The pattern of light diffraction is controlled by the angle of refraction of light as a result of the particle size (Beuselinck et al., 1998). Here, the Fourier lens was used in determination of the diffraction pattern, which leads the refracted light onto a specific detector (Beuselinck et al., 1998). The Fraunhofer optical model uses a refraction index appropriate for sandy soils (Beuselinck et al., 1998), and was here used for particle size determination.

The samples were prepared as described for the pipette method up until and including addition of HCl. The samples were then sieved through a 63 microns sieve, collected in a glass beaker and left for particles to settle. A few drops of 1 M MgCl2 was added to enhance the process. The residue (particles >63 microns) were collected in a glass, dried at 105° C and weighed for comparison with the result from the pipette method. After particle sedimentation, the water was sucked out of the glass beaker, and the remaining material dried at 40° C for three days.

The dried material was carefully homogenised with a spoon. Around 0.2 g (depending on the amount of silt and clay seen from the pipette measurements of each sample was weighed is

preparation for analysis. Then 50 ml 0.5 M sodium pyrophosphate ($Na_4P_2O_7$) was added to the sample, and the solution disparaged for 1.5 minute using an ultrasound rod (at an energy level between 34 and 36 J/ml).

Prior to analysis, laser ray adjustment, water composition control (ensuring absence of particles and air bubbles), bias voltage control (to limit background noise) was carried out. Considering the small amount of soil that is analysed, the particle size composition might not be representative for the whole sample. Variation in mineralogy, flocculation of particles due to iron oxides, non-spherical particle shape and inaccurate preparational sieving are all sources of error. Insufficient material was left for reliable analysis of one of the samples, where only 2.45 g was left when 10 g is required for proper analyses and comparison with the pipette method suggests that results were incorrect. The result is included (table 4.7, soil V2-3), but not considered in data interpretation.

2.9 Data Visualisation and Source Management

The localities visited in the field, including the described landscape transects and localities of GPR measurement, were imported into Arc Map as a point shapefile created in the Norgeskart App by Asplan Viak Internet AS. The open source software drawing programme Inkscape version 0.92 was used to create figures from collected data and photographs, sketch out reflectors in the GPR radiograms, digitalise sedimentary logs and terrain transects as well as figure illustrations of discussed concepts. The free software R and the Microsoft Package Excel (2016) was used for graphical visualisation of data. The software EndNote X8 by Clarivate Analytics is used for source management and citation.

3 Glacifluvial Deposits and the Deglaciation Landscape

3.1 Landscape and Landforms

The digital elevation model (DEM) in figure 3.1 aids the understanding of the nature and distribution of sediments and landforms and connects individual field observations to the deglaciation landscape. The model shows that valley 1 is wide and relatively shallow, valley 2 is narrow and deep, and valley 3 shallow and relatively narrow. The relief of valleys 1 and 3 is less pronounced and their lowest level is at a higher elevation than valley 2. The relationship between the landforms as interpreted from the model is later used to interpret the development of deglaciation in the area.

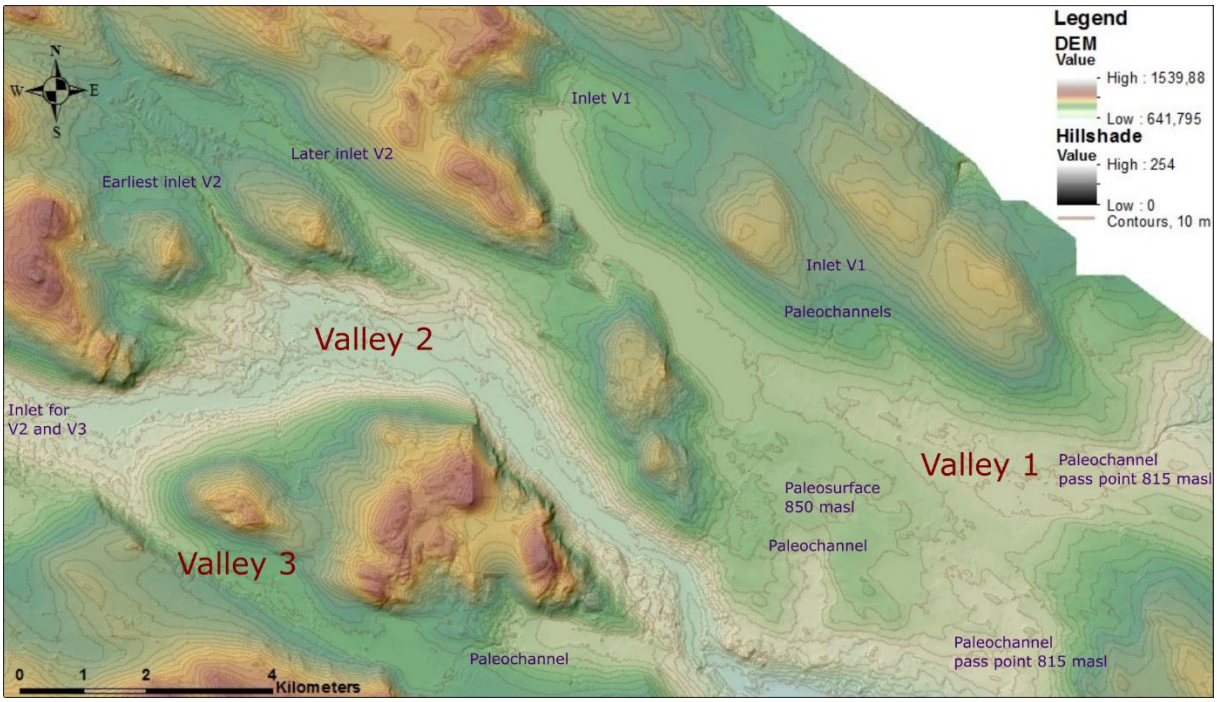

Figure 3.1. Digital elevation model of the study area.

Meltwater inlets and palaeochannels that were active during formation of the studied landforms are marked on the DEM in figure 3.1. Two palaeochannels in the SE corner of the study area connect valley 1 and valley 2. A deep, E-W trending palaeochannels can also be observed in the Eastern part of valley 1. The elevation at the pass points of the palaeochannels is 815 masl. Palaeochannels entering valley 2 can be observed in the NW and along the Northern side of the valley. The valley side gradients increase above 860 masl in valley 1 and 850 masl. in valley 2. There appears to be a palaeo-surface between valleys 1 and 2 at around 850 masl. Evidence for glacifluvial erosion and deposition is found up to around 860 masl in valley 1, 820 masl in valley 2 and 890 masl in valley 3. Various glacifluvial landforms are describe and interpreted in all three valleys.

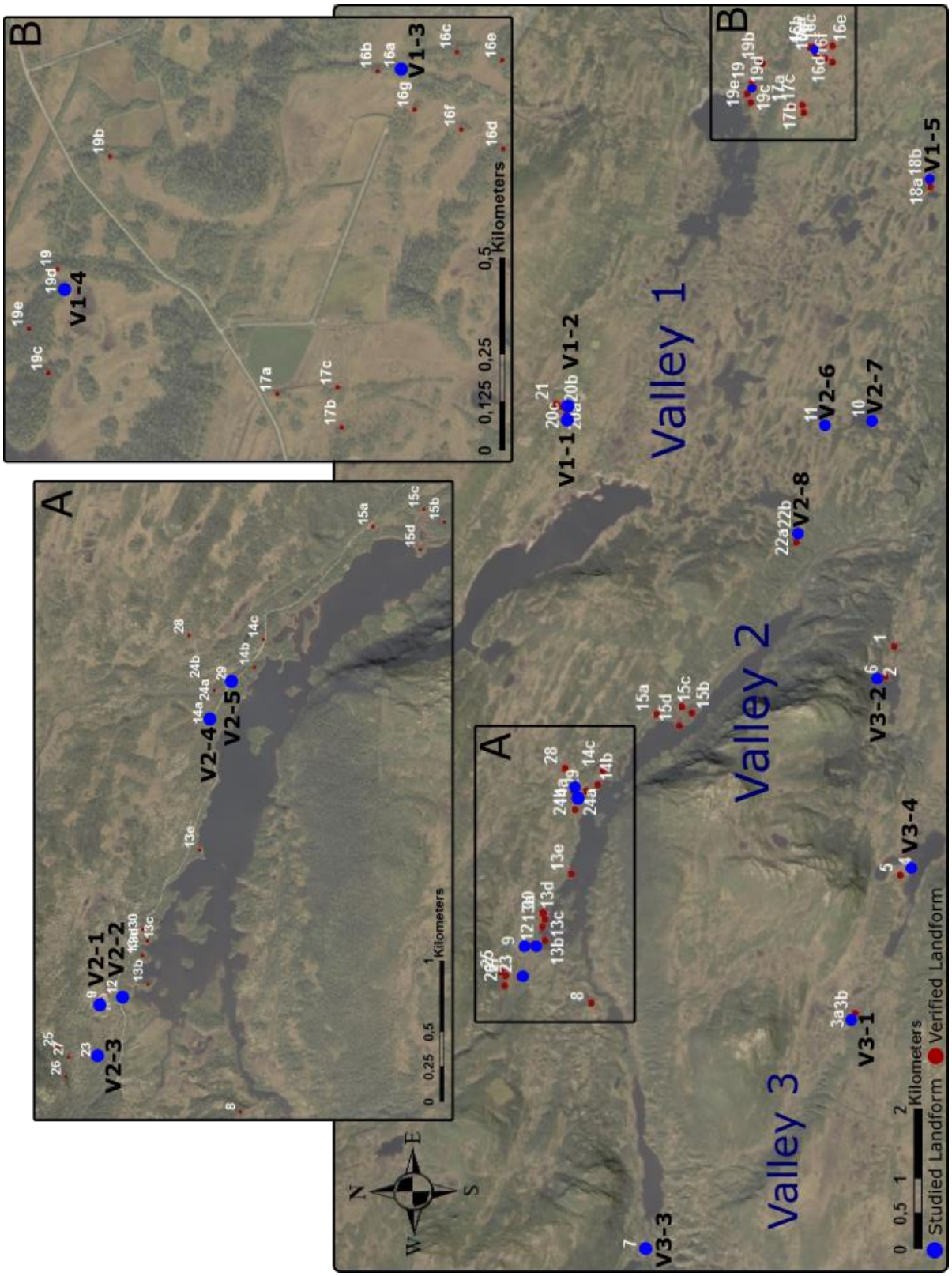

Figure 3.2. Overview of visited localities for landform verification and detailed study. White numbers and red points identify the visited landforms, while black numbers and blue points show landforms that are studied in detail. The numbers in black correlate to table 3.1 and are used in the following chapters.

The visited localities in the study area are shown in figure 3.2 and table 3.1. The visited landforms were chosen from the work of Putnins and Henriksen (2017). In total, 81 localities were visited, and 17 studied in detail. The localities were selected among 475 eskers, 37 "other" meltwater landforms, 454 ribbed moraines and 1397 streamlined landforms (figure 1.5). The landforms studied in detail are assigned a numerical ID with a prefix based on the valley system it is found in (V1, V2 or V3).

Table 3.1. Overview of visited localities (see also figure 3.2). The localities marked in blue are studied in detail and discussed in the chapters that follow. They are assigned a numerical ID based on the valley where the landform is found (e.g. V1-3).

Locality	Mapped Landform (Putnins and Henriksen, 2017)	Field Investigation	Assigned ID
L1	Delta	Three parallel eskers	
L2	Till cover	Basal till overlain by ablation till	
L3	**Not mapped**	**Kame terrace**	**V3-1**
L3b	Not mapped	Kame	
L4	**Kame**	**Kame (surrounded by peat)**	**V3-4**
L5	Esker	Kame	
L6	**Esker**	**Ice-flow parallel esker**	**V3-2**
L7	**Streamlined landform, two deltas in the E**	**Streamlined landform overlain by channel deposits, two outwash plains in the E**	**V3-3**
L8	Streamlined landform	Streamlined landform	
L9	**Not mapped**	**Delta**	**V2-1**
L10	**Ice-flow transverse esker**	**Ice-flow transverse esker**	**V2-7**
L11	**Esker**	**Narrow, short, low esker**	**V2-6**
L12	**Ribbed moraine, type B /till cover/not mapped**	**Sandur plain (valley train)**	**V2-2**
L13a	Ribbed moraine, type B	Ribbed moraine, type B	
L13b	Streamlined landform	Streamlined landform	
L13c	Streamlined landform	Streamlined landform	
L13d	Delta	Uncertain	
L13e	Not mapped	Esker	
L14a	**Not mapped**	**Glacifluvial deposits at shoreline of ice-dammed lake**	**V2-4**
L14b	Delta	Fan	
L14c	Delta	Fan	
L15a	Delta	Distal fan deposits	
L15b	Delta or kame	Kame	
L15c	Not mapped	Esker	
L15d	Streamlined landform	Streamlined landform	
L16a	**Esker**	**Ice-crevasse esker**	**V1-3**
L16b	Esker	Esker	
L16c	Esker	Esker	
L16d	Not mapped	Esker	
L16e	Not mapped	Esker	
L16f	Not mapped	Esker	
L16g	Not mapped	Esker	

L17a	Not mapped	Two parallel eskers	
L17b	Not mapped	Meltwater landform, possibly esker (elongate and wide)	
L17c	Two parallel eskers, Eastern in two parts	Two parallel eskers, Eastern in two parts	
L18	Streamlined landform	Streamlined landform	
L18b	**Esker**	**Chute esker**	**V1-5**
L19	**Esker**	**Small ice-crevasse esker**	**V1-4**
L19b	Esker	Esker	
L19c	Esker on top of streamlined landform	Esker on top of streamlined landform	
L19d	Streamlined landform	Streamlined landform	
L19e	Ribbed moraine, type A	Ribbed moraine, type A	
L20	Esker	Esker	
L20b	**Esker**	**Wide, U-shaped esker**	**V1-2**
L20c	Esker	Esker	
L21	**Esker**	**Narrow, S-shaped esker**	**V1-1**
L22	Esker	Esker	
L22b	**Esker**	**Large chute esker**	**V2-8**
L23	**Delta**	**Fan lobe/deposit, later meltwater erosion**	**V2-3**
L24	Not mapped	Possible lateral glacifluvial deposit	
L24b	Delta	Down cut fan deposit	
L25	Till cover	Border between fan deposit and till cover	
L26	Not mapped	Kame terrace and ice contact	
L27	Mapped, but unidentified	Ice-lateral deposit	
L28	Not mapped	Meltwater plain	
L29	**Delta**	**Fan lobe/deposit**	**V2-5**
L30	Ribbed moraine, type B	Probably ribbed moraine, type B, possibly ice contact	

The field investigation documented additional meltwater landforms that were not mapped by the remote sensing. Some of these were probably too small to be observe in the LiDAR data. On the other hand, the non-mapped landforms are often of comparable size and found close to the mapped landforms. It is possible that some landforms were eliminated because of a high degree of uncertainty. Parallel eskers found in clusters and perpendicular to ice flow, interpreted to have formed in crevasses in the ice, commonly appear to be left unmapped. These are among the landforms of the lowest relief in the landscape. Considering uncertainty, it appears that most of the landforms that are mapped from LiDAR data and included are mapped correctly. Interpretation of landforms as deposited in standing water depends on the model of ice retreat, which appears to require field investigation and hands on sediment description to assess. The landforms studied in detail here (logged and measured with GPR as well as soil profile description and soil sampling) are shown in figure 3.3.

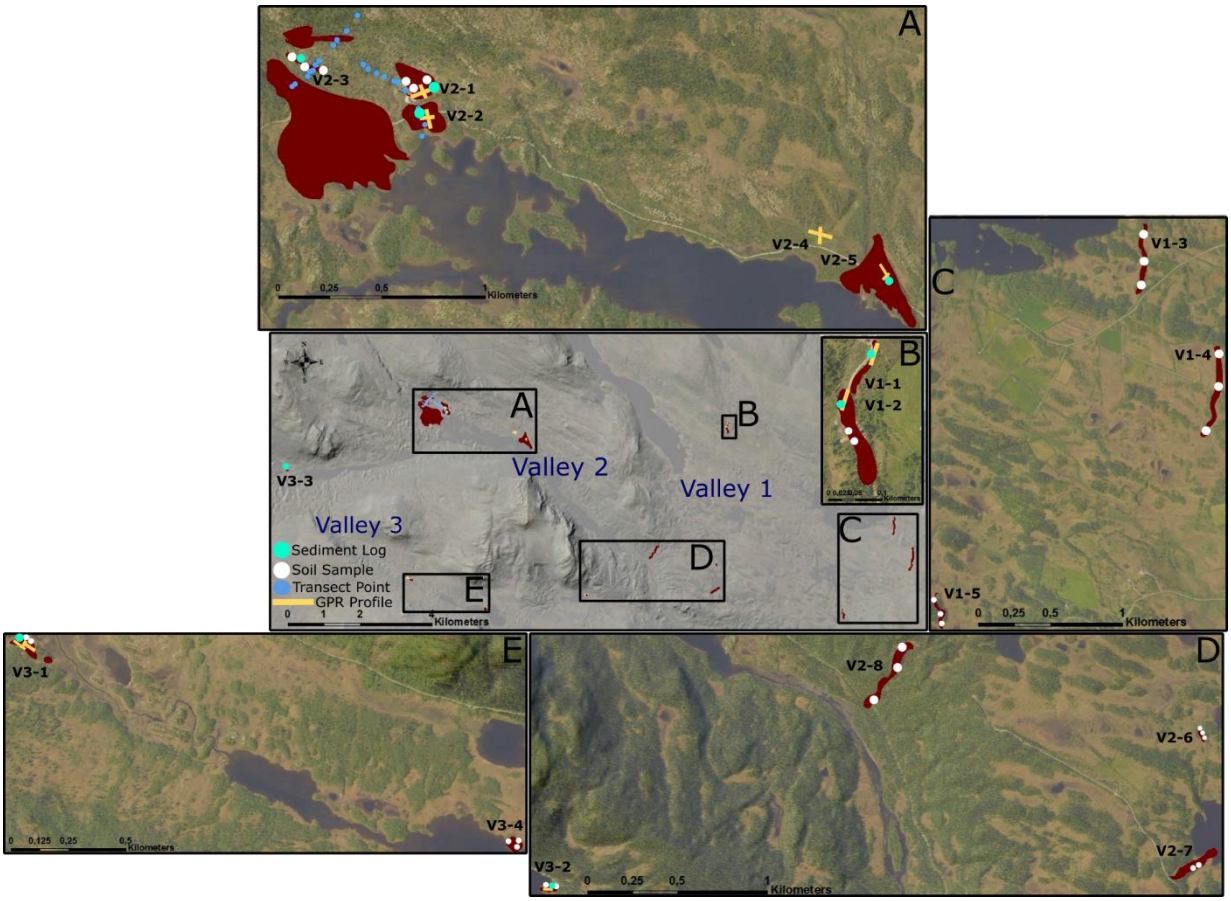

Figure 3.3. Overview of landforms studied in detail. The yellow lines show GPR profiles, blue strings show field transects, white points described and sampled soils profiles and light green points stratigraphic logs. Size, shape and location of landforms are modified from Putnins and Henriksen (2017).

3.2 Sedimentology and Morphology of the Glacifluvial Deposits

All landforms (ridges, terraces, mounds, plains, fans and deltas) are interpreted to be glacifluvial deposits, based on the grain size (sand and gravel), sorting (moderate to high) and rounding (moderate to high) (figure 3.36), flow competence (generally high) (figure 3.36), bedding (high thickness variation), sediment structures (primarily cross-bedding and troughs) and high variability in layering.

All stratigraphic logs are described starting at the C-horizon (50-100 cm below the surface) unless other is specified. Only the uppermost 0.9-3 m of the landforms are described; none of the logs cover entire deposits. All GPR lines are along the topographic highs of landforms and displayed from N (left) to S (right).

3.2.1 Narrow, S-shaped Esker in Valley 1 (V1-1)

Landform description. The landform is an S-shaped ridge (figure 3.4) striking NNE-SSW. It is 222 m long, 2.5 m wide and 4 m high. The stratigraphic log (figure 3.5) is described from slightly S if its midpoint, facing ESE.

Figure 3.4 (right). Photo of the narrow, S-shaped Esker, facing N along the ridge. The sediment log is described from the lower left corner of the picture.

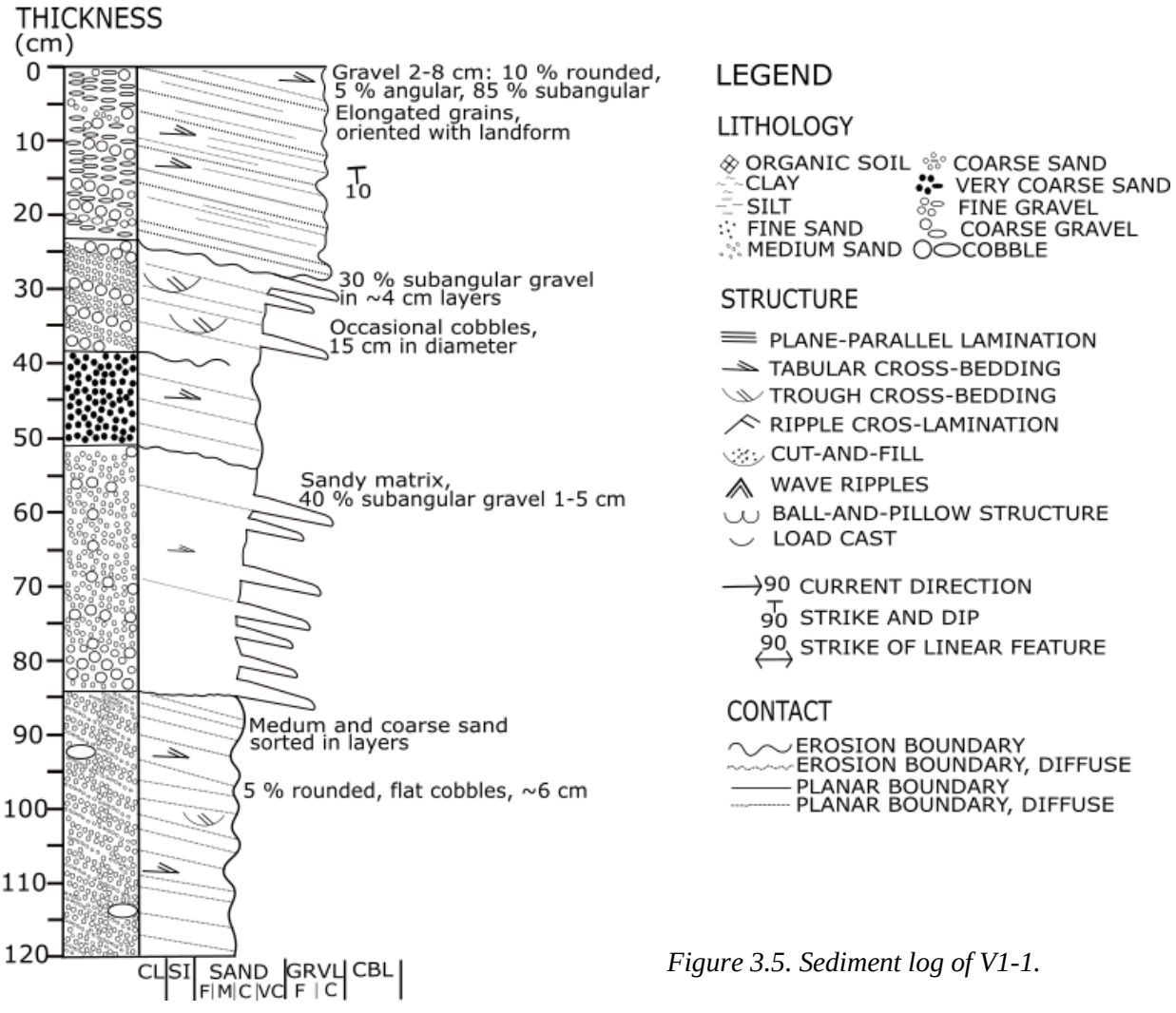

Figure 3.5. Sediment log of V1-1.

Sediment Description. The logged section is reversely graded and dominated by loos, fine and coarse gravel. Beds dipping at 10° towards the S, like the top surface of the landform, occur throughout the outcrop. Thickness of beds varies between 13 and 36 cm, and all boundaries appear erosive. The uppermost bed (0-24 cm) consists of elongate coarse gravel with clasts dipping towards the S. The bed at 24-38 cm consists of well-sorted coarse gravel and coarse sand. The gravel in this bed and at 51-84 cm is subangular with a mean diameter of 4 cm. Very coarse sand and coarse-medium sand are found at 38-51 cm and 84-120 cm, respectively. The lowermost bed (84-120 cm) contains flat cobbles 6 cm in diameter. Tabular cross-bedding is found in all beds, and in the lowermost layer also smaller troughs. The dip of the beds varies throughout.

Sediment Interpretation. The coarsening upward of the sequence suggests a temporal increase in flow regime, from moderate to upper flow regime with time. For the uppermost 24 cm, a combination of strong currents and high material availability likely resulted in deposition of cross-bedded gravel. The alignment of elongated clasts with the landform surface in the upper bed suggests that the sediments were deposited on the slope. The intervals between 24-38 cm and 51-84 cm reflect varying discharge, with gravel deposits at higher flow velocity, sand deposition in quieter conditions, and formation of troughs during events of heavy discharge. The variation is most prominent between 24-38 cm. The filling of troughs represents lateral variation in flow within the channel. The cross-bedded interval at 38-51 cm might represent more stable flow reflected in a high degree of sorting and cross-beds of constant thickness. The interval 84-120 cm contains cobbles possibly deposited by gravity (e.g. sliding). The regularly cross-bedded medium to fine sand indicates a moderate flow regime (Evans and Benn, 1998). The variation in the angle of dip of the cross-bedding along with troughs suggests that flow has migrated laterally within a channel system. Alternatively, variation in the dip of the cross-bedding in the lower bed may suggest that deposition adjusted with landform growth or melting of surrounding ice.

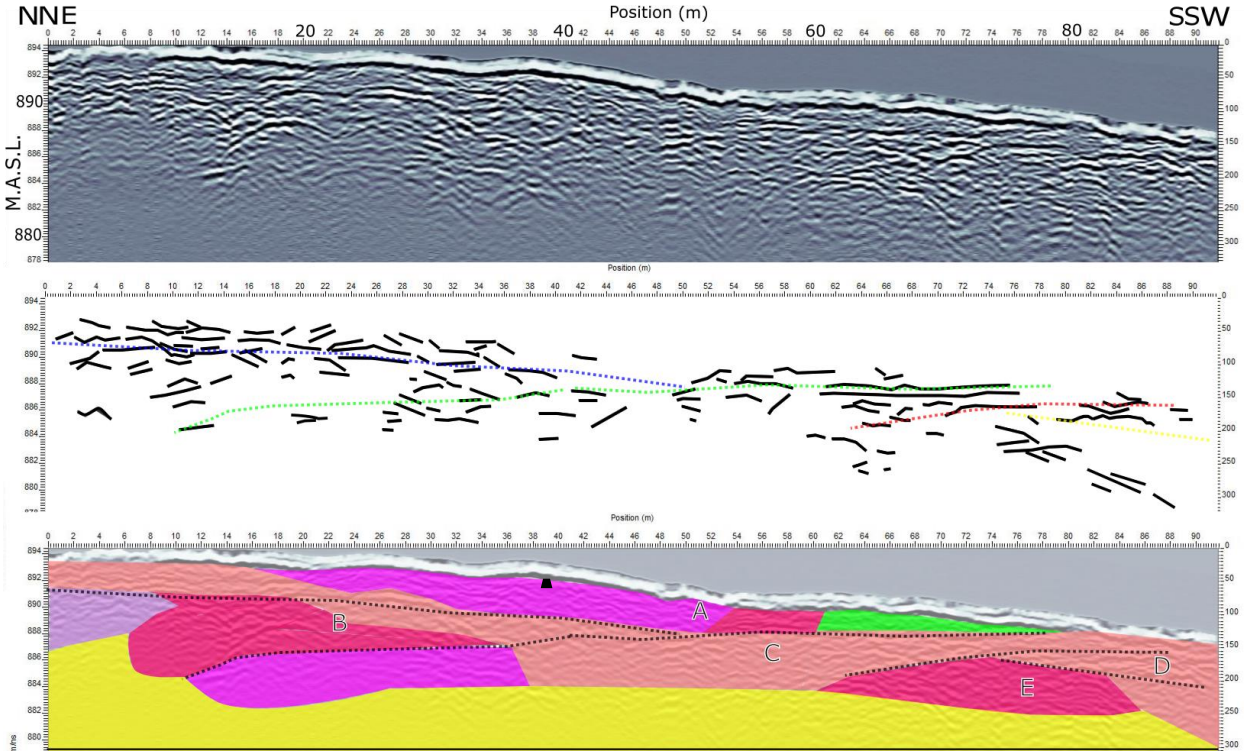

Figure 3.6. Radargram (top), reflectors and interpreted erosive boundaries (middle) and identified facies (bottom) of V1-1, narrow, S-shaped esker, parallel to flow. The boundaries and GPR facies identification are based on figure 2.6. The black trapes indicates where the stratigraphic log is described.

Description of Radargram. The profile contains boundaries that appear to dip in both the NNE and SSW direction (figure 3.6). They are subparallel to the surface of the ridge, hence dip slightly to the SSW. The main reflectors are sinusoidal, subparallel, and sigmoidal. Oblique reflectors are found near the surface in the NNE (unit B), and oblique chaotic reflectors in the SSW (unit A). The subparallel reflectors appear as a lateral continuation of the sigmoidal (units B and E).

Radargram Interpretation. The regradation of the erosional surfaces might be an expression of waning flow with time. The continuity of their dip direction suggests that flow was continuous throughout formation. The repetition of similar facies suggests that similar depositional process occurs in different units. The sinusoidal reflectors in units A and C might represent times of quicker deposition and poorer development of bedding. This can suggest separate flow episodes, where the current strength has decreased towards the end of one depositional sequence (possibly represented by subparallel reflectors). The chaotic reflectors (unit B) could then be an expression of a current occasionally strong enough for boulder transport. The sigmoidal, subparallel and sinusoidal reflectors all represent progradation of the landform in the SSW direction. The prograding and aggrading mode of deposition is like that interpreted by Burke et al. (2015).

Landform Interpretation. The described log (figure 3.5) and upper GPR facies (figure 3.6) dipping in the direction of the top surface of the landform, and the configuration suggest external stabilisation. This glaciofluvial deposit gives a general impression of progradation as all the beds build outwards. This can suggest an ice-walled, but not necessarily an ice-covered environment. Loosely packed sediments suggest deposition under low pressure. Aggrading and prograding GPR facies indicate confined deposition. The esker is possibly formed in an open crevasse in stagnant ice (low pressure environment). Putnins and Henriksen (2017) suggest that all eskers in the area are formed in this way.

3.2.2 Wide, U-shaped Esker in Valley 1 (V1-2)

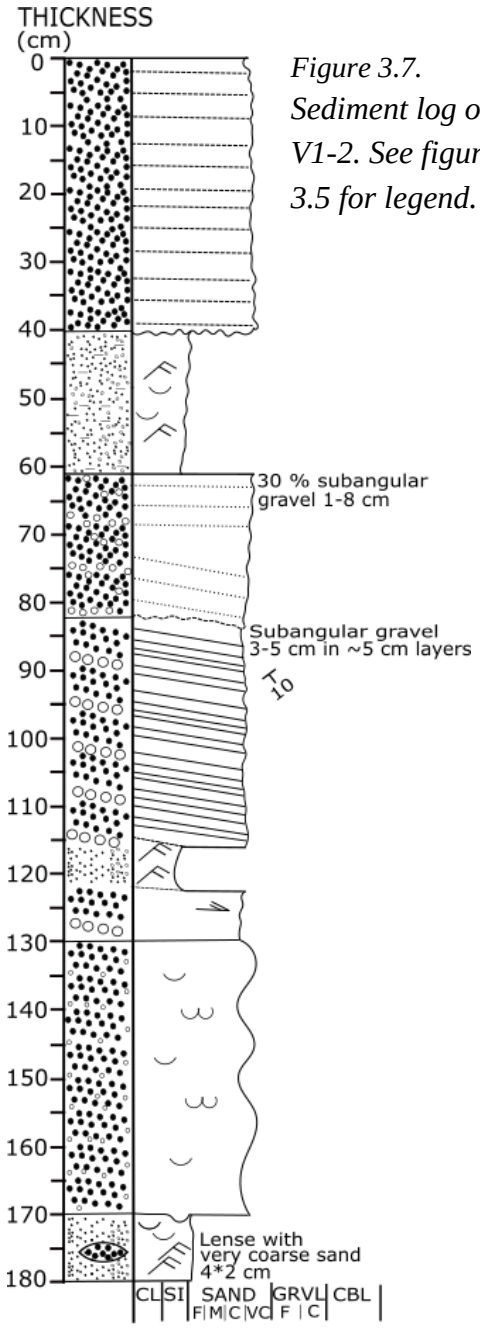

Figure 3.7. Sediment log of V1-2. See figure 3.5 for legend.

Landform description. The landform is a wide, U-shaped ridge curving NE and striking NNW-SSE. It is 265 m long, 30 m wide and 5 m high and appears as a possible continuation of V1-1, narrow, S-shaped esker, described above. The sediment log (figure 3.7) is described from its Northern tip, facing N-E.

Sediment Description. The section is dominated by very coarse sand interbedded with thinner layers of finer material. Beds dip in the direction of the surface slope below 70 cm and are sub-horizontal above. Sedimentary structures such as ripple cross-lamination, load casts, tabular cross-bedding, ball- and pillow structures occur in the silty intervals. The upper 40 cm consist of sorted, very coarse sand with plane-parallel, regularly spaced bedding. An erosive boundary is found at 40 cm (figure 3.7). The interval 40-60 cm consists of silty, fine to medium-grained sand with ripple-cross lamination and load casts. The layer at 60-82 cm contains plane-parallel beds in the upper part and dipping, planar beds in the lower part. It is composed of very coarse sand interspersed with thin layers of fine gravel. An erosive boundary is found at 82 cm, and below is a bedded interval down to 115 cm with layers gently dipping at 10° to the SE. It has thinner layers and is composed of very coarse sand with regularly spaced beds of gravel. Sub-angular

gravel with an average size of 5 cm is found between 60 and 90 cm. A layer of fine sand and ripple-cross lamination occurs at 115-122 cm. A massive bed of coarse sand, with coarse gravel concentrated at its bottom, follows between 122-130 cm. Between 130-170 cm depth is a bed dominated by ball-and-pillow structures and load casts, composed of very coarse sand interspersed with coarse sand. The bottom layer, between 170-180 cm, consists of fine, ripple cross-laminated sand. Its upper part displays load casts and a 2x4 cm lens of very coarse sand.

Sediment Interpretation. The section indicates a moderate flow regime, were deposition has changed repetitively between a quieter (ripple-cross laminated layers of fine sand) and higher energy environment (layers of coarse sand). The erosional boundary at 40 cm points to increasing current that eroded the finer-grained sediments below. Fine sand and ripple-cross-lamination at 40-60 cm suggest relatively calm conditions. Load casts within the interval may have been caused by rapid sedimentation of the sediments above. The cross-bedded, coarser intervals at 60-115 cm were deposited at higher flow regime. The ripple-cross-laminated fine sand at 115-122 cm suggests calmer conditions and possibly deposition in a pond, following an event of stronger currents between 122-130 cm. Intense soft-sediment deformation in the bed at 130-170 cm suggests very rapid deposition. The bottom layer, between 170-180 cm was deposited by weaker currents. Soft sediment deformation and a lens/pillow of coarse sand reflect rapid deposition of the bed above.

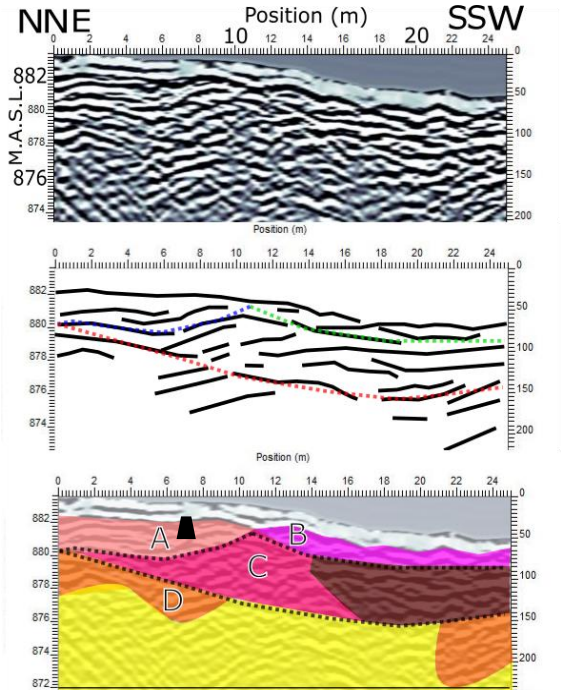

Figure 3.8. Radargram (top), reflectors and interpreted erosive boundaries (middle) and identified facies (bottom) of V1-2, wide, U-shaped esker, parallel to flow. The boundaries and facies identification are based on figure 2.6. The black trapes indicates where the stratigraphic log is described.

Radargram Description. The profile is taken along the wide, U-shaped esker, parallel to flow (figure 3.8). Erosional boundaries are concave and cross-cut each other. The uppermost reflectors are subparallel (unit A) and sinusoidal (unit B), while sigmoidal and trough-shaped reflectors dominate at deeper levels (unit C). Possible dipping reflectors are found in each end of the profile (unit D), with dip directions towards the middle of the profile.

Radargram Interpretation. The facies interpretation is similar to the one for V1-1, the narrow, S-shaped esker. The change from sigmoidal reflectors to troughs within one unit may suggests a quickly changing flow direction and/or flow regime (unit C). The dipping reflectors are likely to be cross-sectional views of channel fills (unit D). The subparallel, sigmoidal and sinusoidal reflectors all represent progradation of the landform in the S-SW direction (units A-C). Various units represent

different flow episodes. The current direction is likely to have changed as the landform evolved. The youngest unit does not show dip in the downflow direction, possibly because the flow was controlled by the landforms own topography (flow down either side). If the spatial conditions were passively affecting deposition and changed during deposition, the landform may have formed in rapidly melting stagnant ice.

Landform Interpretation. The sediment log (figure 3.7) and radargram (figure 3.8) suggest that the esker was possibly formed in a zone between ice blocks, or in a crevasse in stagnant ice like V-1.

3.2.3 Delta in Valley 2 (V2-1)

Landform description. A gravel pit of 30x100 m striking NNE-SSW cuts into the landform (figure 3.9). Shape and extent of the landform are difficult to determine, but it extends at least 20 m further E, possibly up to 150 further N and an unknown distance towards the NW. Assuming the interpretation of the landform as a delta is correct, its elevation suggests a maximum NW extent of 400 m. Two 40 m wide palaeo-channels filled with 70 cm dimeter sub-angular boulders strike E-W. The elevation between the palaeochannels is the same as the elevation of the undisturbed surface of the gravel pit.

The upper 120 cm of the log (figure 3.10) is described in the NW part of the landform facing NNE (point B on figure 3.9) while the lower 40 cm are described from its S-Western part (40 m E and 100 m S) facing S-S-W (point D on figure 3.9).

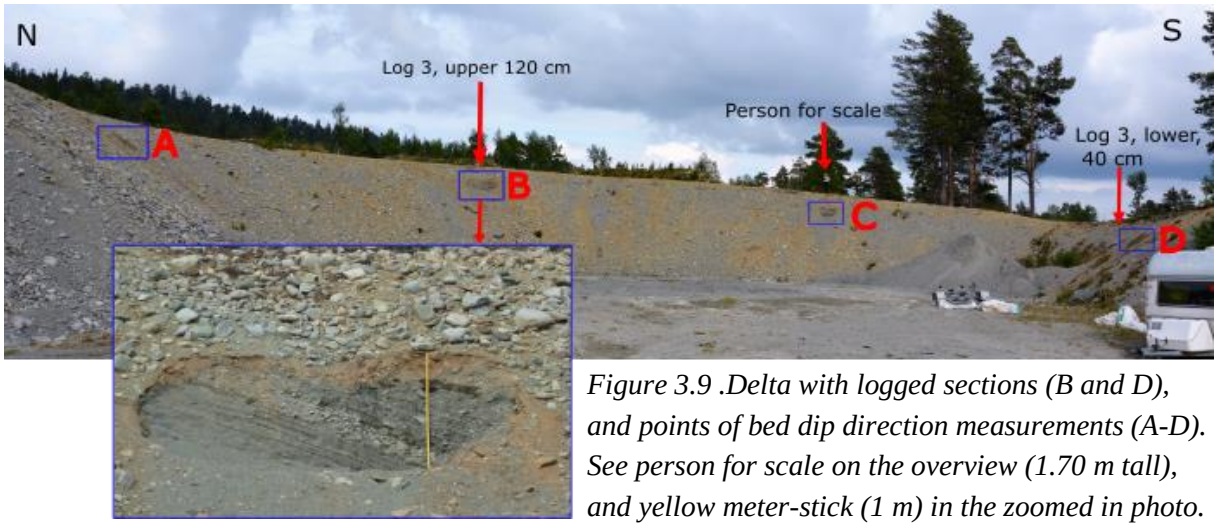

Figure 3.9 .Delta with logged sections (B and D), and points of bed dip direction measurements (A-D). See person for scale on the overview (1.70 m tall), and yellow meter-stick (1 m) in the zoomed in photo.

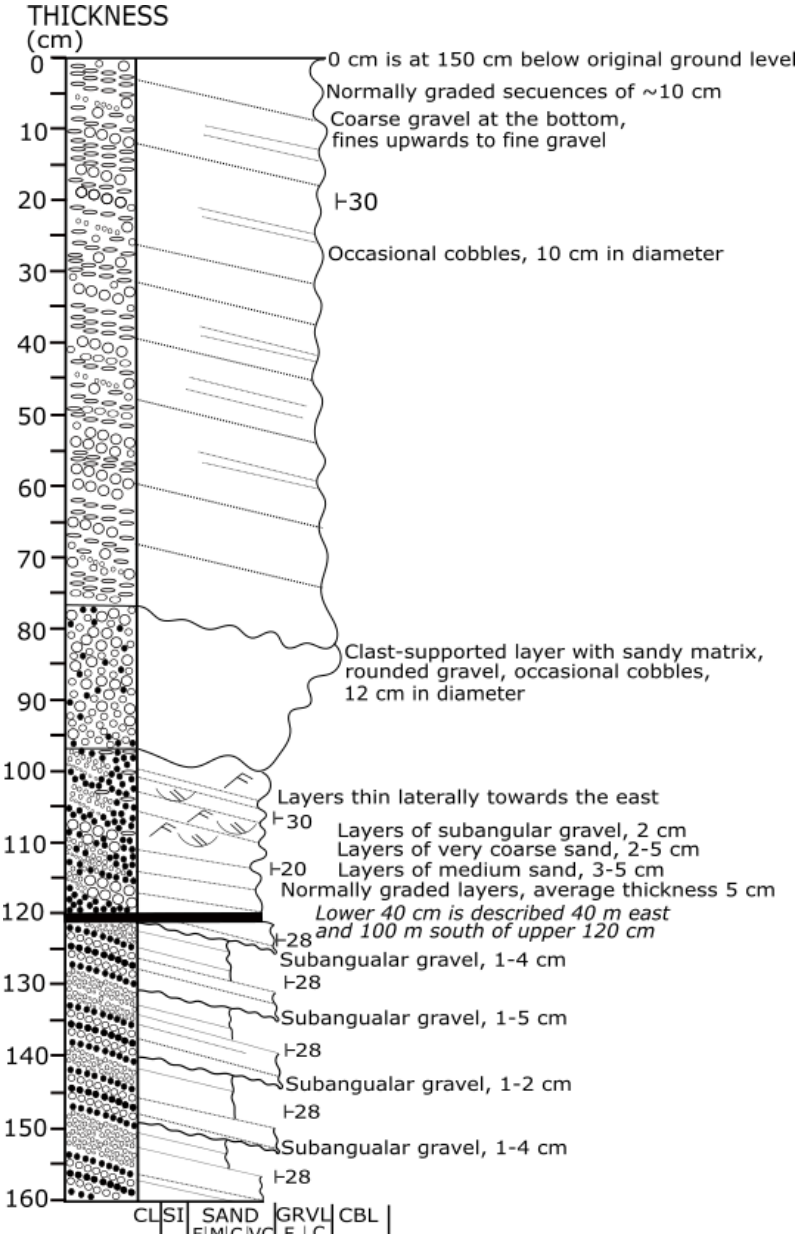

Figure 3.10. Sediment log of V2-1. See figure 3.5 for legend.

Sediment Description. The outcrop is dominated by fine and coarse gravel down to 98 cm depth, and coarse and very coarse sand below. An upper bed 78 cm thick and with an erosive lower boundary has foresets dipping at 30° towards the E. A massive, reversely graded, clast supported bed with sandy matrix and rounded gravel clasts occurs between 78-98 cm. Its lower boundary is erosive. Ripple cross-lamination and trough cross-bedding occur in a layer between 97-120 cm. The bottom 40 cm are dominated by 20 cm thick normally graded beds (very coarse sand and fine gravel at the bottom and coarse sand in the upper part). The beds dip at 28° towards the E.

Above the logged section, layers are subparallel to the landform surface (figure 3.9). Their thickness varies between 5 and 15 cm, and their total thickness vary from 2 m in the NW to 0.5 m in the SE. The layers consist of coarse sand with gravel, and coarse gravel with boulders up to 60 cm diameter. Clasts are sub-angular. The layers contain about 5 % large boulders, 35 % cobbles, 35 % gravel and 25 % sand. Average clast size decreases from around 35-40 cm in the W to 5-10 cm in the SE. The longest axis of clasts are oriented along the strike of the pit wall, larger cobbles dip into the wall, and imbrication is observed in the NW with a direction to the NE.

In addition to the logged points (B and C on figure 3.9), two additional points were measured for strike and dip of dipping beds, height above sea level and thickness of upper horizontal unit (A and C on figure 3.9) (table 3.2).

Table 3.2. Dip and strike of foresets in delta (V2-1), measured at A-D in figure 3.9.

Point on figure 3.9	Dip and dip direction of foresets	Thickness of top sets	Masl of point
A	30°->160°	~2 m	~793
B	30°->140°	~1 m	~792
C	25°->130°	~0,7 m	~791
D	28°->150°	~0,5 m	~768

Sediment Interpretation. The logged section can be interpreted as foresets at a delta with flow towards the SE-SSE. The lake level was falling throughout the delta formation. The reversely graded bed at 78-98 cm might be formed by slumping because of destabilisation of the delta front. The interval 98-120 cm contains sedimentary structures suggesting channel migration. Cross-beds are normally graded and thin in the direction of flow, suggesting that the transport energy decreased in a cyclic manner. The bed may have been deposited by currents with diminishing current strength. The cyclic appearance of the normally graded sand layers with gravel at their base at 120-160 cm can be interpreted as repeated deposition from melting or regular drainage intervals caused by increased flow velocity or material availability. The high degree of sorting and regular bed thickness suggests stable conditions, possibly in relatively deep and stable water. Their cyclic appearance suggest that lake level was stable at the time or decreasing at the rate of delta progradation.

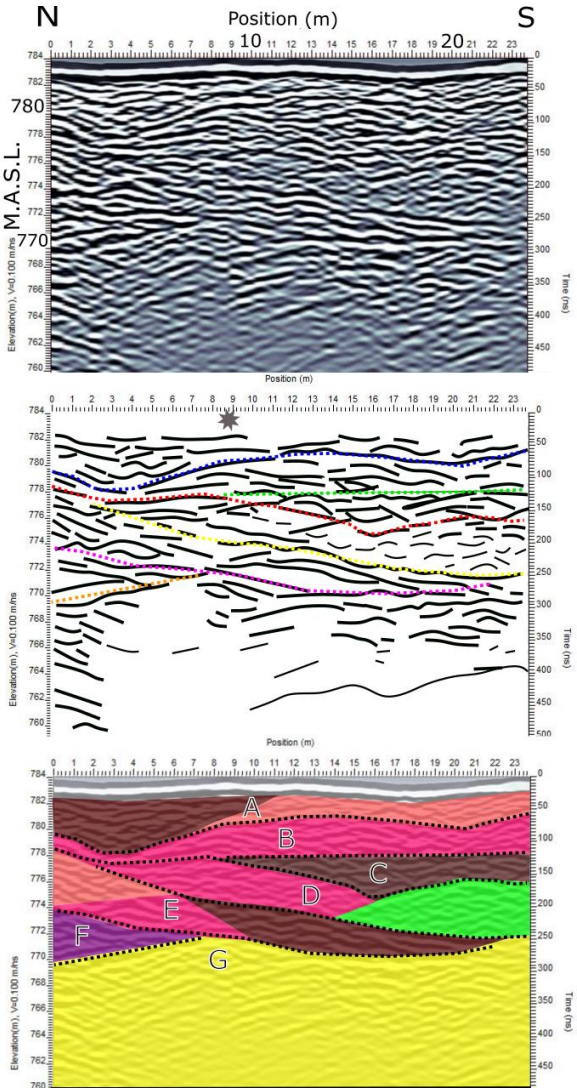

Figure 3.11. Radargram (top), reflectors and interpreted erosive boundaries (middle) and identified facies (bottom), of V2-2, delta, taken parallel to the assumed flow direction. The grey star indicates the intersection with the transverse profile (figure 3.12). The boundaries and facies identification are based on figure 2.6.

Description of Radargram. The profile runs N-S parallel to the assumed flow (figure 3.11). It is taken at the bottom of a gravel pit, hence its flat topography. The main reflectors are sub-horizontal and curved (units A-E), of a moderate dip to both the N and S, but with the Sward direction dominating. They occur at regular vertical intervals of one to five meters, and the units thin towards the S. The profile is dominated by trough- and sigmoidal facies, found within units A, C and E and units B, D and E, respectively. Subparallel (in the upper half, above 774 masl) and oblique divergent and chaotic (in the bottom half, below 776 masl) reflectors also occur. Subparallel reflectors are generally underlain by sigmoidal reflectors, which in turn are underlain by troughs.

The chaotic reflectors in unit D are found in a localised, lens-shaped area to the S between 776 and 773 masl.

Interpretation of Radargram. The trough-shaped and sigmoid reflectors are likely to be channel fills and bars, respectively. The troughs might be cut-and fill sequences. Sigmoidal reflectors might indicate migrating channels (units B-D). The divergent reflectors (unit F) are found at the same depth in both the transverse and parallel directions (figure 3.12), suggesting diversion to both the S and the E. This might suggest lateral changes in the direction of deposition. The lens of chaotic reflectors (unit D) suggests rapid deposition, possibly by gravity flow.

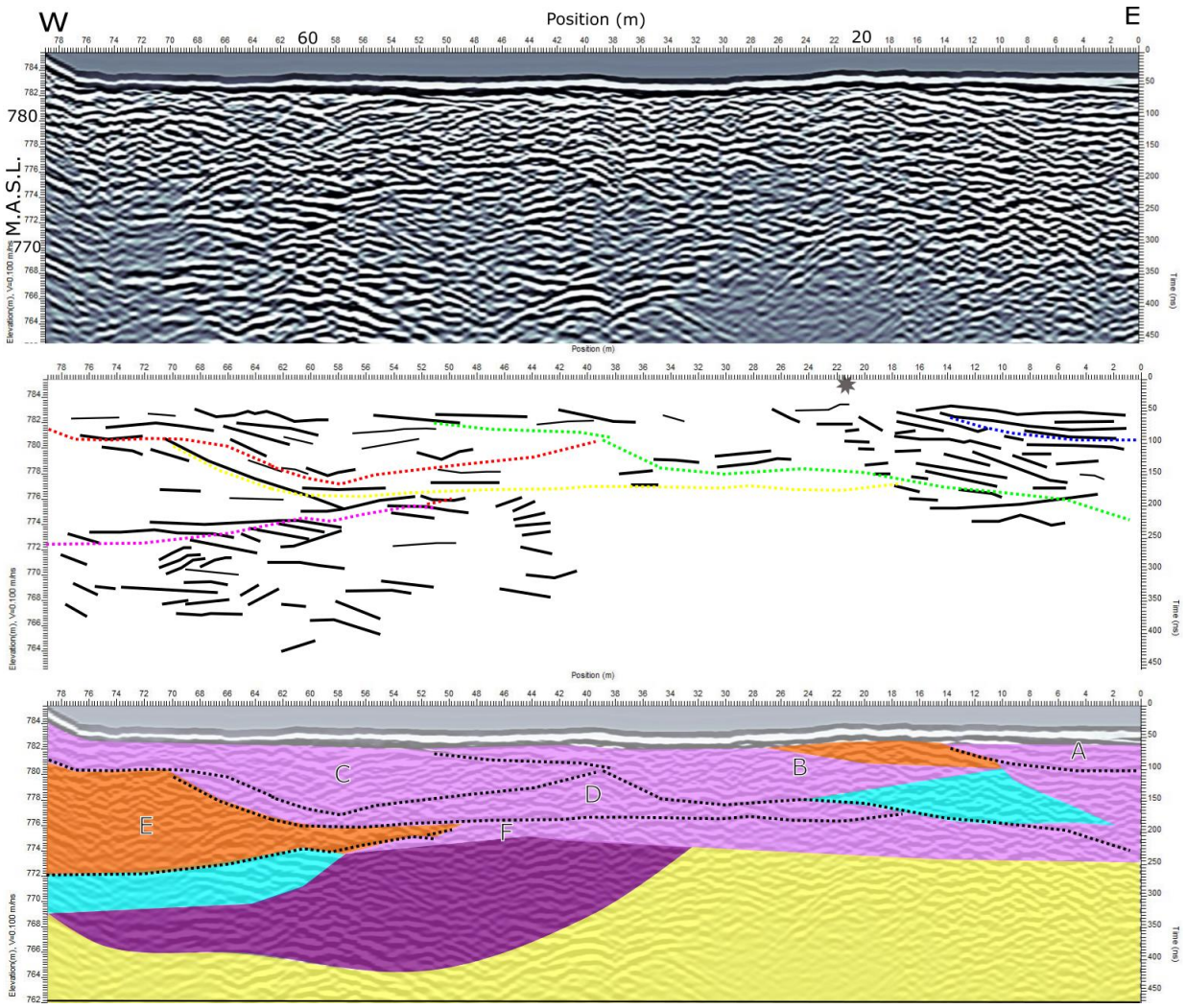

Figure 3.12. Radargram of the V2-1 delta, taken transverse to the assumed flow direction. The grey star indicates where the profile crosses the perpendicular profile. The boundaries and facies identification are based on figure 2.6.

Description of Radargram. The profile runs W-E, transverse to the flow direction (figure 3.12) and is taken at the bottom of a gravel pit, hence its flat topography. The clearest reflectors are sub-horizontal at around 774 masl, and steeply dipping at around 770 masl. The

profile is dominated by dipping reflectors and oblique reflectors, of non-parallel, tangential and divergent nature. Dipping reflectors are found in the upper part of the profile, above 773 masl (units B and E). Most of the reflectors appear to be dipping E. The tangential reflectors appear in close spatial relation with dipping and non-parallel reflectors (units B and F) and are overlain by these. Divergent reflectors appear as a continuation of the tangential (unit F). The reflectors are discontinuous between 38 and 22 m, and the areas below about 761 masl in the W and 772 masl in the E are reflection free.

Interpretation of Radargram. The sediment transport direction has an E component. Unit boundaries, possibly erosive, can be interpreted between 70 and 56 m and 16 and 4 m representing low material availability or a time gap in deposition. These are likely the upper boundaries of delta fore-sets. The dipping and tangential reflectors are found within separate fore sets (units B, E, F). The non-parallel reflectors can represent times of progradation of the delta, where water levels where at a standstill or lowering. If this is the case, the three areas of non-parallel reflectors might reflect three progradational events beginning at a lake level around 774 and 782 masl. The level was then at a standstill before progradation continued when the delta was built out about 20 m further E. The progradation events might suggest that each event deposited about eight meters of sediments, vertically. The dipping reflectors in units B and E are likely cross-stratified beds and can be part of channels of bars. The grey star indicates where the profile crosses the longitudinal profile, indicating that the interpreted cross-stratified beds are part of the channel interpreted in that profile (figure 3.11). The divergent reflectors in unit F might suggest that the rate of deposition changed laterally. The absence of subparallel reflectors suggests that the environment was never transgressive within the interval.

Landform Synthesis and Interpretation. The flow and sedimentation has been to the E and S but the dominating direction is difficult to determine from the GPR data alone. It is likely to have varied throughout deposition. The landform is a prograding delta built out during at step-wise lowering of the lake water level. It is possible that reflectors that appear non-parallel and tangential parallel to flow are sigmoidal transverse to flow, and that dipping reflectors parallel to flow are trough-shaped in the transverse direction.

The deposits above the logged section are delta top sets. The decreasing thickness of beds and size of clast towards the SE and E suggests sediment transport in that direction. The top-sets were formed at palaeo-lake level and their large thickness in the NW suggests high material availability. Grain size decreases in the flow direction and there are no indications of increasing lake levels during deposition.

3.2.4 Sandur Plain in Valley 2 (V2-2)

Landform description. A pit of c. 60x70 m has been dug into the landform. Its original top appears to have been flat (figure 3.13). The sediment log (figure 3.14) is from the middle of the landform looking NW. The lower part of the stratigraphic profile was logged c. 4 m E of the upper part to get a longer and more complete profile (figure 3.13).

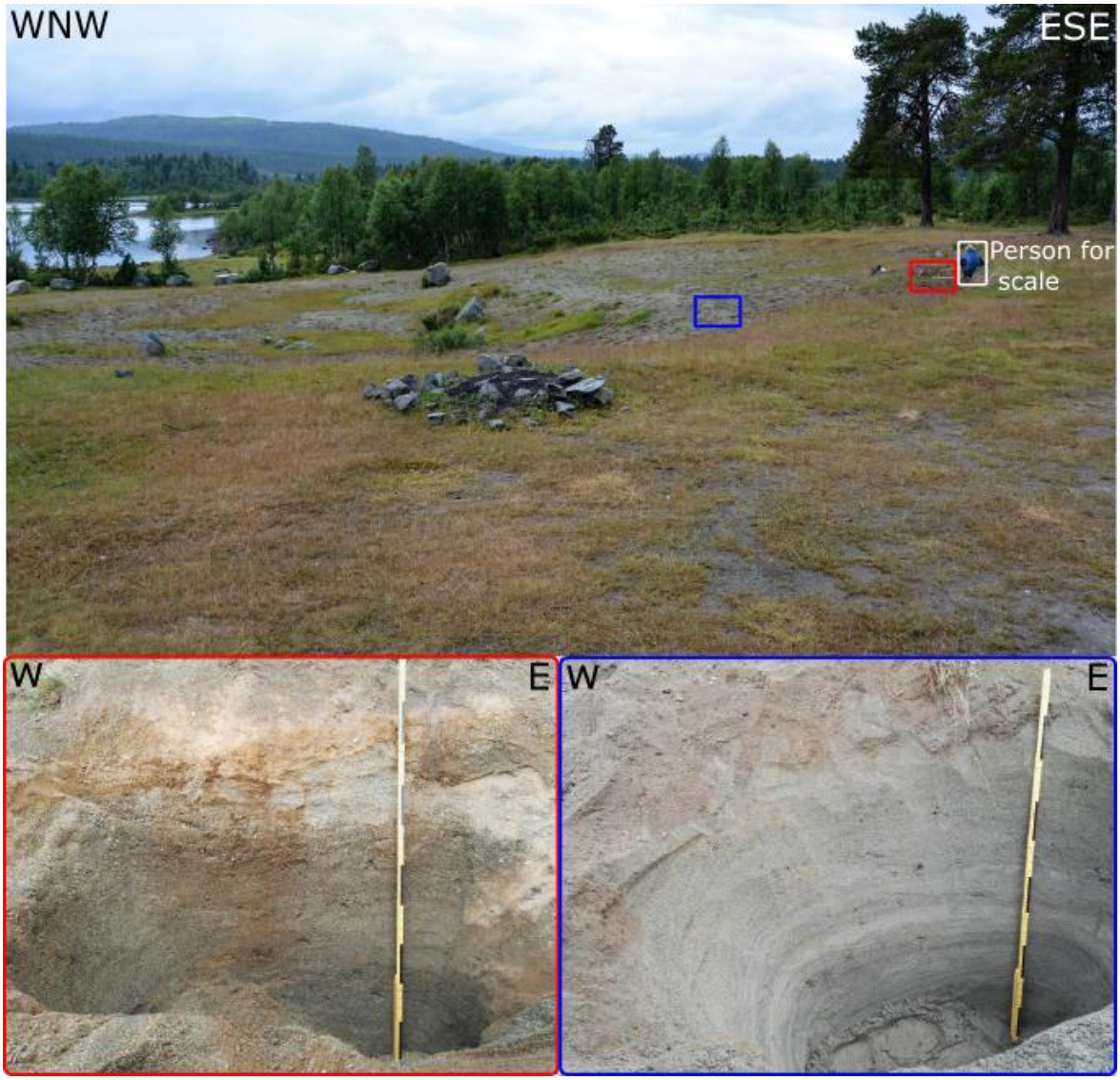

Figure 3.13. Overview of the landform with logged sections. The upper 100 cm of the sediment log in figure 3.14 is from the red area while the bottom 100 cm are from the blue area. See meter-stick for scale (black intervals are 10 cm) and person for scale in overview photo.

Sediment Description. All beds in the log (figure 3.14) are very well sorted, and sedimentary structures frequent. The interval at 0-100 cm is dominated by sub-horizontal, plane-parallel bedding of constant thickness. Layers of fine and coarse gravel dominate the upper 58 cm, while very coarse sand occurs at 58-100 cm. Tabular cross-bedding, ripple cross-lamination and trough cross-bedding occur throughout. The following bed, at 100-129 cm, is characterised by very coarse sand and tabular cross bedding. At 129-142 cm depth, a large

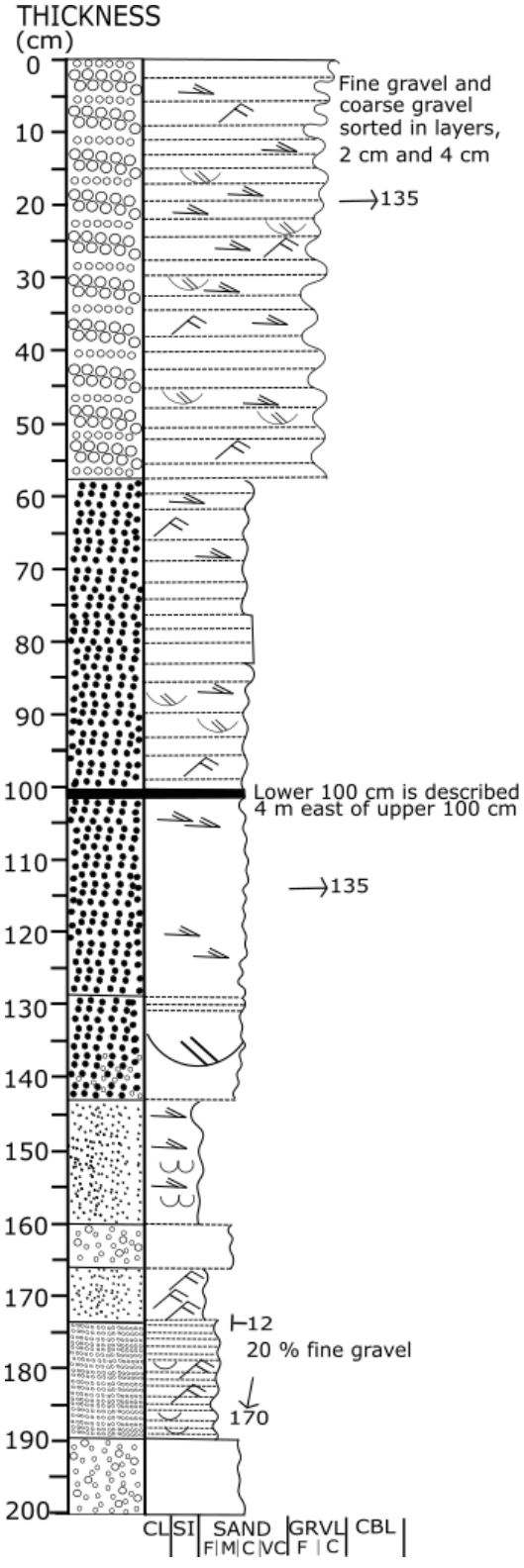

Figure 3.14. Sediment log of V2-2. See figure 3.5 for legend.

trough is overlain by a few plane-parallel beds. Fine and medium sand characterise the interval 142-160 cm, along with tabular cross-bedding as well as ball- and pillow structures at 150-160 cm depth. Two massive layers of coarse sand occur at 160-166 cm and 189-200 cm. Ripple cross-lamination in fine sand is found at 166-174 cm. A grain size change to medium sand occurs at 174 cm, with load structures in addition to ripple cross-lamination, which occurs frequently at 166-189 cm. A current direction towards 135° is observed above 120 cm, and 170° below. The beds dip at 12° towards the E.

Sediment Interpretation. Very well sorted sediments suggest that they were deposited at some distance from the glacier margin. The lower part of the succession, below 142 cm, displays two upward fining intervals starting with gravel. The upward fining and change in sedimentary structures may reflect weakening currents or possibly times of lower lake level following drainage episodes of a lake with water level at around 780 masl. Load casts and ball-and-pillow structures at 174-190 cm and 142-160 cm point to rapid deposition. Currents were possibly relatively stable between 142 and 58 cm, while the upper gravelly part records stronger currents. The trough at 130-140 cm depth can indicate filling of a deeper channel, possibly one of the distributary channels. It was possibly eroded by a significantly stronger flow, and its filling followed by channel migration. Subparallel beds with tabular cross-bedding, trough cross-bedding with troughs transverse to flow, and ripples throughout the unit and especially above 100 cm suggest deposition on a flat, extensive area, probably a river plain with formation of bars. The consistent occurrence of troughs suggests a braided river with migrating channels. There was probably an upward increase in current velocity. This might be due to a lowering of water level or a progradation.

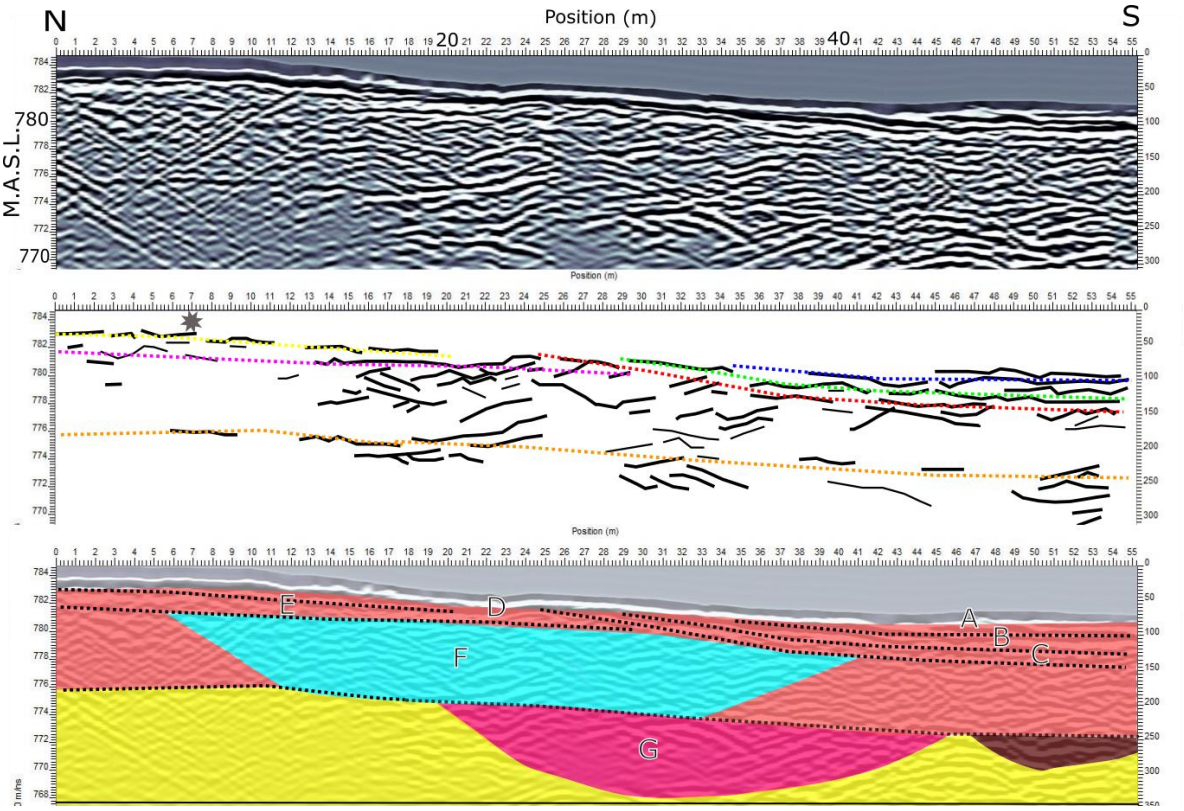

Figure 3.15. Radargram (top), reflectors and interpreted erosive boundaries (middle) and identified facies (bottom) of V2-2, sandur plain, taken parallel to flow. The grey star indicates where the profile crosses the perpendicular profile. The boundaries and facies identification are based on figure 2.6.

Radargram Description. The profile is taken parallel to the sediment transport direction (figure 3.15). The main reflectors are tangential to the erosional boundaries in the middle of the profile, reflector otherwise generally found in the Southern part of the profile, with a general dip to the S. Erosional boundaries are subparallel with a slight dip to the S, and mainly identified at the Southern end of the profile. The uppermost boundaries are tangential to the underlying, giving the appearance of a progressively steeper surface dip with time. The profile is dominated by subparallel, tangential and sigmoidal reflectors, including a trough in the S end at around 774 masl (unit G).

Radargram Interpretation. The tangential reflectors appear to have eroded down into the subparallel ones. The trough is likely to be the fill of a palaeochannel, possibly the same channel that deposited the sediment with sigmoidal reflectors (unit G). Assuming this is true, the channel shifts direction within the same depositional unit suggesting a braided river system. The erosional boundaries give the impression of a tilted area, and possibly deeper erosion after deposition of unit D, at 783 masl. It is possible that the area was flat, but that erosion occurred evenly across the surface and not by channels forming cut- and fill structures. The absence of cut- and fill structures in units A-C suggests that they were deposited in calmer water, probably across a flat, shallow-water area. The grey star indicates

where the profile intersects the flow-transverse profile. It appears that the reflectors at that point are subparallel in both directions. This might suggest that the units found at 782 masl were deposited by sheet floods.

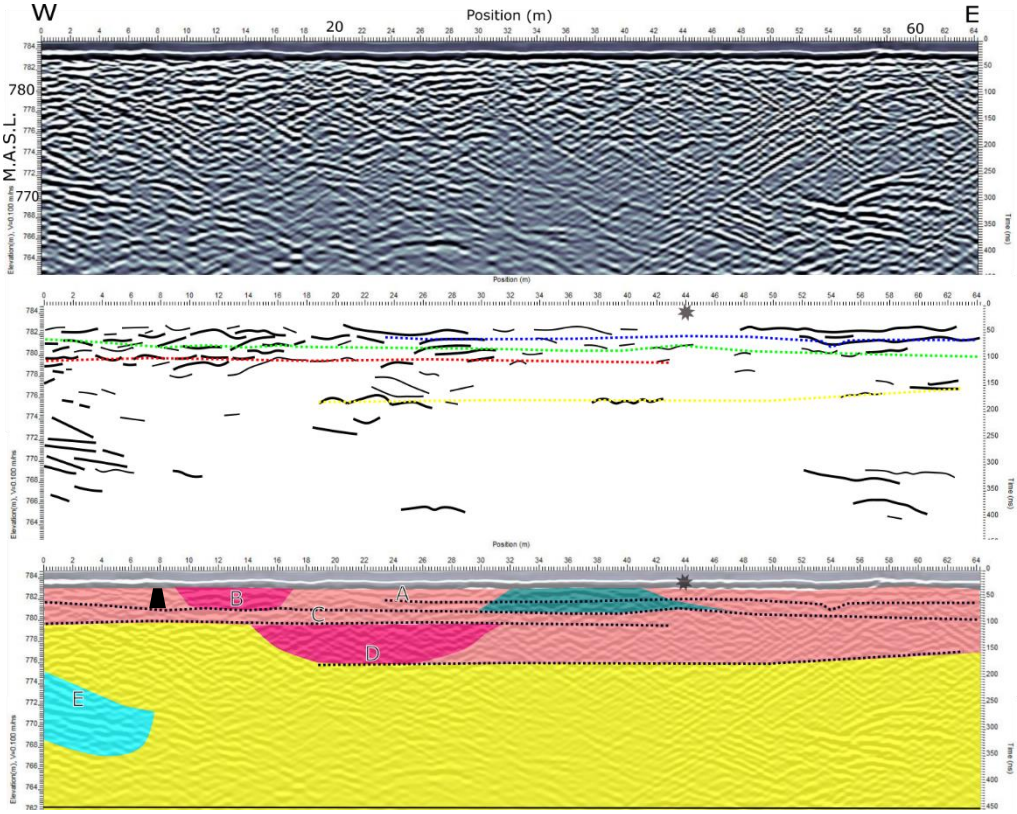

Figure 3.16. Radargram (top), reflectors and interpreted erosive boundaries (middle) and identified facies (bottom), of V2-2, sandur plain, taken transverse to flow. The grey star indicates where the profile crosses the perpendicularly taken profile. The boundaries and facies identification are based on figure 2.6. The black trapes indicates where the stratigraphic log is described.

Radargram Description. The profile is taken transverse to the flow direction on the sandur plain (figure 3.16). The main reflectors are sigmoidal and tangential. Erosional boundaries are identified as plane-parallel, regularly spaced (two to four meters) surfaces. Subparallel (units A-D), sigmoidal (units B and D) and tangential (unit E) facies dominate the profile, while a two-meter thick interval between 30 and 40 m appears discontinuous. The subparallel reflectors alternate with the sigmoidal. No clear dip of the reflectors can be seen, except towards the E among the tangential reflectors.

Radargram Interpretation. The plane-parallel depositional surfaces suggest long-term, low-energy water flow and horizontal deposition. The subparallel reflectors might be the result of sheet floods (units A-D). The sigmoidal reflectors can also represent sheet floods (units B and D), and are possibly the results of bars, potentially migrating channel bars in unit D where the strata are dipping in the flow direction. Both the sigmoidal and tangential reflectors can indicate a dipping surface during deposition, and progradation (units B, D, E). The sigmoidal

and tangential reflectors might be differently oriented expressions of the same channel deposition processes, suggesting that the direction of water flow has changed from a stronger Southern component to stronger Eastern component throughout the interval. The discontinuous reflectors cross erosional boundaries and is therefore unlikely to be the result of primary sedimentary structures.

Landform Interpretation. The landform is a sandur plain that formed as meltwater entered a flat, open area. According to (Banerjee and McDonald, 1975b), the thin gravel beds and structures observed are common in sandur deposits. The GPR facies suggest vertical accretion and progradation. The deposits in this landform are likely to have been laid down after the delta deposits, V2-1. They probably overlay distal delta deposits (bottom set beds).

3.2.5 Eroded Fan Deposits in Valley 2 (V2-3)

Landform description. The landform (figure 3.17) is the second highest of four terraces. It is 250 long, 30 m wide, 6 m high and dips at 20° towards S. The long axis of the terrace strikes 160°. The sediment log (figure 3.18) is from the central part of the terrace, facing N.

Figure 3.17..Photo of fan deposits (V2-3), facing WSW. The yellow line marks the surface of the deposits, likely a fan lobe eroded along the side in the SSE.

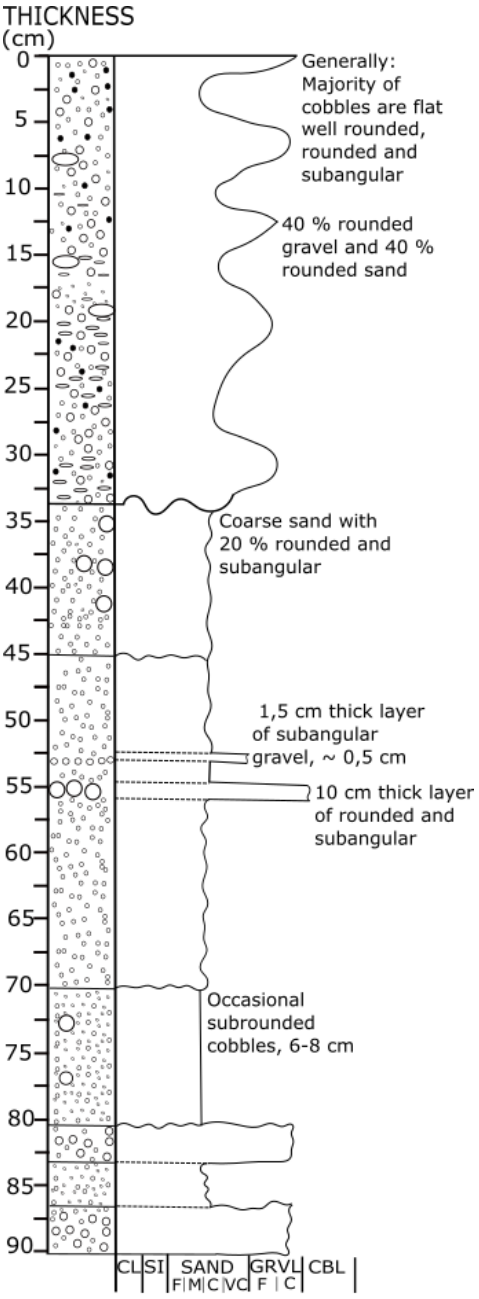

Figure 3.18. Sediment log of V2-3. See figure 2.5 for legend.

Sediment Description. The outcrop is characterised by massive sediments and beds with erosional boundaries. The uppermost bed (0-33 cm) has poorly sorted material ranging from silt to coarse gravel in a matrix of fine gravel. Below 33 cm depth, coarse sand dominates, interspersed with layers of coarse gravel and boulders (figure 3.18). Clasts are flat, circular and rounded in the upper 33 cm, and rounded and sub-angular below 33 cm. Erosive boundaries are found at 33, 45, 70 and 80 cm. The interval between 45-70 cm has some vague plane-parallel beds. All beds appear sub-horizontal, with a gentle dip either in or out of the section.

Interpretation. The logged sequence is found on a terrace, and presence of boulders suggests proximal deposition. If deposition was in an ice-dammed lake, coarse sand and gravel would have been deposited in a proximal position on the flat, while fine sand and silt would be brought further out into the water body. Coarse sediments can be deposited as bedload in subparallel sheets at ice dammed lakes (Herget, 2005). The poorly sorted 33 cm thick bed at the top may have been deposited as a debris flow or in a channel during upper flow regime conditions. Except for occasional large boulders, the interval below 33 cm is well sorted, suggesting redeposited glacifluvial material. Flat, circular cobbles suggest mature material. It is possible that meltwater supply was from the W from the same channel system that deposited the kame terrace in the valley side in the NW corner of Valley 2.

The logged sequence may be part of a fan lobe. The general lack of sedimentary structures can be due to vertical collapse, in which case the sediments might have been laterally supported or overlain by ice. Deposition of the lower beds may have occurred on the proximal part of a fan system influenced by shoreline processes as the lake level lowered. The uppermost bed may have been deposited by gravity flow during erosion of e.g. a kame terrace that was destabilised by ice-wall removal or shore line erosion.

3.2.6 Palaeo-shoreline in Valley 2 (V2-4)

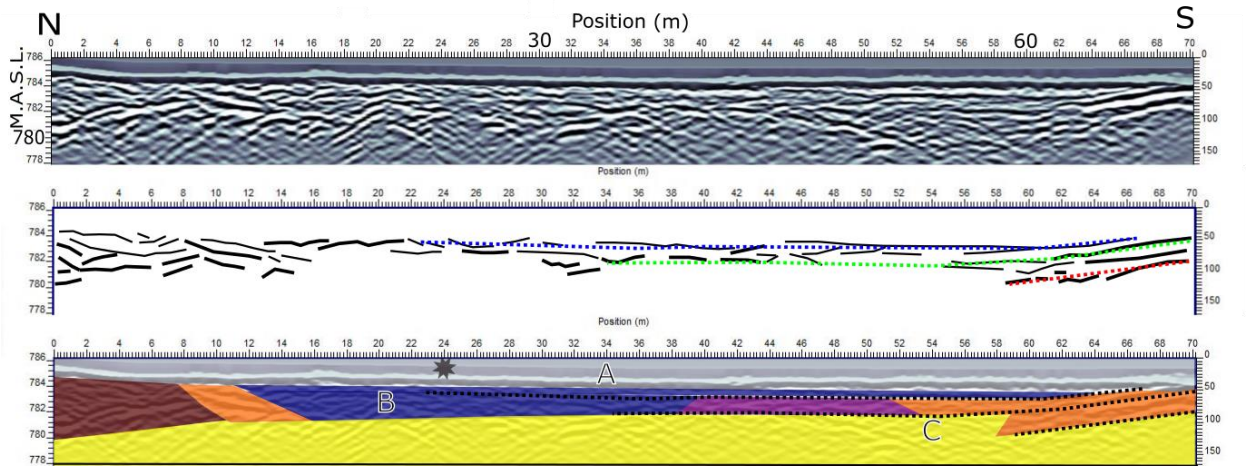

Figure 3.19. Radargram (top), reflectors and interpreted erosive boundaries (middle) and identified facies (bottom), of V2-4 palaeo-shoreline, taken parallel to flow. The boundaries and facies identification are based on figure 2.6. The grey star indicates where the profile crosses the perpendicularly taken profile.

Radargram Description. The profile is taken along the long axis of the terrace (figure 3.19). Three subparallel erosional surfaces are identified in the Southern part of the profile. Dipping reflectors are found in both the N and S (units B-C), trough-shaped reflectors in the N (unit B), and plane-parallel and divergent reflectors in the middle (units A-B). Unit B contains all the reflectors described. The profile is shallow, especially compared to the other profiles.

Radargram Interpretation. The surface of the terrace might represent a palaeo-shoreline. The three oldest erosional boundaries might represent falls in water level. As one unit contains all the identified reflectors (unit B), the depositional environment is variable across the landform. The sequence can be interpreted as a shore-face deposits, where the facies to the very N and S (units B and B/C, respectively) are beach face deposits (based on the shore-face model developed by Prothero and Schwab (2004)). This suggest a progressive regression, where the water level has fallen from just below 786 masl (when unit A was deposited), to a few meters below 784 masl (when unit B was deposited), to a few meters below 781,5 masl.

The plane-parallel reflectors show vertical accretion. The dipping and trough reflectors to the N in unit B can be interpreted as the beach face, or possibly the longshore trough, formed when the water level was a few meters below 784 masl. The plane-parallel reflectors in unit B can possibly be the longshore bar crest, as described by (Prothero and Schwab, 2004). The divergent reflectors that follow may then be part of the slope, or potentially troughs within the longshore bar crest. The dipping facies in unit B can be interpreted as the seaward slope. The erosional boundary between this facies and the dipping facies in unit C suggests that the water

level fell at this time (at 781,5 masl), and a new sequence was deposited where the dipping reflectors represent the beach face.

Alternatively, the sediments were deposited parallel to the valley. The sub-horizontal layers extend in both directions, and channel erosion is difficult to infer. Either way, the homogenous sediment nature and sub-horizontal stratification suggests that the sediments are glacifluvial, and not till. This interpretation excludes the possibility that the landform is erosional (in till) and not depositional. The shallow penetration of the profile suggests that a change occurs a couple of meters down. This can be due to a change in sediment nature, possibly till.

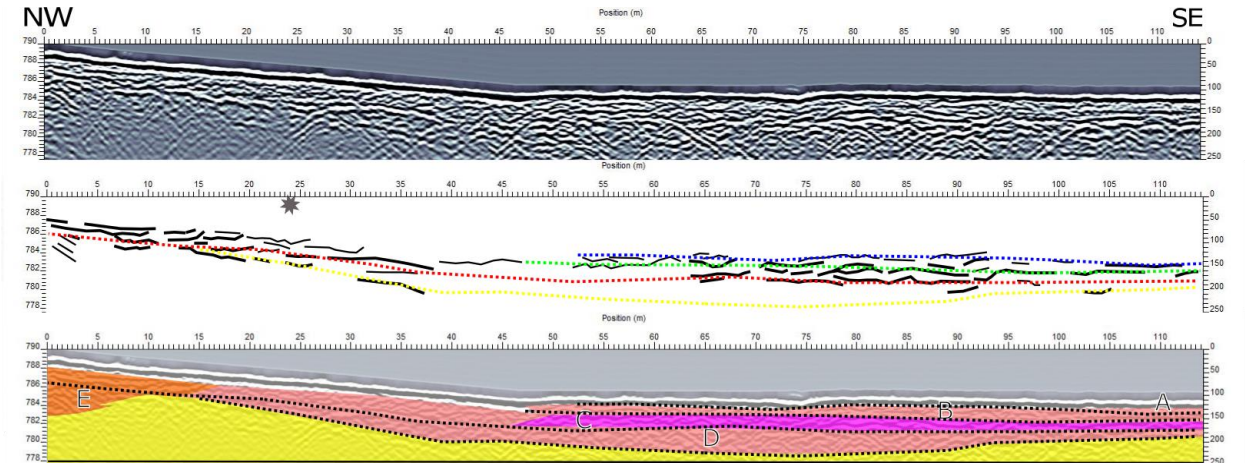

Figure 3.20. Radargram (top), reflectors and interpreted erosive boundaries (middle) and identified facies (bottom), taken transverse to the landform. The boundaries and facies identification are based on figure 2.6. The grey star indicates where the profile crosses the perpendicularly taken profile.

Radargram Description. The profile is taken transverse to the landform (figure 3.20). Subparallel erosional surfaces dipping slightly SE are found at around 786, 784 and 780 masl. The profile is dominated by dipping, subparallel and sinusoidal reflectors. The sinusoidal reflectors (unit C) are found beneath the subparallel in both vertical and horizontal direction. The subparallel (units A-D) are found beneath the dipping in both the vertical and horizontal direction (units A-D). The dipping reflectors appear to be interfingering (units C and E), but the downstream and underlying reflectors are obstructed by hyperbolas. The units are thin, extensive and repetitive.

Radargram Interpretation. The profile is located between two fore shore deposits, and consequently between two water level stands. The interpreted deposits were laid down during the lake level change. The vertical sequence observed consists of upper shore face deposits (dipping reflectors), proximal lower shore face deposits (subparallel reflectors) and distal lower shore face deposits (sinousoidal reflectors). The subparallel reflectors appear as inland deposits above seaward deposits, which implies that a regression has taken place throughout the interval.

The erosional surfaces are found at similar elevation as the ones identified in the crossing profile. The subparallel reflectors in units A-D are likely hummocky cross stratification found at the lower part of the palaeo-shore face. The dipping reflectors are likely to be deposits at the fore shore or the upper shore face. Assuming a regression has taken place throughout the interval, sequence stratigraphy suggests that the younger deposits further inland would be found in the same order vertically as horizontally (Catuneanu, 2006). This implies that the lower shore face deposits are found beneath the upper shore face deposits, which in turn are found underneath the fore shore deposits. This appears to be the case, assuming subparallel reflectors represent proximal lower shore face deposits, sinusoidal reflectors represent distal lower shore face deposits (in unit C), dipping reflectors represent the fore shore (of both units C and E). The horizontal transition of reflectors in unit C suggests that the palaeo-shoreline is curved, so that the straight profile appears transverse in relation to the deposits. Unit C appears to have eroded away distal deposits of unit D. If the radargram indeed show a regressive sedimentary unit, the lowering of water level is likely to be related to drainage of the water body.

3.2.7 Fan Lobe in Valley 2 (V2-5)

Landform description. The landform (figure 3.21) is a NW-SE striking ridge that is 250 m long, 40 m wide and 5 m high. A palaeochannel parallel to the NW side of the fan lobe is shown in figure 3.22. The landform appears to be a lobe of a larger fan (figure 3.23). The larger fan is 750 m long and 310 m wide with a steep slope towards the SE. It is cut through by a road and a gravel pit. The logged section (figure 3.24) is from the middle of the SW side of the ridge facing NW.

Figure 3.21. Photo of fan lobe, facing NW. Yellow line indicate the slope perpendicular to the long axis of the lobe, the orange line runs along the long axis of the lobe.

Figure 3.22. Photo of palaeochannel parallel to the NW fan lobe, facing S.

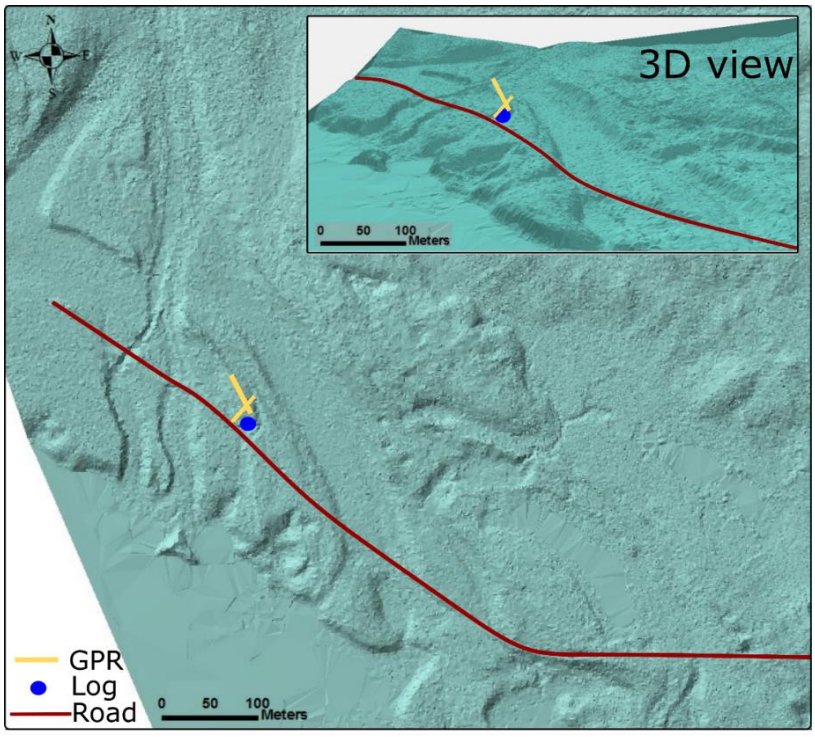

Figure 3.23. Shaded relief visualisation of LiDAR data from landform V2-5 and surrounding areas with a hill shade azimuth at 325°. GPR: GPR profile. Log: Sediment log.

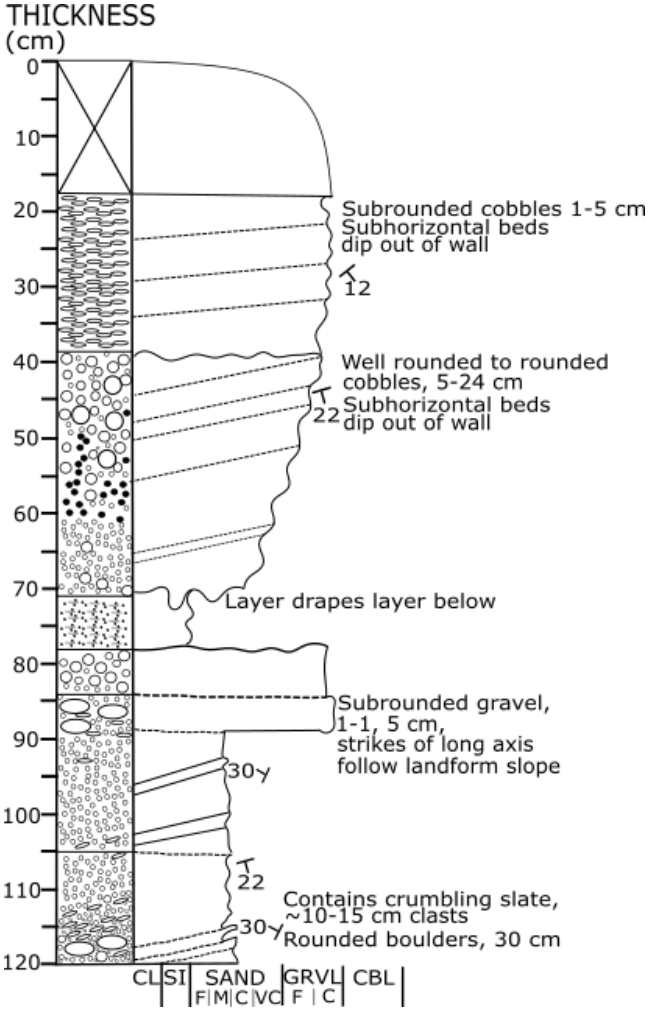

Figure 3.21. Sediment log of V2-5. See figure 3.5 for legend.

Sediment Description. The outcrop is dominated by beds of sorted sand and gravel dipping at 12°-22° and 30° to the SE and NW, respectively (figure 3.24). The interval at 18-39 cm consists of angular coarse gravel and sub-rounded cobbles, angled in the slope direction. Regularly spaced beds dip at 12° towards the S and E. An erosive boundary follows at 39 cm, underlain by a poorly sorted, reversely graded interval from 39-71 cm. Irregularly spaced cross beds dip at 22° with a stronger S component than above. Silty fine sand occurs at 71-78 cm. Sharp, undulating boundaries are found at 71 and 78 cm. Massive, sorted gravel occurs at 78-90 cm; at 84-90 cm with cobbles. At 90-105 cm, coarse sand with steep, S-dipping cross-beds are found. The interval between 105-120 cm also consists of coarse sand, with dipping gravel cross-beds at its base. Elongated clasts are found with long axes in the direction of the hill slope at 81 cm, while rounded boulders with an average size of 15 cm are found below 84 cm.

Sediment Interpretation. The sequence consists of beds with varying grain sizes ranging from silt to cobbles which can suggest a wide range of current velocities. The flow regime appears to have increased from the lower to the upper part of the succession. It is evident from the LiDAR-data that the logged sequence is part of a fan lobe. The alternation between sand and gravel might be a result of changes in which different parts of the fan were active at different times during deposition, as described by (Jo et al., 1997). The coarser, clast-supported intervals, e.g. at 84-90 cm may be deposited by debris flows. Coarsening up intervals and difference in dip of bed foresets suggest channel switching and progradation of bars with lateral displacement of flow. The fine-grained layer at 71-78 cm may have been deposited in a temporarily abandoned channel.

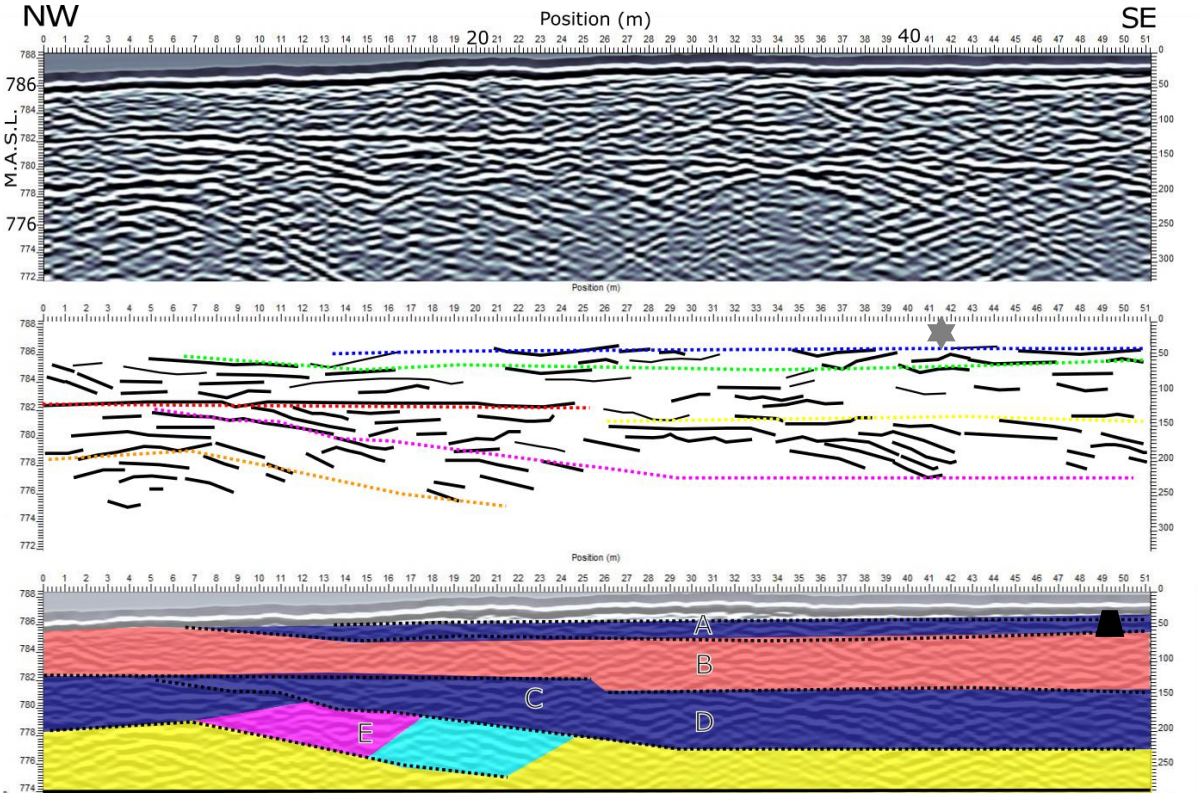

Figure 3.22. Radargram (top), reflectors and interpreted erosive boundaries (middle) and identified facies (bottom), of V2-5, fan deposit, taken parallel to flow. The boundaries and facies identification are based on figure 2.6. The grey star indicates where the profile is cross-cut by the perpendicularly taken profile. The black trapes indicates where the stratigraphic log is described.

Radargram Description. The profile is taken parallel to the direction of flow (figure 3.25). Erosional boundaries are regularly spaced and extensive. They are plane-parallel in the SE and weakly undulating around 780 masl with a dip to the SE. The main reflectors are plane-parallel and subparallel (units A-D). Sinusoidal and tangential reflectors are found in the oldest identified unit (E) just below 780 masl.

Radargram Interpretation. The parallel and subparallel reflectors suggest vertical accretion. According to (van Overmeeren, 1998), glaciofluvial fans can be recognized from a "high reflection amplitude and continuity and parallel stratified sequences". The subparallel reflectors along with clear erosional boundaries support this interpretation (unit B). The lack of channel deposits suggest that the profile is from the lower part of the fan. The sigmoid and tangential reflectors, however, can be interpreted as channel fill (unit E). In that case they are likely to be distributary channels to the lobe and fan deposition must have decreased with time to allow build-up of distal sediments (further from the source) above proximal. It is also possible that the sigmoidal and tangential reflectors represent shingled stacks of sediments in the lower fan, and not channel deposits.

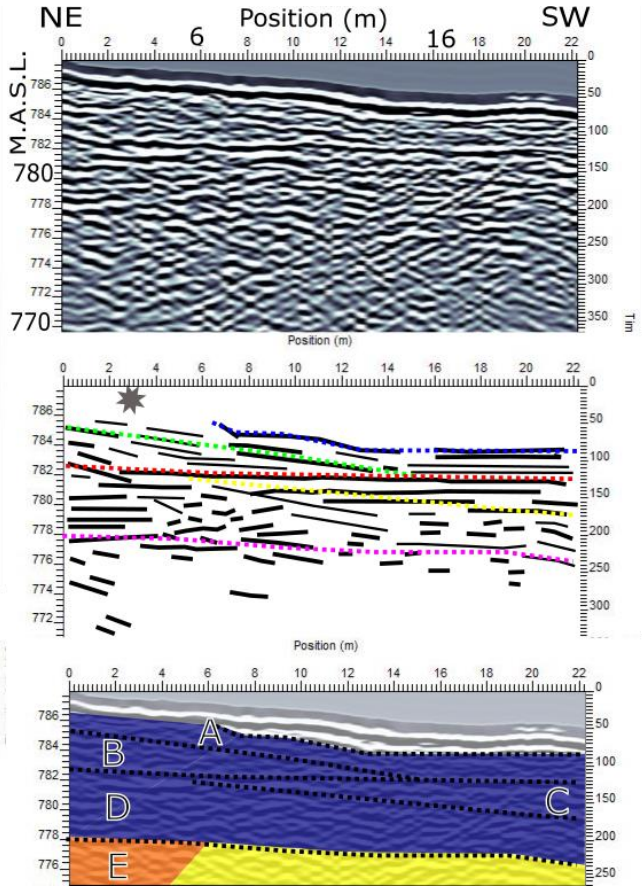

Figure 3.23 Radargram (top), reflectors and interpreted erosive boundaries (middle) and identified facies (bottom), of V2-5, fan deposit, taken transverse to flow. The grey star indicates where the profile crosses the perpendicularly taken profile. The boundaries and facies identification are based on figure 2.6. The grey star indicates where the profile is cross-cut by the perpendicularly taken profile. The black trapes indicates where the stratigraphic log is described.

Radargram Description. The profile is taken transverse to the fan deposit and the direction of flow (figure 3.26). Erosional boundaries extend across the profile and are oblique with a slight dip to the SW. It is dominated by plane-parallel reflectors (units A-D). Dipping reflectors are found in unit E.

Radargram Interpretation. It appears that the plane-parallel reflectors in the upper units are plane-parallel in all directions (units A-D). The dipping reflectors in unit E might be the cross-sectional view of the sigmoidal or tangential reflectors in the perpendicular profile (figure 3.25). If that is the case, they are likely to represent a distributary channel on the lower fan and not shingled stacked deposits. The interpretation is similar to that of the perpendicular taken profile (figure 3.25).

Landform Interpretation. Gravity flow deposits and lateral variation suggest that the sediments are fan deposits. The radargram profiles are from the lower fan and show aggrading units and vertical stacking. The fan has regraded throughout deposition, and a rapid change in deposition occurred around 780 masl.

3.2.8 Kame Terrace in Valley 3 (V3-1)

Landform description. The landform occurs on the S side of valley 3. It is egg-shaped with a NW-SE strike and has very steep N, NW and W sides (30°). The E side is moderately steep (15°), and the S side is flat and continuous. The landform is 86 m long, 40 m wide and 8 m high. The log is from its NW corner facing SSE.

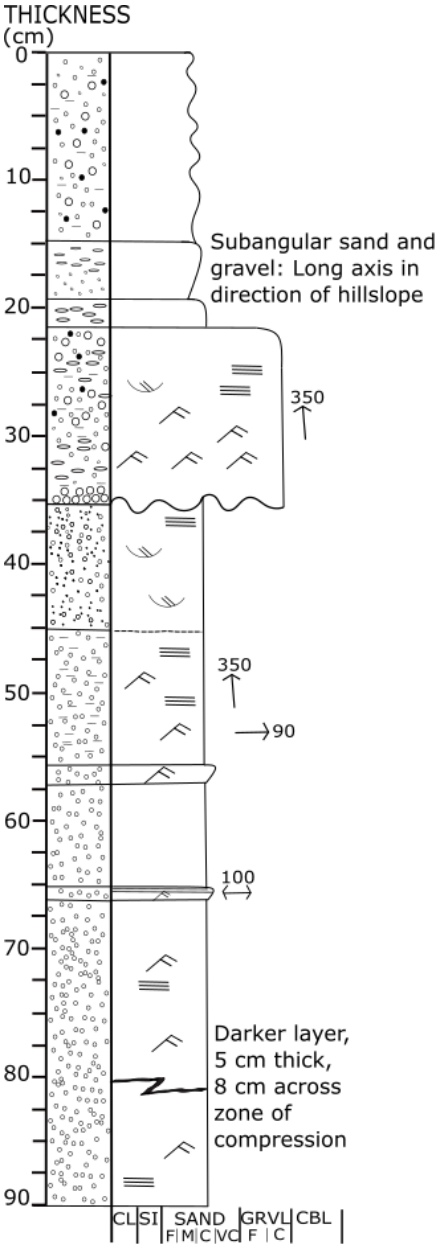

Figure 3.24. Sediment log of V3-1. See figure 3.5 for legend.

Sediment Description. The sediment outcrop is characterised by abundant ripple cross-lamination (figure 3.27). Plane-parallel lamination and through cross-bedding occurs regularly below 22 cm. Dominating grain sizes are sand and gravel, with sorted coarse sand below 58 cm. A bed of massive, gravelly coarse sand occurs at 0-15 cm. Following are two reversely graded layers at 14-19 cm, with the long axis of fine gravel oriented in the direction of the hill slope (down slope). A bed dominated by coarse gravel with ripples, planar lamination and though cross-bedding is found at 21-35 cm depth, above an erosional surface. Sorted coarse gravel occurs in the lower part of the bed, which cuts into beds of fine to coarse sand at 35-45 cm. Upward fining layers of very coarse sand are found at 55-57 cm and 65-66 cm depth. A dark interval, possibly representing a thrust, is found at 80 cm depth. Symmetrical current ripples at 65 cm depth indicate a palaeocurrent direction at 100-280°, while unidirectional palaeocurrent is measured (from asymmetrical ripples) towards 90° at 52 cm and 350° at 28-49 cm.

Sediment Interpretation. The sediments were mainly deposited in the lower flow regime, probably in a braided river system dominated by shallow channels. The poorly sorted, massive layer above 15 cm can represent dumping of sediments during waning current or a vertical collapse, possibly due to ice wall melting. The erosive boundary with sorted gravel at 35 cm depth suggest increasing current velocity and development of a through or a shallow channel. This was subsequently filled with gravelly sediments transported by the river as bedload. In the layer between 22-35 cm, finer particles can have settled down between the coarser particles until it clogged, as described by Frostrick et al. (1984), which suggests a decreased discharge from the current. Normal grading in the top of the bed also suggests decreasing discharge, and the sedimentary structures suggest regular bedload transport. The well sorted coarse-grained sand layers with ripples and planar lamination below 35 cm were probably deposited under moderate current conditions, possibly in an inter-channel area or shallow plain. Episodes of stronger currents are represented by the two upward coarsening layers. Poor sorting above 45 cm may suggest rapidly decreasing current strength. The fault structure at 80 cm suggest a collapse, possibly due to the removal of support from an ice wall.

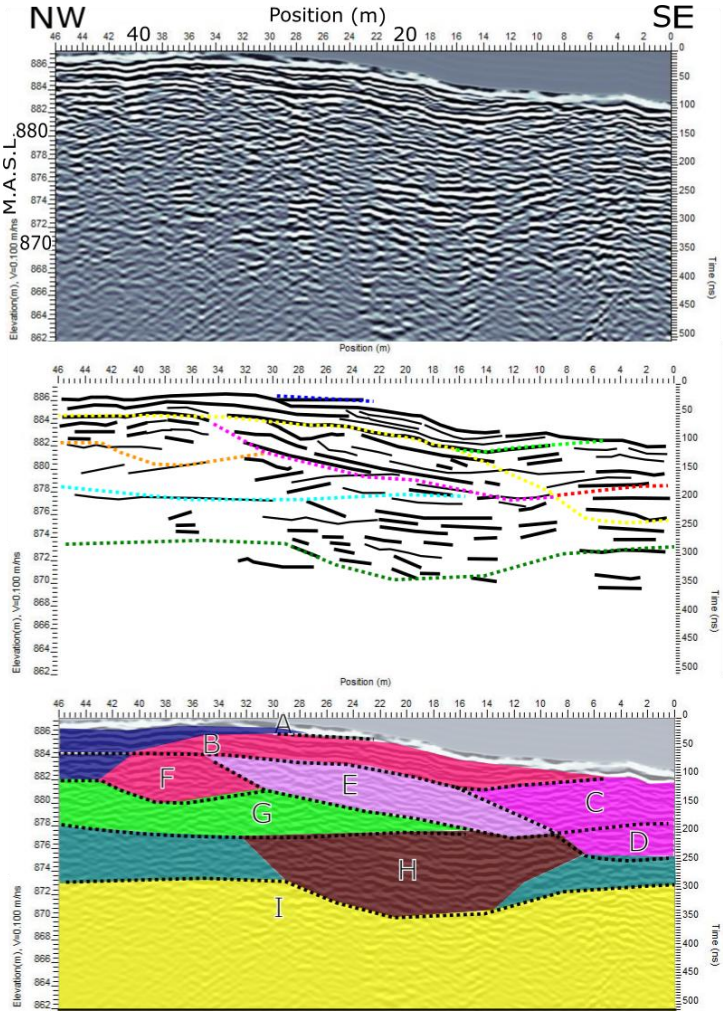

Figure 3.25. Radargram (top), reflectors and interpreted erosive boundaries (middle) and identified facies (bottom), of V3-1, kame terrace, taken parallel to flow along the outer edge of the landform. The boundaries and facies identification are based on figure 2.6. The black trapes indicates where the stratigraphic log is described.

Radargram Description. The profile is taken along the longest axis of the kame terrace, on the NE side, parallel to flow. It has a relatively complicated composition, and its facies are largely divided into separate units (figure 3.28). Oblique erosional boundaries with a weak dip to the SE occur. It contains plane-parallel reflectors in the NW (units A, B, F), sinusoidal reflectors in in SE (units C-D), and sigmoidal, oblique and chaotic reflectors at progressively deeper levels in the middle (units B, E, F-G). The oldest unit (H) contains trough-shaped reflectors in the middle, flanked by discontinuous reflectors at both sides. Sigmoidal reflectors appear as lateral continuation of plane-parallel reflectors (units B and F).

Radargram Interpretation. The variation in type and distribution of facies suggests that the depositional environment has been highly variable. Variation in flow regime and direction has caused variable channel fills and erosion. The trough-shaped reflectors (unit H) might reflect a cross-sectional view of a channel, while the sigmoidal reflectors are a result of an oblique angel relative to the flow (units B, F). The discontinuous reflectors on the sides (unit H) can represent progradation in a lateral direction. They might also be an expression of poor bedding. Both the sigmoidal and oblique reflectors might be an expression of SE progradation of the deposits (units B, E-F). The sigmoidal reflectors can be interpreted as migration of channel bars towards the SE. The change between plane-parallel and oblique reflectors (units A-B, F and unit E, respectively) can be caused by a change in flow regime as well as a change in direction of flow. The chaotic reflectors in unit G can be caused by several factors, e.g. high boulder content, or massive, structureless deposits. It might also be that deposition was rapid, allowing soft-sedimentation to take place. It is most likely a combination, where high energy deposition led to a high boulder content and lack of clear

structures. The sinusoidal reflectors are probably caused by a lack of clear bed development or progradation of the landform to the SE.

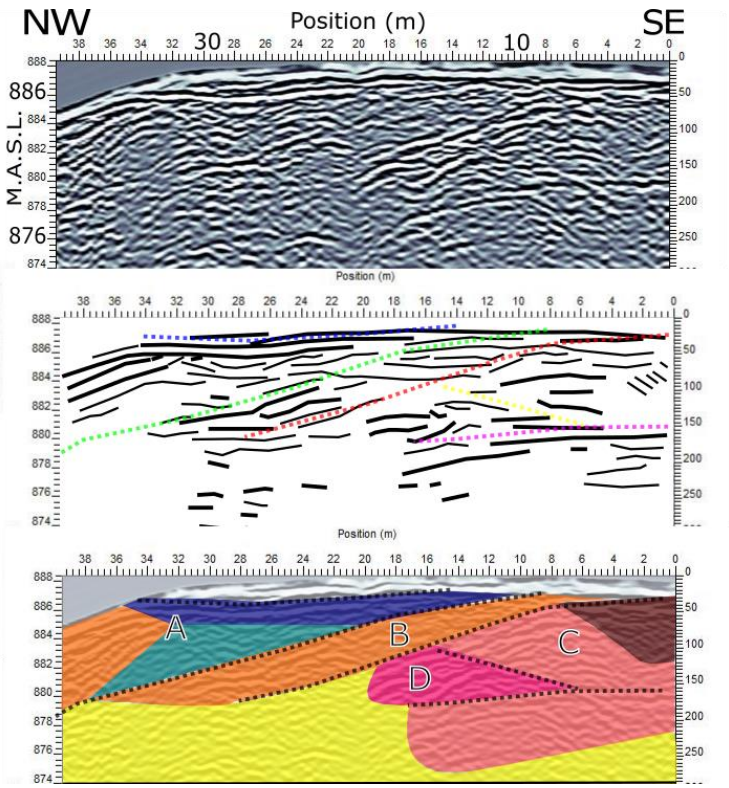

Figure 3.26. Radargram (top), reflectors and interpreted erosive boundaries (middle) and identified facies (bottom), of V3-1, kame terrace, taken parallel to flow at the inner area of the landform. The boundaries and facies identification are based on figure 2.6.

Radargram Description. The profile is taken parallel to the line in figure 3.28, along the longest axis of the kame terrace and parallel to flow, but further from the NE margin (figure 3.29). It contains erosional boundaries that are surface-parallel, and some with apparent dip to the NW. It has a complex structure but contains similar facies to figure 3.28. The main difference is the absence of oblique reflectors. It contains plane-parallel and dipping reflectors in the NW (units A-B), and subparallel, sigmoidal and trough-shaped reflectors in the SE (units CD).

Radargram Interpretation. The absence of oblique reflectors in this profile possibly suggests deposition proximal to the landform edge. be formed proximal to the landform edge. It appears that the landform is very asymmetric in the longitudinal direction. The trough- (unit C) and sigmoidal (unit D) reflectors are channel expressions, and their relative age possibly suggests that the direction of flow changed from mainly towards the E and then towards the SE with time. The chaotic reflectors (unit A) are probably caused by high-energy deposition, and a high boulder content. The upper dipping reflectors (unit A) suggest s high influence of surface topography at the end of formation, where possibly stabilising ice walls were gone.

Radargram Description. The profile links up with the profiles in figures 3.28 and 3.29 but is taken transverse to the landform and interpreted flow direction (figure 3.30). The profile contains subparallel erosional boundaries. The youngest reflectors are subparallel (units A-B), and the older are oblique with an apparent sip to the NE (units C-E). Sigmoidal and divergent reflectors are found in the NE (units C-D).

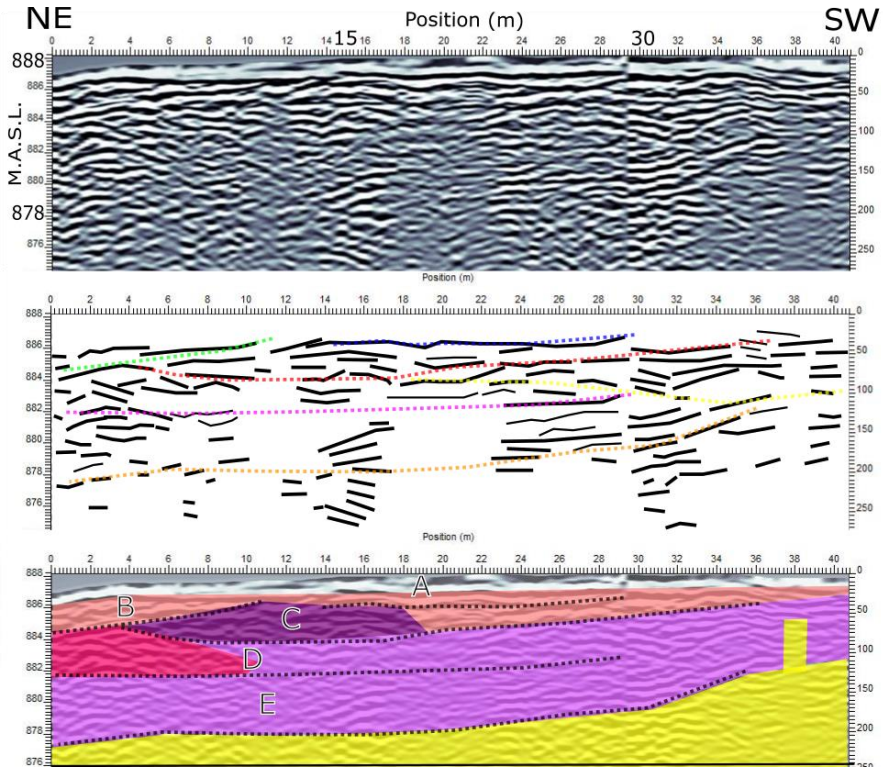

Figure 3.27 Radargram (top), reflectors and interpreted erosive boundaries (middle) and identified facies (bottom), of V3-1, kame terrace, taken transverse to flow. The boundaries and facies identification are based on figure 2.6.

Radargram Interpretation. The landform shows a less complex structure in this direction. The subparallel reflectors (units A-B) are likely the transverse expression of the plane-parallel ones observed in figure 3.28, and the sigmoidal and oblique reflectors (units C-E) probably represent the same lateral progradation of the landform. This suggest that the main direction of progradation was to the E, with both a Southern and Northern component at various times. It is possible that this is a result of a braided channel system throughout formation. The divergent reflectors (unit C) might also be a result of progressive tilting of the surface, possibly due to loss of stability through i.e. removal of the stabilising agent during deposition, such as an ice wall.

Landform Interpretation. The radargrams (figures 3.28, 3.29 and 3.30) suggest that the landform was formed by a complex channel system with the main direction of progradation to the E. Destabilisation structures observed in the sediment log (figure 3.27) suggest that the depositional environment was moderately quiet, and deposition occurred between the valley side and an ice wall. Deposition is variable across the landform suggesting that the depositional environment changed a lot throughout formation.

3.2.9 Ice-flow Parallel Esker in Valley 3 (V3-2)

Landform Description. The landform (figure 3.31), striking E-, is an elongated ridge with steep sides in all direction and the E edge cut by a gravel pit. It is 82 m long, 9 m wide and 7 m high. The log (figure 3.32) is from the NE margin facing SW.

Figure 3.28. Photo of the ice-flow parallel esker, facing S. Note the gravel pit in its W part. Car for scale.

Sediment Description. The outcrop is dominated by beds of sorted coarse and fine sand. Sub-horizontal bedding and bedding subparallel to the surface slope is prominent in coarser layers. The uppermost 9 cm constitute an organic soil horizon. The bed at 9-24 cm consists of weakly dipping, plane-parallel, well sorted layers of fine and coarse gravel. Interbedded coarse and very coarse sand follows at 24-47 cm, with gravel dominating in its lower 10 cm. The beds are subparallel with a moderate dip, and a load cast is found at the bottom boundary. Ripple cross-lamination and tabular cross bedding are found in a silty, fine sand at 47-56 cm. Fine and coarse gravel is present in moderately dipping, plane-parallel bedded layers between 56 and 68 cm. Through cross-bedding, plane-parallel lamination and tabular cross-bedding occurs in a fine sand at 68-78 cm. Massive, sandy gravel occurs between 78 and 82 cm, while at 82-100 cm, layered and sorted very coarse to coarse sand occurs.

Sediment Interpretation. Variation in flow regime, variable discharge and/or sediment availability can be inferred from grain size variations between beds. The change in dip of fore-sets at 24 cm depth suggests migrating channel flow and directional change. The coarser grain size in the upper bed also suggests a strengthening of the current. The grain size change from sand to gravel suggest that either origin of material thereby the flow path, or the strength of the flow, thereby the discharge, changed rapidly. The load cast at the boundary at 47 cm

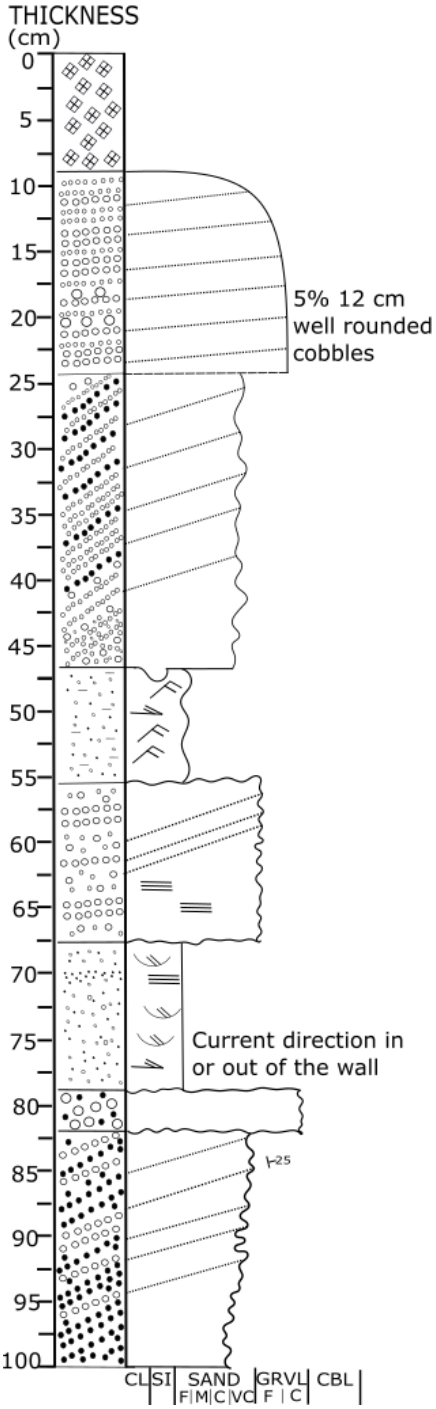

Figure 3.29. Sediment log of V3-2. See figure 3.5 for legend.

suggest rapid deposition and deformation of water-saturated sediments. The upward coarsening seen in the lower and upper parts of the logged sequence could be due to outbursts of dammed meltwater with increasing flow. Stable conditions in the upper flow regime can be inferred between 82-100 cm. The good sorting of the material can suggest currents of similar strength prevailing for a considerable amount of time, and/or a considerable distance of transport. The coarse, massive bed at 78-82 cm suggests upper current regime and rapid deposition. Plane-parallel lamination followed by cross-bedding in the coarse sand at 56-68 cm indicates strong currents and then a shift to weaker currents before (with a possible time gap) deposition of the silty fine sand dominated by ripple-cross lamination. The fine sand interval with cross bedding, plane parallel bedding and ripples at 68-78 cm indicates a flow direction at nearly 90° to the larger cross beds. Coarse sand within the fine sand suggests occasional stronger currents, especially at 70 cm, where plane-parallel laminae have formed.

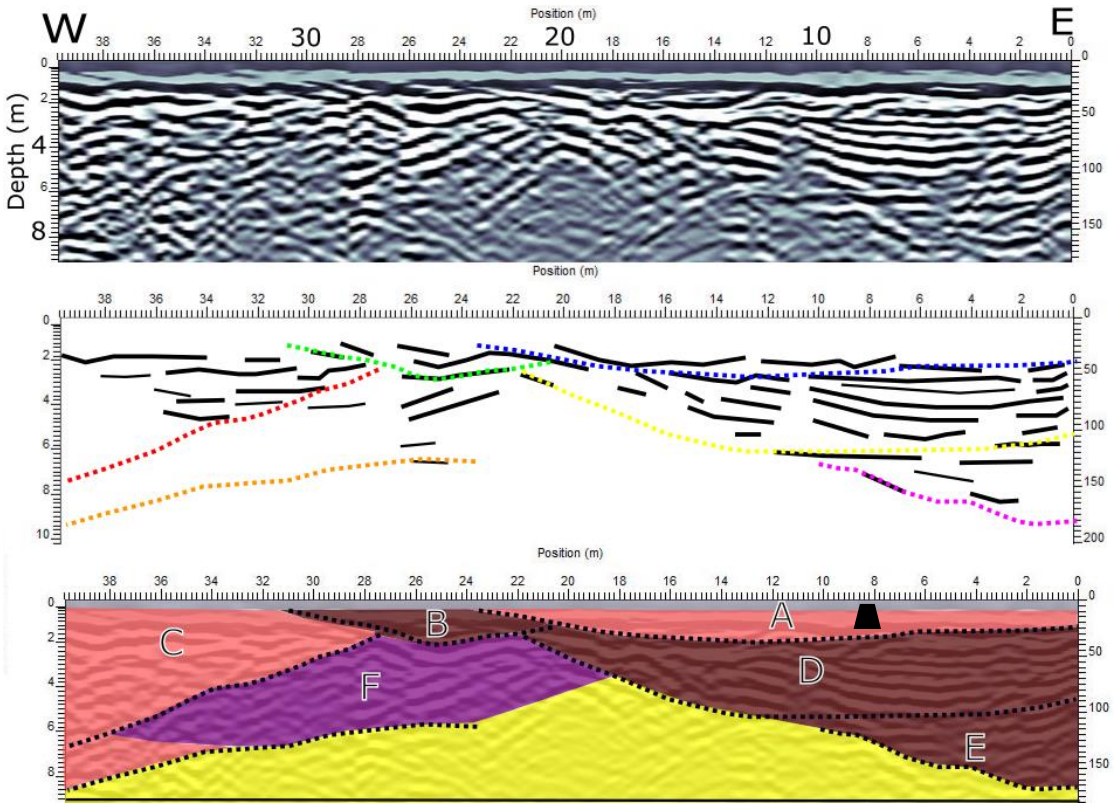

Figure 3.30. Radargram (top), reflectors and interpreted erosive boundaries (middle) and identified facies (bottom), of V3-2, ice-flow parallel esker, taken parallel to flow. The boundaries and facies identification are based on figure 2.6. The black trapes indicates where the stratigraphic log is described.

Radargram Description. The profile is along the ice-flow parallel esker, parallel to flow (figure 3.33). The radargram follows the landform and curves accordingly. Most of the identified reflectors are clear and found in troughs at the W and E ends of the esker. Six erosive boundaries are identified, two with a steep dip the W, two with a moderately steep dip to the E, and two shorter in extent subparallel to the surface. The profile is dominated by trough-shaped (units B, D and E), subparallel (units A, C and F) and divergent (unit F) reflectors. The facies consisting of trough- and subparallel reflectors show a dominating dip direction to the W and E, respectively. The reflection free area peaks in the middle of the landform (unit F).

Radargram Interpretation. The variation among the erosional boundaries suggests variable direction and intensity of flow. The main flow direction appears to be towards the E, with erosive flows down the side of the landform. These flows have deposited sediment transverse to the main flow direction, which in a curving landform gives the impression of a Wward component of flow. The progressive lateral build out of the landform likely resulted in a progressively steeper surface. This is likely to be the cause of the divergent reflectors observed in unit F. The diverging reflectors (unit F) might also be a result of a constantly changing rate of deposition, which is expected for glacifluvial deposits (Jørgensen et al.,

1997). The troughs (units B, D-E) are likely cross-sections of channel fills, while the subparallel reflectors might be a subparallel view of channel deposits. If this is the case, it appears that the flow shifted between various depositional sequences (represented by units). Vertical accretion suggest that deposition was confined by ice walls.

Landform Interpretation. The cyclic sequences of sand and gravel above erosional surfaces observed in the sediment log suggest that the landform is an esker. The GPR facies, showing channel aggradation, suggest that the esker formed sub-glacially. Banerjee and McDonald (1975a) noted that "esker cores often display cyclic sequences of gravel and sand", while Livingstone et al. (2010) noted that "the base of each sequence is often marked by an erosional surface". Banerjee and McDonald (1975a) suggested that the cyclicity in esker cores might be annual, and if true for this landform, would imply that it formed over several years.

3.2.10 Palaeochannel Deposits on Streamlined Landform in Valley 3 (V3-3)

Landform Description. The landform is egg-shaped with N-S strike, 130 m length, 100 m width and 13 m height. It has four topographic highs and is crossed by three E-W striking palaeochannels 3 m deep, 60 m wide and 200 m long filled with rounded boulders 50-100 cm in diameter. A kettle hole with a diameter of 50 m is observed on the N side. Two low-laying connecting meltwater landforms are mapped to the E by (Putnins and Henriksen, 2017).The log (figure 3.35) is from an outcrop (figure 3.34) in the lower SE part, facing N.

Figure 3.31. Photo of section in V-3, facing N. Meter-stick for scale (blackened intervals 10 cm).

Description. The outcrop is dominated by fine and coarse gravel (figure 3.35). The upper five cm constitute an organic soil horizon. An erosively based bed of coarse sand to coarse gravel follows at 5-60 cm. Imbrication is observed at 40 cm depth. Plane-parallel lamination and through cross-bedding dominate the section, with dip direction subparallel to the hillslope. Layers of sorted, coarse and medium sand are found above an undulating boundary at 82 cm. The layers contain trough cross-bedding, tabular cross-bedding and ripple cross-lamination. A lens of very coarse sand with iron precipitation is observed in the lower part. Plane-parallel laminated and trough cross-bedded coarse gravel occurs at 82-90 cm above a diffuse erosional surface with possible soft sediment deformation. The following section, at 90-145 cm, is

massive and compact. It consists of sandy gravel interspersed with boulders. The larger boulders in the bottom interval are well rounded, different to the angular boulders in the layer above.

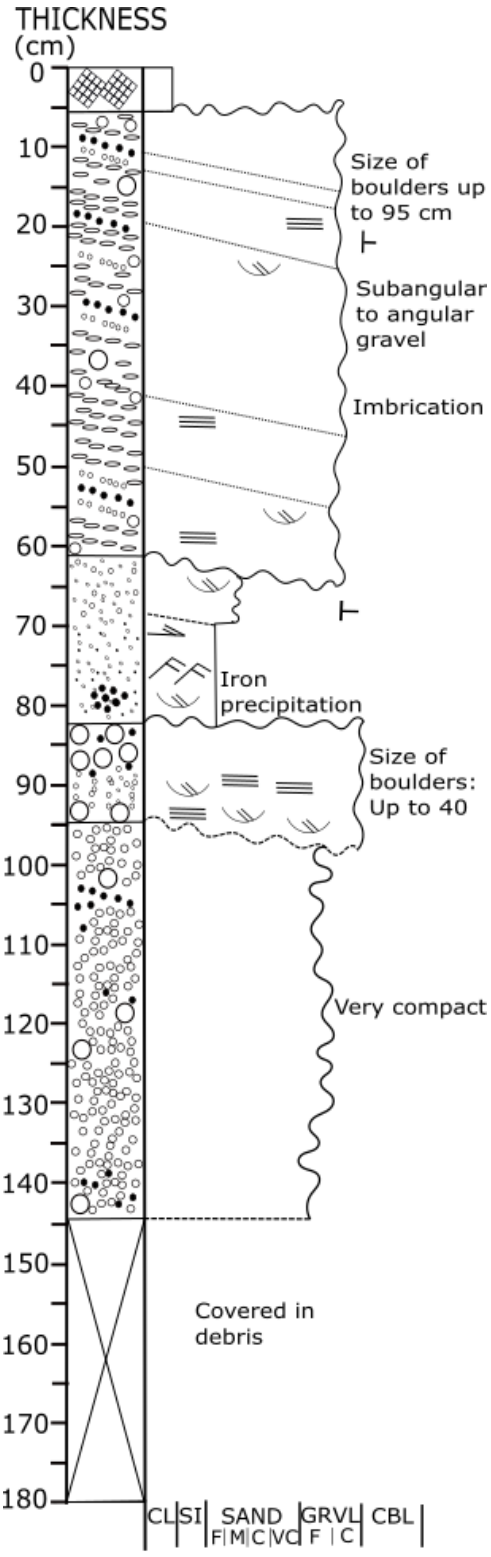

Figure 3.32. Sediment log of V3-3. See figure 3.5 for legend.

Interpretation. Deposition occurred in the upper flow regime, and the sediments suggest either high energy, short-transported material or deposition by gravity, though e.g. sliding on an ice surface. The compacted, massive deposit at the base of the section is till compacted by overlying ice. The deposit was partially formed sub-glacially under flowing ice, and the erosional boundary on top of it represents a time gap. Deposition was on top of a positive landform, which suggests that topographically lower areas were filled with ice at the time, or the whole sequence was deposited sub-glacially, the upper beds under stagnant ice. Deposition of the overlying sequence occurred in the upper flow regime. The first bed with trough cross-bedding and plane parallel stratification may have been deposited in a channel that eroded into the (most likely basal) till. This bed was again eroded by a strong current prior to deposition of the fine-grained, trough cross-bedded and rippled interval at 60-82 cm. Deposition was probably from a migrating flow with variations in current strength. The uppermost gravel bed occurs above a pronounced erosion surface. It has grain size variation that suggests variable discharge. Plane-parallel lamination and cross-bedding suggests deposition in the upper flow regime. Imbrication of clasts at 40 cm depth indicates that the material was carried as bedload. Imbrication within this coarse bed points to waxing and waning of currents. Meltwater may have been discharged at times of high pressure, with possible obstacles to release being topography, sediments or ice. Large boulders in the succession indicate high current velocities. The flow is inferred to have been towards the E above the compact layer, which suggest that meltwater drained into valley 2 by the time the ice was stagnant in the area. It is possible that the bottommost deposits (95-145 cm) can be interpreted as till, but its depth, compaction and absence of fine grains suggest it would not be flow-till

or melt-out till, and hence the degree of sorting and rounding suggest they are most likely glacifluvial deposits containing gravity-deposited clasts.

3.2.11 Remaining Landforms

Six sampled landforms are not studied in detail, i.e. V1-3, V1-4, V1-5, V2-6, V2-8, and V3-4 (figure 3.3). The depositional environment of these has been interpreted from their shape, position, sediment composition, LiDAR data and relation to surrounding landforms and landscape. Shape, position and orientation of these landforms, as well as of the landforms studied in detail, are shown in figure 3.3.

V1-3 and V1-4 are found in clusters of similar landforms, as elongate, low-relief ridges transverse to the ice-flow direction. They are interpreted as eskers formed in crevasses of stagnant ice.

V1-5 and V2-8 are found as single, elongated, extensive, high, high relief, S-shaped ridges transverse to the ice-flow direction, on steep slopes perpendicular to the valley sides. A high content of large, angular clasts are found on top of the landforms, indicating ablation till. The landforms are interpreted as chute eskers, formed sub-glacially under high hydrostatic pressure.

V2-6 is found in a cluster of parallel, narrow, straight, elongate, low-relief ridges transverse to the ice-flow direction. Peat surrounds the area, and it is possible that only the tops of V2-6 and the other landforms are visible. They are interpreted as eskers formed in stagnant ice, possibly in ice crevasses.

V3-4 is found in a low area surrounded by peat, as a semi-circular, singular, low-relief landform. A high content of sorted silt suggests low-energy deposition. The landform is interpreted to have been deposited in the lower flow regime, probably in a depression in dead ice. It may be part of a basin deposit now covered by peat, however, the surrounding topography suggest the landform is a mound, and it is therefore interpreted to be a kame deposit.

3.2.12 Clast Rounding and Flow Competence

The highest degree of clast rounding occurs in valley 2, and the lowest in valley 3 (figure 3.36). The valleys contain landforms that differ in nature and time of formation, which can explain the clast rounding variation. The degree of rounding is likely to be related to the manner of transport, where sub-glacially formed deposits are generally more rounded than supraglacial (Bergersen, 1970). This suggests that better rounding should be found in the

palaeochannel deposits V3-3 and ice-flow parallel esker V3-2, however, this is not the case. According to Bergersen (1970), transport distance is less important for rounding, than transport method. The landforms with the highest degree of clast rounding were not deposited in direct contact with ice (delta, V2-1 and fan lobe, V2-5). The difference can be attributed to a longer transport distance, higher degree of re-sedimentation or higher energy of deposition.

The flow competence of the logged sections shows large variations (figure 3.36). The landforms experienced the strongest flow regime in valley 2, suggesting high discharge. Landforms in valley 3 are found in the lower flow regime, possibly suggesting more quiet flow conditions in this area. Eskers V1-1 and V3-2 were deposited in the lower flow regime, with the ice-flow parallel esker (V3-2) at half the value of the other. The analysis can be misleading, as deposition by gravity through e.g. sliding may contribute large clasts in ice-proximal environments independently of flow regime. It is possible that the large clasts in V1-1 are a result of this process.

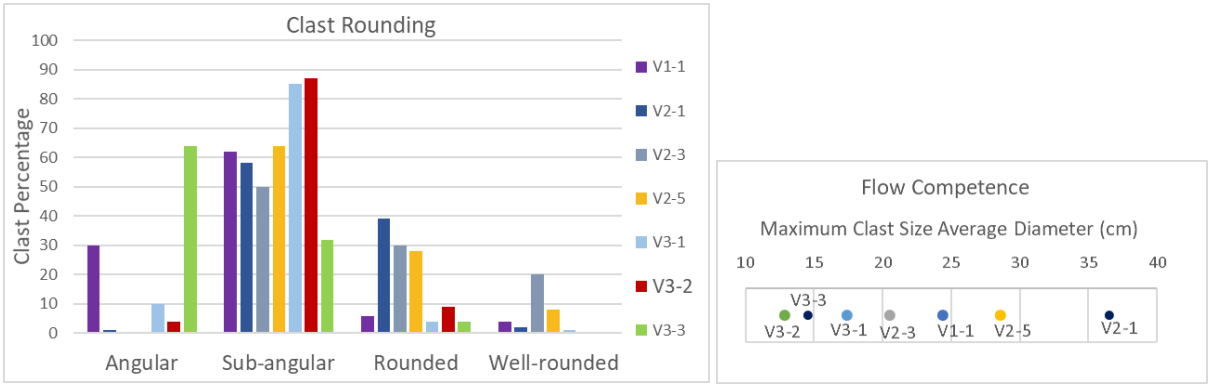

Figure 3.33. Rounding analysis of clasts (left) and flow competence measured for the deposit (right) in logged sections/ landforms.

4 Soil Carbon in the Deglaciation Landscape

4.1 Carbon Stock

The mean carbon stock of the glacifluvial landforms is 7.99 kg/m^2 with a standard deviation (SD) of 4.26. The mean is calculated from $\mu = \Sigma x_i/n$, where μ= the mean, x_i= the individual values and n= the number of values, and the standard deviation from $SD = \sqrt{((1/(n-1)) \Sigma (x_i - \mu)^2)}$, where SD= the standard deviation. The mean and standard deviation is also calculated for the three main groups of landforms (table 4.1), however, the small number of sampled soils (figure 3.3) means that the results for the trend and variation are not necessarily representative. The mineral soil constitutes on average 63.0 % of the total carbon stock (table 4.1).

Table 4.1. The average carbon stock and standard deviation for three main groups of meltwater landforms as interpreted in chapter 3.

Carbon Stock (kg/m^2)	**All landforms (n= 12)**	**Sub-glacial Eskers (n= 3)**	**Ice-flow Transverse Eskers (n= 5)**	**Other Meltwater Landforms (n= 4)**
Total	7.99 (SD= 4.26)	8.67 (SD= 1.74)	8.39 (SD= 5.72)	6.98 (SD= 4.17)
Mineral Soil	5.03 (SD= 4.15)	4.87 (SD= 2.33)	5.85 (SD= 5.91)	4.16 (SD= 3.28)
Organic Soil	2.96 (SD= 3.04)	3.80 (SD= 2.92)	2.54 (SD= 2.22)	2.82 (SD= 4.52)

The calculated average value for total carbon stock of the three main meltwater landform groups studied (sub-glacially formed eskers, eskers formed in crevasses in stagnant ice and landforms formed ice-laterally, sub-aqueously or sub-aerially) show the highest mean and lowest standard deviation in sub-glacial eskers and the lowest mean for "other" meltwater landforms (table 4.1). The relatively high standard deviation of the "other" meltwater landforms reflects the large variety in landforms, where a further distinction between landform should be made to accommodate the differences (chapter 5.3 and 5.4). The ice-flow transverse eskers show a value closest to the mean of all landforms but show a high standard deviation. They exert a considerable influence of the carbon stocks of the glacifluvial landforms despite their variability because they are the largest group, both among the studied landforms (n=5) and overall in the study area (figure 1.5). The low standard deviation in sub-glacial eskers reflect values approaching a mean, which can possibly be linked to parent material (chapter 4.3 and 5.2).

The proportion of the soil carbon stock in the mineral and organic horizon varies slightly between the groups (table 4.1). The mineral soil carbon stock to organic soil carbon stock ratio is highest in the ice-flow transverse eskers and lowest in the sub-glacial eskers group. The ice-flow transverse eskers show a considerably higher mean in mineral soil carbon stock compared to the total landforms average, but also the highest standard deviation, suggesting that some of the eskers within the group show a very high mineral soil carbon stock, whilst some eskers within the group shows a lower mineral soil carbon stock than the overall

average. The sub-glacial eskers show a lower mean and the closest mean to the total landform mean. Among the "other" landforms, the standard deviation of the organic soil carbon stock is significantly higher than the mean, which is due to only two out of the four "other" landforms having an organic horizon, suggesting the necessity of further or revised division. The mean of the two landforms with an organic horizon is 5.64 with a standard deviation of 5.43 which shows that even the two landforms that have an organic horizon still show quite different carbon stock values. However, since having nor organic horizon is a feature of the landforms, the mean is kept, and standard deviation as calculated for all four.

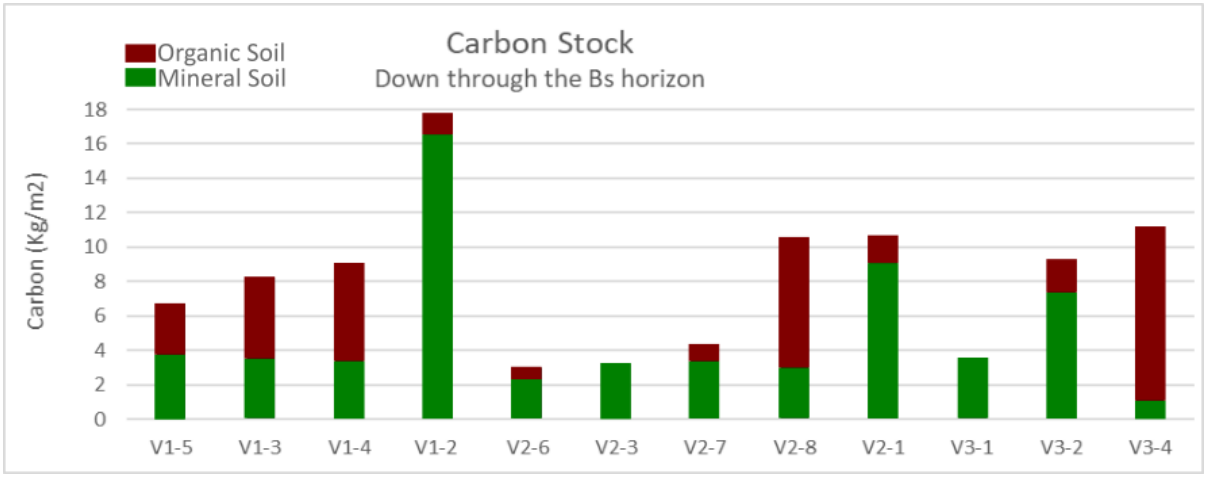

Figure 4.1. Carbon stock of the landforms.

A large variety in the carbon stock of the landforms is evident (figure 4.1). The carbon stock is highest in V-12 and V3-4. It is lowest in the ice- lateral deposits in valley 3 (V3-1) and ice-flow transverse eskers in valley 2. It is higher in landforms of more nutritious parent material and overlaying more nutritious bedrock (chapter 4.3 and 5.2). The mineral soil carbon stock proportion is very high in V1-2 and very low in V3-4, and otherwise proportionally high in V2-1 and V3-2 and proportionally very high in V2-3 and V3-1. The chute eskers show a proportionately high organic soil carbon stock. All non-sub-glacial soils in valley 2 show a low total carbon stock but a high mineral soil carbon stock proportion. Excluding V2-1, the ice-lateral and sub-aerial deposits show the largest mineral soil carbon stock to organic soil carbon stock ratio. Overall, a larger variation is seen in the organic soil carbon stock than the mineral soil, reflecting the stable nature of the carbon in the sub-soil compared to the oxidation-prone, unstable nature of the carbon stored at the surface.

Table 4.2. Overview of parameters in the carbon stock calculation for all horizons.

Horizon	N	Total Carbon (%)		Density (g/cm^3)		Thickness (cm)		Stone and Boulder Content (%)		Carbon Stock (kg/m^2)	
		ų	SD	ų	SD	ų	SD	ų	SD	ų	SD
Oa	1	50.7	-	0.05	-	4	-	35.75	-	0.52	-
Oe	1	43.8	-	0.04	-	3	-	35.75	-	0.26	-
O	11	38.84	13.81	0.18	0.11	6.72	1.58	40.16	13.75	3.83	3.01
A	3	6.12	2.76	0.69	0.17	10.75	6.9	47.17	8.56	1.97	1.03
E	11	1.63	1.52	1.11	0.25	8.77	5.65	40.53	12.66	0.87	0.47
Bs	12	2.4	1.32	1.15	0.23	25.75	16.79	41.13	12.25	3.6	3.55
CB	1	0.2	-	1.48	-	45	-	35.75	-	0.57	-
C	11	0.12	0.14	1.58	0.18	31	18.52	46.69	10.92	0.35	0.35

The carbon stock is calculated from total carbon, horizon thickness and density, and stone and boulder content (table 4.2). In the mineral soil, the Bs horizon shows the highest carbon stock but also the highest variation, and the E horizon the lowest carbon stock and the least variation. A high total carbon value of a thin horizon gives a low carbon stock (e.g. the Bs of V2-1).

The stone and boulder content of the soils can be up to 60 % (Appendix 5). A calculated mean and standard deviation based on horizon is not very useful as the content measured at mean value for the full profiles (chapter 2.5). There appears to be a clustering of the stone- and boulder content into four groups, where the highest content is found in V2-1 and V1-2, and the lowest in V3-4 (Appendix 5). The high stone and boulder content in V1-2 does not appear to lower carbon stock significantly, but the low content in V3-4 appears to allow for a high stock.

The values obtained for total carbon is used to calculate carbon stock without adjustment, and the thickness and density of the soil adjusts the effect of total carbon on the carbon stock calculation. The high thickness and density of the Bs horizons appears to greatly increase carbon stock. The Bs horizons do show a large variation in thickness (SD= 16.79). The low density and low thickness of the organic horizons gives a low carbon stock. The organic horizon thickness shows the least variation across the profiles (SD=1.58). It appears that the combination of a thick horizon and high value for total carbon gives the largest carbon stock (e.g. the Bs of V1-2). The total carbon is highest in the organic horizon but show a large variation (SD= 13.81).

Overall, the high standard deviations and low variation between the means of the landform groups in table 4.1 suggests that division of landforms purely based on landform nature may not be useful for upscaled carbon stock estimation. An evaluation is done of carbon stock in relation the nutrition status in the soil and the parent material, texture, degree of podzolization and overall potential for deep, long-term stabilisation. A revised division the landforms is

done in chapter 5.3, based on the results from chapters 3, 4, 5.1 and 5.2, which also allows for extrapolation to the whole study area (chapter 5.3.4).

4.2 Glacifluvial Soils

Soils are sampled as shown on figure 3.3, and there appears to be a systematic pattern of properties between the valleys. Relatively speaking, the content of active iron and aluminium is high in valley 1 and low in valley 3, CEC is high in valley 1 and low in valley 3, and the content of clay and silt is high in valley 1, high in the Bs horizons in valley 2 and low in valley 3. The significance and implications of the soil properties are discussed throughout the chapter.

Variation is also evident for the described profiles (figure 4.2 and table 4.3). Downward transport appears to be limited by the formation of a very dense layer, possibly cemented by iron and organic matter, within/below the Bs horizon of V3-1. Downward transport appears to strongly follow the coarser grained sediment layers and bed boundaries in V3-2, where soil formation is not strictly vertical, but follows the slope of the landform surface (despite the appearance in thee very narrow photograph). In V2-7, the E horizon is not continuous across the

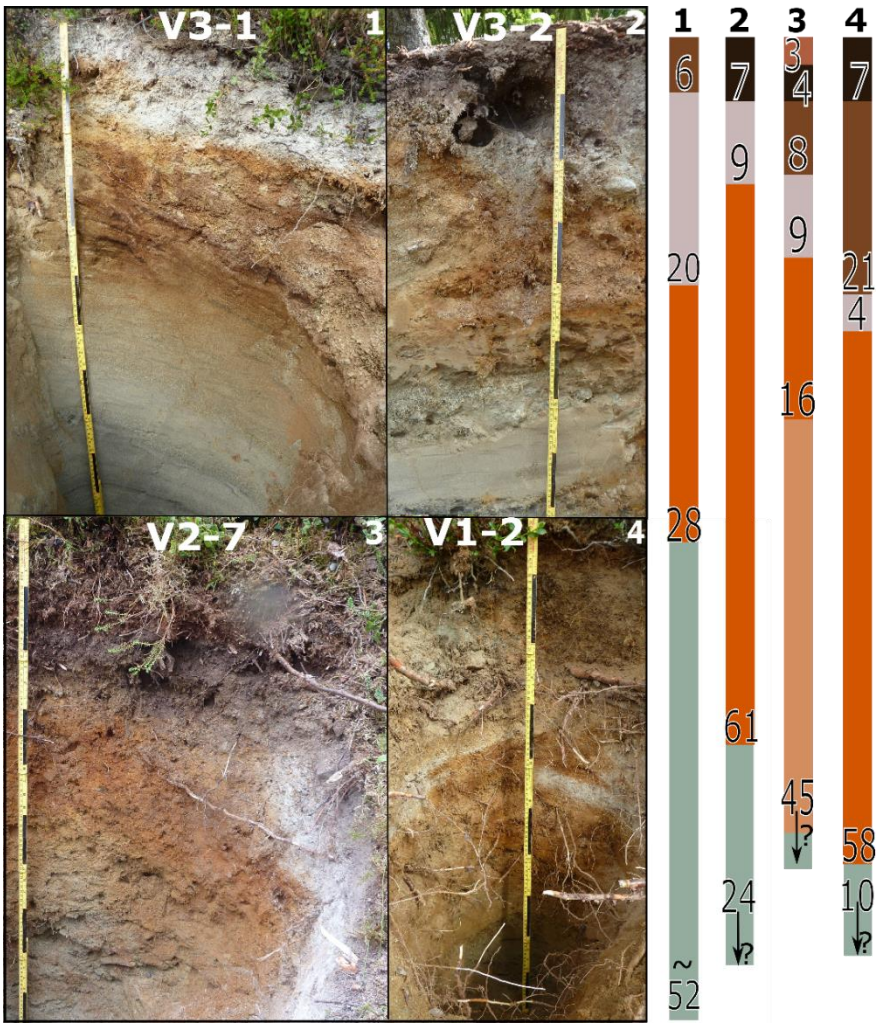

Figure 4.2. Photos of the four described soil profiles (left) and simplified (see meter-stick for scale) visualisation of the horizons (right). Numbers assigned to the horizons indicate their thickness in cm. Light brown: Oe; Black-brown: Oa; Brown: A; Silver: E; Orange: Bs; Orange-grey: CB; Green-grey: C. Landform IDs and numbers that correspond to the horizon model and profile descriptions (Appendix 1) are shown on the photos.

profile, but visible only on the sidewalls. In V1-2, the E horizon appears to be tonguing, and the horizon division is generally more chaotic. There is reason to believe that the eight additional sampled profiles show a similar anisotropy and heterogeneity.

The twelve studied and sampled soils are classified as podzols, but show variation in podzolization, soil nutrition status and carbon stock. The described profiles are sampled down to the C horizon, and/or around 1 m into the mineral soil, and the other soils are sampled down to the Bs horizon. All the sampled soils have a Bs horizon, and all soils but V2-3 have an E horizon. All soils but V3-1 and V2-3 have O horizons, where V2-7 have an Oe and Oa, and V3-2 an Oa horizon. A horizons are found in V3-1, V1-2 and V2-7. As mentioned, CB and C horizons are only included in the described profiles, among which V3-1, V3-2 and V1-2 show a C horizon, and V2-7 a CBs horizon. Full profile descriptions of four landforms (V3-1, V3-2, V2-7 and V1-4) can be found in Appendix 1.

Table 4.3. Overview of described soil profiles. Note that V3-1 does not have an organic horizon and that V2-7 has two.

Soil Property	**V3-1**	**V3-2**	**V2-7**	**V1-2**
Thickness of E (cm)	20	9	9	4
Colour of Bs (Munsell, dry)	7.5YR/7/8	7.5YR/4/6	7.5YR/5/8	7.5YR/5/6
Active Fe + Al in Bs (g/kg soil)	5.8	17.5	24.5	26
Clay in Bs (weight %)	1	2	3	3
Silt in Bs (weight %)	6	19	34	30
Thickness of O (cm)	6 (A)	7	7	7
pH of O	4.65 (A)	4.25	4.21 & 3.69	4.99
CEC of O (cmol/kg)	11 (A)	61.89	89.24 & 120.83	26.84
CEC of Bs	11.99	18.33	4.13	13.62
Ca and Mg in Bs	0.07	0.23	0.14	0.25
Na and K in Bs	0.04	0.18	0.04	0.04
TOC of O (%)	3.64 (A)	23.5	43.8 & 50.7	9.37
TOC of Bs (%)	0.79	1.54	2.01	2.6

Soil properties listed in table 4.3 shows variation in soil nutrition status, soil formation and distribution of carbon within the profiles. All soils are well developed, but V3-1 shows the weakest soil weathering process. Soil nutrition status is highest in V1-2, where the content of base cations is highest in V1-2 and V3-2 and pH is highest is significantly higher in V1-2 than V2-7. The carbon content is very high in the topsoil of V2-7 and very low in its subsoil, where the opposite in true for V1-2 with a very high carbon content in Bs and low in the organic soil.

Table 4.4. Overview of landforms with underlying bedrock, vegetation type and sediment field description. The bedrock identification is from the Synnfjell Map Sheet 1717 III (Hossack and Lutro, 2013). The vegetation (V) is based on Fremstad (1997) (table 2.1). Sediment field description includes percentage distribution of clast roundness and clast size.

ID	Landform	Bedrock	V	Sediment field description % of roundness-size (cm)
V1-1	Narrow, S-shaped Esker	Slate	-	See log
V1-2	Wide, U-shaped Esker	Slate	A2	5 % RC 1-5 cm, 15% CG, 80% CS (see log 2)
V1-3	Esker, crevasse	Slate	A2	5% RC 3-6 cm, 95 % MS
V1-4	Esker, crevasse (small)	Slate	A2	5% SaG 4 cm, 10% G, 85% F-M S
V1-5	Chute Esker	Slate	A2	15% SaC of quartzite and gabbro, 8-10 cm, 5 % FG, 5 % CG, 80 % CS
V2-1	Delta	Arkose and greywacke, rich in K feldspar	A1	See log
V2-2	Sandur Plain	Arkose and greywacke, rich in K feldspar	-	See log
V2-3	Reworked Fan Deposits	Conglomerate, gabbro pebbles	A3 b	See log
V2-4	Palaeo-shoreline	-	-	-
V2-5	Fan lobe	Conglomerate, gabbro pebbles	-	See log
V2-6	Flow-transverse Esker (small)	Slate	A2	10% C 0,5-1 m. 10 % RG 5 mm, 80 % FS
V2-7	Flow-transverse Esker	Slate	A2	Lower: 5% SaG, 15% G, 5% CS, 75% FS. Upper: SAB 5%, AC 15%, 20% G, 60% FS & Si
V2-8	Chute Esker	Dark grey- to greyish black slate	A4	15% SaB, 10 % RC 1-8 cm, 5% RC 50 and 150 cm in the surface. 10% SG 3-8 cm, 10% CS, 40% MS, 10% FS
V3-1	Kame Terrace	Arkose and greywacke, rich in K feldspar	A3 b	See log
V3-2	Ice-flow parallel esker	Conglomerate, gabbro pebbles	A2	See log
V3-3	Palaeo-channel deposits	Arkose and greywacke, rich in K feldspar	-	See log
V3-4	Kame	Arkose and greywacke, rich in K feldspar	A4	90% MS, 10% FS

V= Vegetation: A1=A1, Lichen woodland A2=A2, Cowberry-billberry woodland, A3b= A3b, Heather bog-bilberry – Scots pine mountain woodland, A4=A4, Bilberry woodland. Sediment Field Description: A= angular, Sa=subangular, R=rounded, C=cobble, G=gravel, S=sand, Si=Silt, F=fine, M=medium, C=Coarse, where combinations of letters indicate the degree of rounding of a specific size.

An overview of all profiles, with bedrock, vegetation and sediment field description, is given in table 4.4. All soils show a course texture, with a content of cobbles and boulders around 5-

20 %. The sub-glacial eskers show among the highest contents of cobbles and boulders. The vegetation generally reflects dry conditions and is poorest in valley 2 and riches tin valley 1. The gran size distribution of the fine earth fraction is illustrated in figure 4.3.

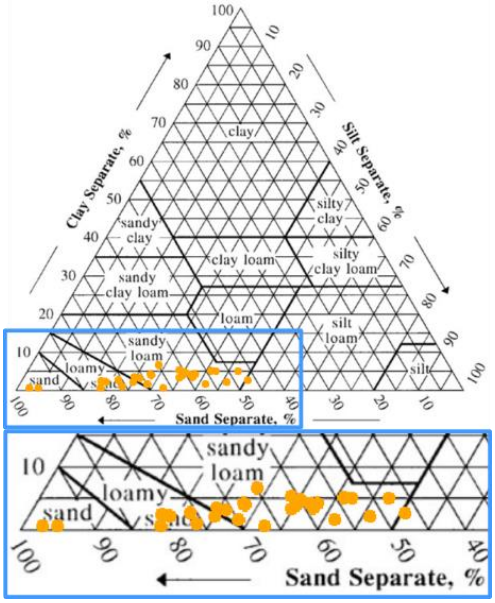

Figure 4.3. Grain size distribution of the soil mineral horizons (30 in total), based on the textural triangle from WRB (2014).

Variation in topography, horizon thickness, stone and boulder content (by visual measurement), sediment field description and landform interpretation are linked in two field transects walked through the largest meltwater landforms mapped by Putnins and Henriksen (2017). Transect 1 was walked parallel to the interpreted sediment transport direction (NW-SE) and transect 2 perpendicularly to this (NE-SW) (figure 4.4). Transect 1 is created from ten measurement points and transect 2 from twelve measurement points (figure 4.5). A simple characterisation of sediments and vegetation was done, as well as classification of and thickness measurements of soil horizons in transect 2 (see chapter 2.4 for method). It was not possible to get through stones and boulders at the surface in transect 1 for soil horizon determination.

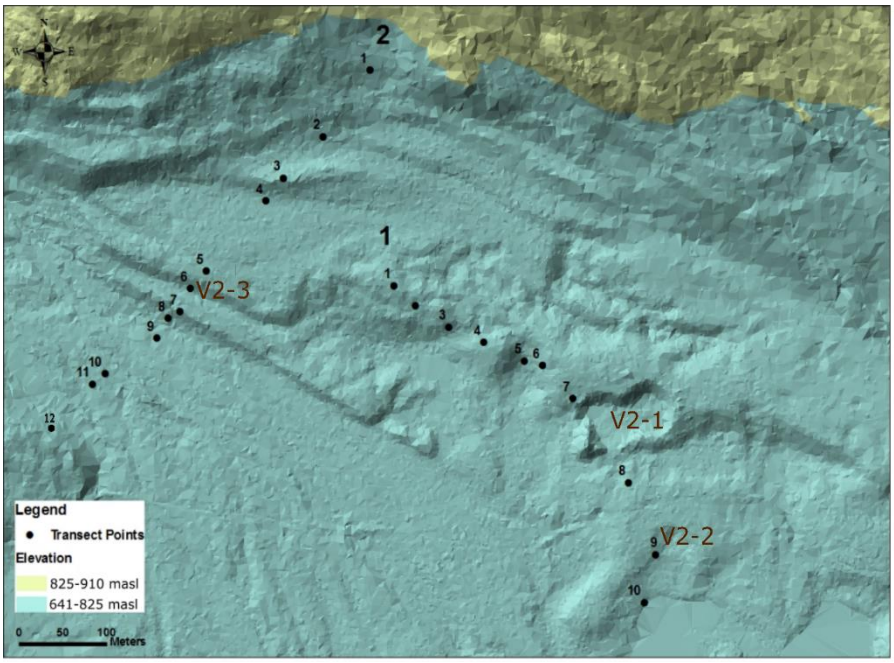

Figure 4.4. Laser data of the landscape at the field transect. Large numbers 1 and 2 identify the transects. Numbered points are correlated to the pink measurement points on the transects in figure 4.5. Transect 1 runs through the delta (V2-1) and sandur plain (V2-2) and transect 2 through the eroded fan deposits (V2-3). Area shaded greenish blue shows glacifluvial deposits. See figure 3.3 for location.

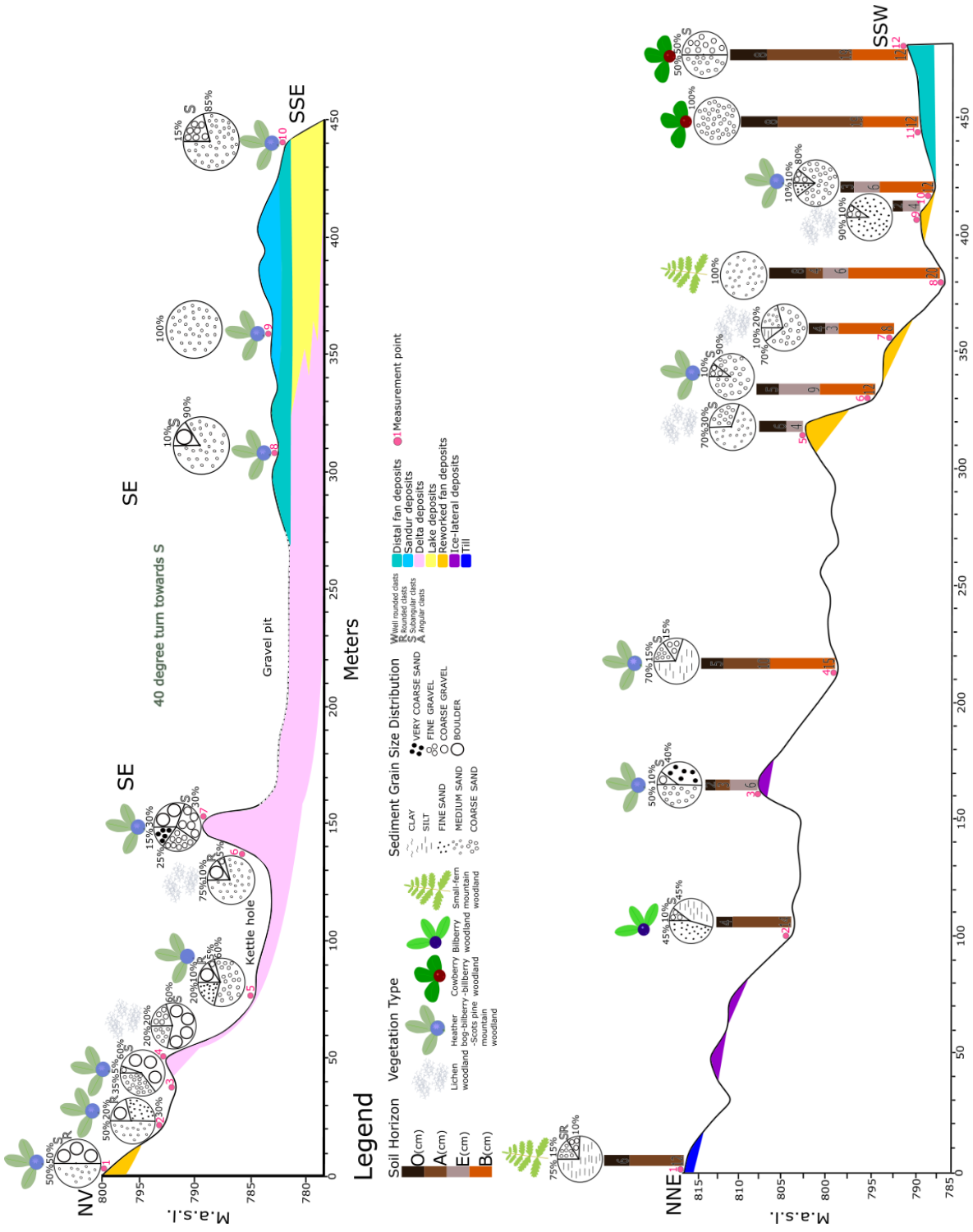

Figure 4.5. Transect 1 (left/upper) parallel to the flow direction and Transect 2 (right/bottom) transverse to the flow direction. Sedimentary grain size, stone and boulder content, vegetation and soil horizon are true field observations, and landforms/depositional environments are interpretations based on observations in chapter 3.

Transect 1 (figure 4.5) described parallel to the flow direction displays grain size distribution of sediments and overlaying vegetation along line 1 shown on figure 4.4. A gravel pit occurs

at its midpoint, where the transect direction also changes. The sediments are coarse and boulder-rich NW of the gravel pit, and significantly finer and better sorted S of it. The driest vegetation is found on the steep slopes.

Transect 2 (figure 4.5) described perpendicularly to the flow direction displays the grainsize distribution of sediments, overlaying vegetation and soil profile along line 2 (figure 4.4). The vegetation is poorest on the fan lobes, and richest between and on the distal fan deposits.

The delta and sandur plain in Transect 1 are separate deposits, and their spatial distribution indicates their temporal relationship. Deposition was continuous from the same source area, but the nature of sedimentation changed. The driest vegetation can be interpreted as the least nutritious soil, which is found along the sides of what is interpreted as a kettle hole within the delta deposit.

Soil weathering processes have been strongest in the proximal fan deposits, most of which were washed by meltwater outflow and possibly wave-activity at a palaeo-shoreline (figure 4.5, Transect 2). The distal fan deposits appear to be the most nutritious (figure 4.5, Transect 2, measurement point 11-12). The strongest soil formation and the most nutritious soil appears to be between fan lobes, where the grain size is finer. It is likely that this depression (measurement point 8) is a distributary channel without pronounced levees, which then can be linked to well-developed, nutritious soils.

No podzolization appears to have occurred in the till (figure 4.5, Transect 2, measurement point 1-2). Till is not a focus of this study, but it is interesting to note that while the till has much of the same material as the glacifluvial deposits (which generally originate from the till), the presence of silt and clay in till prior to soil formation produces quite a different soil. At point 4, the sediment appears to be till that to some extent is eroded by meltwater flow within the fan system. The soil formation appears stronger here than at higher elevation, suggesting a conceptual link between erosive meltwater flow (on till) and how developed the overlaying soil is.

The sediments are assumed to have originated from the same source. The grain size varies because the depositional environment and drainage paths and directions changed between ice-lateral deposition and deposition of the distal fan. Finer sediment in the quiet, distal deposits is likely to be enriched in clay minerals and depleted in quarts and feldspar compared to the coarser components, and the result is less intensive soil weathering processes, more nutritious soils, richer vegetation and thicker horizons.

4.3 Parent material

The flow of ice and meltwater followed the valley systems towards the SE (Putnins and Henriksen, 2017) thus clasts were described and related to lithologies in the study area and in the areas to the N and NW. According to Garnes and Bergersen (1980), the water divide was straight N of the study area at the later stages of deglaciation. The parent material is therefore not likely to have originated further N than the boundaries of the map used in categorisation. Older deposits were removed were meltwater flowed (Garnes and Bergersen, 1980). The interpretation in the four described soil profiles was extrapolated to the sampled profiles (table 4.6) based on proximity of localities, the valley where occur in and the apparent phase flow that dominated the area as described by Putnins and Henriksen (2018).

Considering how conglomerates, tillites and diamictites weather, identifying these lithologies in 2 cm clasts is challenging. Lithologies with quarts and feldspar are more stable and will remain as larger clasts for longer time during ice flow, meltwater transport and soil development (Goldich, 1938). Chemical analyses of the soil samples in the laboratory was done on grain sizes below 2 mm. This grain fraction is likely to be enriched in minerals that weather easily compared to the corresponding relative proportion in the clasts. Despite identification of clast composition, the uncertainty in their origin is therefore large.

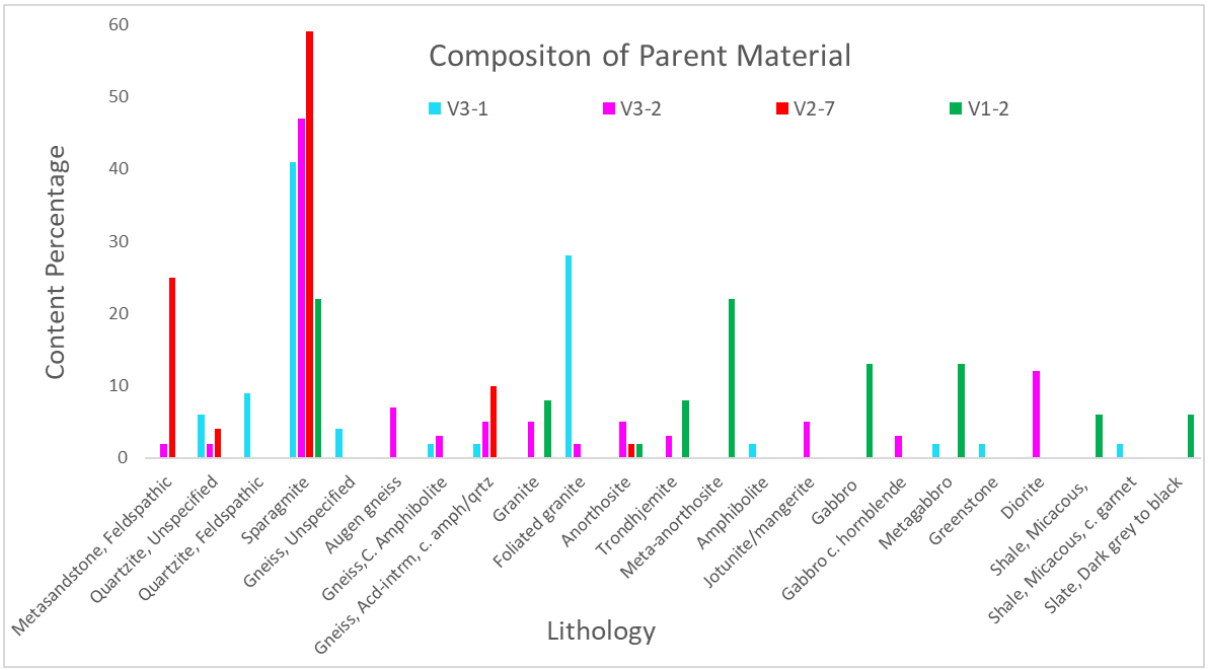

Figure 4.6. Clast analysis of parent material in the four described soil profiles. The colour code corresponds to the colour coding of the plots that follow. The nutrition status of the parent material increases from left to right (table 4.5).

The clast analysis of the parent material of the soils is shown in figure 4.6. All soils are rich in sparagmite, particularly V2-7 which shows significantly less variation and lower distribution

across the lithologies than the other soils. V1-2 is evenly distributed across basic lithologies, and V3-2 across the largest number of lithologies, both acidic and basic. V3-1 is distributed with both very high and very low values across the lithologies.

For comparison between the soils, the parent material composition is divided into six bedrock classes. The classes, along with a numerically calculated value for nutrition status by the equation *Nutrition status of parent material= (∑ (bedrock clast percentage x nutrition status of lithology))/100,* are listed in table 4.5.

Table 4.5. Calculated nutrition level factor for each profile (a value between 1 and 6, where 100% acidic meta-sedimentary and metamorphic clasts would give a value of 1, and 100% basic sedimentary, meta-sedimentary and metamorphic a value of 6).

N.S.B.	Bedrock Class	V3-1 C.P.	V3-2 C.P.	V2-7 C.P.	V1-2 C.P.
1	Acidic meta-sedimentary and metamorphic	15	4	29	0
2	Sparagmite	41	47	59	22
3	Various gneisses	8	15	10	0
4	Acidic-intermediate igneous, meta-igneous and metamorphic	28	32	2	40
5	Basic igneous, meta-igneous and metamorphic	6	3	0	26
6	Basic sedimentary, meta-sedimentary and metamorphic	2	0	0	12
	N.S.	**2.75**	**2.86**	**1.85**	**4.06**

N.S.B.= Nutrition status of bedrock, **N.S.=** Nutrient Status of Parent Material in Soil Profile= *(∑ (bedrock clast percentage x nutrition status of lithology))/100,* **C.P.** Clast Percentage

According to the calculation, the most nutritious soil is found in V1-2, and the least in V2-7. The calculated nutrition status is extrapolated to the other landforms based on valley system and topography, geographic locations, interpreted meltwater feeding origin and direction, surrounding bedrock, and interpreted mode of formation (e.g. transport and deposition) (table 4.4).

The clast analysis of the kame terrace (V3-1) and ice-flow transverse esker (V2-7) suggest that local bedrock (figure 1.2) has had minimal influence, while the bedrock and till material upstream (to the NW, figure 1.2) are more important to the composition of the landform. The bedrock surrounding the wide, U-shaped esker (V1-2) is likely to have exerted a considerable influence, as it covers a large area upstream from the landform and consists of easily erodible lithologies.

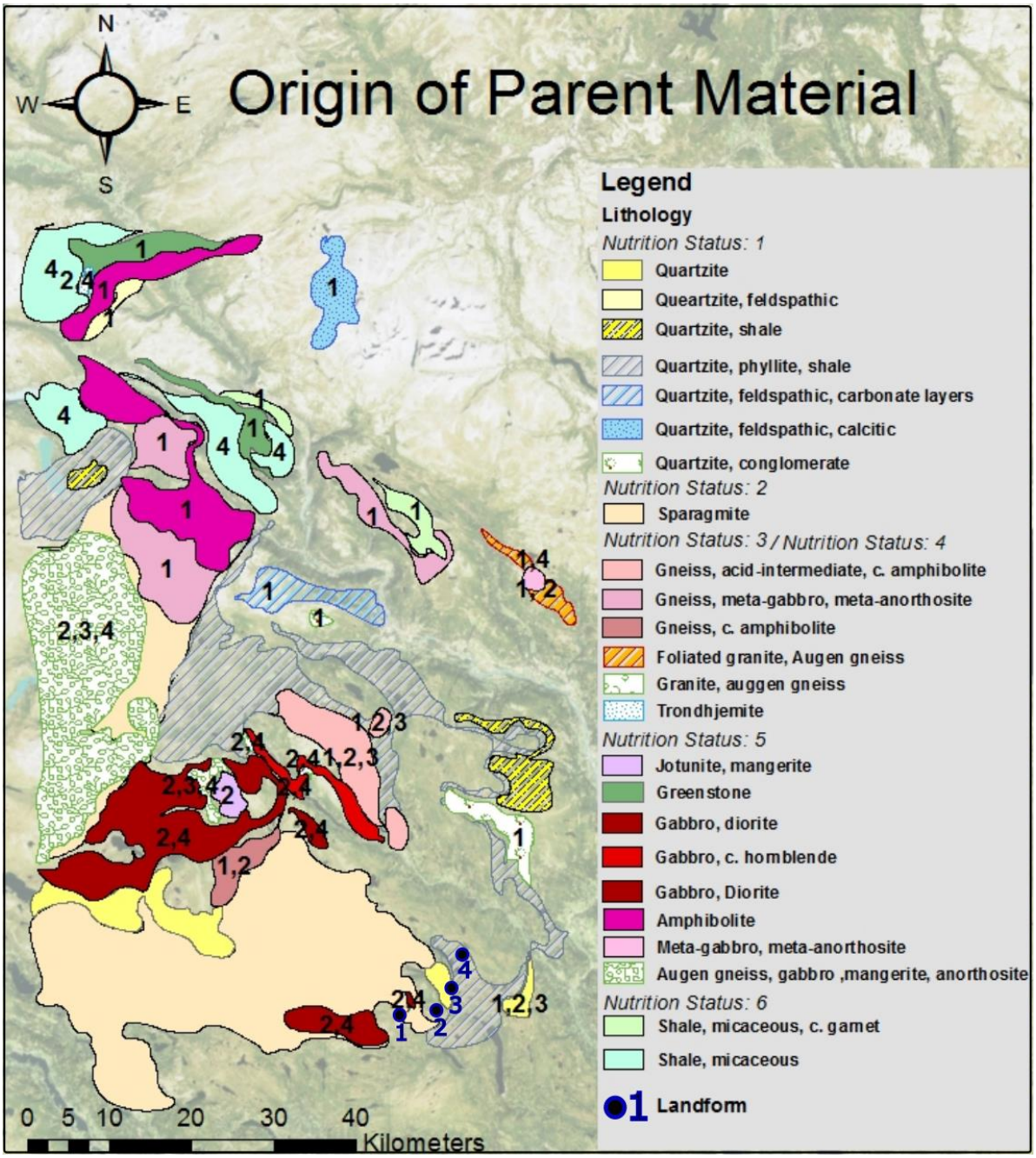

Figure 4.7. Origin of parent material. The overview is from map sheet Lillehammer (Siedlecka et al., 1987). Lithologies with numbers 1,2,3 and 4 are found at V3-1, V3-2, V2-7 and V1-2 (blue dots, soil profile descriptions 1-4 in Appendix 1), respectively. The numbers indicate the lithological content of the parent material of the soil and where it originated. The unnumbered lithologies are found in all soils.

The map of parent material origin (figure 4.7) suggests a widespread origin and distribution of lithologies in the soils. No obvious correlation between the clast composition of the soils and their geographical origin is observed. All profiles contain a high percentage of local lithologies and lithologies from the NW. The wide, u-shaped esker (V1-2) and kame terrace (V3-1) contains the material with the longest transport distance, particularly trondhjemite and greenstone.

Lithologies in the NE are unlikely to have contributed to the clast population. The high sparagmite content suggests that much of the parent material is locally transported (a few to a few tens of kilometres). The wide, U-shaped esker (V1-2) shows longer transport distance, and a more pronounced NW component. This is evident from the high content of Jotun rocks (e.g. gabbro and trondhjemite) and is probably true for the whole of valley 1. On the other hand, it contains larger clasts of easily erodible and underlying slate, suggesting local input has been significant.

The percentage of each of the present lithologies is not indicated by the map but is likely to be significant in interpretation of transport distance. While V2-7 and V1-2 contain fewer lithologies (figure 4.6), the origin is more defined and confined to specific transport paths. These landforms are interpreted as supra-glacial with a formation at a later deglaciation stage. It appears that sub-glacially and laterally formed soils contain a higher variety of parent material, with an origin that is more difficult to infer. The topography of the area around the study area along with the clast composition suggests that the material in V1-2 has originated straight from the N, controlled by the valley topography at the later stage. The parent material of V2-7 is likely to have followed a similar path, but with a stronger W component towards the end. The acidic, homogenous composition suggests mature material, or a path that reflects this lithological composition. As the landform is found downstream valley 2, it is likely that it formed when the ice was largely gone, and large amount of till exposed and re-sedimented.

V1-3 has a high content of foliated granite, which at this map scale is shown only to occur in the E. Trondhjemite constitutes a significant amount of the parent material in V1-2. The lithologies can also be found further S, closer to the study area, but this is not evident from the Lillehammer Map Sheet (Heim, 2017). For a detailed study of the origin parent material, more detailed bedrock maps along with paleontological study are necessary.

Table 4.6. Extrapolation of calculated nutrition status of parent material (table 4.5) to all landforms).

N. S. P. M. [1]	**1.85**	**2.75**	**2.86**	**4.06**	**Uncertain**
Measured	V2.7	V3-1	V3-2	V1-2	V2-1
Extrapolated	V2-6	V3-4	V1-5	V1-3	V2-3
			V2-8	V1-4	

[1] Nutrition Status of Parent Material

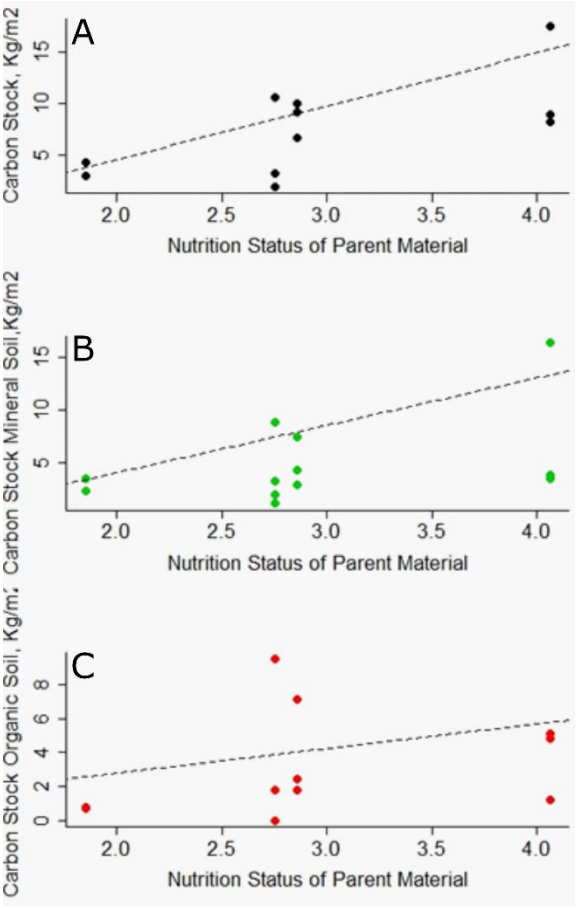

Figure 4.8. Plots of carbon stock of the soils (A), mineral soil only (B) and organic soil only (C) against the nutrition status of the parent material. The trendlines are constructed from the four described profiles (V1-2, V2-7, V3-1 and V3-2).

The carbon stock of the soils, the organic horizons and mineral horizons is plotted against the nutrition status of parent material in figure 4.8. The extrapolation of the model on all soils appears useful with regards to soils carbon, as the four groups show a relative proportional increase between the properties similar to the trend of the described profiles. The more concentrated the points are (in the y-dimension), the less variance within the nutrition status group and the stronger the dependency of carbon stocks on organic material. The carbon stock of a soil profile increases proportionally to the nutritious status of the parent material, largely due to an increase in the Bs horizon. Carbon stock in all horizons appears to increase with the parent material nutrition status.

The plot of carbon stock against the nutrition status for the parent material of the four described soil profiles is strong and positive (figure 4.8 A). The mineral soil shows a linear increase forV2-7, V3-2 and V1-2 with the parent material nutrition status (figure 4.8 B). The discrepancy between the total carbon stock and the organic soil carbon stock indicates how much organic carbon is produced, decomposed, and translocated and preserved in the mineral soil. The organic horizons show the largest difference to the total values in V3-4 and V2-8 (figure 4.8 C). The carbon stock of V2-7 appears to largely be caused by a high organic soil carbon stock, while the carbon stock of V2-1 appears to largely be caused by a high mineral soil carbon stock. The landforms show a difference in Bs horizon carbon stock, where the latter has a value double to that of the former.

Table 4.7. Texture of the soils. L/H= landform/horizon; Cl= clay; Si= silt; S= sand; L= laser measurement (Bs and CB). Note that the laser measurement is done for the clay and silt fraction only. The results are too high in V3-2 due to limited sample material available.

L/H	Cl (%)	Si (%)	S (%)	Cl (%), L.	Si (%), L.
V3-1/E	2	24	74		
V3-1/Bs	0	4	96	9	91
V3-1/C	0	2	98		
V3-2/E	3	50	47		
V3-2/Bs	2	21	77	8	92
V3-2/C	0	4	96		
V2-7/A	2	45	53		
V2-7/E	1	41	58		
V2-7/Bs	0	32	68	7	93
V2-7/CB	0	18	82	6	94
V1-2/A	4	34	62		
V1-2/E	3	37	60		
V1-2/Bs	3	28	69	9	91
V1-2/C	0	2	98		
V3-4/E	1	22	77		
V3-4/Bs	1	28	71	6	94
V2-1/E	4	35	61		
V2-1/Bs	3	24	73	12	88
V2-6/E	5	34	61		
V2-6/Bs	2	18	80	10	90
V1-4/E	4	42	54		
V1-4/Bs	3	25	72	15	85
V1-5/E	4	41	55		
V1-5/Bs	2	17	81	11	89
V1-3/E	5	46	49		
V1-3/Bs	3	37	60	9	91
V2-8/E	3	34	63		
V2-8/Bs	4	38	58	9	91
V2-3/A	6	28	66		
V2-3/Bs	4	28	68	12	88

All soils are coarse-grained (table 4.7). While the percentage and size distribution of sand to a large degree indicates depositional regime, high correlation of clay and silt with various podzolization parameters might suggest that the clay and silt of the Bs horizon is related to soil weathering processes (figure 4.9). The laser measurements (table 4.7) give the most accurate results for clay and silt (note that the laser measurements are cumulative and only include clay and silt). V2-7 and V3-4 show the finest Bs horizon texture, which is interesting in relation to the very low mineral soil carbon stock (figure 4.1). V2-1, of the highest mineral soil carbon stock, shows one of the highest values for Bs horizon clay content. In V2-3, the silt and clay measured by the laser method (bottom row columns 5 and 6) is exaggerated due to limited sample available for analysis (chapter 2.8).

Active Iron and Aluminium in Bs over E against the Bs horizon content of clay and silt (figure 4.9A)

Description. The plot of clay and silt in B against the ratio of the sum of active iron and aluminium in the Bs horizon over E horizon (BEFeAl) shows a moderately strong, positive linear correlation. V1-5 and V2-7 show higher values than the other landforms, where the latter has a lower BECS than average for its BEFeAl value. The V1-2 and V1-3 show a similar linear increase of clay and silt as the other landforms, but at a lower BEFeAl content (the clay and silt to BEFeAl ratio is higher). V3-4 appears to be an outlier, with a high clay and silt and low BEFeAl. All landforms in valley 3 show a high clay and silt to BEFeAl ratio.

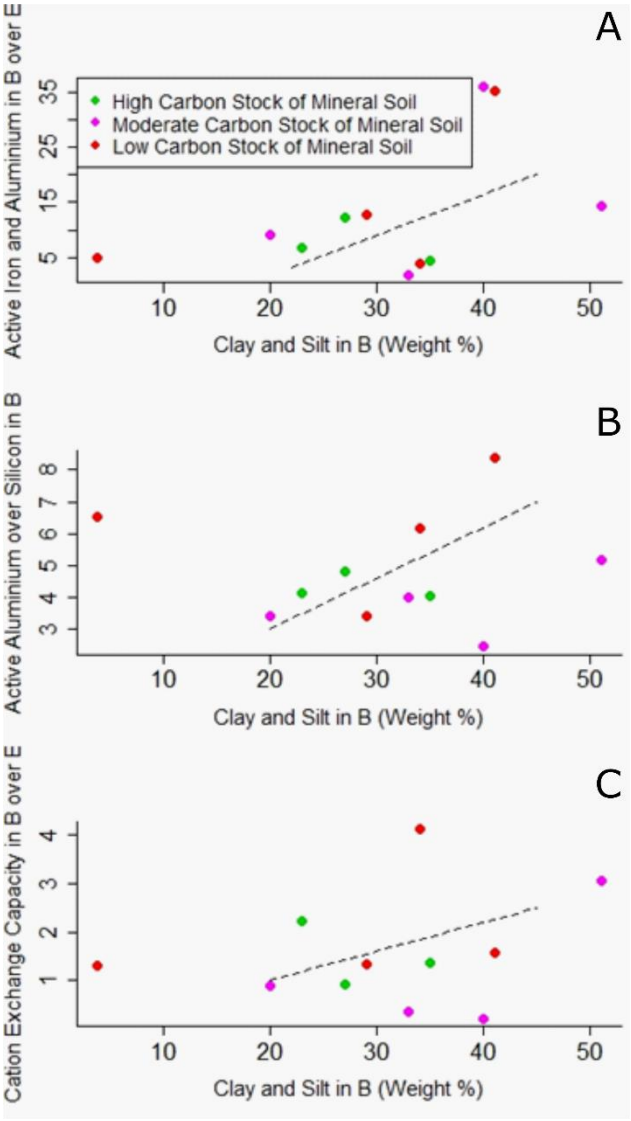

Figure 4.9.Clay and silt content of the Bs horizon and property ratios between the B and E horizons in relation to the mineral soil carbon stock. The trendlines are based on the four described soil profiles.

Interpretation. The BEFeAl indicates degree of podzolization. The relationship between the properties suggests that the processes that cause them are interdependent, or that they are independent signals of similar or different processes. Different starting values of non-pedogenic grain size and minerals give different ratios between the BECS and BEFeAl, but of similar positive nature. A small content of clay and silt in the parent material might give the appearance of a higher or lower BECS than what can be ascribed to soil formation processes. The high clay and silt content in V3-4 suggests geological deposition in quiet conditions.

Active Aluminium over Silicon in B against the Bs horizon content of clay and silt (figure 4.9B)

Description. The plot of the Bs horizon clay and silt and the ratio of active aluminium to silicon in the Bs horizon (BAlSi) is weak, positive and non-linear. The chute eskers and transverse eskers plot at high clay and silt content and show a steep, positive linear relationship at a BAlSi between 0.4 and 1.2. The landforms of lower mineral soil carbon stock show higher ratios for both properties, though V2-8 and V3-4 can possibly be considered

outliers. If they are, landforms of higher mineral soil carbon stock show higher values for both properties.

Interpretation. The BAlSi indicates degree of podzolization. Soils formed from the most and least nutritious parent material (V1-2 and V2-7, respectively) plot at similar ratios, suggesting that the parent material has less influence on these property ratios. The lowest BAlSi to clay and silt content appears to be in soils formed from the most nutritious parent material. Moderate to high values for both properties are associated with the highest mineral soil carbon stock, suggesting stabilisation of carbon by clay in the Bs horizon. There appears to be a proportionality between the ratio of active aluminium to silicon and clay and silt content in the Bs horizons. This is expected, as downward transport of both active aluminium and clay minerals occurs, and aluminium is a key component of the phyllosilicate structure.

CEC of Bs over E against the content of clay and silt (figure 4.9C)

Description. The plot of the Bs horizon clay and silt content against the CEC of Bs over E (BECEC) is moderate, positive and non-linear. The landforms in valley 3 plot in a positive linear trend. The plot can be viewed as a plot of four positive lines of different BECEC to clay and silt ratio. The valley 3 landforms and V1-3 show the highest ratio, followed by V1-5 and V2-6, then V2-1, V1-2 and V1-4, and at the lowest ratio, V2-8 and V2-7. The correlation between the properties appears positive for the low-carbon stock mineral soils, and negative for the high and moderate.

Interpretation. The plot shows a correlation between two properties that indicate downward percolation of material. The clay, silt and exchangeable cation translocation are interdependent processes (as clay minerals contribute a large proportion of permanent charge cation exchange sites (Schlesinger and Bernhardt, 2013)) and can be expected to increase proportionally. The eskers in valley 1 contain the most nutritious parent material and are found in the upper clay and silt range V2-7 is formed from acidic lithologies. It appears that the soils that form from nutritious parent materials show less increase in clay and silt content with an increase in BECEC, indicating better decomposed material at depth and possibly reflecting better conditions (higher nutrient availability) for decomposition at less intense soil weathering.

The BECEC can be expected to change similarly with the BEFeAl and carbon content. A high BECEC to clay and silt ratio can therefore indicate that the decomposition in the soil is associated with stronger weathering processes and more active iron and aluminium oxides. The high ratio is observed in V1-3 and in valley 3. Considering the BECEC in relation to carbon stock (figure 4.1), which show that the carbon content is high in both V1-3 and valley 3 except V3-1, it may only be in V3-1 that a stronger degree of decomposition is clearly related to stronger soil weathering.

The highest mineral soil carbon stock correlate with a lower clay and silt content and higher BEFeAl. This may suggest that a considerable proportion of the mineral soil carbon stock is stabilised by clay at a shallower level than the Bs horizon in soils of stronger soil weathering processes, though the simpler explanation is that it reflects how a higher proportion of carbon is stabilised by oxides and not clay minerals.

4.4 Soil Nutrition Status

The estimated nutrition status of parent material is used to group the landforms in the plots that follow, unless other legend is specified.

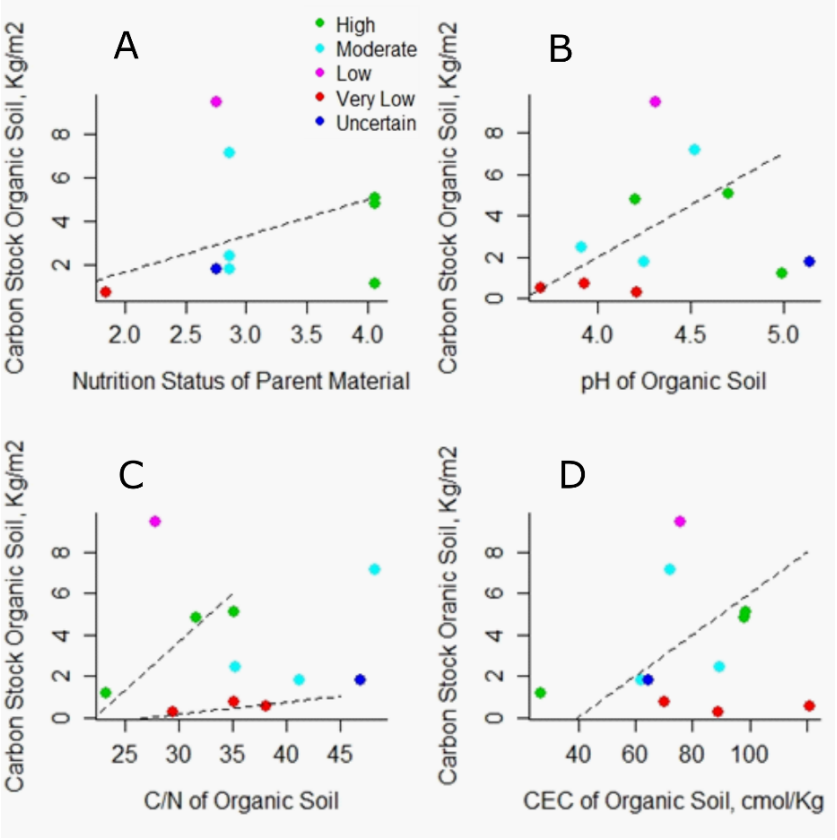

Figure 4.10. Carbon Stock of the organic soil in the soils, plotted against the nutrition status of the parent material (A), the pH of the organic soil (B), C/N ratio of the organic soil (C) and CEC of the organic soil (D). The pH, C/N ratio and CEC are indicators of soil nutrition status and evaluated in relation to the stock of carbon in the organic horizon. V2-7 is plotted twice because it contains two O horizons. Note how the pH of the organic soils seems to be predicted from calculated parent material nutrition status. The legend (A) indicates the parent material nutrition status of the soils.

There appears to be a relationship between the carbon stock of the organic soil and pH, C/N and CEC (figure 4.10). The pH, C/N and CEC of the organic soil are indicators of the nutrition status of the soil, and the correlation suggests that it largely controls the carbon stock of the subsurface along with biochemical decomposition. The calculation of parent material nutrition status seems to predict pH of the organic soil, verifying the method for estimation as well as the property as a carbon stock predictor (figure 4.10 B). Preservation of carbon appears to be controlled by biological factors that limit decomposition for most soils.

The carbon stock of the organic soil is highest in V3-4, V2-8, V1-3 and V1-4. The soils are found at a medium parent material nutrition status (the two former) and at high parent

material nutrition status (the two latter) and at a pH around 4.5 (the middle range in this study). Furthermore, the soil across a C/N ratio range from 25 to 50 (figure 4.10 C), and at a high CEC (between 70 and 100 cmol/kg) (figure 4.10 D), indicating a high soil nutrition status.

The carbon stock of the organic soil is lowest in V1-2, V2-6 and V2-7. The former is formed from nutritious parent material, plots at a high pH (relatively), within a C/N range optimal for production and decomposition (around 24) and at a low CEC. V2-6 and V2-7, on the other hand, plot at the lowest parent material nutrition status, at a low pH, C/N above optimal for decomposition and high CEC.

The organic soil carbon as a component of the total stock indicates whether the total stock can be attributed to temporary preservation in the surface. Comparison with the carbon stock for the total soil profiles, mineral soil only and organic soil only (figure 4.8) suggests that the total carbon stock is very high in V1-2, but very low in V2-7. It appears, therefore, that the similar organic soil carbon stock in the two landforms has different causes. In V1-2, production and decomposition are both high, and the organic material is translocated to depth and added a to an increasing deep stock of carbon. In V2-7, input is also high, decomposition more limited, and the soil carbon biologically stabilised in the surface due to less than optimal conditions for decomposition.

Further comparison with figure 4.8 suggests that the high carbon stock in, V3-4 (kame), V2-8 and V1-5 (chute eskers) and V1-3 and V1-4 (crevasse eskers) can be attributed to high input and good conditions for stabilisation of carbon in the organic soil. Among these, V2-8 has a very high C/N, and the preservation of carbon may predominantly be caused by nitrogen-deficiency and slow decomposition. The high stock in V3-4 appears reflects high stabilisation of carbon in the organic horizon. Overall, the organic soils appear acidic, nitrogen deficient and do not experience optimal condition for production and decomposition.

Key Observations

Based on the observations for the C/N, CEC and thickness of the organic horizons, the nutrition status of the soil is highest in V1-3, V1-4, V1-5 and V2-7. However, decomposition is high in V1-3, V1-4, V1-5 and among the lowest in V2-7. The C/N ratio is above optimal value for decomposition in the organic horizons of V2-1 and V2-8 and optimal for decomposition in the organic horizons of V1-2. The pH of the soils (Appendix 4) generally increases with parent material nutrition status. The Bs horizon seems to be the horizon least affected by acidity of parent material. The O and E horizons are the most affected, and a proportionality exists between the parent material nutrition status and the pH of the E horizon. There is a larger gap between the lower and upper horizons in V2-7, the landform of the least nutritious parent material.

4.5 Podzolization

The mineral soil carbon stock appears to correlate with the active oxide, silt and clay content (figure 4.11). The content of active iron, aluminium and silicon oxides as well as clay and silt are soil weathering products.

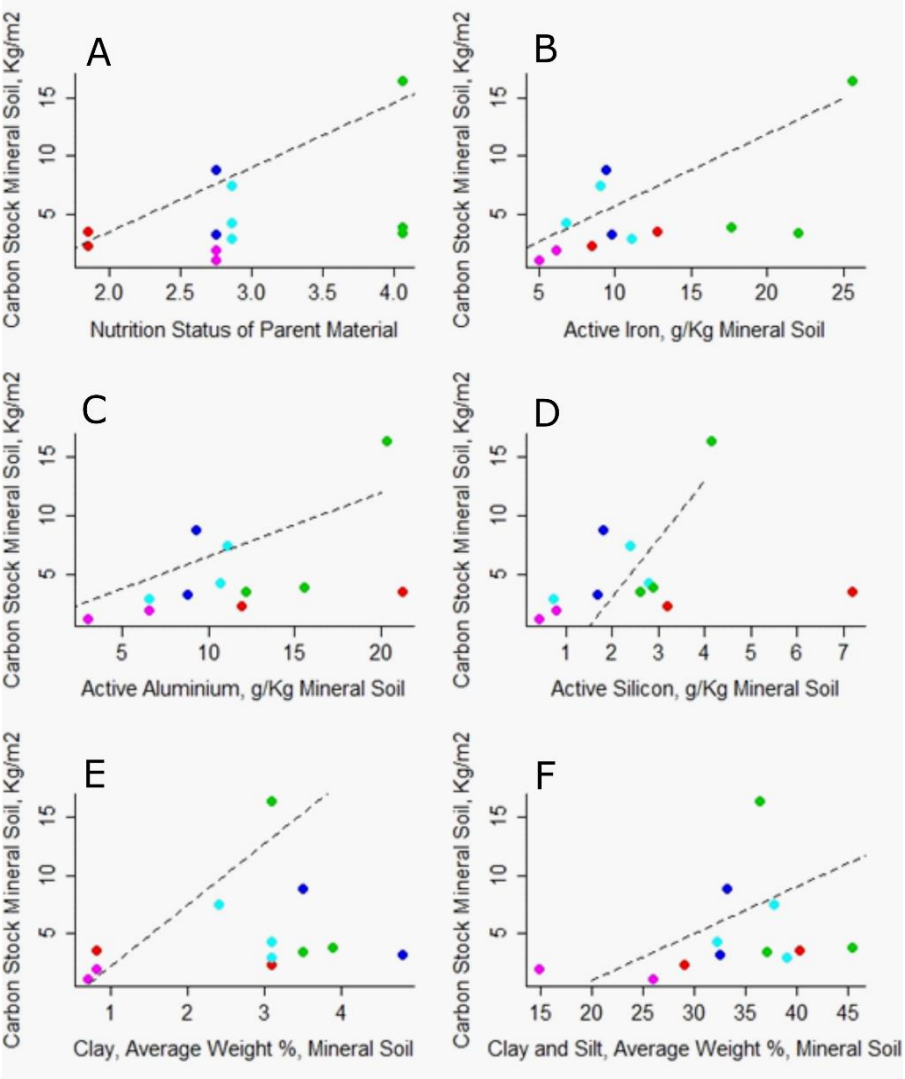

Figure 4.11.Carbon stock of the mineral soil plotted against the nutrition status of the parent material (A), active iron content (B), active aluminium content (C), active silicon content (D), clay content (E) and clay and silt content (F). The trendlines are based on the four described profiles. See figure 4.10 for legend.

The mineral soil carbon stock is highest in V1-2, which is formed from nutritious parent material high in clay and silt. The mineral soil carbon stock and clay content are both high in V2-1, suggesting a correlation, but the clay content is also high in V2-3, which shows a much lower mineral soil carbon stock (figure 4.11 E). The mineral soil carbon stock is high in V3-2 and is formed from moderately nutritious parent material high in silt. The mineral soil carbon stock is lowest in V3-1 and V3-4, which show the lowest values for active iron, aluminium and silicon, as well as clay and silt, and are formed from moderate to low nutrition parent material.

The two plots of mineral soil carbon stock against active aluminium and against silicon are similar, where nutritious parent material soils show a higher active aluminium value

compared to soil of less nutritious parent material (figure 4.11 C and D). The content of active aluminium and silicon is highest for V2-7 and V1-2. According to figure 4.11A, these soils both show a high nutrition status. However, they differ majorly in that the mineral soil carbon stock is highest in V1-2 and lowest in V2-7.

The content of active iron appears to be proportionally related to the parent material nutrition status, and consequently, both appear to proportionally correlate with the carbon stock of the mineral soil (figure 4.11 B) V1-2 is very high in active iron, and V1-3 and V1-4 are also significantly higher than the other soils. It is possible that the amount of active aluminium and silicon indicate productivity, and that active iron is a major contributor to stabilising carbon at depth.

There appears to be a linear proportionality between the active iron and aluminium and carbon stock of the Bs horizons in the landforms (a correlation of ~ 2 when carbon stock is measured in kg/m^2 and iron and aluminium in g/kg), with V2-7 is an outlier (figure 4.11 B and C). The more nutritious the parent material, the higher are both properties. The question arises why V2-7 stands out. It has the least nutritious parent material and a large pool of carbon in the top soil (O and A horizons). Podzolization can be interpreted to be dominated by inorganic complexation of iron and aluminium oxides following silicon weathering (Lundstrom et al., 2000) (figure 4.14 B). It is possible that the translocation of AFe and AAl to the Bs horizon has occurred in this manner, which has either led to a lower amount of organic matter translocation, or to a larger, less stable fraction of what has been translocated.

The carbon stock of the mineral soil appears to increase proportionally with the clay and silt content (figure 4.11 E and F). V2-1 shows the second highest mineral soil carbon stock, medium values for all properties but a high clay content. It appears that the soils with highest mineral soil carbon stock are high in silt and formed from nutritious or moderately nutritious parent material. Some soils high in silt and clay, e.g. V2-7 and V2-8, contain a low mineral soil carbon stock. These soils have a high soil nutrient status, but decomposition appears to be limited by nitrogen. It is possible that other soils, e.g. V3-4, would show a similar trend as V1-2 if the parent material was more nutritious and decomposed carbon contributed to the subsoil was stabilised. It could also show a similar trend as V2-7, if decomposition was biochemically limited.

To assess the carbon stock of the mineral soil in relation to the degree of podzolization, it is plotted against the content of active iron and aluminium in Bs over E and active iron over aluminium in Bs (figure 4.12).

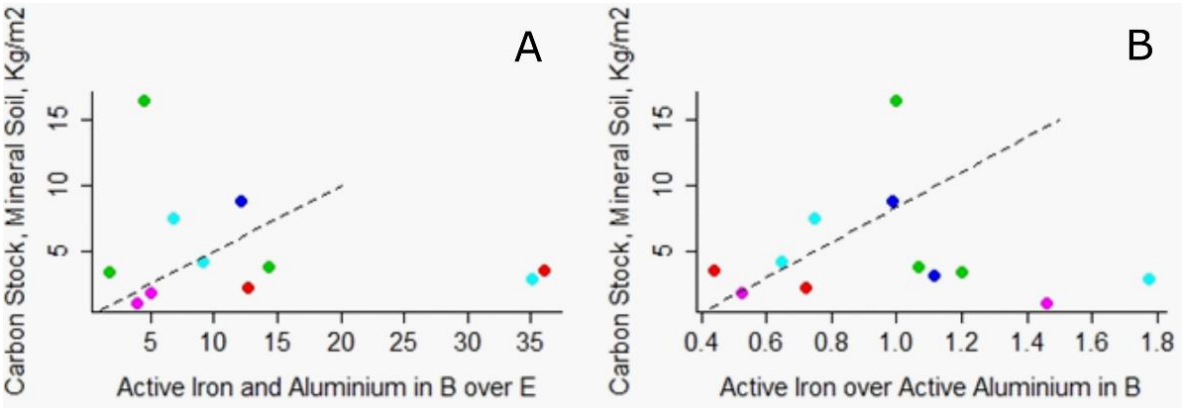

Figure 4.12. Carbon stock of the mineral soils against iron and aluminium. The trendlines display a hypothetical correlation. Soils of more nutritious parent material show a larger increase in mineral soil carbon stock with an increase in both iron and aluminium in Bs over E and iron over aluminium in Bs. See figure 4.10 for legend.

Active iron and aluminium in Bs over E (figure 4.12A)

Description. The plot of the BEFeAl against carbon stock in the Bs horizon shows a weak, positive, possibly linear correlation. Three landforms plot outside the main cluster; V1-2 plots at a high Bs horizon carbon stock and low BEFeAl, and V1-5 and V2-7 at a low carbon stock and high BEFeAl. Considering the plot without those landforms, the correlation is moderate, positive and linear. V2-1 plots at the highest carbon stock within the cluster (dark blue).

*Interpretation***.** The complexation of decomposed organic material with active iron and aluminium suggests that the downward translocation of the latter (seen form the BEFeAl) should increase the recalcitrant carbon content at depth (Blume et al., 2016). It is possible that this is the case, but V1-2, V1-5 and V2-7 are outliers that disturb the correlation in the plot. The landforms contain among the most nutritious (V1-2) and least nutritious (V2-7) parent material in the study. They all show a high clay and silt content in Bs compared to E (table 4.7), which suggests that carbon complexes may form with other (short-transported, non-pedogenic) clay minerals than iron and aluminium oxides (see chapter 5.2.3 for discussion on the binding mechanisms of carbon). The mineral and grain size composition of the parent material may explain both the low BEFeAl and high carbon stock. The landforms within the cluster have a similar parent material nutrition status. It is unclear whether a high and low status is a good reason to exempt the landforms from plot and allow a positive correlation between the properties. Alternatively, separate trendlines should be constructed for various parent material nutrition levels, in which case the trendline is accurate, as the soils it covers are formed from similar material.

Active iron over active aluminium in Bs (figure 4.12B)

Description. The plot of the ratio of active iron over active aluminium in Bs against carbon stock in Bs is positive and linear for the landforms in valley 1. It is weak, positive and non-linear for the other soils.

Interpretation. The ratio of active iron over active aluminium indicates the relative importance of podzolization processes, where a higher ratio indicates a more significant translocation of the (hydr)oxides as organic acid complexes (relative to transport as inorganic complexes) (see paragraph below on the nature of podzolization). The soil formation in valley 1 in particular may driven by processes that stabilise carbon at depth. This suggests that the stock of carbon in the Bs horizon should be higher in the eskers formed in ice crevasses and between stagnant ice blocks overlaying basic sedimentary bedrock. This appears to be true, where a linear increase in the stock of carbon (from 2-4 kg/m^2) is observed for an increase in the AFe to AAl ratio between 8-10. Tre trend is irrespective of landform type and nature of deposition (true for both crevasse and chute eskers) and is therefore likely to be influenced by local bedrock and parent material.

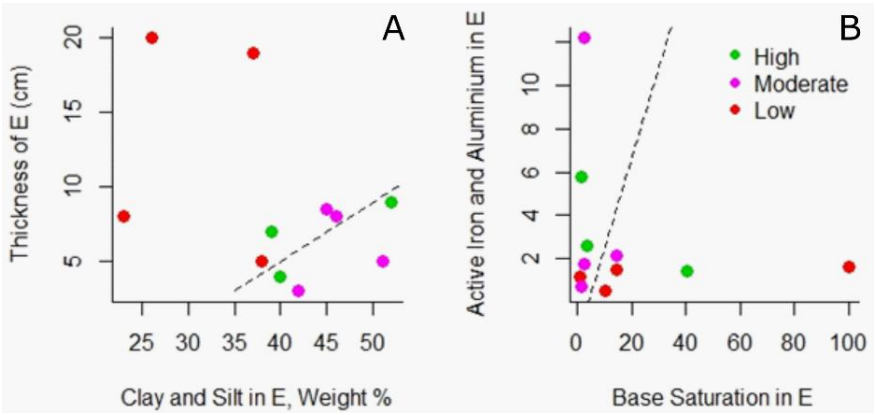

Figure 4.13. Carbon stock and properties of the E horizons. A: Trendline based on soils with a high and moderate mineral soil carbon stock. B: Trendline based on the described profiles. The legend (plot B) indicates mineral soil carbon stock for both plots.

Thickness of E against the content of clay and silt in E (figure 4.13 A)

Description. The plot of the thickness of the E horizon against the clay and silt content in the E horizon is weak, negative and non-linear, but positive and moderately strong for the soils of a high and moderate mineral soil carbon stock. The chute eskers and transverse eskers in both valley 1 and 2 fall on a negative linear line. The E horizon is thickest in valley 3 and in the chute eskers. In the sub-glacial eskers, the E horizon is thicker at a higher clay and silt content. The soils of low carbon stock in the mineral horizons and thin E horizons show the lowest clay and silt content.

Interpretation. At an E horizon thickness below 10 cm, the amount of silt and clay appears to plot above 38 %. There appears to be a proportionality between the properties within this interval, within which all soils of a moderate and high mineral soil carbon stock are found. The soils of the lowest carbon stock in the mineral horizons are less developed and have less surface area for soil processes to occur on. The silt and clay content of the E horizon appears to be significant for stabilising a high or moderately high mineral soil carbon stock.

Active iron and aluminium in E against base saturation in E (figure 4.13 B)

Description. The plot between the AFe and AAl in E and the base saturation in E is weak and L-shaped, but strong, positive and linear for the soils of a low and moderate mineral soil carbon stock. The crevasse eskers in valley 1 plot at a high and relatively high ratio, respectively, and V3-4 and V2-1 at a low and relatively low ratio, respectively. V2-7 and V3-1 plot at the lowest value for both properties. The soils with a high carbon stock in the mineral soil plot at a high content of active iron and aluminium, where V1-2 (of the very highest mineral soil carbon stock value) show a high base saturation.

Interpretation. The soils that preserve carbon in the mineral horizons show a high content of active iron and aluminium and base saturation of the E horizon. The relationship can be used to evaluate the degree of podzolization, where low base saturation and larger translocation of spodic material indicates stronger podzolization. Soils that plot at a high or low ratio has therefore undergone less podzolization. From this plot, V2-7 and V3-1 appear to have undergone the strongest podzolization and are found at the lowest and highest elevation in the area, respectively (see DEM, figure 3.1), suggesting that the influence of elevation on soil formation based on these properties is not essential to consider.

The relative values of the AFe and AAl in the E horizons for V1-2, V3-2, V3-1 and V2-7 are inversely proportional to the calculated nutritional status of the soils (chapter 4.3), with a comparable relative increase in strength between nutritional values and the AFe and AAl plotted here. This suggests that podzolization is strongest on landforms formed from the most acidic material. The strength and nature of podzolization is evaluated in figure 4.14.

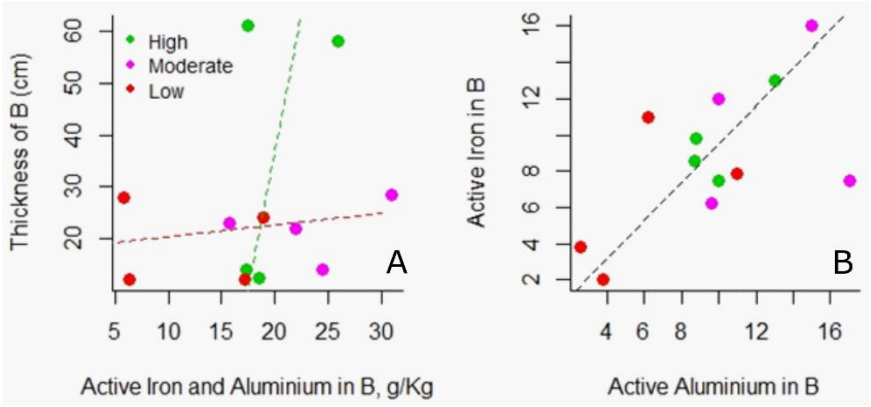

Figure 4.14. Carbon stock and properties of the Bs horizon. A: Green trendline based on the soil that show a high mineral soil carbon stock, and the red trendline is based on the soils that show a low and moderate mineral soil carbon stock. B: Trendline based on the described profiles. Legend (left) indicates mineral soil carbon stock for both plots.

Thickness of Bs against Active Iron and Aluminium in Bs (figure 4.14 A)

Description. The plot of the thickness of B and its content of active iron (AFe) and aluminium (AAl) is moderately strong, positive and linear for soils with a high mineral soil carbon stock, and weak for soils of a moderate and low mineral soil carbon stock. The Bs horizons of V1-2 and V3-2 are double in thickness (around 60 cm) compared to the other profiles but have similar value of Afe and AAl. V1-4 is high in AFe and AAl

relative to other soils of similar Bs horizon thickness. V3-1 and V3-4 are both thin and with a low AFe and AAl value. Soils of a lower carbon stock of the mineral soil plot at a generally lower less variable content of active iron and aluminium in Bs.

Interpretation. A high value of AFe and AAl in a thin horizon can equal lower values in a thicker horizon as volume and concentration balance each other out. A thickness-integrated measure would indicate that V1-2 and V3-2 contain the most active iron and aluminium overall. The AFe and AAl should ideally be weighted for the horizon thickness when compared, as the effect of different concentrations (g/kg soil) may be enhanced by or compensated for in a thick or thin horizon. Higher content of active iron and aluminium in B suggest that the carbon stock of the mineral soil is higher, and that podzolization is a carbon-stabilising process. At the same Bs horizon thickness, the mineral soil carbon stock is higher in soil of higher active iron and aluminium content, suggesting the weathering products may provide a stabilising mechanism for carbon.

Active Iron in Bs against active aluminium in Bs (figure 4.14 B)

Description. The plot of active iron in the Bs horizon against active aluminium in the Bs horizon is moderately strong, positive and linear, and strong for soils with a high mineral soil carbon stock. Two outliers occur, V2-8 at a higher ratio and V2-7 at a lower ratio. The landforms in valley 3 plot at the lowest values, in valley 2 in the middle and in valley 1 at the highest values. The ratio between the properties is highest for the soils in Valley 1, and around 0.5 in the soil of the least nutritious parent material (V2-7). Lower values of both properties are found at lower mineral soil carbon stock, and moderate values for higher mineral soil carbon stock.

Interpretation. Lundstrom et al. (2000) suggested that two processes dominate the podzolization process, and a larger difference between the active iron and aluminium indicates the relative importance of the two soil forming processes. These are “formation and downward transport of complexes of organic acids with Al and Fe” and “silicate weathering followed by downward transport of Al and Si as inorganic colloids”. High Fe versus Al suggests that the former has driven soil formation, here true for V1-5), while high Al versus low Fe suggests that the latter, here true for V2-7. The relative importance of these processes can be linked to parent material. In general, the landforms in Valley 1 display a higher ratio, suggesting that the soil formation in more nutritious parent material is driven by downwards transport of (hydr)oxides with organic acid complexes, while in the innutritious parent material, as inorganic colloids.

Key observations

The mineral soil carbon stock increases more with an increase in all podzolization indicators in soils formed from nutritious parent material. The nature of podzolization appears to affect the mineral soil carbon stock, but it is possible that the correlation is found due to the parent material, where nutritious parent material gives both a higher mineral soil carbon stock and

correlates with podzolization by downwards transport of (hydr)oxides with organic acid complexes. The strength of podzolization, on the other hand, affects the mineral soil carbon stock. Values for both active iron and aluminium are in high mineral horizon carbon stock soils, indicating strong soil weathering processes and a positive correlation. It is possible that the ratio is slightly higher for high carbon stock values, suggesting that iron and aluminium are translocated with organic acids in the soil. This reaffirms the interpretation that podzolization transports and stabilises carbon at depth.

4.6 Carbon Stabilisation

The interpretation that the nutrition status of the soil and the strength of podzolization both affect the mineral soil carbon stock is evaluated by correlating soil properties that indicate both (the thickness and C/N of the O horizon and the ratio of active iron and aluminium in Bs over E, respectively) in relation to the size and proportion on the mineral soil carbon stock. The colour code indicates the amount of mineral soil carbon stock as well as the potential for increased storage. All soils with a high total carbon stock show a high or low mineral soil carbon stock, and none of the soils of a low total carbon stock show a low mineral soil carbon stock to organic soil carbon stock ratio.

Table 4.8. Carbon stock in relation to the proportion of the mineral soil to organic soil carbon stock ratio. The colours correlate to figure 4.15.

Ratio[1]	**High Total Carbon Stock**	**Low Total Carbon Stock**
High	V1-2, V2-1, V3-2	V2-3, V3-1
Moderate	-	V1-5, V2-6, V2-7
Low	V1-3, V1-4, V2-8, V3-4	-

[1]Ratio of carbon stock of mineral soil over carbon stock of organic soil

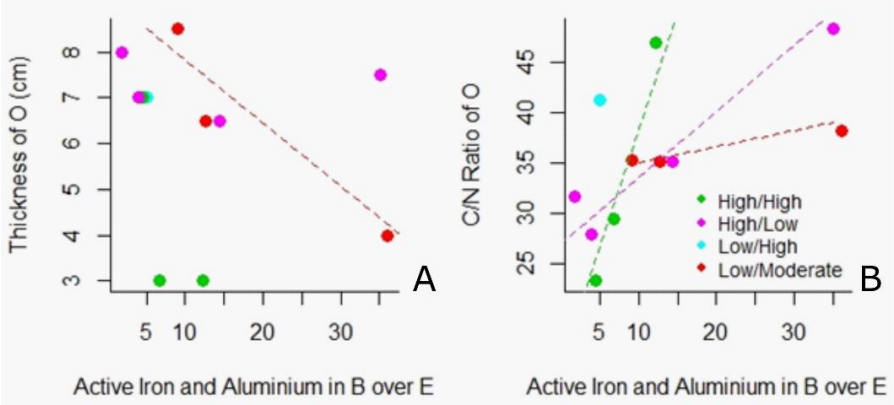

Figure 4.15 Indicators of production and podzolization in relation to the ratio of mineral soil carbon stock to total soil carbon stock. A: Red trendline indicates the soils that store the least carbon at depth. B: Green trendline indicate the soils that store the most carbon in the mineral soil, the red trendline indicate the soils that store the least carbon in the mineral soil and the purple trendline the soils that have a high carbon stock, but not in the mineral horizons. The legend (right plot) indicates the total carbon stock/ratio of mineral soil to organic soil carbon stock for both plots.

Thickness of O against Active Iron and Aluminium in Bs over E (figure 4.15A)
*Description***.** The plot of the thickness of the O horizon against the BEFeAl is moderately strong and negative for soils of a low total carbon stock and/or low mineral soil carbon stock. All soils but V2-1 plot at a total O horizon thickness between 6.0 and 9.0 cm. The chute eskers, transverse eskers in valley 2 and crevasse eskers in valley 1 have the thickest O horizon and are found at the lowest (below 10) and highest (above 35) BEFeAl values. Soils with a high total carbon stock and high mineral soil carbon stock have thin O horizons. Soils with a high total carbon stock and low mineral soil carbon stock have thick O horizons.

*Interpretation***.** The thickness of the O horizon indicates soil nutrition status, and the most nutritious soils appear to be the chute eskers, V2-7 and V1-4. It appears that the most nutritious soils are the ones that are the least and the most developed, of the parent material is the most nutritious and least nutritious, respectively. Soil of a high total carbon stock and high mineral soil carbon stock show thin organic horizons, suggesting little storage of organic material in the surface of the soils. For soils of a low/moderate ratio (see legend), the negative linear relationship between O horizon thickness and BEFeAl might reflect the necessity for strong nutrient extraction to enable decomposition.

C/N ratio of O against active iron and aluminium in Bs over E (figure 4.15B)
Description. The plot of the CNO against the BEFeAl is strong, positive and linear for all four carbon stock categories, and moderately strong and positive when all are considered. Soils of a high total carbon stock show either a very high or very low ratio of mineral soil carbon stock to organic soil carbon stock, and soils of a low total carbon stock show either a high or moderate ratio of mineral soil carbon stock to organic soil carbon stock. Soils that are high in both described properties show a low value for active iron and aluminium in Bs over E, while soils that are high in total carbon stock but low in the mineral/organic soil carbon ratio, show high values for active iron in Bs over E. Soils of a high total carbon stock and high mineral soil carbon stock show a low C/N ratio of O. Soil of a high total carbon stock and low mineral soil carbon stock show similar O horizon C/N ratio as high total carbon stock and high mineral soil carbon stock, but higher active iron and aluminium content in Bs over E.

Interpretation. Soils formed from nutritious parent material plot at low CNO and BEFeAl, and the soils developed from the least nutritious parent material at high CNO and BEFeAl. The parent material determines soil nutritious status (C/N of the O horizon) and consequently, the degree of soil formation, which is stronger at high BEFeAl. A higher CNO suggest that carbon is stabilised biochemically in the surface soil, and a higher BEFeAl provides a higher potential for carbon translocation, complexation and stabilisation in the subsoil.

Interestingly, higher carbon stabilisation in the organic horizon might suggest a higher stabilised stock at depth, possibly suggesting that translocated carbon not necessarily is highly decomposed. Overall, however, carbon stock is highest in the soil developed from the most nutritious parent material. It is possible that a long-term perspective should be considered,

where the stock of carbon might be higher in these soils at the moment but will be higher for a longer period of time in the nutrient deficient soil high in soil weathering products at depth. The sub-glacial eskers (V3-2, V2-8 and V1-5) and delta (V2-7) are found at the highest CNO to BEFeAl ratio, indicating biochemically limited decomposition at a similar degree soil formation. The plot gives the impression of limited decomposition for all soils of a low total and low mineral soil carbon stock (red trendline), which are mainly found in valley 2. Conditions are optimal for decomposition in soils of a high total and high mineral soil carbon stock, which are mainly found in valley 1.

The linear correlation between the CNO and BEFeAl (very steep for high/high ratios, intermediate for high/low ratios (high inorganic soil) and shallow for low/moderate ratios) reflects the dependency of decomposition on nutrient extraction and its effect on carbon stocks. Where both a higher total and mineral soil carbon stock correlate with less increase in podzolization/nutrient extraction at more restricted conditions for decomposition in the organic soil, low carbon stocks correlate with high biochemical stabilisation in the organic soil and increased nutrient extraction at increasing difficulty for decomposition.

Additional observations after O and Bs comparison

It appears that there is a larger difference in CEC of the O and Bs horizons in more acidic parent material (Appendix 4), which relates to a lower organic carbon content. According to Yusoff et al. (2017), organic material is likely to determine the CEC in sandy soils. Proportionality exists between the carbon content and cation exchange capacity in the Bs horizons, but not the other horizons, suggesting that organic carbon is important for nutrient availability at these depths. The CEC is highest in the organic horizons of V3-2 and lowest in V3-1, and highest in the Bs horizons in valley 1 and lowest in the Bs horizon V2-7. Consequently, the carbon stabilised in the mineral soil in valley 2 is more readily decomposed than in valley 1.

The C/N ratio of the O horizon (CNO) against the CEC of the Bs horizon over E horizon (BECEC) shows a weak and positive relationship for high organic soil carbon stock and moderately strong, negative and linear correlation for low organic soil carbon stock. V1-2, V2-7, V3-4 and V3-1 plot within the optimal range for decomposition, across both high and low BECEC. The highest CNO is found in valley 2, and the lowest CNO is found in valley 1. Soils developed from nutritious parent material have a low CNO and low BECEC, suggesting rapid turnover of nutrients in the topsoil, but not necessarily downward translocation of the decomposed matter.

Key observations

Soils of both a high total carbon stock and high mineral soil carbon stock are nutritious with rapid nutrient turnover. Constant biochemical conditions are found within the two soil groups 1) high total high mineral soil carbon stock and 2) low total and moderate mineral soil carbon stock, where the former experience optimal conditions for decomposition and the latter less

than optimal. It appears that soils of a high soil nutrition status (seen from pH, CEC and O horizon thickness) that have undergone strong soil weathering processes not necessarily stabilise the translocated carbon at depth (e.g. V2-7). This is possibly a result of soil formation from an innutritious parent material. Mineral-soil stabilised carbon is more easily degradable in soils formed from innutritious parent material. Carbon in high carbon stock soils are protected by other than biochemical mechanisms.

5 Discussion

5.1 Deglaciation History

The study area was deglaciated by the melting of stagnant ice (Garnes & Bergersen, 1980), and the glacifluvial deposits in the three valleys reflect the ice flow phases interpreted by Putnins and Henriksen (2017). Ice-damming of meltwater upstream from the ice front, formation of a hummocky terrain, kames and kettle holes and deposition of eskers transverse to the ice-flow direction resulted from down-wasting of stagnant ice.

Meltwater deposits in Gausdal Vestfjell are likely to have formed in what Putnins and Henriksen (2017) named the channelized ice flow phase (phase III). Valley 1 is dominated by "Early phase III", valley 3 by "Middle phase III" and valley 2 by "Late phase III". Ice flow persisted in valley 2 the longest. The onset of flow within this phase of ice flow can be identified from parallel esker systems. Sediments were deposited in valley 1 at late stages when ice flow had ceased, and in valley 3, most likely both during flowing and stagnant ice (figure 5.1 A-B). In valley 2, a different dynamic between drainage and deposition occurred, where the nature of drainage and deposition was dominated by meltwater accumulation NW of the ice front (figure 5.1 D-G).

Livingstone et al. (2010) has described how belts of meltwater deposits record an evolving deglaciation landscape where the nature of drainage shifts from subglacial to supraglacial, a system "dominated by ice-walled lakes and ice-contact drainage networks". A similar evolution in deposition has occurred in Gausdal Vestfjell. Eskers deposited in valleys 1 are supraglacial (figures 3.5-3.8), the kame terrace in valley 3 (V3-1, figures 3.27-3.30) is an example of deposition along an ice-contact drainage network (figure 5.1 A), while deposition of fans, delta and plain in valley 2 (figures 3.10-3.16, 3-18) is largely the result of sub-aerial and sub-aqueous deposition in and near an ice-dammed lake (figure 5.1 C-G).

Reconstruction of deglaciation from glacifluvial landforms is difficult, as the spatial relationship between deposition and ice is unclear (e.g. Spooner and Osborn, 2000). It is reasonable to assume that both lateral and subglacial drainage occurred throughout the study area during the last stages of melting. This complicates the interpretation of timing of events, but also shows that processes cannot necessarily be linked to specific time intervals. Spooner and Osborn (2000) suggested that the last stages of valley deglaciation occur as stagnated, down-wasting glaciers, with both subglacial and ice marginal drainage networks.

Drainage of the valleys shifted temporally and spatially (figure 5.1 A-B) and it is unlikely that the stagnant ice melted back at the same time in all three valleys. The topography appears to have played a significant role. Valley 3 is not so deep and did not have the same water accumulation as valley 2. At the inlet of valley 3 (V3-3, figures 3.34 and 3.35), the

sedimentary log shows flow to the E above the compacted sediments. When meltwater drained through valley 3, the area was covered in ice. As the ice melted back, the flow followed the topographic low, which was into valley 2 from the NW (along with input to the valley from the N), which resulted in the filling of an ice dammed lake. Drainage of valley 1, which lack later stage meltwater landforms, was first towards the N, out of the study area through the palaeochannel in the ENE (figure 3.1). Valley 1 also drained towards valley 2, through one of the eroded palaeochannels in the S. Drainage of valley 3 was to the SE, towards the intersection with valley 2 in the S (figure 5.1 A). There was a shift in drainage from valley 3 to valley 2 when the ice in valley 2 was sufficiently low. At this time inflow went from being subglacial under flowing ice, and from then on sediments were deposited in stagnant ice (figure 5.1 B). This suggests that rapid melting and lake formation started almost as soon as the ice flow ceased. The landforms in valley 2 are the youngest and require ice to have receded and for the lake to have formed. The lake is likely to have started sub-glacially, which may have sped up deglaciation of the valley (figure 5.1 B).

The sedimentary evidence from the Northern side of valley 2 suggest a step-wise lowering of the lake level (figure 5.1 D-G). This suggest specific events of drainage, e.g. melting below pass points. The step-wise lowering may alternatively reflect continuous and accelerating drainage coupled with event-based infill of meltwater from melting or drainage upstream from the study area. Drainage can also have occurred continuously, with breaks at certain levels. Stagnant ice melts down in a vertical manner (Garnes and Bergersen, 1980), suggesting that the lake lowering was a result of drainage and not basin extension due to receding ice. The lake is likely to have drained sub-glacially, as the pass point in the S (at the intersection with valley 3 in the SE) shows evidence for high hydrostatic pressure (figure 3.1).

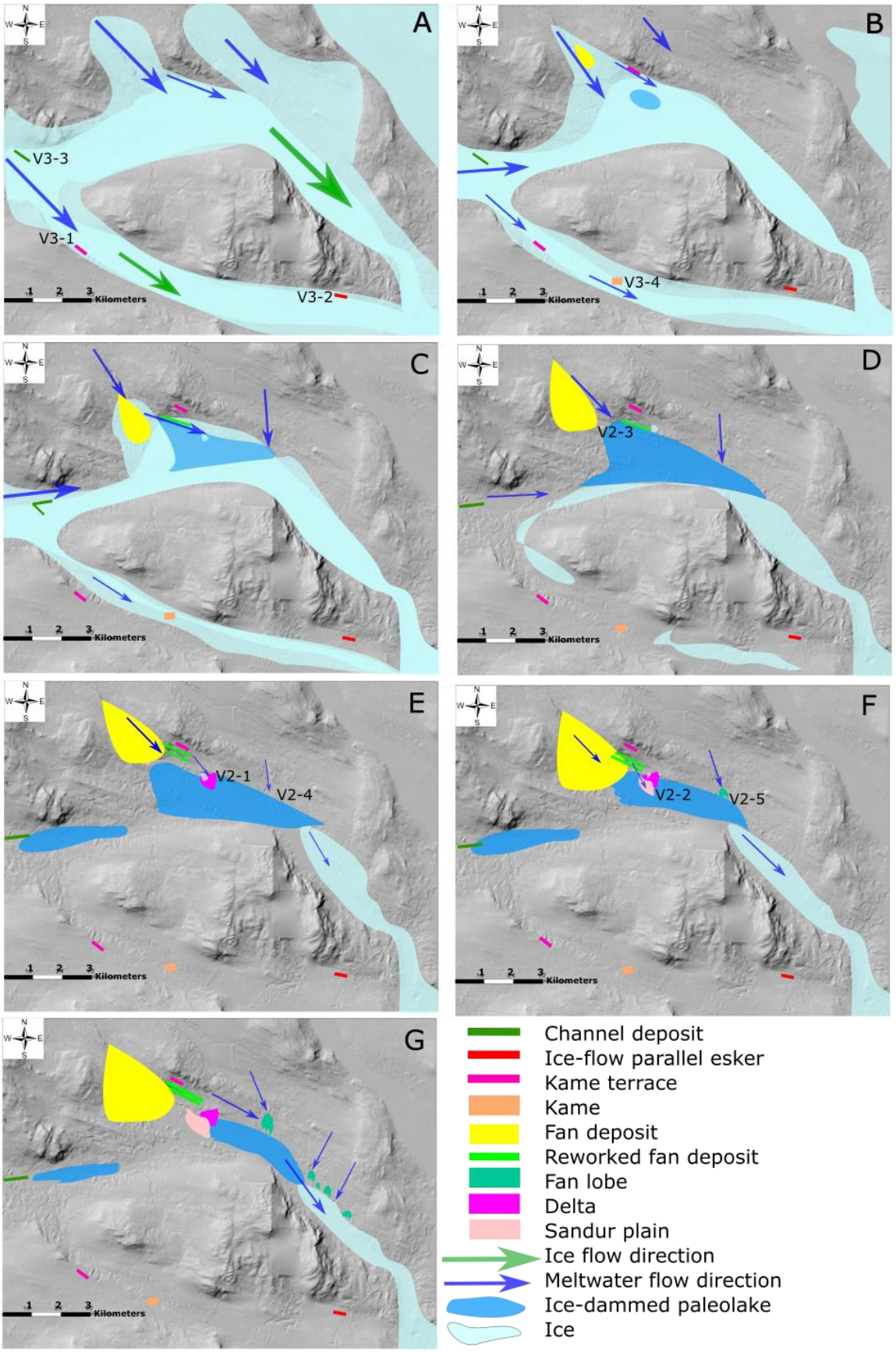

Figure 5.1. Successive time slices illustrating the ice retreat in valleys 2 and 3. The landforms are shown at the time of their appearance. The model is schematic and does not accurately display the elevation of the ice surface.

The drainage followed the ice flow (middle phase III of Putniņš and Henriksen, 2017) towards SE in valley 3 (figure 5.1 A). A kame terrace (V3-1, figures 3.27-3.30) was deposited at the water divide in valley 3, when water drained through valley 3, with ice still present, and thick enough to allow for lateral drainage. The kame further SE (L3b on figure 3.2) is likely to be deposited in the continuation of the channel that deposited the kame terrace at V3-1. Marginal meltwater channels that continue down through the ice to form moulins are, according to Dyke (1993), an indication of cold-based ice, which suggests that the kame terrace may have formed at an early stage of deglaciation. The landforms at this locality are possibly of a similar age as those at the inlet at V3-3. The cluster of eskers, mapped by Putnins and Henriksen (2017), W of V3-1 may represent stagnation of the ice front as it melted down in the valley.

Glacifluvial sediments on top of the streamlined landform at V3-3 were deposited as drainage occurred through valley 3 and ice still covered the inlet at V3-3 (figure 5.1 A). Drainage was SE through valley 3 when the lowermost channel sediments were deposited at the inlet of the valley (V3-3). Following down-wasting of ice in valley 2, drainage was straight E through the Westernmost lake in valley 2 and then SE through valley 2 (figure 5.1 A-B). The compacted deposits at V3-3 (figure 3.35), interpreted as meltwater deposits due to the degree of sorting and rounding, must have been deposited while ice flowed across the area. Consequently, drainage SE through valley 3 partially occurred sub-glacially and when ice was still present. The ice may have been at least as thick as the height of the streamlined landform to allow for sub-glacial deposition on top of it. The palaeochannel at V3-3 can either represent a glacier crevasse or have been formed by a side river in to the valley (valley 3). The drainage patterns along with the high elevation of valley 3 suggests that the landforms in valley 3 are among the oldest in the study area. The main inflows of water to valley 3 at an early stage of meltwater drainage, and later to valley 2 under stagnant ice conditions.

Ice flow persisted in valley 2 the longest (figure 5.1 A). Meltwater drained, mainly sub-glacially and ice-laterally, to the SE through valleys 2 as ice flow stagnated in valley 3 (figure 5.1 A). Kame terraces formed at progressively lower levels along the NW margin of valley 2 as the ice surface lowered (figure 5.1 B). Valley 2 was later fed with meltwater from the N, NW and W (figure 5.1 C). Sub-aerial channel deposits were formed above the sub-glacial deposits at the inlet in the W (V3-3) (figure 5.1 C).

The main and latest drainage is likely to have occurred in valley 2, because the valley is deepest and most profound, and contains landforms that have formed both sub-aerially and in standing water. Meltwater input to valley 2 from the palaeochannels in the N melted and eroded the ice from the bottom. Meltwater accumulated as it was dammed by the ice further downstream the valley (figure 5.1 C-D). As the lake in valley 2 started to drain, progressive lower terraces formed along the N-side of the valley (e.g. V2-4, figure 5.1 E. Ice filled only the lower parts of valley 2 towards the end of the period of glacifluvial deposition (figure 5.1 G).

The landforms in valley 2 are likely to record re-sedimentation of glacifluvial material as the ice disappeared and more material was available for meltwater to reworking. The high degree of rounding (figure 3.36) supports this interpretation. The fan deposits (V2-3) are eroded (figure 3.18) which may have happened at a at a later stage by meltwater inflow from the E or by shoreline activity. The parallel strike of side of the deposit with the fore-sets of the delta (V2-1, figures 3-10-3.12), suggest that the inflow to the lake cross-cut the deposit and that the direction of flow was constant for a considerable time, at least for long enough for fore-set deposition. Tollan (1963) described how material is sorted and re-sedimented into flatter meltwater landforms in lower-laying areas. Such landforms have been mapped mapped by Putnins and Henriksen (2017) downstream in valley 2. It is possible that the terraces in valley 2 (e.g. V2-4, figures 3.19, 3.20 and 5.1 E) are a result of these processes. The meltwater drainage in valley 2 can be summarised from sedimentary logs and GPR profiles (chapter 3.2) and the DEM (figure 3.1) as follows:

Time 1 (figure 5.1 B). Fan (V2-3) starts forming upstream at high elevation (above 820 masl) , filling of the lake begins
Time 2 (figure 5.1 B). Formation of kame terrace (L26 on figure 3.2) (820 masl)
Time 3 (figure 5.1 C). Formation of sub-aerial palaeo-lake
Time 4 (figure 5.1 D). Lake level at the highest before drainage exceeds input (815 masl) (ice front at first esker system) (figure 3.5)
Time 5 (figure 5.1 D). Formation of terrace, ice-lateral channel or palaeo-lake shoreline (V2-4) (801 masl)
Time 6 (figure 5.1 E). Formation of fan deposits (V2-3) (797 masl) (ice front at second esker system)
Time 7 (figure 5.1 E). Formation of delta (V2-1) (794 masl), erosion of fan deposits (V2-3) (797 masl) (ice front at the third esker system)
Time 8 (figure 5.1 F). Formation of sandur plain (V2-2) (782 masl) (ice front at the at fourth esker system)
Time 9 (figure 5.1 F). Formation of distal part of large fan deposit (V2-3) (778 masl)

Meltwater possibly accumulated sub-glacially in valley 2 as soon as ice movement ceased (figure 5.1 B), and landforms might be found below the modern-day lake. However, landforms formed during the filling and draining of the lake might not have been preserved if major meltwater flows were to influence them at a later stage, and the formation of a lake can explain why there are few sub-glacial landforms at low elevations in valley 2. The deeply eroded channel in the NW that formed when the ice still covered the area is possible linked to the earliest filling of the (then subglacial) lake (figure 5.1 B). The same channel system is likely to later have fed the delta, plain and fan. If the maximum lake level was below about 820 masl, the lake would have been drained only through the passage at the intersection of valleys 1 and 2, and not Nwards across valley 1. The lake level would have had to be around 850 masl and blocked in the E towards valley 3 for that to occur. A lake level of 820 masl at

the highest is likely, as it is below the water divide in valley 3 (the kame terrace) and would be contained in all directions in valley 2 and 3 but the SE where the ice front is assumed to reside (figure 5.1 D).

If the lake in valley 2 was ice-dammed, the deposition in ice-crevasses in valley 3 can be related to the step-wise down melting/draining of the meltwater basin (as crevasse eskers are assumed to be located at progressive ice fronts (Putniņš and Henriksen, 2011), figure 5.1 C), and hence down-wasting ice was damming the meltwater in valley 2. It is therefore possible that the sedimentation of the delta flat was synchronous with a cluster of crevasse-fill eskers. If there is no relationship, it is still possible that groups of transverse eskers represent ice front stages during down wasting.

The lateral downcutting and reworking of glacifluvial sediments downstream valley 2 suggests that the glacifluvial deposits might have formed sub-glacially. The extent to which deposition of the large fan NW in valley 2 was subglacial (V2-3, figure 3.18), is uncertain. A generally loose nature of sediments suggests sub-aerial deposition, while very coarse grain sizes suggest short transport distances. Fredin et al. (2013) suggested that deltas along valley sides in ice-dammed lakes often are deposited near the ice-margin. If the terraces along the Northern side of valley 2 (e.g. V2-4, figures 3.19 and 3.20) formed from deposition of lateral channels and the lake existed sub-glacially for a significant time period, the channels that deposited the landforms in valley 2 were ice-lateral. Vertical down wasting in the area complicates this interpretation. The most likely scenario is sub-aerial delta formation in a rapidly changing environment. Landforms at higher elevations can generally be considered older than lower laying landforms upstream (Garnes and Bergersen, 1980). Even if landforms in valley 2 started out as subglacial, the higher parts of the large fan is among the oldest landforms in the area.

Ryder et al. (1991) described how glacial drainage can be affected by down wasting of ice in valleys and suggested that ponding of meltwater generally is a result of drainage systems that are not aligned with the general direction of ice retreat. According to Garnes and Bergersen (1980), isolated ice remnants could remain at higher elevations after the ice retreated and melt away as stagnant ice hence a palaeo-lake dammed by down-wasting ice still can be supplied with meltwater. The interaction of vertical down wasting ice and the relief of valley 2 resulted in several pass points that limited progressive drainage like in valleys 1 and 3.

The deposits and topography surrounding valley 2 suggest that an ice-dammed lake would be restricted in size and duration of existence. Field investigation of the meltwater deposits mapped by Putnins and Henriksen (2017) along the lake bottom in valley 2 have shown that they are flat and extensive, consisting of well sorted and fine grained (silty) sediments. It is possible that they constitute the distal part of the fans described further N in the valley side. Alternatively, they are exposed lake sediments. The GPR profiles along the possible shoreline in valley 2 (V2-4, figures 3.19 and 3.20) suggest that the deposits are glacifluvial (stratified

and sorted). It is possible that they are lake sediments, deposited in lateral channels along the shore. The lack of continuity along the valley side justifies an interpretation as glacifluvial terraces. The filling of the lake occurred laterally from the N resulting in kame terraces in the NW and fans further E, and later the delta and sandur plain. Meltwater input during deposition of the fan was above lake level.

The deposits along the Northern side of valley 2 suggest that drainage occurred along this margin. By the time the lake level would have reached the pass point through valley 3, the ice surface in valley 2 would have been low enough to favour drainage through valley 2. The terraces along the N side of valley 2, interpreted as kame terraces, eroded fan lobes and shoreline deposits, where in the field largely identified based on morphology. Later-stage changes have affected the landforms, such as lateral reworking by channel flow. Tollan (1963) described this process and suggested that it results in the absence of sharp and steep ice-contact deposits. The flat meltwater landforms downstream near the present day lake result from glacifluvial reworking when the ice was almost gone (figure 5.1 F-G).

5.1.1 Glacifluvial Deposition

The proximal deposits of the large fan in the N are found at high elevation (> 850 masl), hence the fan is likely to have started forming at an early stage, sub-glacially or sub-aerially. The fan is likely to have formed throughout deglaciation of the valley, both during lake damming and drainage (figure 5.1 B-F). By determining the nature of the debris flows in the two logged fan deposits in valley 2 (V2-3 and V2-5, figures 3.18-3.20 and 3.24-3.26), the evolution of down-wasting ice and lake drainage can be inferred, as well as the time of deposition relative to the ice position. Sediment-gravity flow deposits can be either sub-aerial or sub-aqueous (Benn and Evans, 2010) (page 406). The reversely graded beds, sharp, erosive boundaries, clast-supported beds and elevated boulders in fine matrix suggest that the deposits downstream in valley 2 (V2-5, figures 3.24, 3.25 and 3.26) are partly formed by sub-aerial debris flows (figures 3.24, 3.25 and 3.26). The loose nature of the deposits upstream in the valley suggests their nature is colluvial, possibly constituting part of a debris cone (e.g. V2-3, figure 3.18). The down-stream deposits suggest deposition occurred along the valley as the ice had receded, but also at low lake levels (5.1 F). The fan deposits further down along the N side of the valley were formed under quieter conditions (figure 5.1 F-G).

Spooner and Osborn (2000) described the nature of delta deposits (figure 3.10) in relation to lake level condition. The authors suggested that gravel beds are formed at low stands, from traction currents or because of increased flow at these times. It might be possible to relate coarser intervals in the delta sequence to drainage events of the lake. The thickest of these intervals is found above an interval with structures indicating shallow water deposition (86-120 cm in the log of V2-1, figure 3.10). Isolated ice-blocks remained along the N-side of valley 2 after the ice retreated (figure 5.1 C), which resulted in kettle holes in the area around

the soon-to-form delta (V2-1, figures 3.11, 3.12 and 5.1 D-E). As the lake level was rising towards its maximum height (figure 5.1 D) the delta was prograding, fed by meltwater from the NW (with a stronger W-E component at first), and ice remnants were covered in deltaic sediments (figure 5.1 E).

In valley 2, a lot of material was available for re-sedimentation by meltwater. The sorted and fine nature of the flat, low-laying deposits along the N side of the valley (figure 1.5) suggest a long transport distance and high degree of re-sedimentation. It is possible that the finest-grained sediments among these are lacustrine, partially covered by the modern-day lake (figure 1.5). The meltwater entered valley 2 mainly from the NE at the latest stage (figure 5.1 G). The deposits along the Northern side in the S of valley 2 are, however, difficult to interpret. They are tentatively interpreted as fan sediments, possibly reworked at a shoreline. Ryder et al. (1991) described deposition of gravel and sand from gravity flows and short-transported meltwater discharge. The coarse and chaotic nature of the sediments along the NW side of valley 2 (figure 5.1 C) suggests a short transport distance, and possibly disturbance or collapse from removal of stability. Ice appears to have been nearby during deposition of these sediments. The erosion of fan sediments along in the NW of valley 2 (e.g. V2-3, figures 3.17 and 3.18) as meltwater drained into the lake from the valley side (figure 5.1 C) may have contributed deposition of finer sediment along the N side downstream.

The nature of the fan and plain (figures 3.14-3.16 and 3.18) NW in valley 2 can be interpreted with regards to surrounding topography. Benn and Evans (2010) (page 534) name outwash deposits limited by narrow valleys in mountainous areas “valley trains”. This is a more appropriate term for the deposits identified as a sandur (V2-2, figures 3.14-3.16). They also describe the formation of these deposits as an integral part of larger fan systems. The valley train constitutes the distal part of a fan, with its proximal part where narrow gorges expand into a broader area. The deeply eroded inlet NW in valley 2 could be considered the equivalent of such a gorge. The fan was probably formed subaerially. Benn and Evans (2010) (page 541) divided sandur environments into four facies associations. The “Platte type” is typically found in the distal part of a sandur, where flow is distributed across shallow and abundant channels. Sandy bedload is transported as migrating bars, and cross-bedding dominates.

According to Fredin et al. (2013), inferring a receding ice-front from esker belts is sensible, as they are most likely formed obliquely to the glacier margin when the front stagnates. Meltwater filling of the ice dammed lake and delta formation in valley 2 may have occurred at the same time as the esker belts. The eskers interpreted to have formed as filling of supraglacial crevasses, V1-1 and V1-2 (figures 3.5-3.8), show the least developed erosional surfaces among the logged deposits. This may suggest, more continuous deposition, short time gaps between depositional events, and/or less variation is deposition including sediment supply and flow regime. The wide eskers in valley 1 (e.g. V1-2, figures 3.7 and 3.8) are composed of sediments that fine outwards from the esker core, which can indicate

accumulation of meltwater in the ice channel during deposition. Livingstone et al. (2010) suggested that ponding of meltwater surrounding esker deposition results in fining outwards sediments, and if true here, might indicate meltwater accumulation supra-glacially or between remaining blocks.

In the eskers, and to some extent kames, coarsening up sequences represent times of major flow, when drainage follows the path displayed by the landform. Intervals of finer sediments might indicate low discharge, or times when drainage was elsewhere. Coarsening upwards of channels, seen in eskers (e.g. figures 3.5-3.8), the kame terrace (figures 3.27-3.30) and the sandur plain (figure 3.14-3.16), can in general be thought to represent times of reactivation of channels. Livingstone et al. (2010) suggested that fining upwards sequences record "backwater outlets" in kames and kame terraces. Layers of silt within the deposits can be considered times of low or no flow, were meltwater accumulates locally and particles settle from suspension. These drapes represent breaks in discharge. The changes in direction of flow often record the evolution of drainage patterns as a result of down-wasting of ice.

Filling of crevasses in valley 1 (e.g. figures 3.5 and 3.7) may have lasted as long as ice was present. The strike of the eskers in the E of valley 1 is similar to the nearby palaeochannel (figure 3.1). These eskers possibly formed during drainage across the valley. They are longer than the other transverse eskers. The channels (especially in the N) record high-pressure flow. There is no clear obstacle in the SE, and the channel was possibly ice-lateral. The implication is a stagnating ice front at this point during extensive drainage. An NE-SW trending ice front (perpendicular to the direction of ice movement), would have created a barrier at the passage in the sharp bend of valley 2.

The eskers in valley 2 are of an equivalent size, shape and orientation to eskers in valley 1, found on a straight NW-SE-trending line perpendicular to ice flow. This might suggest that they formed in an analogous manner at the same time, e.g. in crevasses as the ice front was at this line. The ice-transverse eskers in valley 2 (V2-6 and V2-7) are found at 830 masl and are possibly a result of meltwater drainage between valleys 1 and 2. The DEM (figure 3.1) shows palaeochannels that strike N-S near the eskers. The flat, extensive area surrounding the eskers suggest they are not chute eskers, but possibly formed in stagnant ice. The eskers are not found in clusters such as in valley 1 and 3 (figure 1.5), which are interpreted to be formed by supraglacial ice-crevasse fill, possibly suggesting a different mode of formation. The esker at the sharp bend downstream valley 2 is found on a steep hillside, suggesting it did not form in a crevasse but in a channel under high hydrostatic pressure.

5.2 Soil Carbon Stock and Stability

5.2.1 Carbon Stock

The formation and stabilisation of recalcitrant organic material in soils is essential for understanding the global cycling of carbon in a long-term perspective (Eusterhues et al., 2005). The carbon pools at depth are associated with slower cycling of organic carbon (Trumbore, 2000), as they are resistant to oxidative processes and generally older than the average soil material (Eusterhues et al., 2005). The stabilisation of carbon in a podzol is expected to increase with the soil weathering products clay and silt, and active iron and aluminium oxides (Schlesinger and Bernhardt, 2013). The proportional relationship is true for three of the four described profile (figure 5.2), but V2-7 shows a lower carbon stock than what the content of both clay and silt and iron and aluminium oxides predict. This suggest that other parameters also affect the carbon stock of the soils.

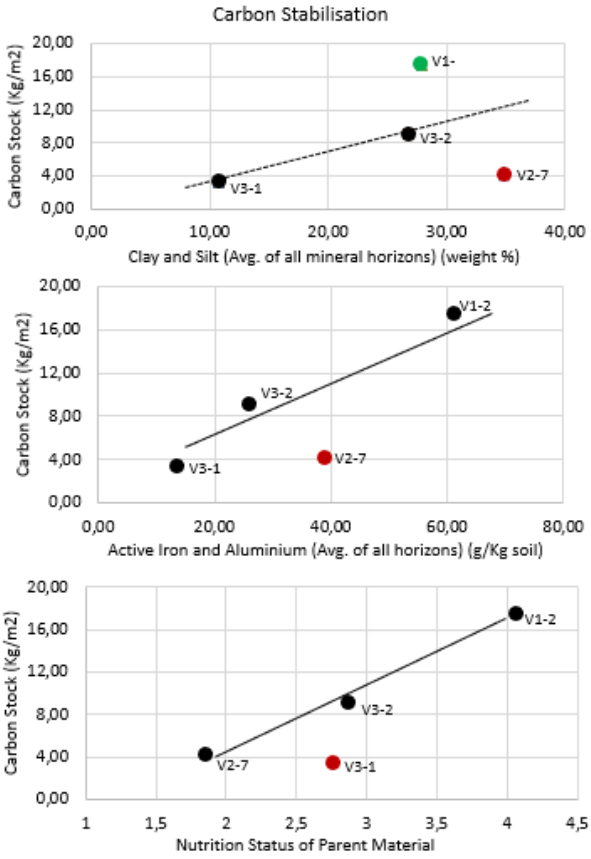

Figure 5.2. Indication of stabilisation of soil carbon by comparison of carbon stock with soil texture, content of active oxides and nutrition status of parent material.

By comparison of carbon stock against the calculated nutrition status, however, V2-7 follows the same trend as the other profiles. Here, V3-1 shows a lower carbon stock than the parent material predicts. It is important to note that the nutrition status is an estimation by a constructed method, and not an absolute measurement like the two other properties. It is possible that the nutrition status of the parent material of V3-1 is an overestimation. Alternatively, other factors are limiting to carbon storage, where differences in moisture regime is likely to be significant.

The carbon stock of V1-2 is higher than predicted by the content of clay and silt and has formed from the most nutritious parent material. Considered in relation toV2-7 formed from the least nutritious parent material and of a lower carbon stock than the texture and oxides predict, it appears that soil carbon stabilisation depends on all three parameters.

The plot of the weight percentage total carbon against carbon stock indirectly displays the effect of horizon thickness, density and stone and boulder content (figure 5.3). A higher total

carbon to carbon stock ratio suggest that the carbon stock is lowered due to a low density and or thin horizon, and/or a large content of stones and boulders. Despite the narrow range in total carbon of the mineral horizon, the carbon stock ranges from ~ 0 to 10 000 g/m^2. The organic horizons plot at a total carbon between 39 % and 52 %, excluding the V3-1 and V3-2. The landforms in valley 1 plot at a lower total carbon to carbon stock ratio than the other. The soils in valley 2 plot between 0 and 2000 g/m^2, and the soils in valley 1 between 2000 and 8000 g/m^2.

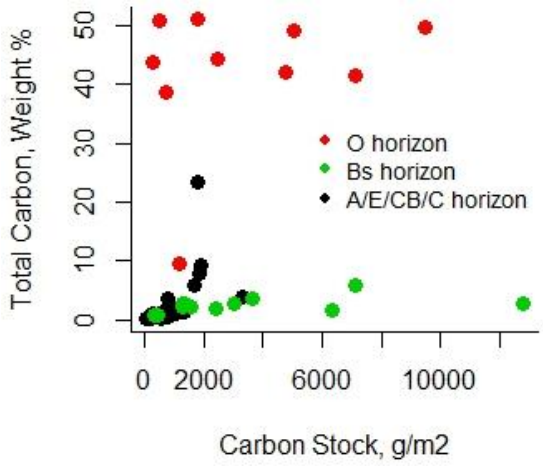

Figure 5.3. Correlation of total carbon (%) with calculated carbon stock.

It appears that the total carbon and the horizon thickness combined best predict the carbon stock of the Bs horizon (table 4.2, figure 5.3 and figure 5.4). Based on the plots of the properties that directly influence the carbon stock calculation, it is evident that the carbon stock is generally higher in V1-2 and lower in V2-7 and V3-1 than predicted. V1-2 shows a higher carbon stock than predicted by density, thickness and stone and boulder content. It is possible that these properties are exaggerated in this soil. V2-7 shows a much lower carbon stock than predicted by total carbon, suggesting that the other parameters may be wrongly recorded. The value if higher than predicted by the horizon thickness, and it is likely that this is where the potential error resides. It plots as predicted with regard to density, and at a lower value than predicted by the stone and boulder content. V3-1 shows a lower carbon stock than predicted by density, thickness and stone and boulder content, suggesting that the former two may be overestimated and/or the latter underestimated. V3-2 falls around the average on the correlation of carbon stock with total carbon, density and stone and boulder content, and has a higher carbon stock than predicted by the thickness. This suggest that the thickness determination may be exaggerated, or that horizon thickness is a poor predictor or carbon stock in sub-glacial eskers.

.

Total Carbon (figure 5.4A). The obtained values of total carbon are considered reliable in carbon stock estimation. Soil organic material (SOM) contains about 58% organic carbon, and can be calculated from total organic carbon by the factor 1.72 (Brady and Weil, 2013). In this study, both the total organic carbon (%) and loss on ignition (an estimate of organic matter) of the soil samples were measured (Appendix 4). Correlation of total organic carbon and loss on ignition are estimated to a regression coefficient of 1.7995, comparable to that given by Brady and Weil (2013). As the accuracy of loss on ignition can be affected by factors such as loss of dust and ash, the size of the sample, temperature variations, furnace type, duration of measurement and clay content (Hoogsteen et al., 2015), the results should ideally have been corrected for, but low clay content in the samples makes the weight correction for water trapped in their crystal structure redundant. However, Jandl et al. (2011) suggest that the carbon content should ideally be measured more than once to ensure representativeness of the sample.

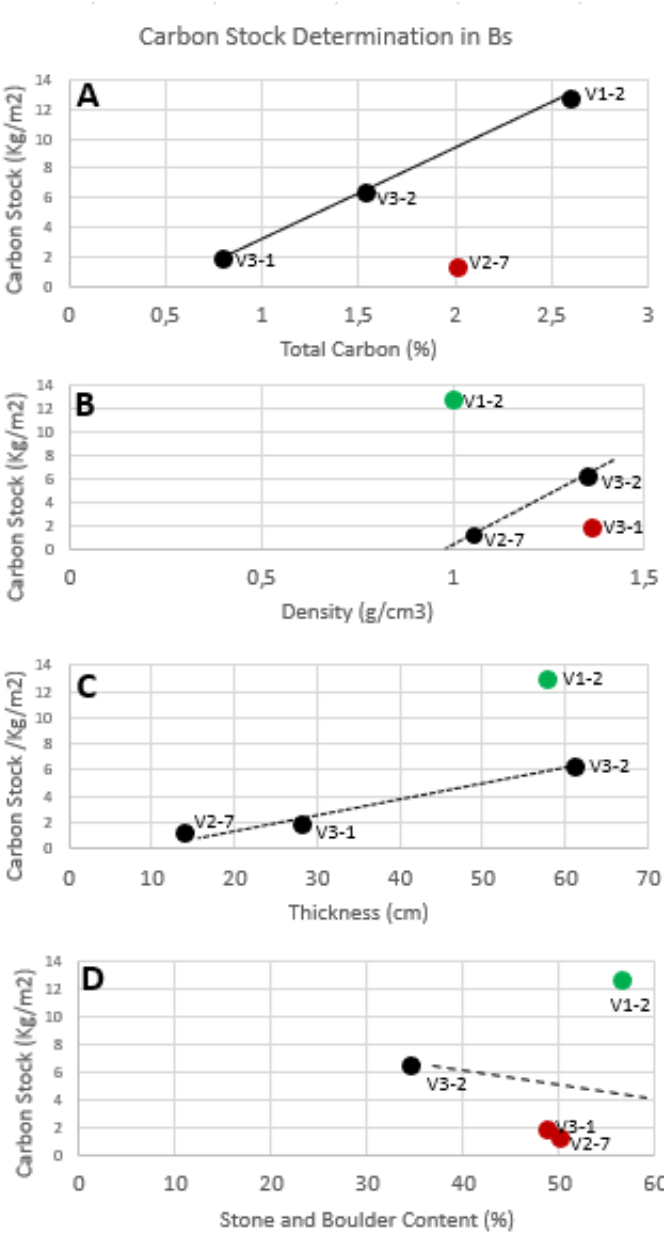

Figure 5.4. Evaluation of the properties that determine carbon stock of the Bs horizons of the described profiles. A: Carbon stock against total carbon; B: Carbon stock against density; C Carbon stock against thickness; D: Carbon stock against stone and boulder content. The trendlines A: Based on the three soils that plot in a linear relationship; B, C, D: hypothetical trendlines.

Density (figure 5.4B). The density of the soils may be inaccurately recorded due to inherent errors from sampling. For organic horizons, and particularly the weakly decomposed horizons, the sampled volume had to be cut loose from the surroundings with the risk of compaction. For mineral horizons, the high content of stones and gravel in a loose, structureless soil made sampling without both loss and inaccurate replacement of potential loss difficult. However, all soils are sampled in the same manner by the same person, which suggests the results are comparable. The systematic error for density estimation by field sampling, however, has been shown to give a carbon stock overestimation

of 36 % (Jandl et al., 2004; Wirth et al., 2004). Additionally, despite the careful procedure for drying, it is possible that some samples, particularly organic horizons, contained water during weighing, inaccurately increasing the carbon stock. Furthermore, the weight, and consequently density of the soil, is calculated without consideration of mineralogy, which to some extent might give a higher value for carbon stock in soils of more nutritious parent material as it most likely contains heavier minerals. Finally, the higher densities of the Bs horizons increases the carbon stock estimation but is most likely an effect of a high content of iron.

Stone and boulder content (figure 5.4C). The estimation of the stone and boulder content is based on a method (chapter 2.5) which requires an area of 500 m^2 and consequently adjustment for landforms of a smaller area. The adjustment might have resulted in an inaccurate number of test points and consequently increased error in the total content estimation. Further, sub-glacially formed landforms (V1-5, V2-8 and V3-2) are likely to be covered in ablation moraine, giving a larger stone- and boulder content than inherent to the meltwater deposit. However, as the stone and boulders would be deposited on the surface, it should be considered as it does affect volume considered in carbon stock evaluation. A significant limitation of the estimation is the exclusion of gravel, the fraction between 2-56 mm. In glacifluvial deposits, mainly consisting of sand and gravel, this fraction is likely to constitute a significant portion of the weight % (confirmed by the sedimentary logs in chapter 3.2). Not subtracting this fraction gives an overestimation of the carbon stock, and the error is likely to be larger in deposits formed in the upper flow regime near the ice front (e. g. in a proximal fan deposit). Despite the poor correlation of carbon stock with the stone and boulder content in these four profiles, the property is likely to be significant at a larger scale. The content is found to be up to 60 % (Appendix 5), which without subtraction would have doubled carbon stock.

Thickness (figure 5.4D). Defining the boundaries between horizons may be done inaccurately, particularly the upper boundary of the uppermost mineral soil horizon (due to mixing) and the lower boundary of the Bs horizon. The uncertainty of the horizon thickness might be particularly large in the sampled (non-described profiles) due to a poorer three-dimensional overview during sampling. Inaccurate separation of organic and mineral soil may lead to exaggerated value in the mineral soil, which Jandl et al. (2011) described as the "the border effect" and a major source of error. This may explain the very large values for carbon stock in V1-2 and V2-1, however, the horizons were sampled at the midpoint (chapter 2.6), and V1-2 falls on the trendline drawn between total carbon and carbon stock.

It would have been sensible to sample the CB and/or C horizons of profiles where the lower boundary of the Bs horizon was shallower than 40 cm. Particularly for V2-7, which has a thinner Bs horizon but a thick CBs horizon, the carbon stock may be underestimated due to the high influence of horizon thickness in the calculation. In this way, the carbon stock would

have been easier to compare (estimation down to 40 cm without regard to horizon types and thicknesses).

If a line was drawn at 40 cm, however, the Bs horizon would barely be included in some soils, and hence the line was drawn at the lower Bs horizon boundary. Consequently, the horizon thickness plays a significant role in determining the total carbon stock, but that is also the true nature of the soils that are sampled. The necessity of considering the horizon thickness in relation to the method used to estimate the stone and boulder content (down to 40 cm) disrupts the carbon stock evaluation, because a Bs horizon that reaches lower than 40 cm naturally results in a soil that contains more carbon and should be included in the total carbon stock for the defined O-through-Bs horizon estimation. Additionally, more downward distribution of material results in a lower concentration, which may underestimate carbon stock when only evaluated down to a specific depth. Thus, recording a thin horizon when it is indeed thin may be more accurate, because the total carbon content concentration may be higher, and a high/low value may compensate for a low/high value of the other. Furthermore, the concentration is likely to decrease from the upper part to the lower part of a horizon, and as the samples are taken at the horizon midpoints, they are assumed to contain an average value for the full horizon thickness.

While sampling done to a specific depth is helpful for detecting changes in soil carbon, sampling down to a specific horizon is sensible when soil genesis is considered (Gruneberg et al., 2010; Jandl et al., 2011). The effect of excluding the CBs horizon of V2-7 in the calculation may however not have been very large. Based in the values in table 4.1, the carbon stock of CB down to a depth of 70 cm would be 0.57 kg, giving a total carbon stock for V2-7 of 4.86 kg/m^2. This value would not bring the soil significantly closer the trendline of carbon stock against silt and clay or active oxides in figure 5.2. Despite the uncertainty regarding thickness, the carbon stock of the four profiles is comparable.

5.2.2 Soil and Parent Material Nutrition Status

Soil organic matter is highest in soils formed from the most nutritious parent material. There is a positive correlation between the calculated nutrient status of parent material and the nutrition status, acidity, and content of weathering products in the soils (figure 4.10). Carbon stock is proportionally correlated to the content of clay and silt in the eskers in valley 1 (table 4.7). The formation of these eskers is interpreted to be from nutritious, short-transported material. The organic horizons of some of them show the largest ratio of carbon input to decomposition (figure 4.10). Furthermore, the soils in valley 1 have accumulated more soil organic carbon in deeper layers (Appendix 5). It is possible that the stock of carbon increases dramatically below a threshold depth (e.g. 50 cm) in nutritious parent material soils due to long term stabilisation. Soils of a high total carbon stock and high mineral soil carbon stock show organic horizons with optimal conditions for decomposition, while soils of low total and

mineral soil carbon stock do not show organic horizons with optimal conditions for decomposition (figure 4.15B).

Valley 1 contains the most nutritious soils which can be attributed to immature sediments (figure 3.36 and table 4.7), and valleys 2 and 3 contain soils formed in less nutritious, coarser and more mature sediment. V1-3 and V1-5 appear to be the most nutritious soils, V3-1 and V2-1 the most innutritious, and the other soils moderately nutritious. The ratio of the O horizon thickness to the O horizon CEC is highest in valley 1 and lowest in valley 2 (table 4.3). This suggests at higher carbon input compared to decomposition in soils formed from nutritious parent material, reflecting the higher carbon stock of these soils.

Decomposition of soil organic carbon in valley 2 is biochemically limited due to the low soil nutrition status. Conditions are not optimal for decomposition and nutrient turnover (table 4.3 and figure 4.15), and particularly low at a low CEC of Bs over E, suggesting less downward translocation of organic carbon (as the CEC is controlled by organic matter in sandy soils) with less decomposition in the top soil. The chute eskers contain more biologically stabilised carbon at a lower degree of soil formation (figure 4.15). The low degree of decomposition (seen from the C/N of the O horizon) and soil formation (seen from the Fe and Al of Bs over E) (figure 4.15) in the chute eskers has resulted in a low mineral soil carbon stock at both high (V1-5) and low (V2-8) parent material nutrition status.

In valley 3, low LOI, thin O horizons and high C/N additionally suggests that soil nutrition status is low (table 4.3 and figure 4.10). V3-4 is nutritious and shows both a high total and organic soil carbon stock (figures 4.8 and 4.10) but is likely to be strongly influenced by its position in the landscape (surrounded by peat) and may not be comparable to the other landforms. It is possible that V3-4 is a “peaty podzol” and should be separated from other podzols in interpretation, as described by Clancy et al. (2015). However, as kames are often found in low-laying dead ice landscape formed from vertical down-wasting, the kame soil studied here is likely to be representative. Overall, the lithological composition of parent material appears to greatly influence the soil nutrition status (figures 4.8 and 4.10).

Clast analysis for determination of mineral assemblage is biased, as some minerals, generally the basic types, weather more easily (Goldich, 1938). Due to the forces of glaciers and glacifluvial transport, e.g. shale and slate will break down easily to smaller particles, while for example quartzite will remain as larger clasts. It is the larger clasts (~ diameter 2 cm) that have been analysed, which might lead to an apparent enrichment of certain (acidic) lithologies. Soil formation processes is considered in relation to the fine earth fraction and interaction is with the finest particles only and may therefore be influenced by minerals other than what the clast analysis predicts.

The landforms of nutrient-rich parent materials show less podzolization (e.g. figure 4.13B). On the other hand, some of the landforms that show least development had acidic starting

compositions. Jenny (1941) suggested stronger podzolization in more acidic parent material, which can be through of as more mature soils on more mature deposits. The strongest podzolization, based on the analysis of the properties, appears to have occurred under a set of optimal conditions: The most acidic parent material and bedrock, but not so robust (metamorphic and to some extent igneous lithologies) it acts as a limit to soil formation. The active silicon content of the Bs horizon is very high at low nutrition status but seems to increase again when the nutrition status is very high (Appendix 4 and table 4.5 and 4.6). This can be explained by stronger nutrient extraction and silicon weathering in the less nutritious soils, and by high production in the very nutritious soil.

The soil formation processes have a similar effect on the minerals that geological weathering does (Blume et al., 2016), and this process occurs intensively during glaciations and meltwater drainage (Benn and Evans, 2010). Consequently, the mineral assemblage in a soil profile is a result of the relative importance of these processes (soil and geological weathering). According to Jenny (1941), monovalent cations dominate acid rocks, and the content of calcium and magnesium is high in basic rocks. It might be possible to assess the parent material nutrition status based on the relative content of sodium and potassium against calcium and magnesium (table 4.3 and figure 5.5).

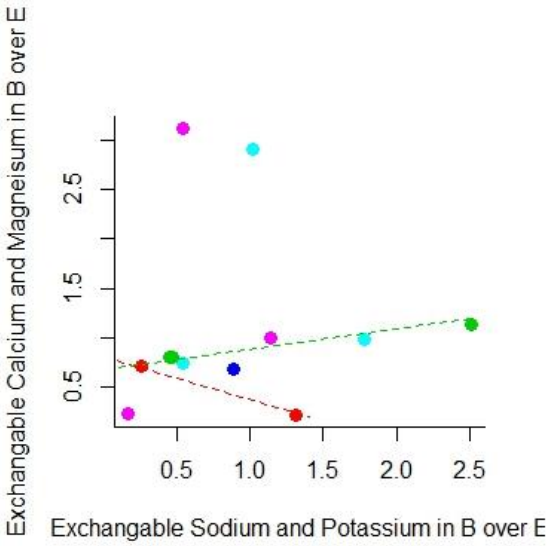

Figure 5.5. Plot of exchangeable calcium and magnesium in the Bs horizon over E horizon (BECaMg) against exchangeable sodium and potassium in the Bs horizon over E horizon (BENaK). The green trendline is based on soils from a nutritious parent material and the red trendline is based on soils from a nutrient-poor parent material. See figure 4.10 for legend.

The plot of exchangeable calcium and magnesium in the Bs horizon over E horizon (BECaMg) against exchangeable sodium and potassium in the Bs horizon over E horizon (BENaK) shows the degree of podzolization in relation to parent material (figure 5.5). The landforms that plot in the bottom left corner are the least developed, and the landforms that plot towards the upper right the most. A BENaK above 1 signifies a soil that is well developed (relative to the others, in this study). Soils that plot at a BECaMg of 1 or above and above a BENaK of 1 are both well developed and developed from nutritious parent material. Soils that plot at a BECaMg below 1 and BENaK above 1 are well developed but starved in nutrients provided by basic lithologies. Overall, the content of Ca and Mg is higher in soils with more nutritious parent material (table 4.3). The cation ratios are biased from the nutrition status of the parent material, as low Ca and Mg ratios in soil with less nutritious parent material would naturally lead to less loss and translocation, e.g.

in V2-7 (table 4.3). It appears that a higher proportion of the available Ca and Mg is utilised when the amount is limited, and consequently, and both the total amount and the amount relative to in shallower layers of exchangeable Ca and Mg at depth may reflect profile parent material nutrition status.

As discussed, soil development indicators are high following intense nutrient extraction from nutrient poor material but are also high in nutritious soils formed from nutritious parent material. According to Vestin et al. (2006), parent material contains more exchangeable calcium and magnesium in deeper horizons (at 25-30 cm). This is true for the present study, where the valley 1 eskers and V2-1 contain the highest Ca and Mg (figure 5.5, table 4.3 and Appendix 4). They also found a correlation between the alkalinity of parent material and iron and aluminium in the soil solution (Vestin et al., 2006). This is evident from the results in chapter 4.3, where iron and aluminium are proportional to the parent material nutrition status (figure 4.11 B-C), particularly for the most nutritious soils. The variations of the properties between organic horizons were minimal, which is explained by the influence of nutrient cycling and atmospheric interaction (Vestin et al., 2006).

It is not only the soil and parent material nutrition status which determine the carbon stock of the subsoil. V3-2 (figures 3.32 and 3.33) and V3-4 are interesting to compare, because they are found in close proximity downstream the same sediment source (figure 4.7) and both contain a higher amount of clay and silt. The soils show a very similar total carbon stock (9.24 and 10.57 kg/m^2, respectively) but a very different mineral soil carbon stock (7.44 and 1.09 kg/m^2, respectively) (figure 4.1). The microclimate is likely to vary greatly between the soils, with lower temperatures, higher air humidity and higher moisture content in the depression surrounding V3-4 (e.g. Jenny, 1941). It is possible that the parent material can predict the total carbon stock of the soil, but that other factors affect the relative distribution throughout the profile.

Chesworth (1973) described soils that contain more oxides as more mature but pointed out that the mineral composition of a soil cannot necessarily be attributed to soil weathering processes. The signal is rather an indicator of geochemistry and how close the system is to the residue state in chemical weathering. More sedimentary bedrock input and till redistribution can therefore indicate stronger soil formation, such as in valley 1 and for V3-2. Here, however, the choice of glacifluvial deposits as parent material minimises the content of non-pedogenic silt and clay-sized particles. The weathering products (both clay minerals and iron, aluminium and silicon oxides) (figure 4.9) are therefore good indicators of soil formation and its relation to carbon stabilisation.

5.2.3 Carbon Stabilisation

The three stabilising mechanisms of carbon in soil are I) chemical recalcitrance, II) protection from decomposers through occlusion and III) interaction with a mineral surface (Berg and McClaugherty, 2003, Jandl et al., 2011). The chemistry of the carbon is not studied here, but the mineral interaction of carbon may be inferred from the soil parent material, texture and weathering products. The fraction considered in terms of stabilisation in this study is stored in the mineral soil, but the carbon can only be mineral-bound after decomposition. Jandl et al. (2011) suggested that the slow decomposition and low (cold-climate) litter quality obstructs mineralogical stabilisation at high altitudes, and because considerable amounts of labile carbon are stored in high elevation ecosystems, they are particularly subject to loss with changing climates. The proportion of mineral soil carbon stock to the total carbon stock in relation to total carbon stock (table 4.8) suggests both the amount and distribution are controlled by the parent material and degree of soil formation (figure 4.15).

The Bs horizon carbon stock varies across the study area but appears to be controlled by additional means to biochemical. The C/N ratio of the Bs horizons are found in a similar range within the interval optimal for decomposition, suggesting both that they contain organic carbon subject that is not stable due to chemical recalcitrance as well as little variance in the biochemical effect on stabilisation. The difference is interpreted to be related to pedogenic and non-pedogenic clay minerals, and the soil weathering products iron, aluminium and silicon (hydr)oxides (figure 4.15).

Bonding of organic material to iron oxides is the most important mechanism for stabilisation in acid soil (Eusterhues et al., 2005). The authors suggest that the stabilisation of this carbon is a result of interactive processes with the iron oxides and clay, and not its chemical composition. In acid soils, iron oxides are positively charged (through the functional OH groups) (Brady and Weil, 2013), which provides the potential for bonding with negatively charged organic material (through the functional OH and COOH groups). Iron oxides from soil weathering processes showed high correlation with mineral soil carbon stock (figure 4.11 B) and the conclusions from Eusterhues et al. (2005) are true for the glacifluvial soils.

The soil organic material is expected to be higher relative to the C/N ratio at depth compared to more shallow layers (Fontaine et al., 2007). This is true for the Bs horizon compared to the E horizon. However, the soil organic carbon relative to the C/N-ratio is highest in the O horizons, and lowest in the CB and C horizons. Fontaine et al. (2007) ascribed the difference to the lack of fresh and energy rich carbon. Eusterhues et al. (2011) noted that this type of carbon compound (e.g. glucose), often is enriched in mineral-organic complexes, and that during complexation processes heavier carbon molecules (e.g. lignin) remain in solution. They suggest that this might explain why easily decomposable organic carbon contribute to the stable carbon pools. The organic carbon enrichment in the Bs horizon might result from a combination of the processes (figure 4.15 B).

Podzolization is a carbon-stabilising process (figures 4.11-4.14). Further, mineral soil carbon stock increases at a faster than linear rate with an increase in all podzolization indicators in soils formed from nutritious parent material (figure 4.12). The charge of soil organic matter changes little under soil acidic conditions (Yusoff et al., 2017), suggesting the binding mechanisms of SOM (figure 5.6) is stable in podzols. Soluble aluminium in podzol Bs horizons is predominantly bound organically (Dahlgren and Ugolini, 1989), which shows that organic complexation is an essential mechanism of the podzolization of soils (Lundstrom et al., 2000). The assumption is that the soil is not affected by acidification (Lundstrom et al., 2000), which points to the sensitivity of podzols to acid input and SOM loss. According to Cornelis et al. (2014), organic acids in podzols have high complexing capacities. It is, therefore, likely that complexation between organic acids and soil weathering products is essential for deep soil carbon stock stabilisation of podzols (figure 4.12 B).

The degree of podzolization varies throughout the area, as may the mechanisms for carbon stabilisation. Binding mechanism (b) in figure 5.6 is likely to dominate in the strongest podzolized soils. Soils formed from parent material of high clay mineral content (e.g. V1-2, V1-3 and V1-4) are likely to contain carbon bound to phyllosilicates (binding mechanism (a)). The higher pH and CEC in valley 1 (table 4.1) suggests that less protonation of oxides occurs, and a higher CEC allows for cation exchange and cation bridging. Podzolization as interpreted from the degree of downward translocation of iron and aluminium (hydr)oxides and other property ratios between the Bs and E horizon (figures 4.14 and 4.12), is strongest in the landforms with the most acidic parent material (figure 4.13 B). V3-2, V2-1 and V1-3 all show medium values for the iron and aluminium oxides in Bs compared to E (figure 4.12A), carbon stock and clay and silt content (figure 4.9).

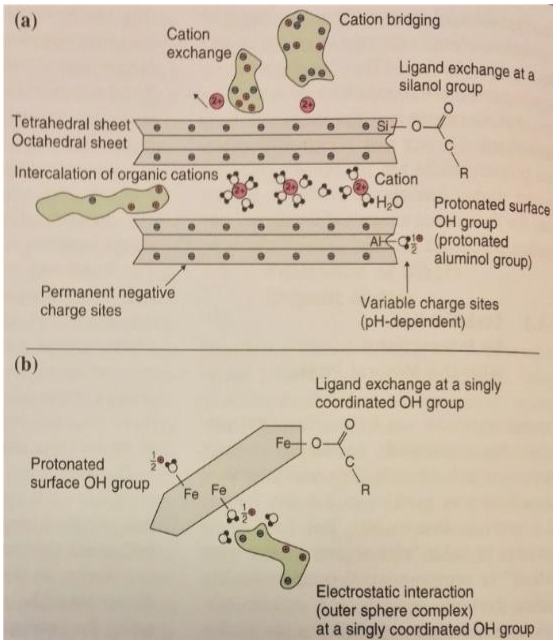

Figure 5.6. The different mechanisms for binding of organic material to clay in soil. (a) Binding between permanently (negatively) charged phyllosilicates by cation exchange, cation bridging and ligand exchange, and (b) Binding on hydroxide/oxide surfaces of pH-dependant charge (positive at low pH) by ligand exchange and electrostatic interaction. Modified from Blume et al. (2016).

In valley 1, the soils are moderately and well developed, in valley 2 more intensive soil weathering and accumulation of finer particles at depth has occurred and in valley 3, low values for both clay and silt in Bs and active iron and aluminium suggest less intensive soil weathering processes (figures 4.9, 4.11, 4.12 and 4.14). In valley 2, the coarse and mature nature of the sediments gives little surface area for soil formation and the stoniness and coarse

grain size of rock fragments allows for good aeration, but poor water retention. V2-1 is possibly formed from longer transported material and contains a larger mix of lithologies, compared to other landforms in the study area.

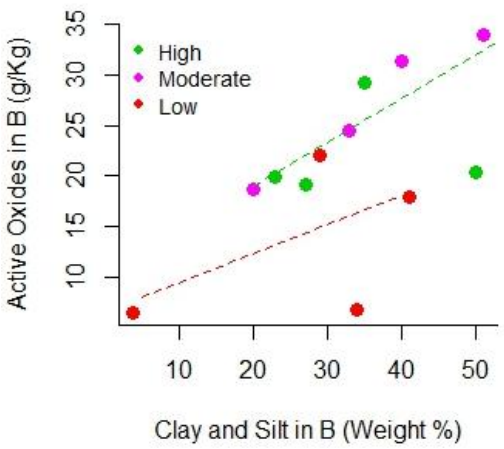

Figure 5.7. Correlation of clay and silt content and active oxide content in the Bs horizon. A linear correlation suggest that a large component of the silt and clay may consist of oxides. The green trendline is based on soils of a high and moderate mineral horizon carbon stock, and the red trendline is based on soils of a low mineral horizon carbon stock. The legend indicates mineral soil carbon stock.

A significant component of the silt and clay fraction consists of oxides (figure 5.7). The correlation is higher for soil of a high and moderate mineral horizon carbon stock (green trendline). The soils that plot at a low ratio (red trendline) are likely to contain silt and clay of a higher phyllosilicate content (clay minerals). The red point that plots below the red trendline is V3-4, suggesting it contains more silt and clay than oxides and that the content may not be a result of soil weathering. The red point that plots above the red trendline is V2-1, suggesting intense soil weathering processes in this soil. The ratios for V3-4 and V2-1 correlate with the lowest and highest interpreted flow regimes of deposition, respectively (chapter 5.3.2). The green point that plots below the green trendline is V2-3, and it is possible that this soil proportionally contains more phyllosilicates than the other soils. This soil is the only one studied that does not have an E horizon (A and Bs only), however, that does not necessarily suggest weaker podzolization.

Cornelis et al. (2014) states that the presence of pedogenic clay is important for the total soil carbon budget. Jobbagy and Jackson (2000) concluded that while climate conditions can predict soil organic carbon in the upper 20 cm of a soil, the content of clay predicts the carbon storage at depth. Non-crystalline minerals and organic carbon are positively related independent of other factors such as climate, and the cycling of carbon on the millennial scale is driven by what is mineral-stabilised (Porras et al., 2018). Considering Bs horizons only, the largest carbon stock is found at a clay and silt content of 20-30 %, and in valley 1, where the Bs horizon carbon stock is highest (excluding V3-2), at a clay and silt content of 20-40 % (table 4.1). It is possible that the clay and silt percentage related to optimal production, decomposition, translocation and deep stabilisation in glacifluvial soils is 20-30 %, and 20-40 % when the landform is found on and downstream basic, sedimentary bedrock (tables 4.1 and 4.4).

Overall, binding of organic matter to clay is significant despite the negative charge of the substances. Even though the total charge of soil organic matter is negative, positive charge

sites occur Brady and Weil, 2010). When organic material is found in a neutral state, it repels water (which is polar) (Prothero and Schwab, 2004), which can explain why it is removed from solution (Kvifte, 2018). The binding of organic carbon to clay minerals may not be charge dependant, or enabled through cation bridging and exchange (Blume et al., 2016). The latter may then require a higher CEC, reflecting the nutrient status of the parent material. The non-crystalline minerals formed from soil processes translocated to deeper layers stabilise and protect organic material (Torn et al., 1997). Torres-Sallan et al. (2017) showed that below 30 cm depth, a larger fraction of the soil organic carbon is associated with and stabilised by clay minerals than in the upper 30 cm (figure 5.8). This illustrates the effect of illuviation of clay on carbon stabilisation.

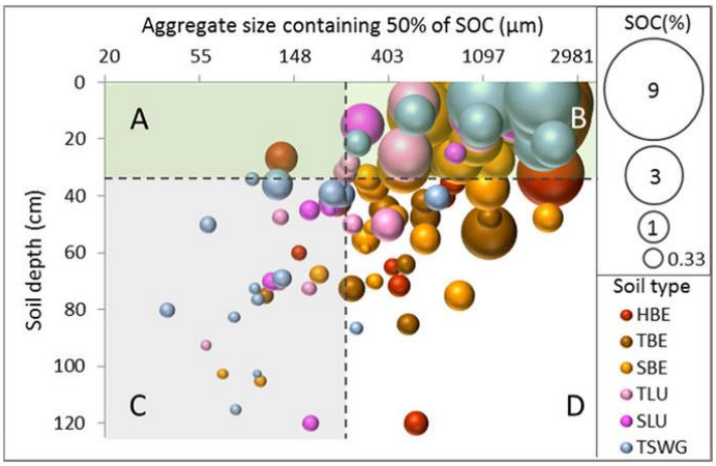

Figure 5.8. Relative distribution of soil organic carbon among various aggregate sizes against depth for various soil types. The upper 30 cm of the soils are displayed in quadrants A and B, and quadrants C and D show the subsoil. Quadrants A and C show where more than 50 % of soil organic carbon is associated with clay minerals, thereby indicating stability. Quadrants B and D show where soil organic carbon is above 50 % only when larger aggregates are considered, illustrating a more unstable fraction. The figure shows that in the subsoil, a larger proportion of organic carbon is associated with clay minerals (quadrant C is fuller compared to D than quadrant A is compared to B). The blue and pink bubbles illustrate soil that have experienced clay illuviation. Figure from Torres-Sallan et al. (2017).

Differences between the E and Bs horizons illustrate the translocation of material (figure 4.12). Proportionality between the aluminium to silicon ratio and content of clay and silt in the Bs horizons in valleys 1 and 2 suggests that they are interdependent in these soils (figure 4.9). Lundstrom et al. (2000) described podzols as soils that have an E horizon depleted in base cations and Al and Fe and enriched in residual Si and a Bs horizon enriched in Fe, Al and organic matter. Consequently, stronger soil formation gives more eluviation of clay minerals, and can be correlated to more mineral-stabilised carbon at depth. Lower content of active aluminium in eskers S in valley 1 suggests that the soils have undergone less soil weathering than the others (figure 4.9). These soils do not show a very high mineral soil carbon stock despite both a high total carbon stock and presence of clay minerals in the parent material, which can possibly be attributed to clay illuviation.

Porras et al. (2018) showed how soil mineral phases have the capacity to retain easily degradable organic material and that it is still unknown how readily decomposable the material is, particularly in changing environments (figure 5.9). It is possible that a significant

amount of organic carbon in high elevation glacifluvial soils is easily degradable (figure 4.15 B). Porras et al. (2018) suggested that the formation of mineral-organic complexes is stronger in a higher moisture regime and with fresh mineral surfaces. The meltwater landforms described in this study are generally well drained, but some are found in depressions and of a smaller vertical relief than the majority. There is however no apparent increase in mineral soil carbon stock of landforms with a higher moisture content. It is possible that higher moisture content promotes iron reduction and thereby limits the ability for organic complexation and even releases previously complexed organic carbon, however, evidence for iron reduction was not observed in the field (stagnic/gleyic properties and mottling). The organic horizons, on the other hand, contain chemically recalcitrant carbon that is not protected by minerals, and the amount is controlled by the input of litter (Eusterhues et al., 2005) and is higher in low-laying landforms (e.g. V3.4).

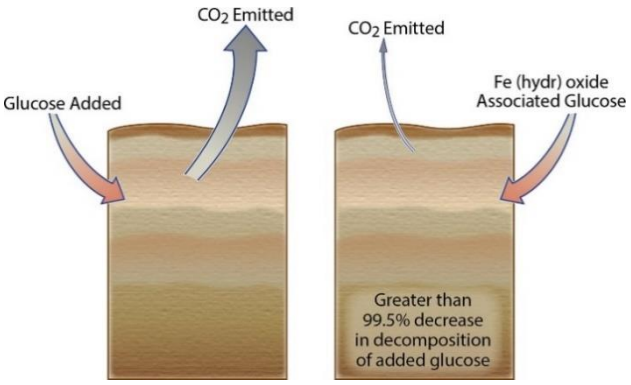

Figure 5.9. Illustration of the stabilising effect of iron (hydro)oxides on readily decomposable organic matter. From Porras et al. (2018).

The effect of mineral maturity on soil carbon is significant at intermediate depths in the soil (at 50-60 cm) (Porras et al. (2018) and the weathering of minerals affects the mechanisms of carbon stabilisation (Jenny, 1941). The weathering of minerals that occurs during soil formation increases the fresh surface percentage, a premise which suggests that stronger podzolization could enhance carbon stock. Short-transported material from local bedrock consisting of easily erodible lithologies in valley 1 can be expected to contain a higher proportion of fresh mineral surfaces, confirmed by the lower degree of rounding (figure 3.36) of the sediments. However, the interpretation from Porras et al. (2008) concerns depths below most of the samples in this study. Soil carbon stabilisation and parent material maturity are related through nutrient release from minerals. The decay of rocks releases various elements with different purposes in the soil (Jenny, 1941). Content of certain minerals, resulting from different parent material (figure 5.5) can therefore show a direct link to soil stability (calcium and magnesium flocculation) and dispersion of clay and humus colloids (sodium and potassium) (Jenny, 1941).

Mikutta et al. (2007) stated that sorption of organic material to mineral phases strongly depends on the chemistry of the soil solution and the reactivity of the mineral surfaces. The sorption processes, which can be illustrated by the ratio between soil organic carbon and the iron oxide content, against the calculated nutrition status of the parent material for the soil profiles, suggests a proportional relationship (a low ratio corresponds to a high nutrition status). The sorption, as interpreted by the described ratio, is low in V2-1, V2-6, V2-7 and V2-8, suggesting lower soil nutrition status and deep soil stabilisation in these soils, and

possibly in valley 2 in general. As the landforms develop by a wide range of sedimentary processes at various stages during deglaciation, the common denominator influencing mineral soil carbon stock is likely to be a significant input of innutritious local bedrock. A weaker, but similar correlation is seen for V2-3 and V3-2, suggesting that acidic parent material leads to a weaker sorption of soil organic carbon to active iron and aluminium in the E horizons. However, the content of active iron and aluminium is particularly low in E horizons of these soils (figure 4.13B), and the hyperbolic nature might strongly affect the ratio.

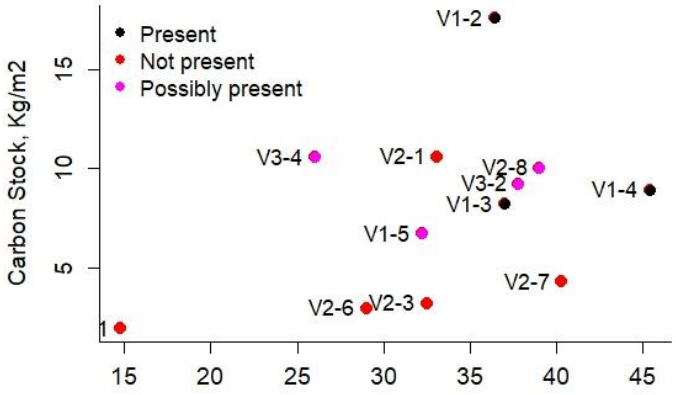

Figure 5.10. Carbon stock against the content of clay and silt in relation to the assumed proportion of clay minerals in parent material. The legend indicates clay minerals in parent material.

There is a difference in carbon stock between glacifluvial landforms with high and low silt and clay content prior to soil formation (figure 5.10). Carbon stock is generally higher in landforms with clay minerals in the parent material (valley 1). However, it appears to be only slightly higher, though always high. Clay minerals in the parent material appear to enhance preservation at depth through complexation, occlusion and stabilisation. Torn et al. (1997) suggested that hydration, large surface area, variable charge and protective geometry of amorphous minerals results in stable organic–mineral bonds. The A horizons are higher in carbon stock for soil with no clay minerals in the parent material (Appendix 5). This is possibly because the carbon is kept in the topsoil at these landforms, with lower decomposition and stabilisation at depth.

Carbon in the soils of valley 1 may be bound to clay minerals, not iron and aluminium oxides. The Bs horizon carbon pool is significantly larger and deeper in V1-2 than other soils (figure 4.14A). Considering the ratio of Fe and Al in Bs over E (figure 4.12A), chute eskers show a high value (and the very highest for V2-8), suggesting a link between podzolization and soil nutrition status in these landforms. The ratio of clay and silt in Bs to the ratio of Fe and Al in Bs over E is higher in valley 1 than elsewhere in the study area (figure 4.9), suggesting that the texture of parent material was finer prior to soil formation (figure 5.10). This is likely a result of the basic sedimentary bedrock in the area, and/or the low-energy deposition in crevasses in the ice. The correlation is also true for V1-2, interpreted to be deposited between stagnant ice blocks, suggesting that the local bedrock is the main controlling factor of this property ratio. The soils show a low ratio of Al to Si in Bs compared to the clay and silt in Bs (figure 4.11 and Appendix 4) but similar to soils formed in the least nutritious parent material (valley 2). It is difficult to assess whether the clay content binding organic carbon in the soils is a result of short-transported material (soils found in the slate and shale areas) or soil weathering processes.

Both weakly podzolized soil formed from nutritious parent material (e.g. V-3 and V1-4) and soils formed from innutritious parent material that have undergone strong soil formation (e.g. V3-2) appear to store carbon in the mineral horizons (figures 4.9, 4.11-4.14), but it is possible that both the stabilising mechanism and the nature of the soil organic carbon are different (figure 5.11). If mineral-surface interactions stabilise carbon independent of chemical recalcitrance (e.g. Eusterhues et al., 2005, Porras et al., 2018), hence sufficient decomposition is not a pre-requisite for deep soil-stabilisation. Intensive nutrient extraction suggests the podzolization processes have been strong in innutritious soil. In these soils, decomposition is limited and the content of iron and aluminium weathering products high and significant for carbon stabilisation. Furthermore, oxides are positively charged in low pH soils. Eusterhues et al. (2005) therefore suggested oxides are more important for stabilising carbon in acid soil. In nutritious parent material soils, better conditions for decomposition are likely to result in soil carbon consisting of larger, more recalcitrant molecules, and the higher content of clay minerals (phyllosilicates) is likely to contribute to and enhance carbon stabilisation (e.g. V1-3, V1-4). The carbon stabilised in nutritious soil may therefore require "fresh carbon" input for further decomposition ((Fontaine et al., 2007), compared to innutritious soil where the mineral-stabilised carbon fraction may consist of a significant amount of smaller organic molecules (figure 5.11).

It is also possible that a link can be drawn between the chemical properties of the soil organic carbon and whether it is stabilised mainly by clay-sized oxides and phyllosilicates from soil weathering processes or non-pedogenic phyllosilicates (figure 5.11). A certain degree of podzolization is however required for translocation of the material to depth, where e.g. V3-4 shows very low podzolization (figure 4.11) and very low mineral soil carbon stock (figure 4.8B) despite a high silt and clay content (table 4.7). All in all, it is important to note that all soils in this study are acidic (table 4.3 and Appendix 4) and that carbon stabilisation by clay-interaction is difficult to discuss as some authors refer to clay as any matter <0.002 mm, and others as aluminium phyllosilicates only.

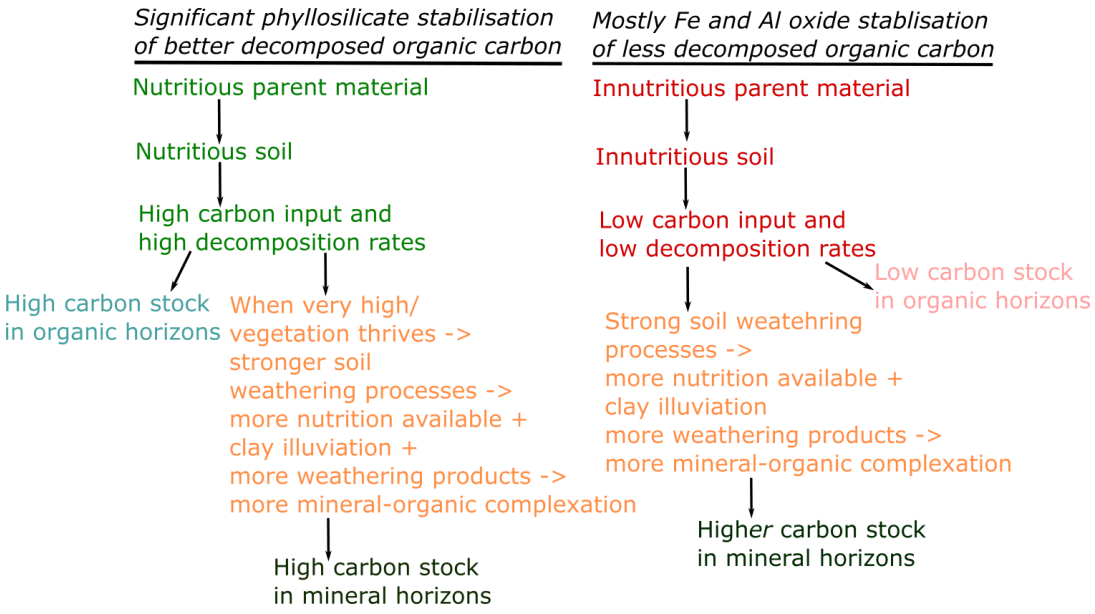

Figure 5.11. Simplified model for mineral soil carbon stabilisation in nutritious and innutritious soils. Black text refers to the stabilising mechanisms, green/red to the high/low potential for stabilisation given by the parent material, orange to soil weathering processes, blue/pink to high/low organic soil carbon, and dark green to the theoretical result of high mineral soil carbon stock.

5.3 Linking Soil Carbon to the Deglaciation Landscape

5.3.1 Carbon Stocks of Forest Soils in Mountainous Ecosystems

The soil of boreal forests is a major carbon sink (Kleja et al., 2008). However, the mineral horizon carbon stocks of such soils vary between ~1 and ~16 kg/m^2, with a mean value of ~5 kg/m^2 (table 4.1). The variation illustrates the difficulty in establishing a representative value even in a restricted environment where most influential factors are kept constant. The organic soil carbon stocks also show great variability, from essentially 0 to 10 kg/m^2, reflecting the interplay between carbon input and decomposition. The average value of carbon stocks of forest podzols in boreal-temperate Scandinavia and Northern Europe has been estimated to 8-25 Mg/ha for organic horizons and 18-45 Mg/ha for the upper 20 cm of mineral soil horizons (Baritz et al., 2010), corresponding to 0.8-2.5 kg/m^2 and 1.8-4.5 kg/m^2, respectively. Hence the stocks in this study show a higher mean and larger variation, where the higher mean may be a result of e.g. the high elevation and less continental climate (e.g. Baritz et al., 2010, Jandl et al., 2011) than the average sample localities. Overall, high variability in podzol carbon stocks is common (Baritz et al., 2010).

The average carbon stock and the carbon stock proportion in mineral and organic soil horizons in this study resembles values from other Norwegian and Swedish podzols. Strand et al. (2016) found the carbon stock of forest mineral soil to be 11.1-19.3 kg/m^2, and Olsson et

al. (2009) found the carbon stock of the full podzol profile down to 50 cm in a Swedish forest to be 8.2 kg/m^2. Furthermore, Strand et al. (2016) found that 60 % of a typical Norwegian forest podzol soil carbon is stored in the mineral horizons, which compares very well to this study where the mean mineral soil carbon stock was found to be 5.03 kg/m^2 (SD= 4.15), constituting 63 % of the full profile carbon stock of 7.99 kg/m^2 (SD= 4.26) (table 4.1). The podzol organic horizons in this study average at 6.72 cm (SD= 1.58) (table 4.1), comparable to both organic horizon thicknesses of Swedish forest podzols at 8.2 cm (Olson et al., 2009, Strand et al., 2016) and previously described Norwegian forest podzols with mean organic horizons of 9.6 cm (Strand et al., 2016). As the horizon thickness in this study is comparable to other studies, it suggests that the organic and mineral soil carbon stock proportions may be comparable for extended areas. Baritz et al. (2011) reported a European forest soil bulk density between ~ 0.6-1.6, which compares to the density trend and variation in this study, where A horizon average at 0.69 g/cm^3 (SD= 0.17) and C horizons at 1.58 g/cm^3 (SD= 0.18) and the remaining mineral soil horizon in the range between (table 4.1).

Carbon stock of forest podzols with similar values in this study, appear in a variety of ecosystems under highly variable geological, biological, topographic and climatic conditions (table 5.1). Considering that the soil carbon stock is calculated down different depths including different horizons, the different studies are difficult to compare. However, the mean carbon stock from this study is found within the interval reports from most authors (e.g. Callesen et al., 2003; Baritz et al., 2010) and is similar to carbon stocks measured to similar depths (e.g. Olsson et al., 2009; Petrenko and Friedland 2015) (table 5.1). Callesen et al. (2003) found the carbon stocks (mineral soil and forest floor) to be texture dependant, reflecting the importance of parent material on carbon stock. The values reported from Petrenko and Friedland (2015) are comparable at similar pH and texture as this study, reaffirming the importance of texture and its relation to soil nutrition status.

The variation in carbon stocks (table 5.1) reflect differences in the geology, in terms of depositional environment (soil texture, stone- and boulder content and landscape relief) and composition and maturity of the sediment (parent material nutrition status). The former may influence the total soil surface area, soil density, nutrient and water retention as well as soil moisture regime, while the latter affects the soil and parent material nutrition status. The stabilisation of carbon in the mineral soil is influenced by their interaction. The accumulation of carbon since deglaciation of Northern Europe has differed greatly on both the continental scale and the scale of the study area.

Table 5.1. Comparison of podzol carbon stock from various studies. Some authors report carbon stocks as kg/m^2, which converts to Mg/ha by the factor 10.

Reference	Carbon Stock (Mg/ha) (soil/depth)	Area	Features
This study	79.9 (down through Bs)	Study area	Elevation: 790-890 masl. Glacifluvial podzol, mountainous forest ecosystem
Callesen et al. (2003)	23-107 (40 cm mineral soil and forest floor)	Scandinavia (latitudes 55°-68° N)	Nordic Northern boreal well-drained forest soils. Texture-dependant carbon stocks
Olsson et al. (2009)	82 (all horizons down to 50 cm)	Sweden	Forest podzol
Schulze et al. (2009)	20 (Bs only)	Germany	Elevation: 770 masl. Similar bedrock. Mineral-associated carbon fraction measured.
Baritz et al. (2010)	11.3-126.3 (mineral soil 0-20/30 cm)	Europe	Continent-wide measurements of European forest soils
Jandl et al. (2011)	50-65 (organic soil and down to 20-30 cm)	Study area	Forest soil in mountain areas, low stature vegetation and low management pressure
Clancy et. al. (2015)	129-139 (all horizons)	Ireland	Forest podzol
Petrenko and Friedland (2015)	~80 (all horizons)	NE USA	Elevation: 400 masl. Hardwood forest. Non-harvested podzol. Similar pH and texture as this study
Strand et al. (2016)	111-193 (mineral soil)	Norway	Forest podzol

Schlesinger (1990) concluded that the accumulation rate of carbon in podzols of temperate and boreal soils during the last 10 000 years has been 0.7-12 g C/m^2 year. The rate suggests that the carbon stock of an average meltwater landform should be 7-120 kg C/m^2. Schulze et al. (2009) noted that the rate is higher at the beginning of soil formation. If the decrease can be assumed to be exponential and described by the natural logarithm, the carbon stock after deglaciation based on the accumulation rate from Schlesinger (1990) can be estimated to 6.99 kg/m^2 by postulating the equation $f(x) = 11.3e^{(-x)} + 0.7$, which gives $\int f(x) = -11.3e^{(-x)} + 0.7x, = \sim -11.3 + 7000, = \sim 6988.7\ g/m^2$. This is comparable to the average value of 7.99 kg/m^2 (SD= 4.26) (tables 4.1 and 5.2) for carbon stock of the glacifluvial soils.

Podzolization processes could have left visible marks on exposed glacifluvial landforms while ice still covered lower areas in the SE. According to Jenny (1941), visible podzolization can happen in 100 years, and Lundstrom (2000) observed podzolization in eskers in cold climate after 330 years (Lundstrom, 200). However, the time gap between onset of podzolization between the landform constitutes a small fraction (~5%) of the time since deglaciation (about 9000 years in the study area). Older landforms formed at the highest altitudes in the NW (V3-1 and V3-4) and younger landforms formed at the lowest altitudes in the SE (V2-6 and V2-7) can be compared, despite uncertainty in their temporal relationship. No conclusion can be drawn regarding the relationship with carbon stock and the time of soil formation after

deglaciation, and differences in soil properties including soil carbon should be attributed to other factors.

It is possible that the differences in carbon stock throughout the areas varies due to difference in elevation between the three valleys (figure 3.1). Jandl et al. (2011) described how carbon accumulates at different rates depending on the elevation, as decomposition slows above the tree line. Carbon stocks particularly increase in the organic horizons and can for a whole profile increase by 4.5 Mg/ha for every 100 masl. (Jandl et al., 2011). On the other hand, the net input of carbon to the soil decreases by ~1 Mg/ha year above 800 masl. The balance between input and decomposition is therefore interesting in the study area, which resides at the treeline ~ 780-890 masl (figure3.1). Carbon decomposition and input may therefore vary greatly between the highest elevated landforms (V3-1, at around 890 masl) and the distal part of the large fan deposits (transect 2, figure 4.5, at around 778 masl). The highest input to decomposition ratio of carbon in the organic soil (figure 4.10) and highest accumulation of carbon in the mineral soil (figure 4.11) is observed in the S of valley 1 at around 820 masl (V1-3 and V1-4). Hence landscape elevation may partly explain the higher carbon stocks in valley 1 resulting in high input and slow decomposition of organic carbon. However, V2-7 and V3-1 have undergone the strongest podzolization (figure 4.13 B) and are found at the lowest and highest elevation, respectively, possibly suggesting that the difference in elevation is not very significant for soil processes in the area.

Because the carbon stock varies among the soils (figure 4.1), the various landforms are grouped to minimise uncertainty in estimation for potential extrapolation. Five factors related to the deglaciation processes may affect the carbon stock of the soils, many of which can to some extent be deduced from remote sensing and map analysis (table 5.2).

Table 5.2. Average carbon stock and standard deviation for five groups of glacifluvial soils.

Factor	**Carbon Stock Mean (kg/m^2)**
All landforms	7.99 (SD= 4.26)
1) subglacial deposition	8.67 (SD= 1.92)
2) high-energy deposition	7.76 (SD= 3.53)
3) strong podzolization	8.90 (SD= 5.73)
4) > 5 m high, steep-sided landform	7.07 (SD= 5.01)
5) high nutrition status (>4) of parent material	11.57 (SD= 5.22)

1) Sub-glacial deposition. The stone- and boulder content is higher in sub-glacially formed eskers, to some extent due to coverage by ablation moraine. Sub-glacially formed eskers are recognised by remote sensing as either a) striking parallel to the ice-flow direction or b) found in steep terrain striking perpendicularly to the contours on a topographic map (chute eskers).

2) High-energy deposition. The mean for this group approached the mean for all landforms, suggesting it exerts a substantial influence on the average value. The density of deposits formed in the upper flow regime is generally lower, due to the larger pore space between

coarser grains/clasts and a limit to how much a coarse deposit (sand and gravel) can be compacted (table 4.7 and Appendix 5). The energy level of deposition is difficult to infer through remote sensing. It is likely to be high for chute eskers and deltas, and lower for landforms comprising flat, extensive areas (e.g. sandur plains and distal fan deposits, figures 3.14 and 4.5) and low-laying areas (hummocky terrain from dead ice deposition, e.g. kames).

3) Strong soil formation. Stronger podzolization releases more nutrients from the parent material, where the quality and quantity depend on its inherent content, gives a higher content of carbon-stabilising weathering products, more intense downward translocation and increased horizon thickness. The degree of podzolization is difficult to infer through remote sensing, however, it is stronger in higher and/or steeper landforms with a relief to the surrounding landscape (which may be inferred from remote sensing by e.g. hill shading) due to increased runoff of soluble cations.

4) Deposition supported by ice or water absent in the modern landscape (> 5m high, steep-sided landform). Tall landforms with steep sides, formed ice-laterally (e.g. kame terrace) or sub-aqueously (e.g. delta) appear to be extremely well drained and production moisture-limited. These landforms are easily recognised by remote sensing, particularly with a variable hill shade effect, as they stand out in the modern landscape.

5) High nutrition status of parent material (>4). A high nutrition status of the parent material correlates with a high carbon stock (figures 4.8 and 4.10). The parent material can be inferred from the bedrock underlaying the landform and found upstream of the ice-flow direction and topography.

Based on the groups in table 5.2, it appears that soil texture is among the most significant for carbon stock. It controls the circulation of water and retention of water and nutrients (Schlesinger and Bernhardt, 2013) When factors 2 and/or 4 are true, the carbon stock of the glacifluvial soil decreases. When factors 1 and/or 3 and/or 5 are true, the carbon stock of the glacifluvial soil increases. The effects of sediment transport and deposition and its relation to texture are discussed in the following chapter.

5.3.2 Soil Carbon and the Nature of Sediment Transport and Deposition

The composition of parent material and depositional regime can be linked to various stages of deglaciation through the nature of transport and deposition, and a conceptual link can be drawn to carbon stock. Based on the mapping of ice flow phases by Putnins and Henriksen (2017) and the interpretation of sedimentary environments in chapter 3 and 5.1, V3-1 and V3-2 are interpreted as deposited in Middle phase III, V2-7 in Late phase III and V1-2 in Early phase III. Meltwater landforms that formed when the ice was active consist of material that

originated NW of deposition, and it is likely that later glacifluvial transport and deposition followed similar paths.

Low carbon stocks are linked to the earlier and latest stages of deglaciation at high (~880 masl) and low elevations (~790 masl), respectively, while the higher carbon stocks are linked to the stagnation of ice at intermediate elevations (~850 masl). High carbon stocks are associated with supraglacial deposition in stagnant ice, including eskers formed in ice-crevasses in and kames. In the ice-crevasse eskers both the mineral soil and organic soil carbon stocks are high, but in the kame the mineral soil carbon stock is very low. Low carbon stocks are associated with high-energy deposition and debris flows of a short transport distances, deposits that may be ice-proximal and/or prone to later meltwater erosion. Low carbon stocks are also associated with ice-lateral deposition. Sub-glacial deposition are associated with high carbon stocks, with a large proportion in the organic horizons.

Correlation between glacifluvial sediments, carbon stock, soil nutrition status and soil formation are evident. In valley 1, the sediments show a low degree of rounding, a moderate flow competence, and a wide range of stone and boulder content. The soils are high in CEC, low C/N ratio and high active iron and aluminium. In valley 2, the sediments show a high degree of rounding, high flow competence and high stone and boulder content. The soils show a relatively high pH and high silt and clay content in the Bs horizon indicating strong soil formation. In valley 3, the sediments show a low degree of rounding and a low flow competence. The soils are low in silt and clay in the Bs horizon, and generally low in active iron and aluminium, indicating weaker soil formation. Generally, the carbon stock is higher in soils formed from locally sourced less mature sediments, transported in less energetic environments en- and supra-glacially. The correlation is evident in valley 1, where V1-2 shows a particularly low degree of rounding, high soil formation and high mineral soil carbon stock.

The degree of rounding (figure 3.36) appears to be independent of landform type and energy of deposition and is therefore likely to be a result of the nature of till and degree of till redistribution. It appears that valley 2 has experienced most till redistribution (chapter 3.2.12). Considering the number of landforms in valley 2 that were deposited when the ice sheet was largely gone (e.g. delta, fan lobe), it is reasonable to believe that they, to a large degree, formed from basal and ablation till. The underlying bedrock may have been of less significance as source for the material. The other landforms, particularly in valley 3, were formed when the ice sheet was still flowing or partly present. The clasts are more angular, with surrounding material consisting mainly of ablation till, probably of more local origin. The ice-flow parallel esker shows a higher degree of rounding than the other landforms but is also interpreted to have formed sub-glacially from redistributed material.

The degree of rounding is related to the origin and transport distance of the sediments. Bergersen (1970) suggested that the glacifluvial material can be divided into two classes,

where one is of local origin dominated by subangular clasts (<20 % rounded), and the other deposited along major drainage channels dominated by rounded clasts (around 50 % rounded). Even though the author refers to deposition on a large scale (where the second class describes deposition in main valleys), a similar model can explain the deposition in the area studied here. The landforms with more rounded clasts might have formed from material transported a longer distance.

Some meltwater landforms were formed when the area was covered by thick ice with ice flow more independent of topography, towards SE (Putnins and Henriksen, 2017)). In these soils, larger clast may have originated at more distant sources. In general, short-transported material appears to predominate, e.g. sparagmite found NW of all soils, and clasts of shale and slate are found in soils overlaying and SE of this bedrock, however lower percentage than the extent of the bedrock area predicts when material is generally short-transported. This is where the particle size differences matter during clast analysis: The soils are likely to contain short-transported material as well, but it occurs as small particles and has been overlooked in the analysis. Paradoxically, it may be the small grain size of this short-transported material that both exerts the strong influence that nutritious parent material and mineral soil carbon stock in valley 1 that causes difficulty in assessing parent material transport-distance.

The transport distance of the parent material can be inferred from the origins map (figure 4.7). Considering two of the described profiles, V2-7 and V1-2, which are found on the same bedrock (slate) but with significantly different parent material, it is evident that a major part originated >4 km upstream from the landform (V2-7), in less nutritious bedrock. Considering the esker formation in stagnant ice for both landforms, the origin of material can be attributed to the last ice flow phase, with a high degree of local bedrock input. The other meltwater landforms in valley 2 and some in valley 3 are likely to be sourced from a wider area than in valley 1. The clast analysis of V1-2 and the other eskers in valley 1, suggests they are probably formed during the Espedal drainage phase. According to Garnes and Bergersen (1980), glacifluvial material consisting of around 30 % Jotun rocks (gabbro, aNosite etc) record the this phase. Hence both a high and deep stock of carbon can be linked to one of the later stages of deglaciation.

The crevasse eskers in valley 1 (V1-3 and V1-4) are compared to illustrate the influence local bedrock. The landforms are found near each other and are interpreted to have formed at the same time and in a similar manner. They have about the same stone and boulder content, similar vegetation, and the Bs horizon content of clay and silt is around 30 % in V1-4 and 50 % in V1-3. However, V3-1 is innutritious, show a high degree of soil formation and lower carbon stock, while V1-4 is nutritious, show large degree of soil formation and higher carbon stock (chapters 4.1 and 4.3). The location of V1-4 gives a larger upstream area consisting of slate, possibly the reason for the variation between the landforms.

Bergersen (1970) further suggested that the transport distance is insignificant compared to the nature of transport, where sub-glacial processes round the material at a higher rate than supra- and en-glacial transport. Sub-glacial eskers and other landforms of rounded material (fan deposits, fan lobe and delta, all in valley 2) contain redistributed till that may have originated from further away, though the glacifluvial transport distance may have been short. The depositional processes in Valley 2 (high degree of redistribution of both basal and ablation till and glacifluvial material) may have resulted in a variety of lithologies present in the parent material of the soils upstream (e.g. V2-1 and V2-3).

Comparison of the deposits V3-2 (figures 3.32 and 3.33) with V1-2 (figures 3.7 and 3.8) with regard to subsurface carbon stock suggest that changes in depositional regime affects the downward translocation of material. The changes in grain size, pore size and connectivity and bed thickness might create hydraulic barriers that retain and contain percolating fluids, which possibly acts as obstacles to downward translocation of carbon. While the ice-flow parallel esker (V3-2) appears to have experienced a large variation in flow regime and sediment supply (figures 3.32 and 3.33), evident from the large variation in grain size (from silt to gravel), bed dip and thickness, the wide, U-shaped esker (V1-2) appears to have experienced more homogenous deposition (figures 3.7 and 3.8), with a relatively constant grain size (coarse sand) and bed thickness. It is also interesting to note that V1-1 and V1-2 are the only (among the logged) ice-crevasse eskers and deposits overall that show poorly developed erosional surfaces (figures 3.5 and 3.7) suggesting less variation in deposition and/or shorter time gaps between depositional events for such landforms. The difference between sub-glacial and supra-glacial channel deposition might therefore affect soil formation and the degree of deep preservation of carbon in the soil. On eskers with steep surfaces sloping in several directions, percolation of solubles, soil formation and carbon translocation occur along the surface slope and not strictly downwards. This is evident in e.g. V3-2, where horizon development does not appear to be vertical, but to follow the landform surface (figure 4.2).

The landscape surrounding the landforms appears to exert a strong influence on carbon stock, however, this has also affected glacifluvial deposition. The field transects (figure 4.5) illustrates the effect of local topography on an evolving soil. Throughout the same landform, the soil horizons are thicker and less podzolized in the low-laying, low relief areas deposited in a lower flow regime (figure 4.5). The landform morphology is a result of the nature of deposition, where for example distal fan sediments build out across flat and extensive areas. The interplay of deposition with the landscape forms the basis for soil formation, as for example fan formation is a result of meltwater discharge from a narrow channel through to an open plain, discharge in a lower flow regime at a later/ quieter stage of deglaciation. The soil formation is deeper in the flatter areas, which gives thicker horizons increasing the carbon pool. Furthermore, a finer texture and lower stone and boulder content, and possibly also higher density due to enhanced compaction in finer texture soils, are likely to increase the stock of carbon. Soils formed in till in the same area have not undergone the same podzolization, probably due to a higher silt and clay content (figure 4.5).

Care must be taken with property analysis of the soils, because the position of the landforms in the landscape appears to affect the carbon stock to a stronger extent than parent material and bedrock variations. Kame terraces found on a hill side and high, steep and coarse-grained deltas are dry, greatly limiting production. The kame in valley 3 (V3-4) is found in a low laying area surrounded by peat, and to some extent this is also true for some of the transverse eskers in valley 2 and crevasse eskers in valley 1. The difference in microclimate effected through runoff and therefore leaching influences the proportion of clay and base cations in the Bs horizons. Kames and eskers formed in ice remnants in depressions, are naturally low-laying, and experience little leaching. The kame (V3-4) shows the largest carbon stock in the area. Landforms made of nutrient-rich parent material appear to be less sensitive to these factors. When landforms are formed downstream from one another and fed by the same meltwater paths at the same time, it is likely that their parent material is similar and that similarities are evident in soil formation and carbon stock. When soil formation on such landforms differ, however, texture, largely a result of deposition, matters (figure 4.5).

The energy level of deposition, inferred flow the flow competence analysis (figure 3.36) and texture of the deposits (table 4.7) can be correlated to the carbon stock. In valley 2, a high flow competence correlates with low degree of soil formation, thin horizons and a low carbon stock. The coarse texture limits carbon input and decomposition through a low surface area for nutrient and water retention capacity and carbon stabilisation, and gravel and cobbles constitute a significant volume of the soil (table 4.4). V2-1 and V2-3 are interesting, as they both shows high flow competence and contains a moderately high amount of silt and clay, possibly illustrating the need for and result of intensive soil weathering processes (figures 3.36 and table 4.7 but note the invalid results for silt and clay in Bs of V3-2). The high content of silt and clay in the soils in valley 1 (table 4.2 and 4.8) correspond to the high carbon stocks. Valley 3 shows the lowest content of silt and clay (excluding the kame, V34) and the lowest flow competence. The deposits are interpreted to have formed under (V3-2) and laterally to (V3-1) flowing ice, suggesting a stable flow regime at the time of deposition correlating to moderate values carbon stocks. The strongest podzolization is found in the soils with a moderately high stone- and boulder content (41-50 %) (table 4.4) and innutritious parent material. High carbon stocks are found both in landforms of a high stone and boulder content of a high parent material nutrition status (V1-2) and landform where the high stone- and boulder content input and decomposition (V2-1). Overall, the energy level of deposition has greatly influences the degree of soil formation and hence mineral soil carbon stock. V3-4 is deposited in the lowest flow regime and show weak podzolization (figure 5.7), correlating with a low mineral soil carbon stock (figure 4.1). V2-1 (figures 3.10-3.12) was deposited in the highest flow regime and show strong podzolization (figure 5.7), correlating with a high mineral soil carbon stock (figure 4.1).

Comparison of mineral soil carbon stock with results from the radargrams (chapter 3.2) is difficult due to the small number of landforms that are both measured with the GPR and

samples for soil. Two of the landforms that show the highest carbon stock, V1-2 and V3-2, both show subparallel GPR facies in the direction parallel to flow at the landform surface (figures 4.1, 3.8 and 3.33). Furthermore, the delta (V2-1) also shows both among the highest carbon stocks and subparallel reflectors in the surface, however, the radargram is not taken at the landform surface where the soil is sampled. It is possible that the mode of sedimentation that subparallel facies reflect, e.g. decreasing current strengths and progradation, provide good conditions for carbon storage. Dipping facies, on the other hand, which may represent channels or bars or simply cross-stratified sequences, may provide poorer conditions, exemplified through the lower carbon stock of V3-1 (figure 3.29). Other landforms where GPR profiles are taken are not sampled, hence the correlation may be a coincidence. However, dipping surfaces may enhance leaching, while horizontal bed boundaries may aid the retention of moisture and nutrients in coarser soils. It is possible that carbon storage is challenging in more complex channel deposits such as a kame terrace (figures 3.28-3.29) compared to more homogeneously deposited eskers (e.g. figures 3.6-3.8), which also really represent one channel only.

The vegetation (table 4.4), reflecting soil nutrition status, is linked to organic soil carbon stocks and indicates soil stoniness (Appendix 5), texture (tables 4.2 and 4.4), and nutrition status of the parent material. The poorest vegetation is recorded on the delta (V2-1) (Lichen woodland), and the richest on the kame, V3-4 and the chute esker in valley 2, V2-8 (Bilberry woodland) (table 4.4). The kame terrace (V3-1) and eroded fan deposits (V2-3) have a fairly poor vegetation, while the remaining landforms are fairly rich (relatively, in this study). The delta (V2-1) is recognised by the highest stone and boulder content, dry vegetation (table 4.4) and strong soil weathering processes. The kame is recognized by the lowest stone and boulder content, richer vegetation and weak soil formation. High organic soil carbon stock correlates with thriving vegetation (e.g. V1-3, V1-4, V2-8, and V3-4), weaker soil formation and high soil nutrition status. Low organic horizon carbon stock correlates with struggling vegetation (e.g. V2-1, V2-3 and V3-1), lower soil nutrition status and more intense soil weathering processes.

Corti et al. (2002) stated that parent material contributes carbon and nitrogen to soil directly through input from rock fragments. The content of carbon and nitrogen depends on the nature of the parent material as well as its resistance to weathering, and the contribution can only be predicted from the parent material itself (Corti et al., 2002). They stated that considering the rock fragment content of carbon and nitrogen is necessary to accurately estimate carbon stock, the stone and boulder content of the soil profiles (table 4.4) is highest in V1-2 and V2-1, landforms of high carbon stock in the Bs horizon. It is however unlikely that the small contributions in the outside pores of rock fragment are significant compared to the soil volume and large total particle surface area that the clasts replace.

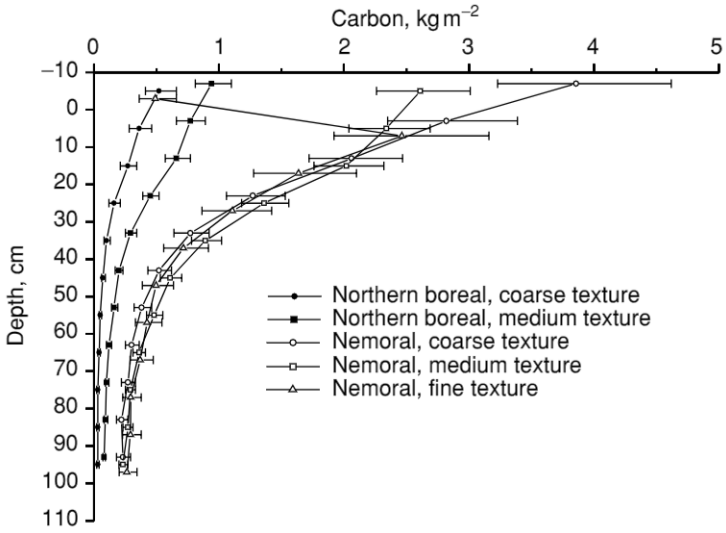

Figure 5.12. Soil organic carbon (with confidence intervals) and its inverse relationship with soil texture in Northern boreal forest soils, comparable to the soils in this study (mean annual temperature= 0° C, mean annual precipitation= 500 mm). From Callesen et al. (2003).

Overall, soil texture appears to exert a major influence on carbon stock. The coarse texture of glacifluvial soils in this study area (figure 4.3) places them in the same category as upland, well-drained soils studied by Callesen et al. (2003). They showed that the carbon stock of Northern boreal forests soils (mineral soil and forest floor) differs between 1.7 kg/m^2 at the lowest in coarse-grained soils and 14.1 kg/m^2 at the highest in in fine-grained soils. Further, they found soil organic carbon content to double in medium textured soils compared to coarse textured soils in the upper 40 cm (figure 5.12). The silt and clay content of the E horizon correlates particularly with mineral soil carbon stock in the soils studied here (figure 4.13A). It is evident that clay content is significant for stabilising carbon in the subsoil (figures 4.9 B and 4.11 E-F).

The content of clay is related to the mode of landform formation. The delta (V2-1) is an outlier, among the soils that show the strongest podzolization and the only soil studied here formed by high energy, late stage deglaciation processes. Generally, the content of clay and silt is higher in eskers, in all horizons, independent of valley and bedrock. The carbon stock of the sub-glacial eskers (V1-5, V2-8 and V3-2) appears to increase linearly with the clay and silt content, suggesting a correlation for this mode of deposition. Most eskers are found on easily erodible bedrock. V3-2, however, is an esker found on less erodible bedrock, and shows high clay and silt in E (figure 4.13A), but average in Bs (figure 4.9). The formation of this esker is, interpreted to be sub-glacial which can explain the variation. The Bs horizons of soils formed from subglacial eskers contain the lowest amount of clay particles. The eskers formed in crevasses in stagnant ice contain the highest amount of clay. The former contains a wide range of parent materials, while the latter are likely to be strongly influenced by surrounding areas of slate bedrock and contain non-pedogenic clay sized particles.

Comparison between soil texture (table 4.7) and carbon stock (figure 4.1) show that the total carbon stock of soils containing a higher percentage sand is lower (figure 5.12). It appears that an increase in the sand fraction from ~60 % to ~80 %, or a halving of the content of clay and silt from ~40 % to ~20 %, can lower carbon stock from ~ 10 kg/m^2 to ~ 40 kg/m^2 (figure 5.13). Strong controls on carbon stock such as moisture regime, soil nutrient status and mineral-complexation are directly influenced by soil texture, which again is directly influenced by the depositional environment and depositional process of the landform. Glacifluvial soil carbon stocks can thus be linked to the formation of the landforms they are found on.

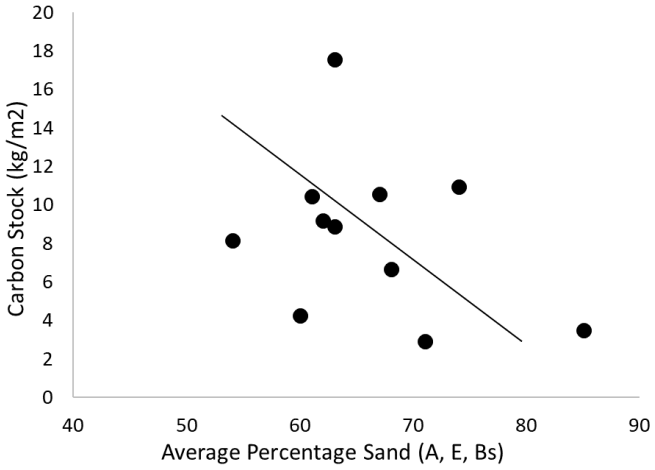

Figure 5.13. Inverse correlation of carbon stock and texture. The percentage clay and silt= 100 %- sand % (table 4.7).

Conceptual relationships exist between carbon stocks, glacifluvial deposits and depositional processes. The higher energy environment deposits (V2-1, V2-3, V2-8 and V1-5) show coarser texture (table 4.2 and 4.4), a higher degree of rounding (figure 3.36) and higher stone and boulder content (table 4.2) than the other deposits. Landforms deposited ice-laterally or in palaeo-water bodies (e.g. V3-1 and V2-1) occur higher than the surrounding landscape. They are very well drained and the soils very dry, and consequently, both production and carbon stock are very low. The steep topography of a typical kame terrace along the NW side of valley 2 is illustrated in figure 5.14.

Figure 5.14.Typical steep slope of an ice-lateral deposit, here illustrated by a kame terrace at 820 masl in the NW part of valley 2 (L26, figure 3.2).

Landforms developed in lower energy environments (V1-3 and V1-4) show a high carbon stock at depth for both well- and less developed soil. This is likely because of a higher amount of silt deposition and clay minerals and better sediment sorting, which provides the potential for water retention and nutrients. In a less developed and moderately nutritious soil (V3-4), it

appears that the carbon is not translocated to depth. Low-laying landscape surrounding a kame (V3-4) is shown in figure 5.15. A summary and numerical evaluation of carbon stocks in relation to depositional processes, soil nutrition status and soil formation is given in the following chapter.

Figure 5.15. Low-laying area surrounding a typical kame, here illustrated by V3-4 (the area vegetated by birch).

5.3.3 Deep Carbon Storage

Mineral soil carbon stock in higher in nutritious, well-developed soils formed from sediment deposited in a stable and moderate flow regime (figures 4.11-4.14). The analysis of the significance of parent material and soil nutrition status, podzolization and the stabilisation of carbon at depth can be summarised as: *Stabilisation Potential= Soil Nutrition Status x Podzolization x Parent Material Nutrition Status x Depositional Process x Depositional Environment,* or *SP= Ns x Pz x Pm x Dp x De.* Soil nutrition status can be low or high, or = ½ or 1, podzolization can be weak or strong, or = 1/3 or 1, the nutrition status of parent material can be low or high, or = ¼ or 1 , the depositional process can be subglacial or not subglacial, or = ½ or 1, and the depositional environment can be ice-lateral/ice-proximal/shallow sub-aqueous/prone to erosion or none of these, or= 1/3 or 1. A value close to 1 predicts optimal potential for stabilisation of carbon in the mineral soil of glacifluvial podzols.

The numerical values of the properties have been set to take their relative importance into account. The development of a carbon stock at depth requires the input and decomposition of carbon. Downward translocation is essential and stabilisation by clay particles necessary for preservation. The nutrition status of the parent material appears to greatly influence the input, decomposition, podzolization and stabilisation, and is assigned the largest value range. The effect of the variation in input-decomposition appears to be lower than the difference in podzolization between the soils (figure 4.15), and the significance of the former is assigned a lower value than the latter.

Sediment maturity (seen from clast rounding, sorting and mineral composition, table 4.4 and 4.6 and figure 3.36) and heterogeneity and anisotropy of the grain size, pore volume and bed thickness within the deposits appear to be higher in sub-glacial landforms compared to supraglacial (e.g. logs V3-2 and V1-2, figures 3.32 and 3.7). The relationship suggests that

input, decomposition and podzolization might be limited due to limited nutrient extraction and/or hydraulic obstacles to both capillary rise and percolation within the profile. Sub-glacial eskers also have a higher stone and boulder content, possibly because they are covered in ablation till. The chute eskers (V2-8 and V1-5) show high input and carbon stock in the organic soil, but low carbon stock at depth. This suggests that the carbon is ether not translocated to or stabilised at depth. The sediment maturity as evaluated from the mineral content (figure 4.6) does not appear to increase with sub-glacial deposition, however, Vorren (1977) suggested that the mode and distance of subglacial transport in the area gives a higher degree of rounding. Additionally, White et al. (1996) suggested that parent material of less surface area undergoes soil weathering at a slower rate. The sediment maturity is considered in the equation through the parent material, nature and energy level of deposition, though it may be wrongly interpreted due to the lack of representative landforms.

Table 5.3. The potential for mineral soil carbon stabilisation in the landforms. Ns= Soil nutrition status; Pz= Podzolization; Pm= Parent material; Dp= Depositional process; De= Depositional environment; SP= Stabilization potential.

Landform	Ns	Pz	Pm	Dp	De	SP
V1-2	1	1	1	1	1	1
V1-3	1	1/3	1	1	1	1/3
V1-4	1	1/3	1	1	1	1/3
V1-5	1	1/3	1	1/2	1	1/6
V2-1	1/2	1	1/4	1	1/3	1/24
V2-3	1/2	1	1/4	1	1/3	1/24
V2-6	1/2	1	1/4	1	1	1/8
V2-7	1/2	1	1/4	1	1	1/8
V2-8	1/2	1/3	1/4	1/2	1	1/48
V3-1	1/2	1	1/4	1	1/3	1/24
V3-2	1/2	1	1/4	1/2	1	1/16
V3-4	1/2	1/3	1/4	1	1	1/24

Deep carbon preservation potential varies among the landforms, though some factors are not included in the analysis. The lowest mineral soil stabilisation potential can be assigned to sub-glacial eskers, delta, kame and proximal fan deposits, and the highest to wider crevasse fill eskers. The depositional regime of the landforms (chapter 5.1 and figure 5.1) affects the estimation through soil texture and landform relief. However, it appears that moderate flow regimes can deposit large grain sizes, probably because of short transport distances of flow- and melt out till (e.g. in V1-2). Landforms of high stone- and boulder content can show high carbon stock (e.g. V2-1), and no functional relationship between the properties is observed on the scale of this study. The estimation does not consider the elevation of the landforms, which may influence the balance of carbon input and decomposition (Jandl et al., 2011). The estimation suggests that the parent material nutrition status enhances carbon stabilisation in the subsoil, even when other factors are limiting.

The evaluation fits with the results from table 4.2, where ice-flow transverse eskers show the highest carbon stock. However, the carbon stock of table 4.2 show the whole profile, while the estimation in table 5.3 concerns stabilisation in the mineral soil. The organic soil carbon stock of the subglacial eskers is generally high (figure 4.1), giving a high total carbon stock despite the estimated low potential for mineral soil stabilisation. V3-2 is an exception and shows a high mineral soil carbon stock. This may be explained by the moderately high parent material nutrition status (table 4.5) despite the low value assigned when the choice was high or low, or the high content of clay and silt (table 4.7). Alternatively, it may simply be a result of unrepresentative or inaccurate sampling as variation within the profile is large (e.g. sediment nature, figure 3.32) and the soil formation processes not vertical. The relationship with deposition process, soil formation, soil nutrition status and mineral soil carbon stock is summarised in table 5.4.

Table 5.4. Summary of degree of podzolization against deep carbon stock, including soil nutrition status, in relation to the depositional environment. See plots in chapters 4.1, 4.4 and 4.5 for carbon stock, soil nutrition status and degree of podzolization. "Early" and "Late" are used as relative terms, based on the deglaciation interpretation in chapter 5.1. The soils coloured in green, purple and red show high, moderate and low soil nutrition status, respectively.

Bs Carbon Stock	Well-developed soil	Less developed soil
Very High[1]	Supraglacial deposition in/between stagnant/blocks of ice **(V1-2)**	-
High Carbon[2]	Supraglacial deposition in stagnant ice **(V1-4)**	Sub-glacial channel deposition **(V3-2)** Late, high energy sub-aqueous deposition **(V2-1)**
Moderate[3]	High pressure sub-glacial channel deposition **(V2-8)** En- or supraglacial deposition in stagnant ice **(V2-7)**	Supraglacial deposition in stagnant ice **(V1-3)** High pressure sub-glacial channel deposition **(V1-5)** High energy, sub-aerial deposition, followed by strong erosion **(V2-3)**
Low[4]	Late Ice-flow Phase/Early Ice stagnation ice-lateral deposition **(V3-1)**	En- or supraglacial deposition in stagnant ice **(V2-6)** Earlier supraglacial deposition in stagnant ice **(V3-4)**.

[4]= 0-0.5; [3] = 0.5-2; [2] = 2-8; [1] = 8-12, kg C /m^2 (Bs horizon).

Based on the summary in table 5.4, which shows a relatively good fit with the results from table 5.3, it appears that a conceptual link can be drawn between the nature of glacifluvial deposition, soil formation and deep stock of carbon. Supraglacial deposition in stagnant ice appears to correlate with both well-developed soils and high carbon stock at depth, and less developed soils with low carbon stock at depth for moderately nutritious soils. It appears that soils formed from landforms deposited in high energy environments are less developed with a moderate to high carbon stock at depth. It appears that en-glacially and ice-laterally deposited landform correlate with a low to moderate carbon stock at depth.

The degree of soil weathering is uncertain. The properties that are used to evaluate the degree of soil formation, such as chemical, clay and iron content, may be inherited from the parent material. A higher content of conglomerates, tillites and sedimentary rocks in general in the glacifluvial sediment, the stronger the weathering signal independent of soil formation (e.g. Chesworth, 1973). The effect is likely to be true for V3-2, formed downstream tillites and conglomerates (figure 1.2). Additionally, note that a distinction in the evaluation is made between intense soil weathering processes and the degree of development in the soils, where e.g. the coarse texture of V2-1 has resulted in strong soil weathering, but the low nutrition status of the soil still results in a soil that is not very well developed.

The nutrition status of the soils appears to influence the process correlation. Innutritious soils appear to have a high carbon stock at depth when they are less developed and formed from high energy, sub-aerial deposits, and lower carbon stock at depth when better developed and formed from ice-lateral deposits. It appears that the innutritious soils follow the opposite trend, as stronger soil formation does not increase the deep stock of carbon, potentially suggesting that strong soil weathering releases little nutrients if the parent material contains little to release. Nutritious soils of a high carbon stock at depth appear to be formed by both high- and low energy, sub- and supraglacial deposition. Nutritious soils appear to compensate for lower degree of soil formation with regards to the deep stock of carbon. In highly nutritious soils, the deep stock of carbon can be high despite a lower degree of soil formation.

Bias during selection of landforms for detailed study occurred, where soil profiles were described in clearly identifiable and visible landforms of clear boundaries with the surrounding landscape. Naturally, this implies that the landforms are higher, have steeper sides, and are isolated from the surroundings. They all show relatively strong soil formation, which may be a result of this common denominator: landform morphology. Either way, it is interesting to note that such landforms, of a morphology clearly identifiable from LiDAR data, possibly can be assessed for degree of soil formation independent of parent material. Overall, the small number of samples gives no statistical significance in the described correlations and are not necessarily representative and useful for generalisation. The detailed study of each landform nonetheless makes correlation for specific groups possible. An attempt of extrapolation of carbon stocks for the whole study area is made in the following chapter.

5.3.4 Carbon Stock of the Glacifluvial Soils Across the Study Area

Extrapolation of the calculated carbon stock is made to include all meltwater landforms in the study area, however, the processes that determine the carbon stock of the soil cannot be accurately determined without field investigation. Hence the landforms are grouped in a manner that allows distinction by remote sensing and map studies; sub-glacially and non-sub-glacially deposited eskers and other meltwater deposits, and the nature and influence of the

local bedrock on the deposits (figure 5.16). The parameters that carbon stock is calculated from are not possible to determine through remote sensing, however, from the evaluation (tables 5.3 and 5.4) they appear to be related to the type of landform through the energy level and mode of deposition (density and stone and boulder content). To allow for upscaling of the carbon stock measurements, six assumptions are postulated:

1st assumption: The bedrock upstream indicates the lithological composition of all landforms. The radii of influence can be inferred by comparing the bedrock clast composition with the bedrock map. Sub-glacial landforms contain more long-transported material.
2nd assumption: Material transport has followed the same direction as ice flow, and the topography of the ice surface and later of the terrain.
3rd assumption: Soil formed from nutrient poor parent material have undergone stronger soil weathering processes.
4th assumption: Soil formed from nutritious parent material are nutritious and experience higher organic carbon input and decomposition.
5th assumption: Podzolization is essential for deep carbon translocation and proportionate to deep soil carbon stock in innutritious parent material soils.
6th assumption: Sub-glacial landforms have experienced a larger variation in flow regime, resulting in hydraulic barriers within the soil that limits downward translocation, and are likely to be covered in ablation moraine, giving a landforms surface and soil profiles with a high stone and boulder-content.
7th assumption: The values obtained for the few studied landforms are representative for upscaling.

Jandl et al. (2011) stated that some soils, including podzols, show a significant dependence on parent material compared to relief and climate, which allows upscaling of values for soil carbon stock on a regional scale with regards to bedrock. Hence, they suggested that georeferencing of maps may allow estimation on the continental scale with a small number of samples for glacifluvial soils.

Table 5.5. Overview of eskers for extended area extrapolation. Lithologies are from map sheet Synnfjell (Hossack and Lutro, 2013). «Local» refers to the local, underlaying lithology as well as the lithology in a cone shaped area upstream from the profile (<5 km radii for non-subglacial landforms and <10 radii km for sub-glacial landforms). Numbers in parenthesis is carbon stock in kg/m^2, down through the Bs horizon.

	High Nutrient Status of Local Bedrock	**Low Nutrient Status of Local Bedrock**
Subglacial	V1-5, Small Chute Esker (6.72)	V3-2, Ice-flow Parallel Esker (9.24) V2-8, Large Chute Esker (10.50)
Non-sub-glacial	V1-3, Larger Crevasse Esker (8.20)	V2-6, Small Ice-flow Transverse Esker (2.96)
	V1-2, Wide, U-Shaped Esker (17.58)	V2-7, Ice-flow Transverse Esker (4.29)
	V1-4, Small Crevasse Esker (8.92)	

The large variation in carbon stock across the studied landforms (table 4.1 and figure 4.1) suggests that extrapolation to a number of landforms about 50 times what are studied is may lead to great over- and underestimations of values. Comparison with various studies (table 5.1), however, suggests that the obtained values are both within a range and of similar variation as previously found (e.g. Baritz et al., 2011). There appears to be less variance within the groups than between, which suggest that the grouping is reliable (table 5.5). On the other hand, the results are not statistically reliable due to the small number of landforms. A detailed study of a large enough number is not possible in this project, but a test of the method is carried out by using the constructed model to calculate the carbon stock of a landform that is already measured (table 5.6).

Carbon stock values are higher for soils formed from landforms downstream nutritious bedrock, and larger variation is observed between landforms that are not formed sub-glacially (figure 4.1 and table 4.1). This suggests that the carbon stock of soils in sub-glacial landforms are less affected by the local bedrock, and that the material composition has larger variance and an average nutrient status. The subglacial landforms show a lower carbon stock in the nutritious bedrock group and vice versa. The degree of podzolization appears to have insignificant effect on carbon stock for subglacial eskers but increase carbon stock in the other. This is particularly true for eskers in nutritious bedrock areas, as the highest carbon stock is found in the strongest podzolized, most nutritious group (V1-2 and V1-3).

The premises for extrapolation suggests that sub-glacial eskers show a value for parent material approaching the mean in the constructed method (= 3). The transport distance for

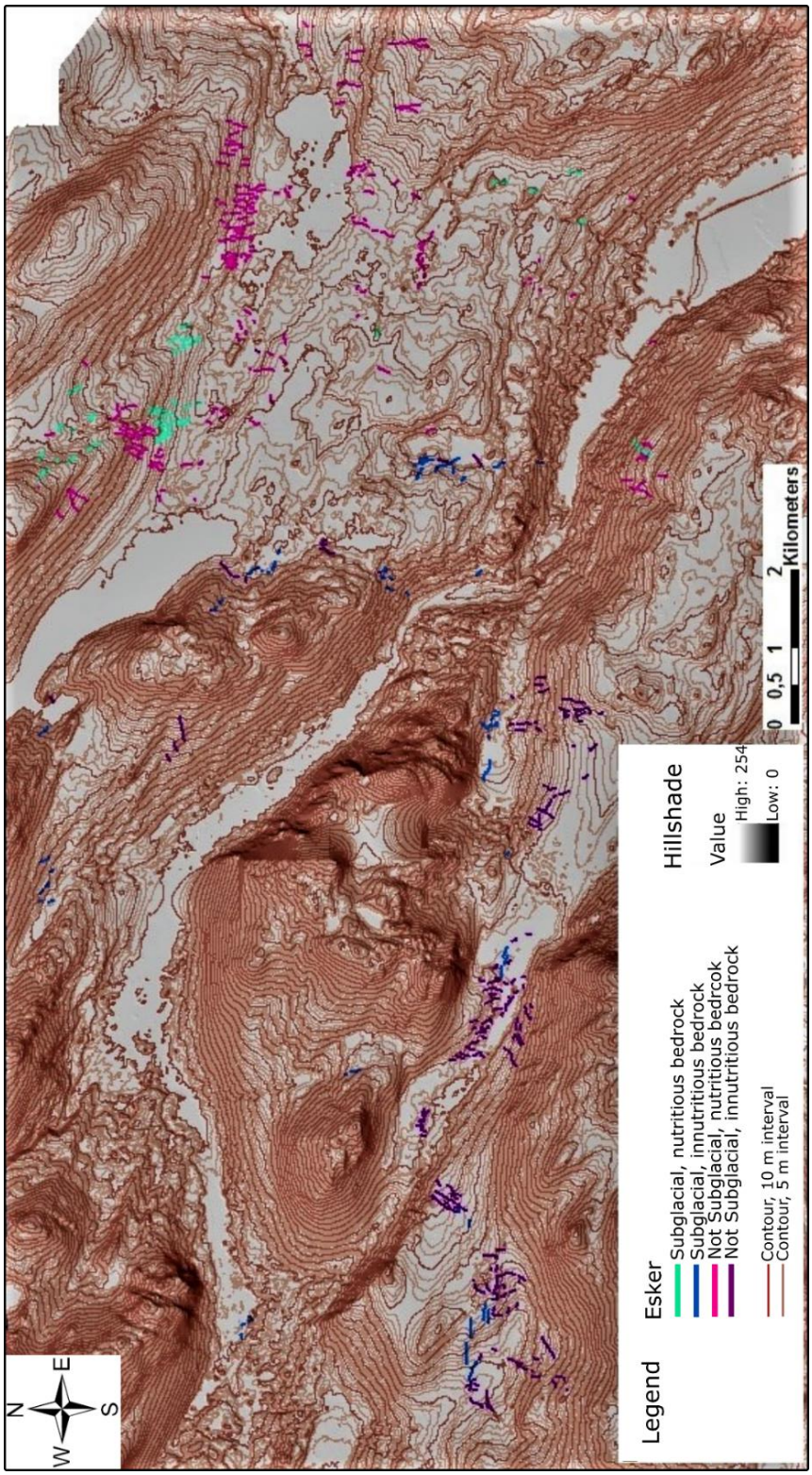

Figure 5.16. Nature and distribution of eskers for soil carbon estimation, classified according to landscape, depositional process and local bedrock influence.

parent material is estimated after comparison of bedrock clast analysis composition (figure 4.6) with the bedrock map (figure 1.2). Comparing the parent material nutrition status for V3-1 and V3-2 (2.75 and 2.86, respectively) where V3-2 is found downstream V3-1 in the same valley, suggests that the assumption can be true. However, V3-2 is found closer to more basic bedrock (conglomerate with gabbro pebbles, figure 1.2). Figure 4.6 suggests that the parent material of V3-1 contains lithologies of a similar transport distance as V3-2, however, the small number of potentially long transported clasts makes the interpretation difficult. It is also possible that specific clasts have a local source, but that the scale of the Lillehammer Map Sheet used for evaluation did not allow their recognition.

The extrapolation of carbon stock to all eskers in the area is done based on the bedrock criteria outlined above, as well as the categorization of chute eskers (found on steep slopes) and ice-flow parallel esker as subglacial. The underlying topography

and directional sense of the landforms can be inferred from the contour lines and hill shade developed from the digital elevation model. By georeferencing the bedrock map onto the landforms -, hill shade - and contour files (see chapter 2.4 for method), the nature of the local bedrock, underlaying topography and directional sense of esker can be evaluated. Figure 5.16 shows all 475 eskers in the study area (Putnins and Henriksen, 2017) grouped according to the system in table 5.5.

Length is the only dimensional parameter that can be obtained for the eskers in the meltwater landforms map by Putnins and Henriksen (2017) (figure 1.5). An interesting feature of the map is the distribution of eskers transverse to the ice flow direction in the various bedrock areas (figure 1.2). There appears to be both a higher number of transverse compared to ice-flow parallel eskers, as well as more clustering (figure 1.5). The observation excludes the eskers along the Northern side of valley 1 (around the kame), which are found on steep slopes and most likely represent chute eskers. An average width of landforms in each group is calculated based on the studied landforms, and the length of each landform given in the map. The area of each esker is calculated and summarized for each group, and the total carbon stock of each group estimated. The results are shown in figure 5.17.

Carbon stock values used for the meltwater landforms in valley 2 are from the delta and reworked fan deposits (V2-1 and V2-3). The values are quite different (figure 4.1), and a significant part of the landforms along the valley side are outwash plains, distal deposits and possibly even lacustrine deposits. The geographical position of landforms along valley 2 is interpreted to reflect time of deposition (chapter 5.1) and the material origin may have changed throughout deposition. An average of the values obtained in the valley is used (obtained from the delta and the fan deposits). The values used for the meltwater landforms in valley 1 are extrapolated from the kame, kame terrace, and ice-flow parallel esker. In the Southern end of valley 2, for what appears to be small fans originating in the N, the value for the small chute esker is used.

Parent material origin in meltwater landforms other than eskers is estimated from geographical position and depositional environment/time of deposition. LiDAR data and orthophotos are used to evaluate the nature of the mapped meltwater landforms, and proximity and similarity with sampled soil landforms. Where sampled landforms do not occur nearby, and/or the mode and time of formation is clearly different, the source of material determines the extrapolation value, e.g. the values for the kame terrace is used for the washout plains at the inlet of valley 1. Underestimation rather than overestimation is likely to occur in these situations. The texture and stone and boulder content of the delta and eroded, proximal fan deposits are likely to be coarser and higher than the landforms the carbon stock is extrapolated to. The carbon stock may therefore be underestimated in the “other” meltwater landforms, because lower stone and boulder content allows for a higher carbon concentration and, and higher fraction of silt and fine sand enhances production, decomposition and stabilisation. However, many of these landforms are likely to be fan deposits.

Overall, the largest carbon stock is found on the landforms the largest surface area but is higher in soils formed from nutritious parent material for a specific size. It is lowest in short, sub-glacial eskers. The width of the eskers is estimated from the mean (see above), hence the surface area and carbon stock estimation may be misleading as e.g. sub-glacial eskers may be wider than ice-flow transverse eskers (figure 3.3). As discussed in chapter 5.2.2, the parent material nutrition status may predict the total carbon stock, but not the relative proportion in the mineral soil. Hence the stocks of carbon extrapolated in figure 5.17 may give no indication of the stock of stable carbon.

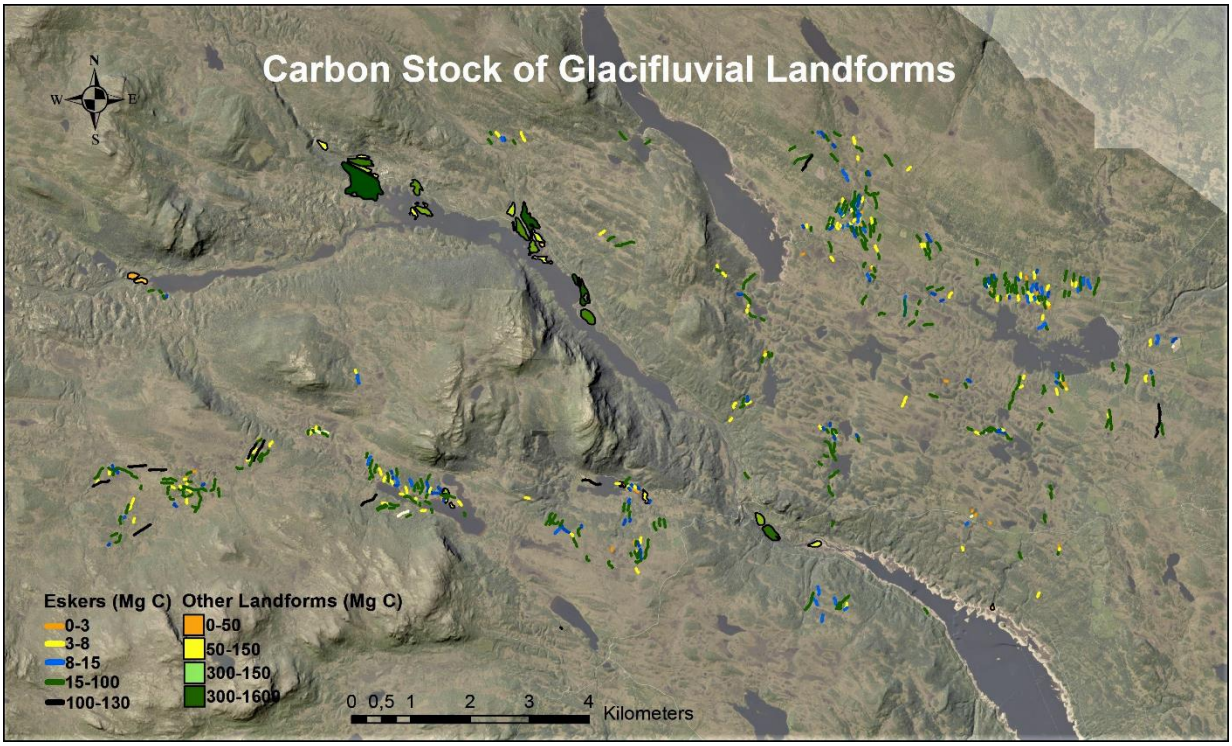

Figure 5.17. Carbon stock extrapolation to all glacifluvial landforms in the study area.

In order to verify the method for upscaling, the carbon stock of a landform from one of each of the four constructed groups are compared to the value calculated from field and laboratory measurement (table 5.6). All landforms chosen for comparison are interpreted to have experienced weak soil weathering processes (figure 4.11), eliminating the variable. The result shows that the carbon stocks are exaggerated in the extrapolated results, particularly for meltwater landforms other than eskers. The lowest exaggeration is found in eskers in low nutrition bedrock areas, with an underestimation in subglacial eskers. Other meltwater landforms, the extrapolated value was more than doubled than the measured. It is not surprising that the result is inaccurate, due to the small area and large variety in landforms, as evident from e.g. the organic soil carbon stocks of these landforms (table 4.1). The general exaggeration might be a result of stronger podzolization of most studied landforms than the landforms compared. It is possible that the influence of a high parent material nutrition status is easily overrated when a soil has experienced little soil weathering. The smallest error in the

group that constitutes most of the landforms in the area (ice-flow transverse eskers, figure 5.1), is good news for extrapolation, however, caution should be note that the values measured is based on a small area and is susceptible to error.

Table 5.6. Comparison of carbon stocks in estimated based on field and laboratory measurement and from extrapolation for the five constructed groups.

Landform Group	Representative Landform	Landform Area (m^2)	Measured Carbon Stock (Mg)	Extrapolated Carbon Stock (Mg)	Error
SE, High BA NS	V1-5	13 800	92 705	136 206	+ 47 %
SE, Low BA NS	V2-8	14 508	145 799	97 494	- 33 %
TE, High BA NS	V1-4	23 127	189 710	267 159	+ 40 %
TE, Low BA NS	V2-6	610	1 807	2 214	+ 22 %
OML, Low BA NS	V2-3	2 220	7 153	15 213	+ 113 %

SE= Subglacial esker, TE= Ice-flow transverse esker, OM= Other meltwater landform, BA= Bedrock area, NS= Nutrition status

5.3.5 Glacifluvial Soils and the Short-term Carbon Cycle

Contribution of glacifluvial soil carbon to the atmosphere as CO_2/unit area can be estimated. The carbon that resides at depth is not in constant exchange with the atmosphere, and its translocation to the atmosphere would constitute an unbalanced flux. Furthermore, the degeneration of soil structure that would occur with loss of organic material would lower nutrient and water retention capacity, limit production and decomposition and decrease the potential for storage of soil carbon in the future. The total value of the soil carbon of glacifluvial landforms in the area is 16 430 Mg, among which eskers constitute 10 837 Mg and other landforms 5 593 Mg (table 5.7). The average ratio of the soil carbon stock of the landforms studied to the soil carbon of the mineral soil only is 1.55 (avg. total amount = 7.80 and avg. mineral soil amount = 5.02) (figure 4.1 and table 4.2). Hence two-thirds of the soil carbon of the glacifluvial landforms have the potential for surplus contribution to the atmospheric in a temporal perspective. The carbon stock of soil carbon can be converted into CO_2 equivalents by the factor 3.67, as the atomic weight of carbon and oxygen through *((12.00 g/mol + (16.00 x 2) g/mol) / 12.00 g/mol* gives the conversion factor. The total area of the ~500 meltwater landforms constitute 166.64 ha (1 666 429 m^2). Two-thirds of the glacifluvial soil carbon in the area (16 430 Mg) is 10 954 Mg, which is equal to 241 Mg CO_2. A summary is given in table 5.7.

Table 5.7. Carbon Stock and CO_2 equivalent across the deglaciation landscape

	Carbon Stock (Mg)	**Carbon Stock Mineral Soil (Mg)**	**CO_2 Equivalent (Carbon stock mineral soil) (Mg)**
Eskers	10 837	7 225	26 516
Other Meltwater Landforms	5 593	3 729	13 684
All landforms (166.64 ha)	16 430	10 954	40 200
Average (Mg/ha)	99	66	241

In glacifluvial landforms of a deglaciation landscape in uncultivated, highland areas in the boreal vegetation zone and cold climate, therefore, soil carbon can release 241 Mg of CO_2 per hectare not balanced by any sink equivalent. The mean value for carbon stock in Mg/ha is slightly higher than the mean based on the 12 studied landforms (7.99 kg/m^2 which equals 79.9 Mg/ha). The higher mean also affects the carbon equivalent CO_2 estimation. Additionally, the fraction of soil organic carbon that resides in the mineral soil appears highly variable. Kleja et al. (2008) found the fraction to be 77-88 % in three spruce ecosystems in Sweden. The sites were located at an altitude of 190-320 masl in mean annual air temperature of 1.2-5.5° C, potentially illustrating an increased downward distribution of soil carbon at higher temperature and lower elevation.

It appears that the carbon pool of glacifluvial soils is sensitive to change, and that utilisation will require maintenance of the natural ecosystem. Afforestation is a popular mean of carbon capture and sequestration, but Clancy et al. (2015) showed that turning podzols into forest may increase the flux of CO_2 to the atmosphere. Disturbance and drainage of the podzols might affect the inherent carbon stock. At the same time, Petrenko and Friedland (2015) predicted that deforestation of these soils will cause loss of carbon and lower the potential for future sequestration, through heating and compaction. They showed how harvest slowly but drastically can decrease the inherent carbon stock of the soils across a century. It is possible that both afforestation and deforestation of the areas studied will cause a similar change, despite the major difference that it is neither densely forested nor cultivated. Torres-Sallan et al. (2017) concluded that soils subject to clay illuviation, soils in which the stock of carbon is largely associated with the clay fraction, are sensitive to changes in land use. They stated that deeply stored soil carbon may be lost if the mechanistic relationship between the clay fraction and carbon is disturbed. Though soil carbon is largely stabilised by oxides studied here (which, however, constitutes a significant part of the clay fraction (figure 5.7)) and the authors referred to a different setting and, a similar situation might occur.

The carbon in the upper soil that is not mineral-stabilised may be destabilised in a warmer climate. Jandl et al. (2011) stated that temperature is the main predictor for soil carbon stock in the study area, possibly predicting substantial changes in higher temperatures. Decomposition increases with warming (Schlesinger and Bernhardt, 2013), and the acceleration can possibly exceed the rate of stabilisation. Callesen et al. (2003) concluded that

coarse soils are more sensitive to mean annual temperature and precipitation than finer soils. The unstable soil carbon fraction is likely to constitute at least a third of the total carbon stock of the soils, equivalent to 120.62 Mg CO_2/ha.

Jandl et al. (2011) suggested that the effect of warming on net ecosystem exchange increases with altitude, hence that carbon stocks of soils in mountains ecosystems such as Gausdal Vestfjell may be more sensitive to increased temperatures. They showed that the increase in CO_2 flux (evaluated from the net ecosystem exchange) resulting from warming at peak growing season in higher elevation mountain/tundra heath ecosystems went from ~ 0.1 to ~ 0.4 g CO_2/m^2 hour. The flux corresponds to 10-40 kg CO_2/ha hour, or the CO_2 equivalent of 1 hectare carbon from the upper horizons of the soil studied here (121 Mg) in 18 days. However, these processes require complex modelling and the calculation is inaccurate for many reasons, among them that the change is not likely to be linear, and that various feedback mechanisms are likely to be activated that move the system towards new equilibrium states. Soil organic carbon will depend on input as well as decomposition, and studies have also shown soil organic carbon to increase with temperature and precipitation (e.g. Callesen et al., 2003).

Overall, it appears that the carbon stock of podzols show variation across the recently deglaciated Northern Hemisphere (table 5.1), but that upscaling of small-scale studies can be used to estimate the carbon pools of vast areas (chapter 5.3.4) as well as its possible influence on the larger, changing environment. On the other hand, the glacifluvial landforms constitute only 5.5 % of the study area (~30 km^2), and the carbon stocks might not represent many of the soils in the deglaciation landscape. They may however provide a minimum value for its high content other, finer-grained deposits.

6 Suggestions for Future Research

- To enhance the understanding of the effect of parent material nutrition status on carbon stock: Mineralogical studies of the fine earth fraction of the soil (e.g. by total element analysis by ICP) in combination with clast analysis, consideration of palaeochannels/meltwater erosion features feeding the landforms for improved understanding of parent material composition and large-scale bedrock maps.
- To evaluate stabilisation and dynamics of organic matter in glacifluvial soils: Measurement of the hot water extractable organic carbon (HWOC) to determine the proportion of labile carbon.
- For more accurate carbon stock evaluation and to possibly assess the effect of carbon input and decomposition rates: Inclusion of soil moisture regime/ microclimate and altitude of landform.
- Evaluate the carbon stock of peat and peaty soils that cover the vast areas of negative relief landforms of the deglaciation landscape (e.g. meltwater basins, palaeochannels, kettle holes, channel complexes of wash out fan systems).

7 Conclusions

Gausdal Vestfjell was deglaciated by down-wasting of stagnant ice, with damming of meltwater by the stagnant ice front in the SE. Drainage occurred in stages, and kame terraces formed at high elevations (~820-890 masl) record a progressive lowering of the ice surface. Subaerial and subaqueous deposits such as fan, delta and plains at lower elevations (780-810) record the final stages of deglaciation. The glacifluvial sediments are generally sorted, subangular and in a textural range from fine sand to gravel. The flow regime was highly variable, although mainly un the upper flow regime. Well-developed erosional surfaces are observed in all deposits except eskers formed supra-glacially in ice crevasses. Deposition by gravity occurred in fan and ice-crevasse esker deposits.

The carbon stocks can be linked to depositional environments and processes during deglaciation. Early and late stage deposition at high (~890 masl) and low elevation (~790 masl), respectively, resulted in low carbon stocks, while deposition from stagnating ice at intermediate elevations is linked to high carbon stocks (~850 masl). Low-relief eskers formed in ice-crevasses perpendicularly to the ice movement direction at around 850 masl and with around 30 % Jotun rocks are attributed to the Espedal Drainage Phase. Soil texture varies greatly as result of large variations between and within depositional environments and depositional processes and exerts a major influence on carbon stocks through water circulation, moisture and nutrient retention and mineral-organic occlusion and complexation.

In general, the high energy flow of glacifluvial deposits has resulted in a low clay and silt content which limits carbon input, decomposition, translocation and stabilisation. While 63 % of the glacifluvial soil carbon is stabilised through mineral occlusion and complexation, 37 % is unstable and found in the organic horizons. However, the mineral soil carbon stock constitutes appear to constitute either a very high or very low proportion in soil of a high carbon stock.

The carbon stock of the glacifluvial deposits of the deglaciation landscape varies between ~ 3 and 18 kg/m^2, with an average value of 7.99 kg/m^2 (SD= 4.26) (down through the Bs horizon). The organic soil carbon stock shows a variability of 0-9.48 kg C/m^2, and an average of 2.96 kg C/m^2 (SD= 3.04). The mineral soil carbon stocks also show large variation, with values ranging from 1.09 to 16.40 kg C/m^2, and an average of 5.03 kg C/m^2 (SD= 4.15). A rate for podzol carbon accumulation rate given by Schlesinger (1990) provided the basis for theoretical estimation of accumulation since deglaciation, found to be ~ 7 kg/m^2, comparable to the measured values for carbon stock.

Proportionality exists between the mineral soil carbon stock, parent material nutrition status, content of clay minerals and iron and aluminium oxides. The ratio of soil organic carbon to the active oxide content shows sorption of soil organic carbon to mineral phases and is

proportional to the parent material nutrition status, suggesting stabilisation of carbon through mineral-organic complexes. The proportionality between degree of podzolization and mineral soil carbon stock is a result of higher nutrient extraction, more clay illuviation and more mineral-organic complexation. A doubling of clay and silt content from 20 % to 40 % increases carbon stock from ~4 kg/m^2 to ~10 kg/m^2. Proportionality is found between mineral soil carbon stock, base saturation and sorption of soil organic carbon to active iron and aluminium.

The total carbon stock appears higher in soils that show high parent material nutrition status and degree of podzolization, and in landforms deposited sub-glacially. The nutrition status of parent material may predict the total carbon stock of a soil, but not the proportion found in the mineral soil. In soils formed from more nutritious parent material, more recalcitrant organic carbon is stabilised by clay minerals, while in soils formed from innutritious parent material, the organic carbon is likely to be more labile and mainly stabilised by soil weathering products including iron and aluminium oxides.

Analysis of the significance of carbon input/decomposition, podzolization and parent material nutrition status on the stabilisation of carbon at depth can be summarised as *stabilisation potential= soil nutrition status x podzolization x parent material x depositional environment x depositional process, which* yields a numerical value for the potential for mineral soil carbon stabilisation. The results from glacifluvial soils in this area, which fit relatively well with the mineral soil carbon estimation, suggest that deltas (top-sets), (proximal) fan deposits and (variable and/or high energy flow) sub-glacial eskers have the lowest potential, and wider/larger supra-glacial crevasse fill eskers the highest.

The transport distance and time since deglaciation does not exert a control on carbon stock, but the nature of transport and deposition does. Sediment immaturity correlates proportionally with carbon stock, and both are higher in low-energy, supra-glacial environments. Where the stone and boulder content and flow competence of a sediment are moderate, the properties exert little control on soil formation. When the degree of rounding, flow competence and stone and boulder content are high, soil formation appears to be strong, but soil nutrition status low. Low degree of rounding and low flow competence exert no influence on soil nutrition status and soil formation in acidic parent material but enhance both in nutritious parent material.

Landforms deposited in the upper flow regime and/or, ice-laterally or ice-proximally and/or deposition resulting in high landform relief have lower carbon stock, particularly in the organic horizons (which are thin or absent). Further, landforms consisting of complex channel systems, e.g. kame terraces, may have a lower potential for mineral soil carbon storage, while, landforms of more homogenous deposition, e.g. supraglacial eskers, may have a higher. The former is represented by dipping GPR facies displaying e.g. bars and cross-stratified beds, and

the latter by subparallel reflectors displaying quieter environments, decreasing currents and progradation.

Sub-glacial and supra-glacial channel deposition appear to give different potential for the downward translocation of carbon. Subglacial eskers show a variable material and depositional regime, whereas supra-glacial eskers appear more homogenous. The hydraulic containment of material in sub-glacial eskers might be limiting to the supply and stabilisation of carbon to the deep soil. High energy sediment deposition results in poorly developed, innutritious soils. Low energy deposits that have undergone little soil formation, are nutritious, but store carbon in shallower horizons. Low nutrition soils appear to store less carbon at depth with stronger soil formation, opposite to the nutritious soils. Ice-lateral and deltaic deposits give innutritious soils that store little carbon at depth. Bio-chemically stabilised carbon storage in the organic soil is highest in kame and chute eskers. Soils formed from immature sediment deposited in crevasses in stagnant ice, are generally less developed with a high carbon stock at depth, and well developed with an even higher carbon stock at depth.

Carbon stock in the Bs horizon is influenced by the nature of podzolization in soils formed in and downstream areas consisting of slate. A higher amount of translocated organic acid complexes with iron and aluminium (hydr)oxides increases the carbon stock proportionally. The organic carbon is stabilised by the (hydr)oxides and is part of a long-term carbon pool. The soils formed from the least nutritious parent material has a lower pool of carbon in the Bs horizon than what is expected from the amount of iron and aluminium (hydr)oxides, suggesting that the hydroxides were translocated through other mechanisms (e.g. inorganic complexes following silicate weathering). A conceptual link can be drawn between parent material fertility, nature of podzolization and Bs horizon mineral stabilised carbon stock.

Local bedrock exerts a considerable influence on parent material for both sub-glacial, supra-glacial and ice-lateral deposits, and is particularly influential on carbon stock when it is composed of slate, increasing both parent material nutrition status and carbon stock. The origin of the parent material appears insignificant otherwise, except when the glacifluvial deposits are composed of material from a wider area, which gives a more intermediate parent material nutrition status.

Subsoil carbon stock can be assessed from LiDAR data and upstream bedrock maps, without sampling and analysis. Extrapolation of the measured values for carbon stock to the whole study area shows that the surface area of the landforms is the dominant factor for total carbon stock estimation. For equally sized landforms, the nutrition status of the local bedrock predicts the carbon stock.

Loss of unstable carbon accumulated since the deglaciation in the glacifluvial deposits in Gausdal Vestfjell due to increased temperatures can potentially amount to ~121 Mg/CO_2/ha.

Loss of loss mineral-stabilised carbon through for example land use change can contribute to ~ 241 Mg CO_2/ha.

The carbon stock values obtained here are similar to values found for forest soils in mountainous ecosystems in other studies, and extrapolation of smaller scale measurements can facilitate accurate soil carbon stock estimations across vast areas of the recently deglaciated Northern Hemisphere.

8 References

ANNAN, A. P. 2003. *Ground Penetrating Radar. Principles, Procedures & Applications,* Sensors & Software Inc.

BANERJEE, I. & MCDONALD, B. C. 1975a. Nature of Esker Sedimentation. *Glaciofluvial and Glaciolacustrine Sedimentation, Society of Economic Paleontologists and Mineralogists Special Publication,* 23**,** 132-254

BANERJEE, I. & MCDONALD, B. C. 1975b. *Nature of esker sedimentation,* Society of Economic Paleontologists and Mineralogists

BARITZ, R., SEUFERT, G., MONTANARELLA, L. & VAN RANST, E. 2010. Carbon concentrations and stocks in forest soils of Europe. *Forest Ecology and Management,* 260**,** 262-277.

BARON, J. 1992. *Biogeochemistry of a subalpine ecosystem,* New York, Springer-Verlag.

BENN, D. I. & EVANS, D. J. A. 2010. *Glaciers and Glaciation,* Oxon, UK, Hodder Education.

BERG, B. & MCCLAUGHERTY, C. 2003. *Decomposition, Humus Formation, Carbon Sequestration* Springer

BERGERSEN, O. F. 1970. Undersøkelser av steinfraksjonens rundingsgrad i glasigene jordarter *NGU* 266**,** 252-262.

BERGERSEN, O. F. & HOFSETH, E. H. 1987. *Bind 1 Fra Istid til Viktingtid forhistorie* Lillehammer, Thorsrud a/s.

BEUSELINCK, L., GOVERS, G., POESEN, J., DEGRAER, G. & FROYEN, L. 1998. Grain-size analysis by laser diffractometry, comparison with the sieve-pipette method. *Catena,* 32(3)**,** 193-208.

BLUME, H., BRÜMMER, G. W., FLEIGE, H., HORN, R., KANDELER, E., KÖGEL KNABNER, I., KRETZSCHMAR, R., STAHR, K. & WILKE, B. 2016. *Scheffer/Schachtschabel Soil Science,* Berlin, Germany Springer-Verlag Berlin Heidelberg

BOCKHEIM, J. G., GENNADIYEV, A. N., HAMMER, R. D. & TANDARICH, J. P. 2005. Historical development of key concepts in pedology. *Geoderma,* 124**,** 23-36.

BRADY, N. C. & WEIL, R. R. 2013. *Elements of the Nature and Properties of Soils,* Harlow, United Kingdom, Pearson Education Limited.

BREMMER, J. M. & MULVANEY, C. S. 1982. *Methods of Soil Analysis Part 2* Madison, Wisconsin, USA, American Society of Agronomy, Inc.

BURKE, M. J., BRENNAND, T. A. & SJOGREN, D. B. 2015. The role of sediment supply in esker formation and ice tunnel evolution. *Quaternary Science Reviews,* 115**,** 50-77.

CALLESEN, I., LISKI, J., RAULUND-RASMUSSEN, K., OLSSON, M. T., TAU-STRAND, L., VESTERDAL, L. & WESTMAN, C. J. 2003. Soil carbon stores in Nordic well-drained forest soils - relationships with climate and texture class. *Global Change Biology,* 9**,** 358-370.

CATUNEANU, O. 2006. *Principles of Sequence Stratigraphy,* Elsevier Science.

CHESWORTH, W. 1973. Parent rock effect in genesis of soil. *Geoderma,* 10**,** 215-225.

CLANCY, M., JOVANI SANCHO, A. J., CUMMINS, T. & BYRNE, K. 2015. *The need to disaggregate podzols and peaty podzols when assessing forest soil carbon stocks*.

CORNELIS, J. T., WEIS, D., LAVKULICH, L., VERMEIRE, M. L., DELVAUX, B. & BARLING, J. 2014. Silicon isotopes record dissolution and re-precipitation of pedogenic clay minerals in a podzolic soil chronosequence. *Geoderma,* 235**,** 19-29.

CORTI, G., UGOLINI, F. C., AGNELLI, A., CERTINI, G., CUNIGLIO, R., BERNA, F. & SANJURJO, M. J. F. 2002. The soil skeleton, a forgotten pool of carbon and nitrogen in soil. *European Journal of Soil Science,* 53**,** 283-298.
DAHLGREN, R. A. & UGOLINI, F. C. 1989. Aluminium fractionation of soil solutions from unperturbed and tephra-treated spodosols. *Soil Science Society of America Journal,* 53**,** 559-566.
DANIELS, R. B. & HAMMER, R. D. 1992. *Soil geomorphology,* New York Wiley.
DAVY, H. 1813. *Elements of Agricultural Chemistry,* London
DOKUCHAEV, V. V. 1879b. *Chernozeme (terre noire) de la RussieD'Europe,* St. Petersburg.
DYKE, A. S. 1993. Landscapes of cold-centered Late Wisconsinan ice caps, Artctic Canada. *Progress in Physical Geography* 17**,** 223-247.
ENGLUND, J. O. 1973. Stratigraphy and Structure of the Ringebu-Vinstra District, Gudbrandsdalen; with a Short Analysis of the Western Part of the Sparagmite Region in Southen Norway. *NGU Bulletin 18,* 293**,** 1-58.
ERIKSSON, C. P. & HOLMGREN, P. 1996. Estimating stone and boulder content in forest soils - Evaluating the potential of surface penetration methods. *Catena,* 28**,** 121-134.
EUSTERHUES, K., RUMPEL, C. & KOGEL-KNABNER, I. 2005. Stabilization of soil organic matter isolated via oxidative degradation. *Organic Geochemistry,* 36**,** 1567-1575.
EVANS, D. J. A. & BENN, D. I. 1998. *Glaciers and Glaciation,* London, Edward Arnold.
EVANS, D. J. A. & BENN, D. I. 2004. *A Practical Guide to the study of Glacial Sediments* London, Edward Arnold.
FAO 2006. World reference base for soil resources 2006. A framework for international classification, correlation and communication. 4th ed. Rome: Food and Agriculture Organization of the United Nations.
FLINT, R. F. 1957. *Glacial and Pleistocene Geology,* New York, John Wiley & Sons.
FONTAINE, S., BAROT, S., BARRE, P., BDIOUI, N., MARY, B. & RUMPEL, C. 2007. Stability of organic carbon in deep soil layers controlled by fresh carbon supply. *Nature,* 450**,** 277-U10.
FREDIN, O., BERGSTRØM, B., EILERTSEN, R., HANSEN, L., LONGVA, O., NESJE, A. & SVEIAN, H. 2013. Glacial landforms and Quaternary landscape development in Norway. *Quaternary Geology of Norway,* 13**,** 5-25.
FREMSTAD, E. 1997. *Vegetasjonstyper i Norge,* Trondheim, NINA Norsk Institutt for naturforskning, Direktoratet for naturforvaltning.
FROSTRICK, L. E., LUCAS, P. M. & REID, I. 1984. The infiltration of fine matrices into coarse-grained alluvial sediments and its implications for stratigraphical interpretation. *Journal of the Geological Society,* 141**,** 85-94.
GARNES, K. & BERGERSEN, O. F. 1972. Ice Movements and Till Stratigraphy in the Gudbrandsdal Area. Preliminary Results *Norsk Geologisk Tidsskrift* 26**,** 1-16.
GARNES, K. & BERGERSEN, O. F. 1980. Wastage features of the inland ice sheet in Central South Norway. *Boreas,* 9**,** 251-269.
GEE, G. W. & BAUDER, J. W. 1986. *Particle-size analysis,* Madison, Wisconsin, USA.
GOEHRING, B. M., BROOK, E. J., LINGE, H., RALSBECK, G. M. & YIOU, F. 2008. Beryllium-10 exposure ages of erratic boulders in southern Norway and implications for the history of the Fennoscandian Ice Sheet. *Quaternary Science Reviews,* 27**,** 320-336.
GOLDICH, S. S. 1938. A Study in Rock Weathering. *Journal of Geology,* 46**,** 17-58.

GRINDERUD, K., RASMUSSEN, H., NILSEN, S., LILLETHUN, A., HOLTEN, A. & SANDERUD, Ø. 2008. *GIS: geografiens språk i vår tidsalder,* Tapir Akademiske Forlag.
GRUNEBERG, E., SCHONING, I., KALKO, E. K. V. & WEISSER, W. W. 2010. Regional organic carbon stock variability: A comparison between depth increments and soil horizons. *Geoderma,* 155**,** 426-433.
HEIM, M. 01.10.17 2017. *RE: The Bedrock of Lillehammer.* Type to AUTHOR.
HERGET, J. 2005. Reconstruction of Pleistocene Ice-Dammed Lake Outburst Floods in the Altai Mountains, Siberia. *Geological Society of America Special Papers,* 386.
HOOGSTEEN, M. J. J., LANTINGA, E. A., BAKKER, E. J., GROOT, J. C. J. & TITTONELL, P. A. 2015. Estimating soil organic carbon through loss on ignition: effects of ignition conditions and structural water loss. *European Journal of Soil Science,* 66**,** 320-328.
HOSSACK, J. & LUTRO, O. 2013. *Berggrunnskart, Synnfjell, 1717 III,* 1:50 000. Trondheim: Norwegian Geological Survey.
JANDL, R., RODEGHIERO, M. & OLSSON, M. 2011. *Soil Carbon in Sensitive Europen Ecosystems* Chichester, UK, Wiley-Blackwell.
JENNY, H. 1941. *Factors of soil formation. A System of Quantitative Pedology*
JO, H. R., RHEE, C. W. & CHOUGH, S. K. 1997. Distinctive characteristics of a streamflow-dominated alluvial fan deposit: Sanghori area, Kyongsang Basin (Early Cretaceous), southeastern Korea. *Sedimentary Geology,* 110**,** 51-&.
JOBBAGY, E. G. & JACKSON, R. B. 2000. The vertical distribution of soil organic carbon and its relation to climate and vegetation. *Ecological Applications,* 10**,** 423-436.
JOFFE, J. S. 1936. *Pedology,* New Brunswick, NJ, Rutgers Univ. Press.
JØRGENSEN, P., SØRENSEN, R. & HALDORSEN, S. 1997. *Kvartærgeologi,* Bergen Landbruksforlaget.
KARTVERKET 2018. https://www.kartverket.no/.
KLEJA, D. B., SVENSSON, M., MAJDI, H., JANSSON, P. E., LANGVALL, O., BERGKVIST, B., JOHANSSON, M. B., WESLIEN, P., TRUUSB, L., LINDROTH, A. & AGREN, G. I. 2008. Pools and fluxes of carbon in three Norway spruce ecosystems along a climatic gradient in Sweden. *Biogeochemistry,* 89**,** 7-25.
KROGSTAD, T. & BØRRESEN, T. 2015. Field and Laboratory Methods. *In:* SCIENCES, D. O. E. (ed.). Ås: Norwegian University of Life Sciences.
KVIFTE, A. 03.05. 2018. *RE: Binding of organic matter to clay minerals*
LARSSON, J. Y. 2000. Veiledning i bestemmelse av vegetasjonstyper i skog. Ås: Norsk institutt for jord- og skogkartlegging.
LAWSON, D. E. 1981b. *Sedimentological characteristics and classification of depositional processes and depositsin the glacial envrionment,* Hanover, NH, Cold Regions Research and Engineering Laorratory.
LIVINGSTONE, S. J., EVANS, D. J. A., COFAIGH, C. O. & HOPKINS, J. 2010. The Brampton kame belt and Pennine escarpment meltwater channel system (Cumbria, UK): Morphology, sedimentology and formation. *Proceedings of the Geologists Association,* 121**,** 423-443.
LUNDSTROM, U. S., VAN BREEMEN, N. & BAIN, D. 2000. The podzolization process. A review. *Geoderma,* 94**,** 91-107.
MAURING, E., KOZIEL, J., LAURITSEN, T., RØNNING, J. S. & TØNNESEN, J. F. 1995. Målinger med georadar : Teori, anvendelse, teknikker og eksempler på opptak. NGU Report No. 94.024.

MIKUTTA, R., MIKUTTA, C., KALBITZ, K., SCHEEL, T., KAISER, K. & JAHN, R. 2007. Biodegradation of forest floor organic matter bound to minerals via different binding mechanisms. *Geochimica Et Cosmochimica Acta,* 71**,** 2569-2590.
MOEN, A. 1987. The regional vegetation of Norway; that of Central Norway in particular. *Norwegian Journal of Geography* 41**,** 179-226.
MOEN, A. 1998. *Vegetasjon,* Hønefoss.
MULDER, V. L., DE BRUIN, S., SCHAEPMAN, M. E. & MAYR, T. R. 2011. The use of remote sensing in soil and terrain mapping - A review. *Geoderma,* 162**,** 1-19.
MUNSELL 2010. Munsell Soil Color Charts : with Genuine Munsell Color Chips. Grand Rapids, MI: Munsell Color.
NEAL, A. 2004. Ground-penetrating radar and its use in sedimentology: principles, problems and progress. *Earth-Science Reviews,* 66**,** 261-+.
NELSON, D. W. & SOMERS, L. E. 1982. *Total Carbon, Organic Carbon and Organic Matter,* Madison, Wisconsin, USA, American Society of of Agronomy, Inc.
NGU. 2018. *Database for løsmasser* [Online]. [Accessed 26.02. 2018].
NORA. 2017. *What is LIDAR?* [Online]. National Ocean Service - National Oceanic and Atmospheric Administration - United States Department of Commerce. [Accessed 18.09.17 2017].
NVE, MET.NO & KARTVERKET. 2018. *SeNorge.no* [Online]. [Accessed 26.02. 2018].
OLSEN, L. 1983. A method for determining total clast roundness in sediments *Boreas,* 12**,** 17-21.
PETRENKO, C. L. & FRIEDLAND, A. J. 2015. Mineral soil carbon pool responses to forest clearing in Northeastern hardwood forests. *Global Change Biology Bioenergy,* 7**,** 1283-1293.
PIERZYNSKI, G. M., SIMS, J. T. & VANCE, G. F. 2005. *Soils and Environmental Quality* Boca Raton, FL, USA, CRC Press.
PORRAS, R. C., PRIES, C. E. H., TORN, M. S. & NICO, P. S. 2018. Synthetic iron (hydr) oxide-glucose associations in subsurface soil: Effects on decomposability of mineral associated carbon. *Science of the Total Environment,* 613**,** 342-351.
PROTHERO, D. R. & SCHWAB, F. L. 2004. *Sedimentary geology: An introduction to sedimentary rocks and stratigraphy,* New York, W. H. Freeman.
PUTNINS, A. & HENRIKSEN, M. 2017. Reconstructing the flow pattern evolution in inner region of the Fennoscandian Ice Sheet by glacial landforms from Gausdal Vestfjell area, south-central Norway. *Quaternary Science Reviews,* 163**,** 56-71.
RETCH, G. 2017. Germany Retch GmbH. [Accessed 09.09.17 2017].
RYDER, J. M., FULTON, R. J. & CLAGUE, J. J. 1991. The Cordilleran Ice Sheet and the Glacial Geomorphology of Southern and Central British Colombia. *Géographie physique et Quaternaire* 45**,** 365-377.
SCHLESINGER, W. H. 1990. Evidence from chronosequence studies for a low carbon-storage potential of soils. *Nature,* 348**,** 232–234.
SCHLESINGER, W. H. & BERNHARDT, E. S. 2013. *Biogeochemistry: An analysis of global change* Amsterdam, Netherlands, Elsevier Academic Press.
SCHULZE, K., BORKEN, W., MUHR, J. & MATZNER, E. 2009. Stock, turnover time and accumulation of organic matter in bulk and density fractions of a Podzol soil. *European Journal of Soil Science,* 60**,** 567-577.
SIEDLECKA, A., NYSTUEN, J. P., ENGLUND, J. O. & HOSSACK, J. 1987. *Berggrunnskart over Lillehammer,* 1:250 000. Trondheim: Norwegain Geological Survey
SMITH, K. A. & MULLINS, C. E. 2001. *Soil and Enviromental Analysis: Physical Methods,* New York, Marcel Dekker Inc.

SPOONER, I. S. & OSBORN, G. D. 2000. Geomorphology and Late Wisconsinan sedimentation in the Stikine River Valley, northern British Columbia. *Quaternary International,* 68-71**,** 285-296.
STRAND, L. T., CALLESEN, I., DALSGAARD, L. & DE WIT, H. A. 2016. Carbon and nitrogen stocks in Norwegian forest soils - the importance of soil formation, climate, and vegetation type for organic matter accumulation. *Canadian Journal of Forest Research,* 46**,** 1459-1473.
STROEVEN, A. P., HATTESTRAND, C., KLEMAN, J., HEYMAN, J., FABEL, D., FREDIN, O., GOODFELLOW, B. W., HARBOR, J. M., JANSEN, J. D., OLSEN, L., CAFFEE, M. W., FINK, D., LUNDQVIST, J., ROSQVIST, G. C., STROMBERG, B. & JANSSON, K. N. 2016. Deglaciation of Fennoscandia. *Quaternary Science Reviews,* 147**,** 91-121.
TOLLAN, A. 1963. Trekk av isbevegelsen og isavsmeltningen i Nordre Gurdbrandsdalens Fjelltrakter *In:* NGU (ed.). NGU: NGU.
TORN, M. S., TRUMBORE, S. E., CHADWICK, O. A., VITOUSEK, P. M. & HENDRICKS, D. M. 1997. Mineral control of soil organic carbon storage and turnover. *Nature* 389**,** 170-173.
TORRES-SALLAN, G., SCHULTE, R. P. O., LANIGAN, G. J., BYRNE, K. A., REIDY, B., SIMÓ, I., SIX, J. & CREAMER, R. E. 2017. Clay illuviation provides a long-term sink for C sequestration in subsoils. *Scientific Reports,* 7**,** 45635.
TRUMBORE, S. 2000. Age of soil organic matter and soil respiration: Radiocarbon constraints on belowground C dynamics. *Ecological Applications,* 10**,** 399-411.
UNIVERSITY OF MINNESOTA, C. O. F., AGRICULTURAL AND NATURAL RESOURCE SCIENCES 2017. *http://ral.cfans.umn.edu/tests-analysis/icp-analysis* [Online]. University of Minnesota, College of Food, Agricultural and Natural Resource Sciences. [Accessed 15.09.07 2017].
VAN OVERMEEREN, R. A. 1998. Radar facies of unconsolidated sediments in The Netherlands: A radar stratigraphy interpretation method for hydrogeology. *Journal of Applied Geophysics,* 40**,** 1-18.
VAN REEUWIJK, L. P. 1993. *Procedures for soil analysis,* Wageningen, The Netherlands, International Soil Reference and Information Centre, ISRIC.
VESTIN, J. L. K., NAMBU, K., VAN HEES, P. A. W., BYUND, D. & LUNDSTRÖM, U. 2006. The influence of alkaline and non-alkaline parent material on soil chemistry. *Geoderma,* 35**,** 97-106.
VORREN, T. O. 1977. Weichselian Ice Movement in South-Norway and Adjacent Areas *Boreas,* 6**,** 247-257.
WHITE, A. F., BLUM, A. E., SCHULZ, M. S., BULLEN, T. D., HARDEN, J. W. & PETERSON, M. L. 1996. Chemical weathering rates of a soil chronosequence on granitic alluvium: I. Quantification of mineralogical and surface area changes and calculation of primary silicate reaction rates. *Geochimica et Cosmochimica Acta,* 60**,** 2533-2550.
WIRTH, C., SCHULZE, E., SCHWALBE, G., TOMCZYK, S., WEBER, G., WELLER, E., BÖTTCHER, H., SCHUMACHER, J. & VETTER, J. 2004. Dynamik der Kohlenstoffvorräte in den Wäldern Thüringens. *Abschlussbericht zur,* 1.
WRB, I. W. G. 2014. International Soil Classification System for Naming Soils and Creating Legends for Soil Maps. *World Soil Resources Reports No. 106.* Rome: FAO.
YUSOFF, K. H. M., ABDU, A., SAKURAI, K., TANAKA, S. & KANG, Y. M. 2017. Influence of agricultural activity on soil morphological and physicochemical properties on sandy beach ridges along the east coast of Peninsular Malaysia. *Soil Science and Plant Nutrition,* 63**,** 55-66.

Appendix 1 Soil Profile Descriptions

V3-1, Profile 1 884 m.a.s.l. Kame Terrace, valley 3 Described: 25/07/2017

UTM Coordinates 32V 539886 E 6783896 N
Position Medium gradient hill, upper slope (shoulder), convex slope surface form in both vertical and horizontal direction. Moderately steep slope gradient, oriented towards the EEN (at 60º)
Climate Annual average precipitation 1000-1500 mm. Annual average temperature +1-0 º C
Weather Partly cloudy during description, no rain in the last week
Soil climate regime
Frigid soil temperature, ustic soil moisture
Parent material
Glacifluvial material, sand and gravelly sand. Clasts of Andesite, Meta-andesite, Feldspathic metasandstone, Feldspathic quartzite, Gneiss, Granite
Bedrock Arkose and greywacke
Age and nature of land surface
Late Pleistocene/Early Holocene, ice covered. No anthrogeomorphic influence, only natural loss by erosion
Vegetation Deciduous shrub, Heather bog-bilberry – Scots pine mountain woodland
Land use National Park
Rock outcrops None
Coarse surface fragments Few, stones and boulders (48,6 volume percent of upper 40 cm)
Erosion Slight water and wind erosion, active at present, 5-10% of area affected
Degree of drainage Well drained
Groundwater level Below profile depth
Profile depth 106 cm

Classification Arenic Ortsteinic Podzol (Densic)

Horizon	Depth (cm)	Description
A	6-0	Dark grey (10YR/4/1) (coarse sand); moderately decomposed peat; weak, angular blocky, very fine soil structure; loose when dry and moist; non-sticky; non-plastic; very high porosity, many medium, interstitial voids; few very fine and fine, many medium and few coarse roots; abrupt, wavy horizon boundary
E	0-20	White (2,5Y/8/1) loamy fine sand (very coarse and coarse sand); abundant subrounded, strongly weathered fine and medium gravel; weak, angular blocky, very fine soil structure; loose when dry and moist; non-sticky; non-plastic; very high porosity, many medium, interstitial voids; many very fine, few fine and medium and very few coarse roots; clear, wavy horizon boundary
Bs	20-35	Reddish yellow (7,5YR/7/8) fine sand (very coarse and coarse sand); abundant subrounded, strongly weathered fine and medium gravel; weak, single grained, fine soil structure; loose when dry and moist; non-sticky; non-plastic; very high porosity, many medium, interstitial voids; few very fine, fine and medium and no coarse roots; clear, smooth horizon boundary
Bx	35-48	Dark brown (7,5YR/3/4) (medium and fine sand); very few, fine, black (7,5YR/2,5/1) mottles, with a distinct contrast and sharp boundary with matrix; weak, massive, fine soil structure; fast loose when dry and moist; non-sticky; non-plastic; very low porosity, very few, very fine interstitial voids; discontinuous, pisolithic cemented mass of iron-organic matter; no roots; clear, irregular horizon boundary
C	48-100	Reddish grey (2,5YR/6/1) fine sand (coarse, medium and fine sand, sorted within sedimentary layers); weak, layered (coherent), fine soil structure; loose when dry and moist; non-sticky; non-plastic; very high porosity, fine, interstitial voids common; no roots

V3-2, Profile 2 844 m.a.s.l. Ice-flow Parallel Esker, valley 3 Described: 25/07/2017

UTM Coordinates 32V 544820 E 67834004 N
Position High-gradient hill, crest (summit), convex slope surface form in both vertical and horizontal direction. Steep slope gradient, oriented towards the NNE (at 34º)
Climate Annual average precipitation 1000-1500 mm. Annual average temperature +1-0 ºC
Weather Partly cloudy during description, no rain in the last week
Soil climate regime
Frigid soil temperature, ustic soil moisture
Parent material Glacifluvial material, sand and gravelly sand. Clasts of Meta-andesite, Amphibolite, Augen Gneiss, Acid Gneiss, Granite
Bedrock Conglomerate, gabbro pebbles
Age and nature of land surface Late Pleistocene/Early Holocene, ice covered. No anthrogeomorphic influence, only natural loss by erosion
Vegetation Deciduous shrub, Cowberry-bilberry woodland
Land use National Park
Rock outcrops None
Coarse surface fragments Few, stones (34,9 volume percent of upper 40 cm)
Erosion Slight water and wind erosion, active at present, 0-5% of area affected
Degree of drainage Well drained
Groundwater level Below profile depth
Profile depth 101 cm

Classification Episkeletic Podzol (Arenic, Fragic, Geoabruptic)

Horizon	Depth (cm)	Description
Oa	7-0	Brown (7,5YR/4/2) organic material; moderately decomposed peat; weak, subangular blocky, very fine soil structure; loose when dry and moist; non-sticky; non-plastic medium porosity, common with fine, interstitial voids; common with very fine, fine and medium and few coarse roots; clear, wavy horizon boundary
E	0-9	Light grey (7,5YR/7/1) loam, (coarse sand); common with subrounded, weathered stones; weak, single grained, very fine soil structure; loose when dry and moist; non-sticky; non-plastic; high porosity, commo with fine, interstitial voids; few very fine and fine, very few medium and no coarse roots; gradual, irregular horizon boundary.
Bs	9-70	Strong brown (7,5YR/4/6) loamy fine sand (coarse sand); common with subrounded, weathered stones; few, fine, strong brown (7,5YR/5/8) mottles, with a distinct contrast and sharp boundary with matrix; weak, single grained, very fine soil structure; loose when dry and moist; non-sticky; non-plastic high porosity, commo with fine, interstitial voids; continuous, platy cemented mass of silicate or clay; very few very fine and fine and no medium and coarse roots; possibly a few, large, infilled burrows; diffuse, broken horizon boundary.
C	70-94	Grey (5YR/5/1) fine sand (medium sand); very few subrounded, weathered fine gravel; common with coarse, Yellowish red (5YR/5/8) mottles, with a distinct contrast and sharp boundary with matrix; weak, layered (coherent), very fine soil structure; fast loose when dry and moist; non-sticky; non-plastic; high porosity, common with fine, interstitial voids; no roots

V2-7, Profile 3 832 m.a.s.l. Ice-flow transverse Esker, valley 2 Described: 27/07/2017

UTM Coordinates 32V 548483 E 6783597 N
Position Medium-gradient hill, middle slope (back slope), slope surface form convex in vertical and concave in horizontal direction. Moderately steep slope gradient, oriented towards the V (at 270º)
Climate Annual average precipitation 1000-1500 mm. Annual average temperature +1-0º C
Weather Rain during description, rain without heavy rain in the last 24 hours
Soil climate regime Frigid soil temperature, ustic soil moisture
Parent material Glacifluvial material, sand and gravelly sand. Clasts of Andesite, Meta-andesite, Feldspathic metasandstone, Feldspathic quartzite, Gneiss, Granite, Quartzite, anorthosite
Bedrock Slate
Age and nature of land surface Late Pleistocene/Early Holocene, ice covered. No anthrogeomorphic influence, only natural loss by erosion
Vegetation Deciduous shrub, Cowberry-bilberry woodland
Land use Nature Reserve
Rock outcrops None
Coarse surface fragments Very few, boulders (50,0 volume percent of upper 40 cm)
Erosion No evidence
Degree of drainage Moderately to well drained
Groundwater level Below profile depth
Profile depth 103 cm

Classification Umbric Podzol (Arenic)

Horizon	Depth (cm)	Description
Oe	7-4	Brown (7,5YR/4/4) organic material; moderately decomposition of peat; weak, subangular blocky, fine soil structure; loose when dry and moist; non-sticky; non-plastic; low porosity, common with fine, interstitial voids; many very fine, fine and medium and few coarse roots; abrupt, wavy horizon boundary
Oa	4-0	Dark brown (7,5YR/3/4) organic material; very low to low decomposed peat; common with subrounded, weathered stones; moderate, subangular blocky, fine soil structure; loose when dry and moist; non-sticky; non-plastic; low porosity, common with fine, interstitial voids; common with very fine, fine and medium and few coarse roots; abrupt, wavy horizon boundary
A	0-8	Dark reddish grey (5YR/4/2) sandy loam (fine sand); very few subrounded, weathered coarse gravel (15%) and stones (1%); few, fine, strong brown (7,5YR/5/8) mottles, with a distinct contrast and sharp boundary with matrix; moderate, subangular blocky, fine soil structure; loose when dry and moist; non-sticky; non-plastic; low porosity, commo with fine, interstitial voids; common with very fine, fine and medium and few coarse roots; abrupt, broken horizon boundary
E	8-17	White (5YR/8/1) sandy loam (fine sand); common with subrounded, weathered coarse gravel (20%) and stones (3%); common with coarse, Yellowish red (5YR/5/8) mottles, with a distinct contrast and sharp boundary with matrix; moderate, subangular blocky, fine soil structure; fast loose when dry and moist; non-sticky; non-plastic; low porosity, common with fine, interstitial voids; few very fine, fine, medium and coarse roots; abrupt, broken horizon boundary
Bs	17-33	Strong brown (7,5YR/5/8) sandy loam (fine to medium sand); common with subrounded, weathered medium and coarse gravel (20%) and stones (5%); few, fine, strong brown (7,5YR/4/6) mottles, with a faint contrast and clear boundary with matrix, occurs predominantly around gravel and stones; moderate, subangular blocky, fine soil structure; loose when dry and moist; non-sticky; non-plastic; low porosity, few fine, interstitial voids; few very fine and fine and very few medium and coarse roots; possibly a few, large, infilled burrows; gradual, irregular horizon boundary
CB	33-96	Olive grey (5Y/4/2) loamy fine sand (coarse sand); many subrounded, weathered medium and course gravel; common with coarse; moderate, subangular blocky, fine soil structure; fast loose when dry and moist; non-sticky; non-plastic; low porosity, common with fine, interstitial voids; few very fine and fine and no medium and coarse roots

V1-2, Profile 4 878 m.a.s.l. Wide, U-shaped Esker, Valley 1 Described: 31/07/2017

UTM Coordinates 32V 548709 E 6788035 N
Position High-gradient hill, upper slope (shoulder), slope surface form concave in vertical and convex in horizontal direction. Steep slope gradient, oriented towards the V (at 260°)
Climate Annual average precipitation 1000-1500 mm. Annual average temperature +1-0° C
Weather Partly cloudy during description, rain without heavy rain in the last 24 hours
Soil climate regime
Frigid soil temperature, ustic soil moisture
Parent material Glacifluvial material, sand and gravelly sand. Clasts of Amphibolite, Meta-aNosite, Gabbro, Meta-gabbro, Micaceous Shale, Dark slate, Granite, Jotunite/mangerite
Bedrock Slate
Age and nature of land surface Late Pleistocene/Early Holocene, ice covered. No anthrogeomorphic influence, only natural loss by erosion
Vegetation Deciduous shrub, Cowberry-bilberry woodland
Land use National Park
Rock outcrops None
Coarse surface fragments Common, stones (56,5 volume percent of upper 40 cm)
Erosion Slight erosion by mass movement, 0-5% of area affected, active at present
Degree of drainage Moderately well drained
Groundwater level Below profile depth
Profile depth 100 cm
Classification Episkeletic Glossic Podzol (Eutric)

Horizon	Depth (cm)	Description
O	7-0	Brown (10YR/3/3) organic material, low to moderately decomposed peat; few, subrounded, weathered coarse gravel; weak, subangular blocky, fine soil structure; loose when dry and moist; non-sticky; non-plastic; low porosity, common with fine, interstitial voids; many very fine and fine, few medium and common with coarse roots; abrupt, wavy horizon boundary
A	0-21	Dark reddish grey (10YR/3/4) sandy loam (coarse sand); few, subrounded, weathered coarse gravel; weak, single grained, fine soil structure; loose when dry and moist; non-sticky; non-plastic; low porosity, common with fine, interstitial voids; many very fine and fine and common with medium and coarse roots; clear, wavy horizon boundary
E	21-25	White (10YR/6/2) sandy loam (medium sand); very few, subrounded, weathered coarse gravel (20%) and stones (3%); common with coarse, Yellowish red (5YR/5/8) mottles, with a distinct contrast and sharp boundary with matrix; weak, single grained,, very fine soil structure; fast loose when dry and moist; non-sticky; non-plastic; low porosity, common with fine, interstitial voids; very few very fine and fine, few medium and no coarse roots; abrupt, broken horizon boundary
Bs	25-83	Strong brown (7,5YR/5/6) sandy loam (medium sand); very few, subrounded, weathered coarse gravel; weak, single grained, very fine soil structure; loose when dry and moist; non-sticky; non-plastic; low porosity, few fine, interstitial voids; very few very fine and fine and common with medium and coarse roots; possibly a few, large, infilled burrows; gradual, wavy horizon boundary
CB	33-96	Olive grey (5Y/4/2) loamy fine sand (coarse sand); many subrounded, weathered medium and course gravel; common with coarse; moderate, subangular blocky, fine soil structure; fast loose when dry and moist; non-sticky; non-plastic; low porosity, common with fine, interstitial voids; few very fine and fine and no medium and coarse roots

Appendix 2 Bedrock Clast Count

Bedrock clast count of the four described soil profiles.

Lithology	**No. M.s. L./S.** [1]	**V3-1**	**V3-2**	**V2-7**	**V1-2**
Metasandstone, Feldspathic	38	0	1	13	0
Sparagmite	16	21	21	13	16
Quartzite, Unspecified	1,14,34,41,52,53, 56, 57/9,12	3	1	2	0
Quartzite, Feldspathic	2,32, 37, 39, 47	5	0	0	0
Shale, Micacous	5,7	0	0	0	3
Shale, Micacous, c. garnet	10	2	0	0	0
Slate, Dark grey to black	14,52, 53/1,2,3,9,12	0	0	0	3
Gneiss, Unspecified	13	2	0	0	0
Augen gneiss	28,30,50	0	3	0	3
Gneiss,C. Amphibolite	19	1	1	0	0
Gneiss, Acd-intrm, c. amph/qrtz	21	1	2	5	0
Granite	8,28	0	2	0	4
Foliated granite	50	15	0	1	0
Gabbro	23,25,30/7	0	0	0	7
Gabbro c. hornblende	25	0	2	0	0
Metagabbro	49	1	0	0	7
Amphibolite	2,11,13,35	1	0	0	0
Greenstone	4	1	0	0	0
Jotunitt/mangeritt	3,29	0	3	0	0
anorthosite	30	0	3	1	1
Meta-aNosite	13,49	0	0	0	12
Trondhjemite	1	0	2	0	4
Diorite	23,24	0	5	0	0

[1] Assigned number on lithology from mapsheets Lillehammer/Synnfjell, after Siedlecka et al. (1987) and Hossack and Lutro (2013), respectively.

Appendix 3 Soil Sample Rock Fragment Rounding

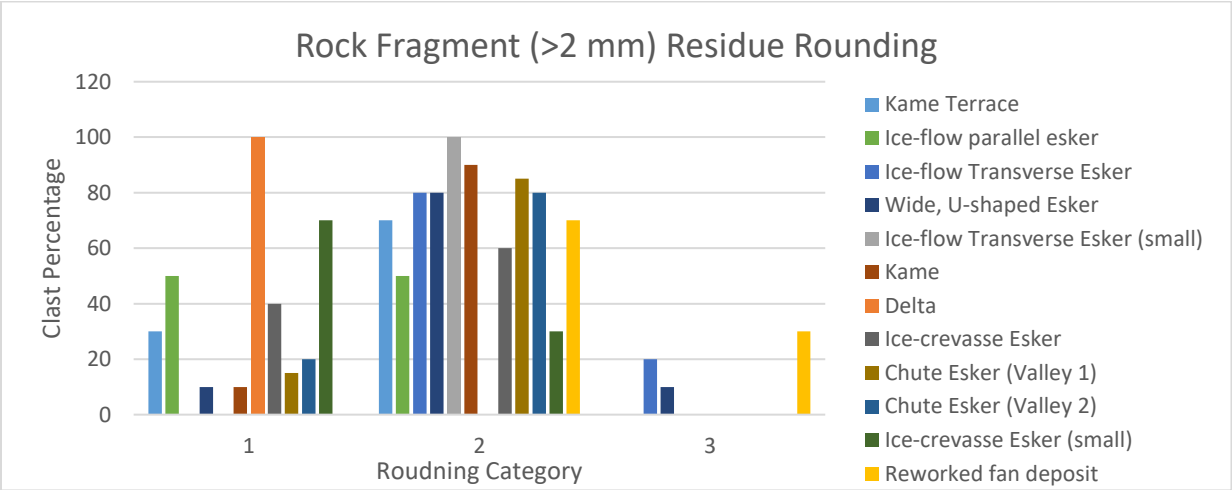

The degree of rounding of the rock fragment residue of all sampled profiles. 1= Angular, 2= Subangular, 3= Rounded. Note that the rock fragment percentage varied greatly between the samples and is reflected in the uncertainty in comparison.

Appendix 4 Soil Chemical Analysis

Landform	Horizon	Tot C (%)	Tot N (%)	C/N	pH	LOI (w. %)	CEC (cmol/kg)	BS (%)	Na+ (cmol/kg)	Mg2+ (cmol/kg)	K+ (cmol/kg)	Ca2+ (cmol/kg)	H+ (cmol/kg)	Tot Ox. (g/kg)	Fe (g/kg)	Al (g/kg)	Si (g/kg)
V3-1	A	3,64	0,17	22	4,65	8,6	11,00	9,09	0,13	0,15	0,19	0,53	10,00	5,91	3,60	2,10	0,21
	E	0,29	0,05	6	4,46	1,13	9,27	1,09	0,00	0,03	0,04	0,04	9,17	1,16	0,51	0,65	0,00
	Bs	0,79	0,05	15	5,22	2,18	11,99	0,92	0,00	0,02	0,04	0,06	11,88	6,38	2,00	3,80	0,58
	C	0,04	0,03	1	5,66	0,13	7,33	3,37	0,13	0,02	0,04	0,06	7,08	0,88	0,27	0,47	0,14
V3-2	O	23,50	0,57	41	4,25	41,93	61,89	9,79	0,26	1,66	0,74	3,40	55,83	5,26	2,30	2,90	0,06
	E	1,00	0,06	17	4,63	2,45	8,23	3,76	0,13	0,05	0,05	0,08	7,92	2,60	1,50	1,10	0,00
	Bs	1,54	0,08	19	5,3	4,01	18,33	2,21	0,13	0,05	0,05	0,18	17,92	19,90	7,50	10,00	2,40
	C	0,05	0,03	2	5,77	0,27	8,43	3,58	0,13	0,02	0,07	0,09	8,13	0,69	0,20	0,39	0,10
V2-7	Oe	43,80	1,49	29	4,21	76,02	89,24	16,43	0,26	2,40	5,00	7,00	74,58	1,22	0,47	0,66	0,09
	Oa	50,70	1,33	38	3,69	92,03	120,83	3,79	0,28	0,76	1,64	1,90	116,25	0,87	0,36	0,51	0,00
	A	9,13	0,34	27	4,26	15,27	32,13	2,07	0,13	0,13	0,31	0,10	31,46	9,10	4,90	3,90	0,30
	E	0,77	0,05	14	4,09	1,56	19,02	1,42	0,13	0,02	0,04	0,09	18,75	0,68	0,34	0,34	0,00
	Bs	2,01	0,09	23	5,34	5,45	4,13	4,21	0,00	0,02	0,04	0,12	3,96	31,40	7,50	17,00	6,90
	CB	0,20	0,04	5	5,45	0,71	1,38	9,42	0,00	0,02	0,04	0,07	1,25	3,38	1,00	1,80	0,58
V1-2	O	9,37	0,40	23	4,99	19,49	26,84	16,17	0,00	0,74	0,60	3,00	22,50	11,98	5,60	5,70	0,68
	A	3,90	0,20	20	5,07	8,07	19,70	1,61	0,00	0,07	0,07	0,18	19,38	15,05	8,30	5,90	0,85
	E	0,89	0,05	19	4,96	2,24	9,93	1,37	0,00	0,02	0,04	0,08	9,79	5,90	4,30	1,50	0,10
	Bs	2,60	0,11	23	5,54	6,79	13,62	2,14	0,00	0,02	0,04	0,23	13,33	29,20	13,00	13,00	3,20
	CB	0,29	0,04	7	5,82	1	0,19	100,00	0,00	0,02	0,04	0,14	0,00	4,41	1,00	2,60	0,81
V3-4	O	49,80	1,79	28	4,31	91,49	75,98	19,37	0,32	3,40	2,00	9,00	61,26	0,92	0,52	0,40	0,00
	E	1,28	0,07	18	4,44	2,88	0,27	100,00	0,00	0,08	0,06	0,14	0,00	1,62	1,20	0,42	0,00
	Bs	0,83	0,07	11	5,68	1,91	1,13	26,22	0,13	0,03	0,05	0,09	0,83	6,82	3,80	2,60	0,42
V2-1	O	51,00	1,09	47	5,14	90,73	64,72	36,25	0,26	5,00	6,80	11,40	41,26	0,58	0,32	0,26	0,00
	E	5,88	0,19	31	6,61	9,9	15,78	40,56	0,00	1,00	3,70	1,70	9,38	1,42	0,83	0,59	0,00
	Bs	5,68	0,21	27	5,98	11,88	14,51	33,98	0,13	1,00	2,40	1,40	9,58	19,10	8,60	8,70	1,80
V2-6	O	38,80	1,10	35	3,93	71,47	70,20	16,30	0,26	2,40	1,58	7,20	58,76	1,45	0,73	0,72	0,00
	E	2,24	0,09	24	4,03	4,57	4,89	14,67	0,00	0,10	0,10	0,52	4,17	1,49	0,54	0,95	0,00
	Bs	2,67	0,09	29	4,94	7,53	6,48	3,59	0,00	0,05	0,07	0,11	6,25	22,10	7,90	11,00	3,20
V1-4	O	42,10	1,33	32	4,2	74,76	98,22	17,27	0,36	4,40	3,20	9,00	81,26	9,00	8,00	1,00	0,00
	E	1,33	0,06	23	4,41	3,31	12,59	2,41	0,00	0,09	0,07	0,15	12,29	12,32	10,00	2,20	0,12
	Bs	1,74	0,07	26	4,97	4,82	4,54	3,52	0,00	0,04	0,05	0,06	4,38	24,50	12,00	10,00	2,50
V1-5	O	44,20	1,25	35	3,91	80,45	89,56	13,93	0,26	2,40	1,62	8,20	77,08	1,50	0,73	0,77	0,00
	E	2,14	0,08	28	3,98	4,55	13,92	2,73	0,00	0,11	0,08	0,19	13,54	1,74	0,64	1,10	0,00
	Bs	2,66	0,04	72	4,93	15,88	12,30	1,81	0,00	0,05	0,06	0,11	12,08	18,60	6,20	9,60	2,80
V1-3	O	49,20	1,40	35	4,7	91,04	98,72	17,28	0,26	4,00	3,20	9,60	81,66	1,16	0,68	0,48	0,00
	E	0,82	0,12	7	3,99	3,24	3,90	14,62	0,00	0,15	0,08	0,34	3,33	2,16	1,60	0,56	0,00
	Bs	3,65	0,14	26	4,96	9,15	11,97	2,48	0,00	0,06	0,07	0,17	11,67	33,90	16,00	15,00	2,90
V2-8	O	41,60	0,86	48	4,52	84,65	72,40	21,74	0,34	2,40	3,00	10,00	56,66	0,78	0,49	0,29	0,00
	E	1,27	0,10	13	3,91	2,58	6,74	10,33	0,00	0,14	0,09	0,47	6,04	0,49	0,11	0,38	0,00
	Bs	2,01	0,11	18	5,37	5,1	10,66	8,16	0,13	0,12	0,12	0,50	9,79	17,94	11,00	6,20	0,74
V2-3	A	7,79	0,28	28	4,24	13,82	19,77	9,36	0,00	0,58	0,29	0,98	17,92	4,49	2,80	1,60	0,09
	Bs	2,64	0,13	20	5,18	5,83	12,21	2,68	0,00	0,10	0,07	0,16	11,88	20,30	9,80	8,80	1,70

Tot C= Total Carbon Content, Tot N= Total Nitrogen Content, LOI= Loss on Ignition, BS= Base Saturation

Appendix 5 Carbon Stock Calculation

Landform	Horizon	Tot C (%)	Thickness (cm)	Density (g/cm^3)	Stone and Boulder Content (%)	Carbon Stock (kg/m^2)
V3-1	A	3.64	6.0	0,70	48.64	0.79
	E	0.29	20.0	1,36	48.64	0.78
	Bs	0.79	26.0	1,36	48.64	1.94
	C	0.04	52.0	1,50	48.64	0.22
V3-2	O	23.50	7.0	0,17	34.92	1.8
	E	1.00	9.0	1,21	34.92	1.09
	Bs	1.54	61.0	1,35	34.92	6.35
	C	0.05	24.0	1,45	34.92	0.08
V2-7	Oe	43.80	3.0	0,04	35.75	0.26
	Oa	50.70	4.0	0,05	35.75	0.52
	A	9.13	8.0	0,53	35.75	1.93
	E	0.77	3.0	1,27	35.75	0.29
	Bs	2.01	16.0	1,05	35.75	1.28
	CB	0.20	45.0	1,48	35.75	0.57
V1-2	O	9.37	7.0	0,41	56.50	1.18
	A	3.90	21.0	0,93	56.50	3.3
	E	0.89	4.0	0,85	56.50	0.3
	Bs	2.60	58.0	1,00	56.50	12.8
	C	0.29	17.0	1,79	56.50	0.74
V3-4	O	49.80	7.0	0,27	15.34	9.48
	E	1.28	8.0	1,53	15.34	0.63
	Bs	0.83	12.0	1,13	15.34	0.46
V2-1	O	51.00	3.0	0,12	59.78	1.8
	E	5.88	7.0	0,64	59.78	1.69
	Bs	5.68	14.0	1,40	59.78	7.12
V2-6	O	38.80	6.5	0,07	35.75	0.72
	E	2.24	5.0	1,06	35.75	0.95
	Bs	2.67	24.0	1,39	35.75	1.3
V1-4	O	42.10	8.0	0,14	42.48	4.8
	E	1.33	8.0	0,95	42.48	1.01
	Bs	1.74	22.0	0,99	42.48	2.39
V1-5	O	44.20	8.5	0,07	37.09	2.45
	E	2.14	8.5	1,19	37.09	1.24
	Bs	2.66	23.0	0.86	37.09	3.02
V1-3	O	49.20	6.5	0,16	30.23	5.07
	E	0.82	5.0	1,05	30.23	0.22
	Bs	3.65	28.5	0,69	30.23	3.63
V2-8	O	41.60	7.5	0,23	49.31	7.15
	E	1.27	19.0	1,06	49.31	1.34
	Bs	2.01	12.0	1,24	49.31	1.56
V2-3	A	7.79	8.0	0,60	47.80	1.86
	Bs	2.64	12.5	1,29	47.80	1.36

Norges miljø- og biovitenskapelige universitet
Noregs miljø- og biovitskapelege universitet
Norwegian University of Life Sciences

Postboks 5003
NO-1432 Ås
Norway